Investigations of the DEAD-box helicase eIF4A

Nicola Marie Phillips, BSc., MSc.

Thesis submitted to the University of Nottingham for the degree of Doctor of Philosophy

July 2011

Abstract

Eukaryotic Initiation Factor (eIF) 4A is the most abundant initiation factor and the prototypical member of the DEAD-box family of helicases. Once recruited to the cap-binding complex, eIF4F, eIF4A unwinds inhibitory RNA secondary structure in the 5' untranslated region (UTR) of mRNAs, promoting efficient ribosomal scanning to the start codon. The requirement for eIF4A in translation initiation correlates with increasing 5' UTR length, suggesting that regulating the activity of eIF4A may affect the translation of particular mRNAs. It is well established that the transcripts of genes involved in cell cycle control and proliferation have long 5' UTRs; therefore altering the activity of eIF4A may affect these genes specifically.

A cross-discipline approach was used to investigate eIF4A helicase activity to obtain information regarding both the mechanics of helicase activity and the biological impacts of its inhibition. Recombinant eIF4A helicase activity, the stimulatory effect of eIF4B and the effect of known eIF4A inhibitors was first analysed using an ensemble helicase assay. Due to the limitations of this method a single molecule technique utilising optical tweezers was developed to investigate helicase activity at a higher force resolution. Optical tweezers were used to 'trap' and manipulate a dual-labeled RNA:DNA construct containing a central stem-loop hairpin known to be inhibitory to ribosomal scanning attached to functionalised microspheres. Although instrumental failure prevented the completion of these experiments, initial force extension curves using this molecule were obtained. Once established, this single molecule system may be used to observe eIF4A activity with its accessory protein eIF4B and known eIF4A inhibitors.

15-deoxy-delta(12, 14)-prostaglandin J_2 (15d-PGJ_2) is a newly identified natural inhibitor of eIF4A activity which induces apoptosis and is implicated in the resolution of inflammation. The translation of specific mRNAs affected by 15d-PGJ_2 treatment of HeLa cells was analysed by translational profiling coupled to microarray analysis. No correlation, however, was seen between those transcripts that were translationally repressed and their 5' UTR length or composition.

Acknowledgements

Firstly I would like to thank my supervisors Keith Spriggs and Stephanie Allen for all their help and advice throughout my project. I would also like to thank Anne Willis, Martin Bushell, Lia De Moor and Catherine Jopling for access to their superior knowledge of science. Thanks to the University of Sussex, Korner travelling fund for enabling me to travel to Berlin to collaborate with JPK and to Joost Van Mameren and Anna Wozniak of JPK for their help using their optical tweezer systems and Phil Williams for helping me with the analysis of the data. Thanks to Jonas Emsley and Paul McEwan for the cells and vectors required for the *Drosophila* expression system and advice.

Especial thanks to Keith who I feel has gone above and beyond the call of duty as a supervisor - I've loved working with you and 4A and I'm going to miss you both a lot. I would also like to thank him and his partner Hilary Collins for their help in the final, quite manic stage of handing this in. Thanks to everyone in the RNA biology group and LBSA past and present who have helped along the way, particularly Andrew Bottley for enthralling chats, Sasha Kondrashov for his endless knowledge and enthusiasm, Tiffany Hamilton and Kirsti Hill for advice and tissues, Helois Radford and Helen Booden for always being available for a pint, Laura Cobbold, Yi Wen Kong, Melissa Chen, Lucy Young and Helen King for providing ears aplenty and Andrew Lewis for always being available for duck walks.

Thanks to my Mum and Dad who have always encouraged me and have been a huge source of support throughout the last few years (and all of my life come to think of it!). Thanks to my 'inlaws' Pam and Ed Blenkinsopp for providing lots of encouragement in addition to vast quantities of wine, chocolates and flowers throughout the years. Thanks to Sophie Cunningham and Michelle Ramsay for only being a phonecall away.

Lastly, thanks to Aidan Blenkinsopp who has been a hero all along the way, I probably would not have started this without your encouragement and I definitely would not have finished it! You have been absolutely brilliant and I can't thank you enough.

Table of Contents

List of Figures

List of Abbreviations

15d-PGJ$_2$	15-deoxy-delta(12, 14)-prostaglandin J$_2$
4E-BP	eIF4E-binding proteins
A Site	Aminoacyl site
ADP	Adenosine diphosphate
ADP-BeF$_x$	ADP-beryllium fluoride
ADP-AlF$_x$	ADP-aluminium fluoride
ADPNP	Adenosine 5'-[8, y-imido] triphosphate
AFM	Atomic Force Microscopy
AML	Acute myeloid leukaemia
APAF1	Apoptotic protease activating factor 1
APS	Ammonium persulphate
ATF4	Activating transcription factor 4
ATP	Adenosine 5'- triphosphate
BSA	Bovine Serum Albumin
CamKII	Calmodulin-dependent protein kinase II
CDKA	Cyclin dependent kinase A
cDNA	Complementary deoxyribonucleic acid
CDS	Coding sequence
cIAP	Cellular inhibitor of apoptosis
CKs	Casein kinases
CPE	Cytoplasmic Polyadenylation Element
CPEB	Cytoplasmic Polyadenylation Element Binding Protein
CPSF	Cleavage and Polyadenylation Specificity Factor
COX	Cyclooxygenase
C-TD	C-terminal domain
dATP	Deoxyadenosine 5'-tripohosphate
dCTP	Deoxycytidine 5'-triphosphate
DAPF	Death associated protein 5
dGTP	Deoxyguanosine 5'-triphosphate
DMEM	Dulbecco's Modified Eagles Medium
DNA	Deoxyribonucleic acid
DNase	Deoxyribonuclease
dNTP	Deoxyribonucleotide 5'-triphosphate
dsRNA	Double stranded RNA
DTT	Dithiothreitol
dTTP	Deoxythymidine 5'-triphosphate
DPP	Decapentaplegic
E Site	Exit site
ECL	Enhanced Chemiluminescence
E. coli	*Escherichia coli*
EDTA	Ethylene Diamine Tetraacetic Acid
EDSF	Ectodermal dysplasia/skin fragility syndrome
eEF	Eukaryotic Elongation factor
eIF	Eukaryotic initiation factor EMCV
EPL	Expressed Protein Ligation
ER	Endoplasmic reticulum
ERK	Extracellular signal-related kinase
EtBr	Ethidium Bromide

FCS	Fetal calf serum
FHS	Fetal horse serum
FRET	Fluorescence resonance energy transfer
GADD34	Growth arrest and DNA-damage inducible protein 34
GAP	GTPase activating protein
GDI	GDP dissociation inhibitor
GEF	Guanine nucleotide exchange factor
GTP	Guanosine triphosphate
GSK	Glycogen synthase kinase
HCl	Hydrogen chloride
HCV	Hepatitis C virus
HBS	HEPES-buffered Saline
HeLa	Human cervical epithelial carcinoma cells
Hepes	N-2-Hydroxyethylpiperazine-N'-2-Ethanesulphonic Acid
HRI	Haem-regulated eIF2α kinase
HRP	Horseradish peroxidase
HSP	Heat shock protein
HSV	Herpes simplex virus
IFN-γ	Interferon-γ
IPTG	Isopropyl-β-d-Thiogalactopyranoside
IREs	Iron response elements
IRES	Internal ribosomal entry site
IRP	Iron response proteins
ITAF	Initiation factors and trans-acting factors
ISR	Integrated stress response
Kb	kilobase
kDa	Kilodalton
LB	Lysogeny Broth
LSU	Large ribosomal subunit
MAPK	Mitogen-activated protein kinase
MEK1/2	Map or ERK kinase 1 or 2
miRNA	MicroRNA
mRNA	Messenger ribonucleic acid
mRNP	Messenger Ribonucleoprotein
mTOR	Mammalian target of rapamycin
NEB	New England Biosciences
NMR	Nuclear magnetic resonance
NOM	Nucleolar MIF4G-containing protein 1
N-TD	N-terminal domain
NTP	Nucleoside triphosphate
ORF	Open reading frame
P Site	Peptidyl site
PABP	Poly-A Binding Protein
PAGE	Polyacrylamide gel electrophoresis
Paip	Poly(A)-binding protein (PABP)-interacting protein
PAK2	p21-activated protein kinases 2
PAP	Poly(A) polymerase
PB	Processing bodies
PBS	Phosphate buffered saline

PCR	Polymerase Chain Reaction
PDCD4	Programmed cell death 4
PKPs	Plakophilins
PP1	Protein phosphatase 1
PPARγ	Peroxisome proliferator-activated response-γ
RBM4	RNA binding motif 4
RF	Release factors
RISC	RNA-induced silencing complex
RNA	Ribonucleic acid
RNase	Ribonucleic acid hydrolase
RNPS	Ribo-nucleo proteins
RPs	Ribosomal proteins
RRL	Rabbit reticulocyte lysate
RRM	RNA Recognition Motif
rRNA	Ribosomal RNA
S2	*Drosophila* Schneider (S) 2 cells
S6 K	S6 kinase
SDS	Sodium Dodecyl Sulphate
SELEX	Systematic Evolution of Ligands by Exponential Enrichment
SFs	Superfamilies
SGs	Stress granules
SH-SY5Y	Human neuroblastoma cell line
SPR	Surface plasma resonance
siRNA	Silencing ribonucleic acid
SSC	Saline-sodium citrate buffer
ssRNA	Single stranded RNA
SSU	Small ribosomal subunit
TAE	Tris acetic acid EDTA buffer
Taq	Thermus aquaticus
TBE	Tris-borate EDTA buffer
TBS	Tris buffered saline
TBST	Tris Buffered Saline Tween
TE	Tris-EDTA
TEMED	Tetramethylethylenediamine
TGF-β	Transforming growth factor-β
TOPs	5' terminal oligopyrimidine tracts
tRNA	Transfer RNA
uORF	Upstream open reading frame
UTR	Untranslated Region
UV	Ultraviolet
Vhs	Virion host shutoff

1. Introduction

1.1 Helicases

DNA replication, the production of messenger RNA (mRNA) and the synthesis of proteins are all integral elements of cell maintenance, growth and division. The polynucleic acids at the centre of these processes are able to form stable secondary and tertiary structures that must be unwound to create a single-stranded template accessible to DNA/RNA modifying enzymes. The molecular motors capable of catalysing the separation of DNA or RNA duplexes are known as helicases. By utilising the conformational changes induced by nucleoside triphosphate (NTP) binding and/or hydrolysis, helicases are able to dissociate the strands of a nucleotide hybrid or dislocate bound proteins from the nucleic acid chain.

Initially helicases were identified and classified by sequence analysis of conserved motifs which resulted in their assignment into three large superfamilies (SFs) or 2 smaller families (Fs), termed SF1 - 3 and F4 - 5 (Gorbalenya *et al.*, 1988a; Hodgman, 1988; Gorbalenya *et al.*, 1989; Gorbalenya *et al.*, 1990) (for review see (Gorbalenya and Koonin, 1993). Amongst these motifs are the Walker A and B boxes (motifs I and II), which facilitate NTP binding and hydrolysis and are a feature of most NTPases (Walker *et al.*, 1982), and an "arginine finger" which aids coupling of NTP hydrolysis to conformational change (Rittinger *et al.*, 1997; Scheffzek *et al.*, 1997; Nadanaciva *et al.*, 1999). It later became apparent that the motifs used in these sequence analyses are actually common to a much larger subset of proteins called translocases, which couple NTP hydrolysis to nucleic acid translocation, and that helicases are a subset of this group of enzymes. A new method of categorising helicases using a number of biochemical properties has therefore been developed and consequentially helicases are now assigned to one of six superfamilies; firstly according to their sequence and structure (as with Gorbalenya's method) and then by a number of biological criteria (rate; directionality; processivity; step size and active/passive mechanism of action) (Singleton *et al.*, 2007). Structurally, the superfamilies fall into two categories:

those that form a ring structure, usually as hexamers, are members of SFs 3 - 6 and those that are not toroidal belong to SFs 1 and 2.

Members of SFs 1 and 2 share seven or eight conserved sequence motifs (Gorbalenya *et al.*, 1989) distributed in a 'helicase core' flanked by highly variable C- and N-terminal regions. Crystallographic analyses of proteins from these superfamilies show the helicase core folded to form two RecA-like domains, joined by a flexible linker of varying lengths. The conserved motifs responsible for NTP binding and hydrolysis and nucleic acid binding are positioned in the cleft between the two domains (Hall and Matson, 1999; Caruthers and McKay, 2002). Despite the high level of sequence similarity between the conserved domains, members of SFs 1 and 2 perform diverse roles within the cell at different levels of processivity. These differences can in part be attributed to variations in the N and C terminal domains, which determine nucleic acid affinity and allow the binding of other proteins and protein complexes that position and direct the activity of the helicase.

1.2 DEAD-box helicases

Using additional sequence, structural and mechanistic characteristics, helicases of SFs 1 and 2 can be further subdivided into smaller groups (Fairman-Williams *et al.*, 2010). The largest of these sub-groups is the DEAD-box subfamily of SF2, grouped according to previously identified motifs common to NTPases (Gorbalenya *et al.*, 1988a; Hodgman, 1988) and the sequence of the putative helicase eukaryotic initiation factor (eIF) 4A (Linder *et al.*, 1989). DEAD-box helicases are highly conserved between kingdoms and across species; *Saccharomyces cerevisiae* expresses 26 DEAD-box proteins (de la Cruz *et al.*, 1999), while 11 additional proteins are encoded in the human genome (Abdelhaleem *et al.*, 2003). The abundant number and expression of DEAD-box genes is perhaps indicative of the wide range of cellular activities that they are involved in, from mRNA transcription to decay, through mRNA splicing; translation; transport and modification (de la Cruz *et al.*, 1999; Abdelhaleem *et al.*, 2003; Abdelhaleem, 2005). DEAD-box proteins display a non-sequence

specific preference for RNA, discriminate for ATP and are bidirectional, a feature that distinguishes them from other members of SF2 and helicases in general.

1.2.1 Structure and conserved motifs

Like other members of SFs 1 and 2, the DEAD-box helicase core comprises two domains, which form RecA-like folds. Conserved motifs within these domains assume similar tertiary positions in the cleft formed between them (see figure 1.1). In the absence of nucleotide and ssRNA the domains do not interact and exist in a variety of open conformations, indicating the flexibility of the linker between the two domains. In the presence of ATP or ATP analogues and ssRNA, the helicase core adopts a closed, compact structure, as observed with limited proteolysis studies (Lorsch and Herschlag, 1998b; Henn *et al.*, 2002; Cheng *et al.*, 2005; Low *et al.*, 2007), single molecule FRET analysis (Theissen *et al.*, 2008), Expressed Protein Ligation (EPL) studies (Karow *et al.*, 2007) and comparisons of crystal structures (Caruthers *et al.*, 2000; Story *et al.*, 2001; Cheng *et al.*, 2005; Andersen *et al.*, 2006; Bono *et al.*, 2006; Sengoku *et al.*, 2006; Collins *et al.*, 2009; Nielsen *et al.*, 2009; von Moeller *et al.*, 2009). Structural analysis also revealed complex interactions between elements within the conserved motifs and the substrate (Bono *et al.*, 2006; Sengoku *et al.*, 2006).

DEAD-box proteins contain the eight conserved sequence motifs originally used to define their family, plus three additional motifs in a core region of 350 – 400 amino acids, as shown in figure 1.2 (Gorbalenya *et al.*, 1988b, 1989; Linder *et al.*, 1989; Tanner *et al.*, 2003). The N-terminal domain (N-TD) contains motifs Q, I, Ia, GG, Ib, II and III and the C-terminal domain (C-TD) contains IV, QxxR, V and IV. It is the conserved D-E-A-D (Asp-Glu-Ala-Asp) amino acid sequence, located in motif II that gives rise to the family's name. By using a combination of mutational analysis and biochemical testing, the ATP binding, ATP hydrolysis, ssRNA binding and helicase activities of the enzymes have been assigned to each sequence motif (summarised in Table 1) (Blum *et al.*, 1992; Pause and

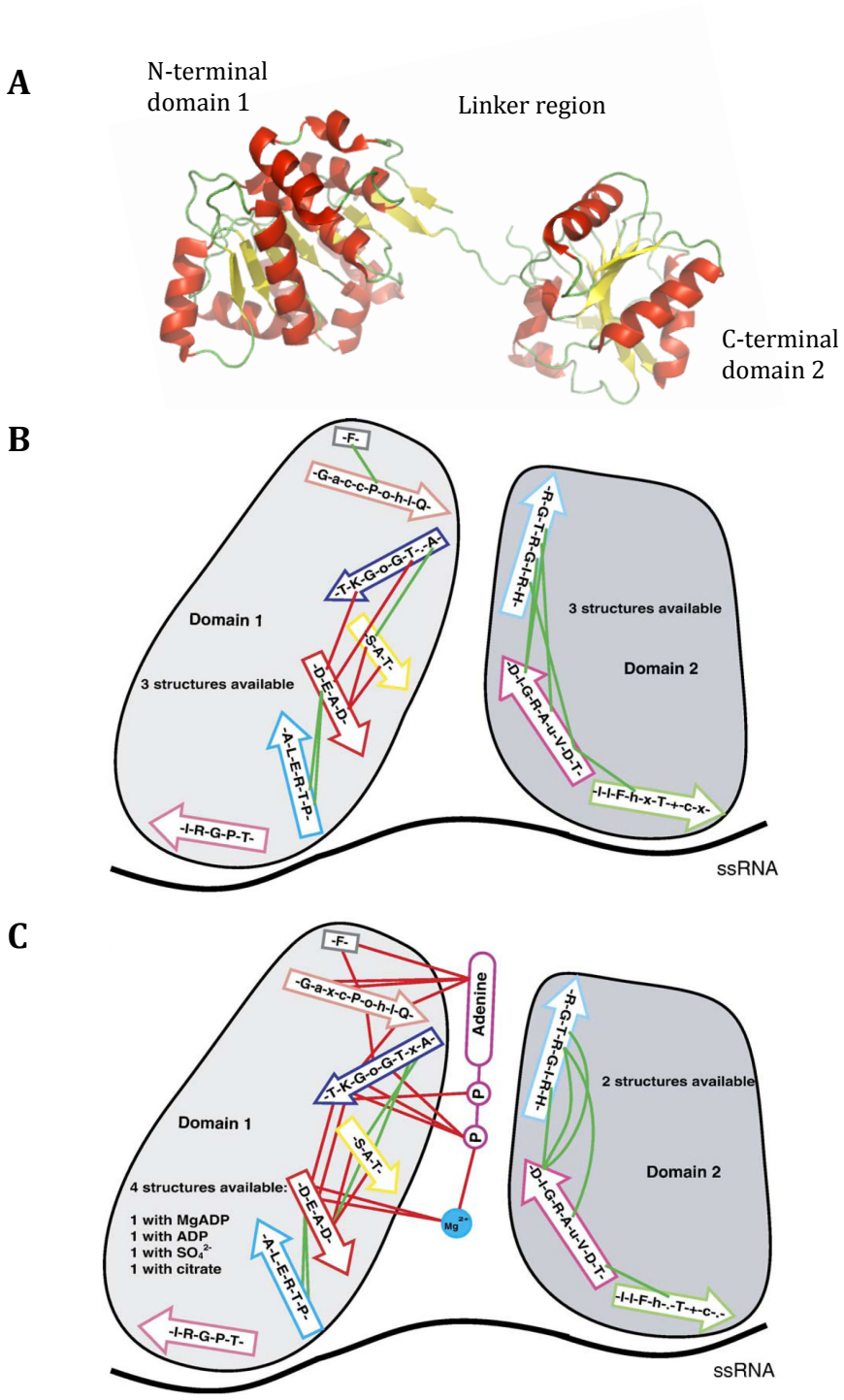

Figure 1.1. Tertiary structure and conserved motif organisation of the DEAD-box proteins. A. Ribbon drawing of yeast TIF1/eIF4AI (PDB ID code 1FUU). Two compact domains form RecA-like folds. The alpha helices are represented in red and the beta sheets in yellow. Image drawn using PyMOL Molecular Graphics System, Version 1.2r3pre, Schrödinger, LLC. **B. & C. Schematic diagram of the motif arrangement within the helicase cleft of the DEAD box proteins B.** in the absence of ATP. **C.** in the presence of ATP. Motifs are represented by coloured arrows using the colour scheme shown in figure 2. Motif interactions are indicated by red or green arrows to demonstrate observed and predicted interactions respectively (Diagram taken from Cordin *et al.*, 2006).

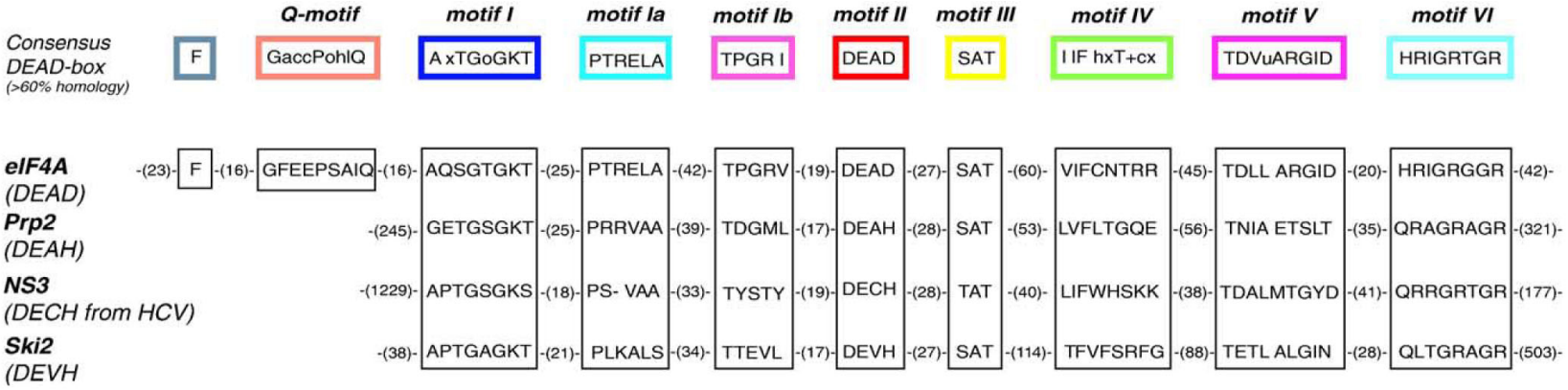

Figure 1.2- Conserved motifs of DEAD-box helicases and DEAD-box related helicases. (Taken from Cordin *et al.* 2006). Symbols used: o – S; T; I; L; V. x – any residue. a – F; W; Y. c – D; E; H; K; R. h – A; F; G; I; L; M; P; V; W; Y. + - H; K; R. u – A; G.

Table 1. Sequence and function of the conserved motifs in DEAD-box helicases

Name	Sequence	Summary	References
Q	$Fx_{16}G(F/Y)x_2PT(A/P)IQ$	Selects specifically for adenine base of ATP, required for ssRNA binding and conformational changes associated with ATP binding and hydrolysis.	(Tanner *et al.*, 2003; Cordin *et al.*, 2004)
I	AxTGSGKT	Walker A motif. Crucial for the ATPase activity of the helicase. Contains a P-loop, characteristic of ATP and GTP binding proteins, and a conserved lysine which contacts the β- and γ-phosphates directly and through Mg^{2+} and water.	(Saraste *et al.*, 1990; Pause and Sonenberg, 1992; Caruthers and McKay, 2002; Shi *et al.*, 2004; Andersen *et al.*, 2006; Bono *et al.*, 2006; Sengoku *et al.*, 2006; von Moeller *et al.*, 2009)
Ia	PTRELAxQ	Involved in RNA binding. Contacts QxxR motif when RNA is bound, may therefore contribute to the closed conformation of the helicase.	(Bono *et al.*, 2006; Sengoku *et al.*, 2006)
GG doublet	GG	Forms part of the RNA binding pocket.	(Bono *et al.*, 2006; Sengoku *et al.*, 2006; von Moeller *et al.*, 2009)
Ib	TPRG(V/L)	Involved in RNA binding.	(Bono *et al.*, 2006; Sengoku *et al.*, 2006)
II	DEAD	Walker B motif. Crucial for ATP binding and hydrolysis, contacts the β- and γ-phosphates directly and through Mg^{2+} and water.	(Pause and Sonenberg, 1992; Andersen *et al.*, 2006; Bono *et al.*, 2006; Sengoku *et al.*, 2006; von Moeller *et al.*, 2009)
III	SAT	Interdomain interaction with motifs II, VI. Mutation to Ser213 and Thr215 abolished helicase activity whilst maintaining RNA binding and ATPase activities.	(Pause and Sonenberg, 1992; Caruthers and McKay, 2002; Sengoku *et al.*, 2006)
IV	$(L/I)(V/I)Fx_2(T/S)$	Interacts with RNA. Required for the ATP-dependent cooperative binding of RNA.	(Bono *et al.*, 2006; Sengoku *et al.*, 2006; Banroques *et al.*, 2008)
QxxR	Qx_2Rx_6F	Involved in RNA binding. Contacts motifs Ia when RNA bound.	(Bono *et al.*, 2006; Sengoku *et al.*, 2006)
V	L(V/I)(A/C)TDVAARG(L/I)D	Interacts with ATP and RNA.	(Bono *et al.*, 2006; Sengoku *et al.*, 2006)
VI	YxHR(V/I)GRT(A/G)R(A/F)	Interacts with α, β and γ phosphates of ATP. Interdomain interaction with domain II.	(Pause *et al.*, 1993; Story *et al.*, 2001; Caruthers and McKay, 2002; Bono *et al.*, 2006; Sengoku *et al.*, 2006)

(Blum *et al.*, 1992; Pause and Sonenberg, 1992; Pause *et al.*, 1993; Cordin *et al.*, 2004; Banroques *et al.*, 2008). In brief, motifs Q, I and II with contributions from VI coordinate ATP binding and hydrolysis by the enzyme, motif III appears to be involved in coupling ATP hydrolysis to conformational changes of the domains and motifs Ia, GG, Ib, IV, QxxR, V and VI form a bipartite RNA binding site across the two domains.

The growing number of protein structures identified in the presence of ssRNA and ATP analogues has confirmed those findings described above and suggests a complex network of motif coordinated inter-domain contact (Caruthers *et al.*, 2000; Story *et al.*, 2001; Caruthers and McKay, 2002; Shi *et al.*, 2004; Cheng *et al.*, 2005; Andersen *et al.*, 2006; Bono *et al.*, 2006; Sengoku *et al.*, 2006; Collins *et al.*, 2009; Nielsen *et al.*, 2009; von Moeller *et al.*, 2009). In agreement with the crystal structure analyses, EPL studies of the *Bacillus subtilis* RNA helicase YxiN demonstrated that for nucleotide binding to occur, both helicase domains must be present (Karow *et al.*, 2007). Visualisation of the helicase core in the presence and absence of ATP or analogues of ATP and ssRNA has allowed in-depth analysis of the substrate specificity of DEAD-box proteins. A stable ssRNA binding site formed by residues on both the N- and C-TD of the helicase is only formed when the ATP binding site is occupied in the helicase cleft, bringing together the two domains to form a bipartite RNA binding site (Bono *et al.*, 2006; Sengoku *et al.*, 2006). This site is not correctly aligned in the absence of ATP which may explain the low affinity of the 'helicase core' for ssRNA (Rogers *et al.*, 1999; Karginov *et al.*, 2005; Grohman *et al.*, 2007; Mohr *et al.*, 2008). DEAD-box helicases show no preference for nucleic acid sequence and this was accounted for by the multiple contacts existing between the residues in the binding site and the ribose backbone of ssRNA, but none with the bases (Bono *et al.*, 2006; Cordin *et al.*, 2006; Sengoku *et al.*, 2006). In addition, residues in the helicase core contact the 2' hydroxyl (-OH) groups of the ribose backbone, favouring RNA over DNA (Peck and Herschlag, 1999; Rogers *et al.*, 2001a; Bono *et al.*, 2006; Sengoku *et al.*, 2006). To date, all crystal structures with bound nucleotide and ssRNA display a kink in the phosphate-ribose backbone caused by α-helix 7 of the helicase sterically hindering the stacking arrangement of the

nucleotides (Story *et al.*, 2001; Shi *et al.*, 2004; Cheng *et al.*, 2005; Bono *et al.*, 2006; Sengoku *et al.*, 2006). It has been suggested that this unusual feature of DEAD-box helicases contributes to atypical unwinding as it prevents the A-form conformation of RNA (Sengoku *et al.*, 2006).

1.2.2 Mechanism

Processive helicases are able to unwind long stretches of DNA/RNA duplex by repeatedly facilitating the hydrolysis of NTPs whilst translocating along the nucleic acid chain. DNA helicases are vital components of the replication, recombination and repair machinery of cells and are very processive, unwinding duplexes that are kilobases in length (Bjornson *et al.*, 1996; Patel and Picha, 2000). By contrast, most RNA helicases have comparatively poor helicase activity. Biochemical studies show that members of the DEAD-box helicase family, although functionally active, may only unwind short duplexes before chain release occurs and are therefore termed non-processive (Linder, 2006, and references therein). Accordingly, the functions that they are involved in; local RNA structure remodeling; the disruption of RNA/protein complexes and RNA annealing require helicase activity only over a short stretch of RNA. The comparative difference in activity signifies that DEAD-box helicases employ an alternative mechanism of action.

It is thought that ATP-hydrolysis after RNA binding triggers conformational changes that facilitate helicase translocation and disrupt RNA duplexes. It is unclear, however, how these conformational changes are able to disrupt RNA duplexes or at which stage in the nucleotide-hydrolysis cycle this structural rearrangement occurs. The binding affinity of DEAD-box proteins was first investigated using pulse-chase experiments testing eIF4A (Lorsch and Herschlag, 1998a), and more recently by single molecule FRET analysis using fluorescently labeled ATP and ADP to research DbpA and YxiN respectively (Talavera and De La Cruz, 2005; Karow *et al.*, 2007). The results of these studies suggest that DEAD-box proteins are able to bind ADP with a higher affinity than ATP. This may account for the product inhibition of ATPase activity

observed for eIF4A (Lorsch and Herschlag, 1998a). The affinity of DEAD-box proteins for ssRNA was higher in the presence of ATP and drastically reduced in the presence of ADP, which demonstrates a coupling between nucleotide state and RNA binding (Lorsch and Herschlag, 1998a; Iost *et al.*, 1999; Cordin *et al.*, 2004). The γ-phosphoryl group, proposed to act as a switch to initiate domain rearrangement as observed in many NTPases, may drive helicase activity (Smith and Rayment, 1996; Vale, 1996). This may in-part explain how ATP binding and hydrolysis can bring about ssRNA binding and release and why DEAD-box helicases are non-processive; the rapid dissociation of substrates after ATP hydrolysis would release the protein and allow it to diffuse away from the RNA molecule before rebinding ATP for a subsequent round of activity. In this model, the processivity of the enzyme is directly linked to its ability to remain associated with the RNA after ATP-hydrolysis or unwinding. As it has been demonstrated that the core region of the DEAD-box helicase binds RNA with very low or negative affinity when no nucleotide or ADP is present in the helicase cleft, then this is probably coordinated by additional sequences in its C- or N-TD or by additional binding proteins (Lorsch and Herschlag, 1998a; Henn *et al.*, 2008; Nielsen *et al.*, 2009).

Studies analysing the nucleotide-cycle of DbpA have shown that the nucleotide transition state ADP-P_i has the highest affinity for RNA, and that a release of the inorganic phosphate induces a conformation change which is unfavourable for RNA binding (Henn *et al.*, 2008). The use of ATP analogues, which mimic the various transition states throughout nucleotide hydrolysis, allow RNA binding and helicase activity to be analysed at each step of the NTP cycle. Interestingly, it has been shown that non-hydrolysable ADP-beryllium fluoride (ADP-BeF_x), which represents groundstate ATP, allows duplex unwinding to occur, but ADP-aluminium fluoride (ADP-AlF_x), which represents a transition state after ATP hydrolysis, or ADPNP does not (Liu *et al.*, 2008). This signifies that RNA strand separation can occur in the absence of ATP hydrolysis. Separation, however, cannot occur in the absence of ATP (or a groundstate analogue) and ATP hydrolysis is required for the release of the enzyme and multiple rounds of activity (Liu *et al.*, 2008). Furthermore, helicases that disrupted short helices,

which only required one round of unwinding to separate them, on average hydrolysed fewer than one ATP molecule (Chen *et al.*, 2008). In addition to this, ATP bound to the helicase core was only hydrolysed in half of the unwinding events observed (Chen *et al.*, 2008). These data suggest that ATP hydrolysis does not induce the conformational changes responsible for helicase activity, but that ATP binding is necessary for the helicase to assume an active state, capable of duplex unwinding and ATP hydrolysis. Consistent with this, the separation of longer duplexes, involving repeated rounds of helicase binding, unwinding and release, require higher concentrations of ATP (Rogers *et al.*, 1999; Chen *et al.*, 2008).

DEAD-box helicases appear to have a unique mechanism of unwinding RNA secondary structure that is not shared by even their closest relatives, the DExH-box family of helicases. The DExH-box protein NPH-II is unable to unwind duplexes in the presence of ADP-BeF_x (Liu *et al.*, 2008), and, as mentioned above, the resolved crystal structures of other SF2 members display different α7 helix positioning which would not distort the A-form geometry of their nucleic acid substrate. Current structural and biochemical analysis of DEAD-box helicases, as summarised above, has led to the proposal of a model where ATP binding in the helicase cleft allows closure of the cleft and stabilises RNA binding. This closed conformation induces a kink in the RNA, which occurs without ATP hydrolysis and disrupts local base pairing. The closed conformation and formation of the kink is also formed in the presence of the transition state analogues ADPNP and ADP-AlF_x, however, this isn't enough to cause RNA unwinding. It would therefore seem that a hydrolysis-competent state, only formed in the presence of ATP or its groundstate analogues, is necessary to produce helicase activity. This helicase activity would precede or occur with ATP hydrolysis, which would release bound ssRNA and regenerate the enzyme, enabling further cycles of helicase activity to occur. This theory would tightly couple unwinding activity to ATP hydrolysis, though the latter may follow, or be caused by the former (Liu *et al.*, 2008; Hilbert *et al.*, 2009).

1.2.3 N and C terminal extensions

Unlike the helicase core, the sequence and size of the flexible linker and C- / N-TDs vary considerably among helicases. The possession of additional domains may provide DEAD-box proteins with extra mRNA binding motifs and/or protein docking sites and may even encode for alternative activities. Therefore it may be these domains which dictate the efficiency and location of the helicase (Yang and Jankowsky, 2005; Halls *et al.*, 2007; for review see Hilbert *et al.*, 2009). Sterically, the additional domains may also stabilise RNA binding of the helicase core by closing the RNA binding domain (Fairman-Williams *et al.*, 2010).

The smallest DEAD-box protein possessing helicase activity is eIF4A, which, as it does not contain either C or N terminal extensions, is effectively representative of the DEAD-box 'helicase core'. The RNA binding ability and helicase activity of eIF4A is lower than that of the other members of this family and truncations of other DEAD-box proteins that remove the C and N terminal domains reduce RNA binding activity to that of eIF4A (Karginov *et al.*, 2005; Grohman *et al.*, 2007; Mohr *et al.*, 2008). Substitution of the flexible linker of eIF4A with that of the *Drosophila* helicase Vasa enhanced the ATPase activity of the protein indicating that this region may also have a role in enzyme regulation (Low *et al.*, 2007).

Due to the ineffectiveness of the helicase core to bind ssRNA it is thought, and has been demonstrated, that many DEAD-box proteins act in concert with other proteins, which has the effect of increasing their activity. These additional proteins can also direct the activity of the helicase to particular regions of the cell, or to particular RNAs. Due to a lack of C and N termini it is unsurprising that eIF4A is one such example, displaying a minimal helicase activity as a monomer that is greatly increased upon the addition of cofactors. Representative of the minimal 'helicase core', eIF4A has been exploited as an example DEAD-box helicase to explore the mechanism and functions of this family. However, in its own right eIF4A is an important enzyme involved in the regulation of translation initiation and is the focus of the following study.

1.3 eIF4A - the prototypical DEAD-box helicase is involved in translation

eIF4A is considered the prototypical DEAD-box helicase, due to its lack of C- and N-TDs in addition to the well documented role of this protein in translation initiation. The process of translation follows three phases - initiation, elongation and termination and it is during the initiation phase that the main regulatory mechanisms occur. Control of new protein synthesis is affected by mRNA primary, secondary and tertiary structures and a plethora of initiation factors, many of which are phosphorylated or cleaved in response to external and internal signals. As with the majority of initiation factors, eIF4A was first isolated and then characterised from the salt washes created during the purification of intact 40S ribosomal subunits from rabbit reticulocyte lysates and mouse Krebs ascites cells (Sundkvist and Staehelin, 1975; Safer *et al.*, 1976; Benne *et al.*, 1977). eIF4A is highly conserved in bacteria, archaea and eukaryotes and has been identified as the most abundant of translation initiation factors, expressed at levels higher than ribosomes in yeast and mammals (Duncan and Hershey, 1983; Conroy *et al.*, 1990; von der Haar and McCarthy, 2002).

Yeast *S. cerevisiae* expresses two isoforms of eIF4A, TIF1 and TIF2, that are identical in amino acid sequence but have variable non-coding regions (Linder and Slonimski, 1989). Knocking out either TIF1 or TIF2 in yeast has little or no effect on the cellular phenotype, but knocking out both proteins is proved lethal (Linder and Slonimski, 1989). Higher eukaryotes express three isoforms of eIF4A; I, II and III. As in yeast, eIF4AI and II have very similar amino acid sequences, sharing 91 % homology in murine cells (Nielsen and Trachsel, 1988) and 89 % in humans (see figure 1.3). They are both located within the cytoplasm but display differential expression patterns which are both tissue (Nielsen and Trachsel, 1988) and cell cycle specific (Williams-Hill *et al.*, 1997). This may be due to differences in mRNA expression and stability caused by variations in the promoter sequences and 5' and 3' untranslated regions (UTRs) of the mRNAs (Nielsen *et al.*, 1985; Nielsen and Trachsel, 1988; Williams-Hill *et al.*, 1997). The conserved motifs of eIF4AIII are very similar to eIF4AI and II but

less overall homology to eIF4AI is observed (65 % amino acid sequence match) (see figure 1.3) (Li *et al.*, 1999).

In 1980 Kozak identified that during protein synthesis 40S ribosomal scanning required ATP (Kozak, 1980b) and it was later discovered that the protein consuming ATP was eIF4A (Seal *et al.*, 1983). Depletion of TIF1 from a cell-free *S. cerevisiae* translational system caused translational repression which was restored upon replacement of TIF1 (Blum *et al.*, 1989). A mutant variant of TIF1, A667V, affecting the alanine residue in motif I (Walker A), prevents the ATPase and helicase activity of the protein and inhibits the translation of the majority of mRNAs in the cell (Blum *et al.*, 1992). In addition, dominant negative mutants of eIF4A inhibit translation (Pause *et al.*, 1994) signifying that eIF4A plays a crucial role in translation initiation, which will be described in detail below.

1.4 Translation

Proteins form an integral part of cellular biology, contributing structurally and catalytically to most cellular activities. Translation is the process of protein synthesis which has three distinct stages: (i) initiation, in which protein factors aid in the recruitment of the ribosome to the mRNA; (ii) elongation, in which the ribosome migrates along the mRNA, translating the coding nucleic acid sequence into a peptide chain; and (iii) termination, in which a termination signal triggers the release of the polypeptide chain and the ribosome from the mRNA and the latter is recycled for a further round of protein synthesis. In addition to the energy required to actually synthesise the peptide chain itself, a significant amount of the cell's resources is devoted to generating proteins and ribonucleoproteins (RNPs) that coordinate translation. Due to this expenditure it is unsurprising that the process of protein synthesis is tightly regulated, and can be altered quickly in response to a vast array of cellular environments and stresses. Such regulatory mechanisms either affect the mRNA directly or act upon the interacting factors that facilitate message translation. This control typically occurs at the point of translation initiation.

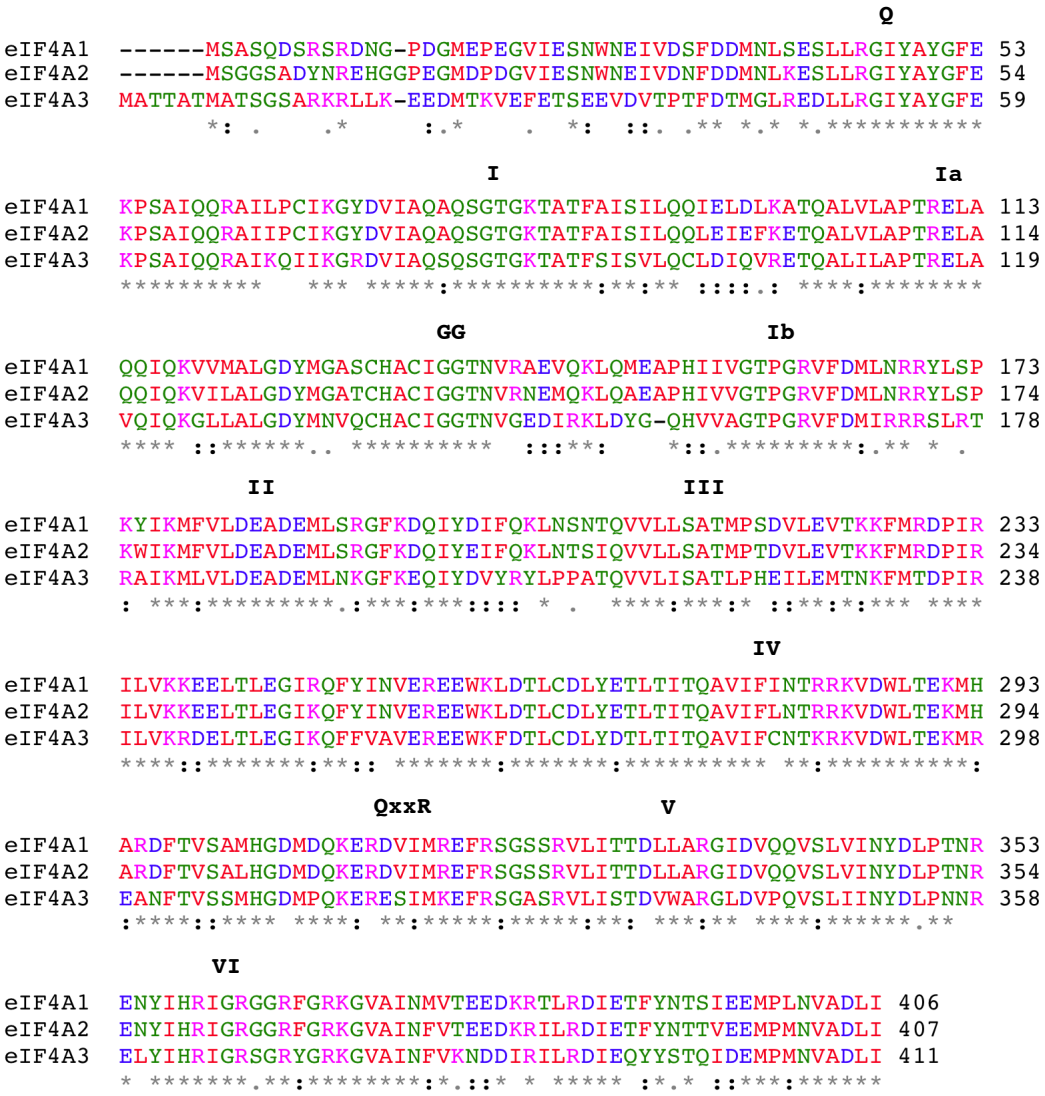

Figure 1.3 - Sequence alignment of the three human eIF4A homologues, highlighting the conserved DEAD-box sequence motifs.
Alignment was performed using ClustalW, EMBL-EBI software (Chenna *et. al*, 2003).
Amino acid key: RED – Small (small + hydrophobic (including aromatic Y)); BLUE – Acidic; MAGENTA – Basic; GREEN – Hydroxyl + Amine + Basic + Q.
Alignment key: * - common residue; : – conserved substitution according to amino acid properties; . – semi-conserved substitution.

Under nutrient rich conditions the cell is committed to a higher level of protein synthesis, while conversely, under conditions of nutrient deprivation or cellular stress, such as viral infection, hypoxia, heatshock and DNA damage, the cell will employ rapid mechanisms to down-regulate global translation to coordinate energy resources towards directing a response towards these environments. The expression of some genes, however, is still required in order to maintain cellular homeostasis or facilitate the rescue, or alternatively the death of the cell. mRNAs may possess features within their primary or secondary structure that provide a target for translational control; this will be discussed in 'Alternative mechanisms of translation initiation' (section 1.9).

1.5 Signaling pathways to translation

A cellular response to adverse conditions may be mediated by a number of signaling cascades that culminate in the targeted downregulation, modification, cleavage, sequestration or degradation of components of the initiation complex, termed initiation factors (Deribe *et al.*, 2010). Alterations that occur to specific factors and the effect these have on function will be introduced throughout this chapter, however an outline of the pathways involved is briefly described below.

The phosphorylation status of each initiation factor is an important mechanism by which translation may be controlled. The two main signaling pathways implicated in this process are the mTOR/PI3K/Akt pathway and the mitogen activated protein kinase (MAPK) pathways. The mammalian target of rapamycin (mTOR) cascade is largely responsible for the growth 'decisions' taken by the cell. This pathway is responsive to growth factors, hormonal stimuli and nutrient availability and, in adequate conditions, promotes protein synthesis (White and Sharrocks, 2010). mTOR binds the protein GβL and forms two complexes, MTORC1, with Raptor (regulatory associated protein of mTOR), and MTORC2, with Rictor (rapamycin insensitive companion of mTOR). These complexes directly phosphorylate the 70 kDa ribosomal protein S6 kinase (S6K) and the serine/threonine kinase Akt respectively. MTORC1 and S6K may

directly phosphorylate initiation factors or other binding proteins, increasing protein synthesis whereas Akt promotes MTORC1 activity.

Though several MAPK signaling cascades exist in metazoans, two in particular influence translation initiation; the 'classic' cascade consisting of Raf, Map or ERK kinase 1 or 2 (MEK1/2) and extracellular signal-related kinase (ERK) which signals in response to mitogens or growth factors and activates the mitogen-activated protein kinases, Mnk1 and Mnk2 and the 90 kDa S6 kinase family, Rsks 1 - 4, and a cascade that culminates in p38 kinase which also activates Mnk1 in addition to mitogen-and-stress activated protein kinase, Msk1 (Waskiewicz *et al.*, 1997).

Apoptosis, or programmed cell death, is a cascade of events that occurs in response to a variety of intracellular or extracellular signals that ultimately lead to the death of the cell. The onset of apoptosis or severe cellular stress rapidly inhibits global translation (Deckwerth and Johnson, 1993; Morley *et al.*, 1998; Zhou *et al.*, 1998; Scott and Adebodun, 1999) by altering the phosphorylation state or causing the cleavage of some initiation factors and thereby affecting their ability to form complexes (for review see (Clemens *et al.*, 2000). The signaling cascades involve the Bcl-2 family of proteins that can be pro- or anti-apoptotic, the Apoptotic protease activating factor 1 (Apaf1) and a family of cysteine proteases, called caspases, of which the activation of caspase 3 results in the cleavage of downstream targets, such as the initiation factors, or their kinases (Fischer *et al.*, 2003). Some cleavage events render proteins involved in translation ineffective, however others alter their function and direct them to an alternative mode of translation initiation; this will be discussed in further detail below.

1.6 The mechanism of eukaryotic translation

Prokaryotic and eukaryotic mechanisms of translation initiation vary greatly in their levels of complexity, however their general consensus is the same, involving the positioning of a complete ribosome correctly on an mRNA and facilitating its translation.

1.7 The ribosome in translation

The ribosome is a large complex comprised of ribosomal (r) RNAs and proteins (RPs) arranged in a small (SSU) and large (LSU) subunit (30S and 50S in bacteria, 40S and 60S in eukaryotes respectively). The main function of the ribosome is to migrate along an mRNA translating nucleic acid sequence into a peptide chain for which it catalyses the peptide bond formation. A large commitment of the cell is to its ribosomal content, which in growing yeast is estimated to occupy between 30 - 40 % of its cytoplasmic volume (Warner, 1999). A growing yeast cell produces approximately 2000 ribosomes per minute which requires ~ 60 % of the cells transcriptional energy to produce rRNAs (Warner, 1999). This estimate is in addition to the energy required for transcription, splicing and translation of the mRNAs encoding the RPs (Warner, 1999). Ribosome biogenesis is highly regulated in response to nutrient availability and a number of external and internal stimuli. The mammalian target of rapamycin (mTOR) signaling pathway in part coordinates this control and also regulates a number of other translation factors (Beretta *et al.*, 1996; Powers and Walter, 1999; Gingras *et al.*, 2001). This is one of many regulatory mechanisms that affect translation by targeting the production, modification or degradation of initiation and elongation factors, or other components of the translational machinery, however, a major contributor to the regulation of a gene's expression is also the primary and secondary structure of the mRNA encoding it.

Pre-mRNAs are processed cotranscriptionally to add a methylated GTP (m^7GpppN) cap to the 5' end of the mRNA, remove the non-coding introns by splicing and add a poly-adenylated (polyA) tail to the 3' end (Shatkin, 1976; Bentley, 2005). The mature mRNAs consists of a coding region comprised of triplet units termed codons (Crick *et al.*, 1961), which encode amino acids, flanked by untranslated regions (UTRs) that contribute to the regulation of each message's translation. The degeneracy of the genetic code means that an amino acid can be encoded by more than one codon, however, each codon only encodes one amino acid. Codons are decoded by the anticodon site of a transfer RNA (tRNA) that is charged with the corresponding amino acid at its 3' end.

tRNAs are small RNA molecules with a 'clover-leaf'-like secondary structure that is folded into an 'L' shaped tertiary structure with the anticodon loop and the amino acid group located at the end of each arm (Kim *et al.*, 1973; Robertus *et al.*, 1974b, a). The attachment of an amino acid to a tRNA is catalysed by an amino acid-specific aminoacyl-tRNA synthetase, which recognises the 3' acceptor stem and anticodon sequences of the tRNA. Codon/anticodon pairs were assigned by radiolabelling individual tRNAs and incubating them with different RNA triplets and isolated ribosomes, which would form a complex if the codon was recognised by the tRNA (Nirenberg and Leder, 1964). In addition to binding the exact complement of their anticodon, some tRNAs are isoaccepting and are able to pair with codons that contain one non-matching or 'wobble' base, but still encode the same amino acid.

During translation the complete ribosome (70S in bacteria, 80S in eukaryotes) migrates along the coding region of an mRNA and tRNAs are moved through three binding sites at the interface of the small and large subunits: the A (aminoacyl) site; the P (peptidyl) site and the E (exit) site (see figure 1.4). Complementary aminoacylated tRNAs are delivered to the A site of the ribosome by elongation factor (eEF) 1A and are positioned so that each anticodon associates with the mRNA chain. Here the peptidyltranferase activity of the ribosome transfers the polypeptide chain attached to the tRNA in the P site to the amino acid of the tRNA in the A-site and then translocates along the mRNA to the next codon. This translocation moves the tRNA in the A-site, now attached to the peptide chain, into the P-site, the tRNA in the P-site into the E site and the tRNA in the E-site is released. The A site is now unoccupied allowing the next charged complementary tRNA to join the system. The elongation process is repeated until one of three stop codons (UAG, UAA, UGA) is reached, triggering the termination of translation. Termination codons are not recognised by tRNAs, but by class one release factors (RFs 1 and 2 in bacteria, eRF1 in eukaryotes) which prompt the hydrolysis of the ester bond attaching the peptide chain to the tRNA occupying the P-site, and the release of the protein from the ribosome (Scolnick *et al.*, 1968; Capecchi and Klein, 1970; Caskey *et al.*, 1970). In bacteria a class 2 GTPase release factor, RF3, removes

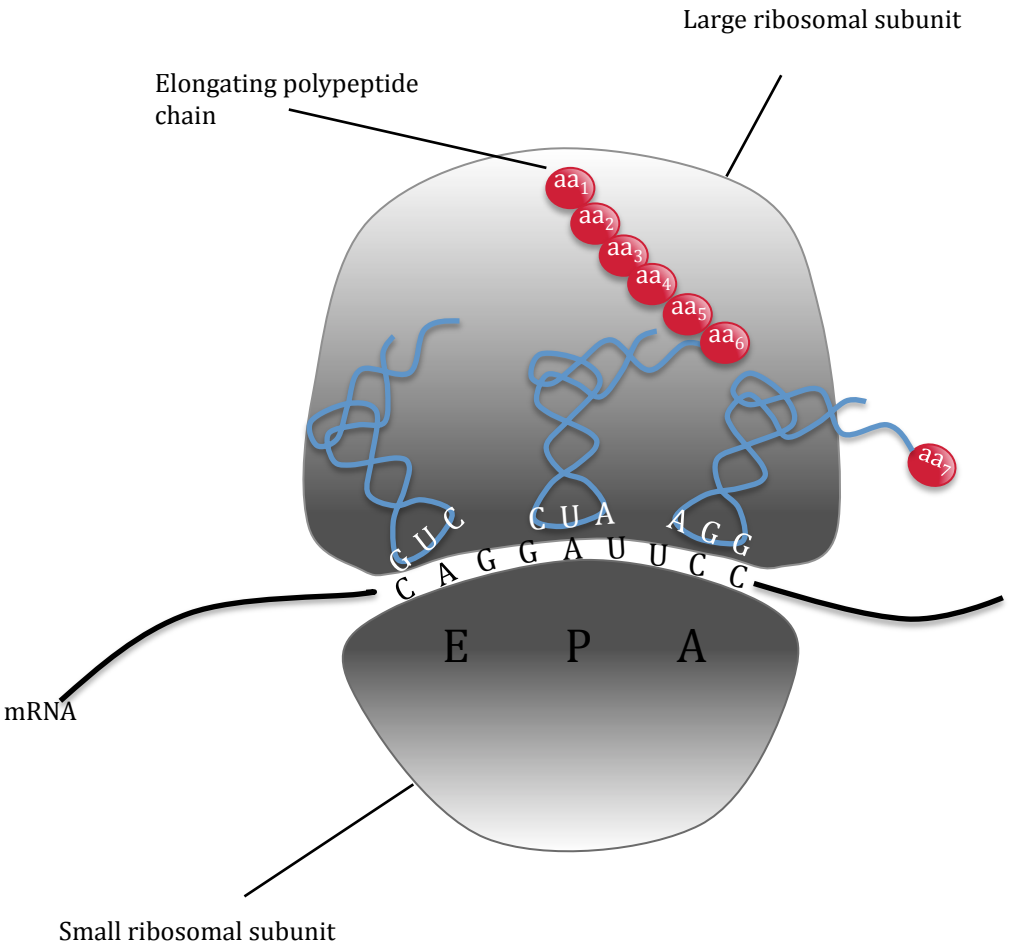

Figure 1.4 – tRNA progression through the complete 80S ribosome. Schematic diagram demonstrating the progression of the tRNA (blue) through the ribosome during translational elongation. A, P and E (in black) depict the aminoacyl, peptidyl and exit site respectively. Red circles depict amino acids (aa).

the class 1 RF from the A-site by hydrolysing its bound GTP after the tRNA in the P-site is deacylated and the ribosome has started to translocate (Freistroffer *et al.*, 1997; Zavialov *et al.*, 2001; Zavialov *et al.*, 2002). The 70S ribosome is then recycled by the ribosomal release factor (RRF), IF3 and EFG in a GTP-dependent manner (Janosi *et al.*, 1996; Karimi *et al.*, 1999; Inokuchi *et al.*, 2000; Agrawal *et al.*, 2004). The mechanism of translation termination is less well characterised in eukaryotes but appears to be distinct from that of prokaryotes (Mitkevich *et al.*, 2006). eRF1 promotes and stabilises the GTP binding of the RF3 homologue, eRF3 (Mitkevich *et al.*, 2006) and in turn eRF3's GTPase activity greatly stimulates eRF1 dependent hydrolysis of the amino-tRNA bond (Zhouravleva *et al.*, 1995). Ribosome recycling in eukaryotes also varies from the mechanism employed by prokaryotes and will be addressed later in this introduction.

1.8 The mechanism of translation initiation

Although translation initiation differs between prokaryotes and eukaryotes, each culminates with a functioning ribosome positioned at the beginning of the coding region of an mRNA. The process by which the ribosome identifies its starting place has been thoroughly investigated. One of the first breakthroughs arose from the discovery that a formylated version of the amino acid methionine is incorporated into bacterial proteins at their amino (N) terminus, but not internally within the peptide sequence (Marcker and Sanger, 1964; Marcker, 1965). This finding led to the discovery that two methionine tRNAs ($tRNA^{Met}$) exist; initiator tRNA ($tRNA_i^{Met}$) is required to initiate protein synthesis and $tRNA^{Met}$ is required during translation elongation (Clark and Marcker, 1966). In bacteria, after aminoacylation, the sequence of the acceptor stem of the initiator tRNA promotes formylation of the amino group of methionine by met-tRNA transformylase producing *N*-formylmethionine- or *f*Met-$tRNA_i^{fMet}$ (Lee *et al.*, 1991; Lee *et al.*, 1992). The formyl group prevents peptide chain extension in the amino direction and is important for tRNA recognition by the initiation factors and the 70S ribosome (Petersen *et al.*, 1976). In eukaryotes, unmodified methionine is incorporated at the start of the peptide chain, but the sequence of $tRNA_i^{Met}$ is important for its incorporation into the pre-initiation

complex and can't be replaced by $tRNA^{Met}$ (Von Pawel-Rammingen *et al.*, 1992). Analysis of the codons that $tRNA_i$ is able to bind to indicated that translation would primarily initiate from an AUG codon and less efficiently from a GUG or UUG codon (Nirenberg *et al.*, 1965; Sundararajan and Thach, 1966). In both bacteria and eukaryotes, the initiator tRNA is positioned in the P-site of the ribosome by initiation factors which also promote its association with the start codon of an mRNA.

In order to distinguish the correct start codon from out-of-sequence and non-initiating methionine codons, the initiation codon of both bacterial and eukaryotic mRNAs is contained within a consensus sequence that directs the initiation of translation, albeit in very different ways. In bacteria this is a 6 base sequence (AGGAGG), called the Shine-Dalgarno (SD) sequence, which is located 4 - 10 nucleotides upstream of the initiation codon (Shine and Dalgarno, 1975). The 16S rRNA in the 30S SSU contains an anti-SD sequence that, when bound to the SD sequence of an mRNA, positions the start codon in, or in close proximity to, the ribosomal P-site (Shine and Dalgarno, 1974; Steitz and Jakes, 1975). The 30S SSU is part of a pre-initiation complex with IF1, IF2-GTP and IF3 that, after 16S rRNA binding to the SD sequence, promotes the arrangement of *f*Met-$tRNA_i^{fMet}$ in the P-site to facilitate its association with the start codon (La Teana *et al.*, 1995). IF1 and IF3 are then released from the complex and the 50S LSU binds to the SSU, aided by IF2, which then arranges the *f*Met-$tRNA_i^{fMet}$ into a position favourable for translational elongation. This in turn stimulates IF2 to hydrolyse its bound GTP which releases it from the initiation complex, leaving a complete 70S ribosome primed with *f*Met-$tRNA_i^{fMet}$ in its P-site, ready for translational elongation (reviewed by (Laursen *et al.*, 2005)).

Rather than assemble the translational machinery at the start codon, the majority of eukaryotic mRNAs are predicted to be translated by a mechanism where the 40S SSU and a host of initiation factors are first recruited to the 5' proximal cap and then 'scan' the 5' UTR until they reach a start codon in the correct context (Kozak, 1978, 1980a). Translation initiation is thought to proceed from the first AUG encountered, which was demonstrated by the

introduction of an AUG codon upstream of an existing start codon. This AUG insert was able to supplant the original AUG as a translational start site (Kozak, 1983; Iacono *et al.*, 2005).

Sequence analysis of eukaryotic mRNAs have identified a common motif surrounding the initiation codon, GCC**R**CCAUG**G**, where R is a purine (Kozak, 1981; Pesole *et al.*, 2000; Iacono *et al.*, 2005). Mutational analysis of these residues suggests that the purine in position -3 (If A of start codon is +1) and the G in position +4 aid ribosomal recognition of the start codon (Kozak, 1986b), though there is no evidence of a direct interaction with the 40S SSU. It has been suggested that the +4 position may also be highly conserved as it encodes the first residue of the penultimate amino acid. The terminal methionine is removed from the polypeptide chain shortly after it emerges from the ribosome by methionine aminopeptidase and the size of the penultimate amino acid is thought to influence this activity (Moerschell *et al.*, 1990). Analysis of vertebrate protein sequences identified alanine as the favoured penultimate amino acid (Xia, 2007; Sanchez, 2008). Interestingly this residue is primarily encoded by the alanine codon GCG that is generally underrepresented in proteins (Sanchez, 2008).

1.9 Cap-dependent translation initiation

As mentioned above the scanning mechanism, also referred to as cap-dependent translation initiation, is employed by the majority of mRNAs in order to facilitate their translation. Cap-dependent translation initiation involves the formation of a number of intermediary complexes that collectively assist in the recruitment of a small ribosomal subunit to the 5' cap of an mRNA, the scanning of this subunit to the translational start codon and the subsequent formation of the complete 80S ribosome capable of translational elongation. This complicated process is illustrated in figure 1.5 and described in detail below.

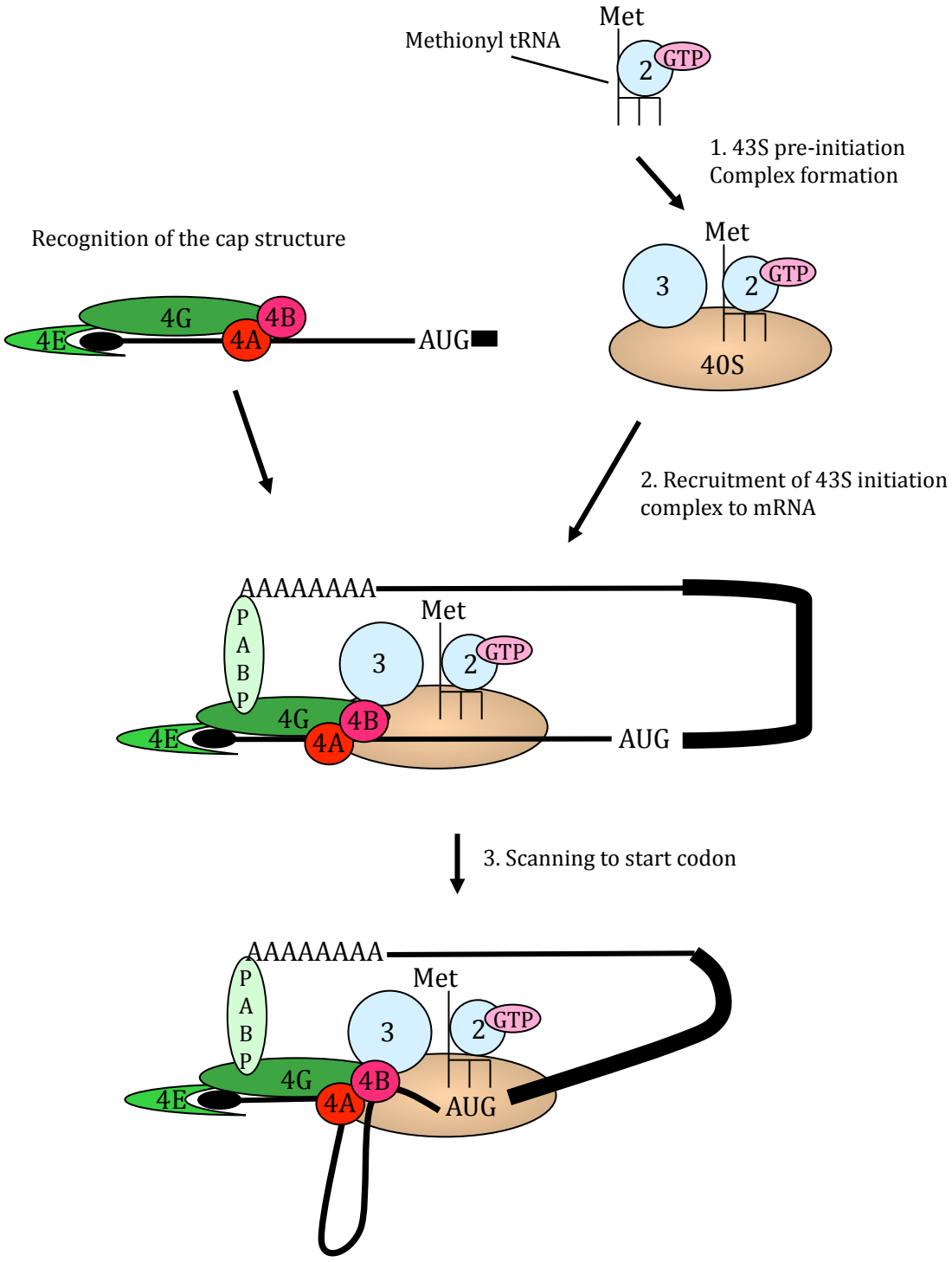

Figure 1.5. Cap dependent translation initiation
Schematic diagram showing the process of cap dependent translation initiation. Step 1. the 43S initiation complex is formed and the mRNA cap structure is recognized by eIF4F proteins. Step 2. The 43S initiation complex is recruited to the mRNA and the closed loop complex is formed. Step 3. 43S scans to the start codon and translation occurs. The abbreviation 'eIF' is omitted from each factor.

1.10 Ribosomal subunit dissociation

The first step in translation initiation is to separate the 40S SSU from the 60S SSU. Ribosomes cycle between their actively translating form bound to translation factors and mRNA and a stable non-active free form existing in ribosomal pools within the cytoplasm of the cell according to the growth state of the cell (Kaempfer, 1969; Kay *et al.*, 1971; Cooper *et al.*, 1976). The stable associations between the 40S and 60S subunits mean that the complete 80S ribosomes present in the ribosomal pools have to be actively separated in order to for them to resume translation initiation (Kaempfer, 1970). Alternatively, the 40S and 60S ribosomal subunits, released from an mRNA after the termination of translation, need to be prevented from re-associating with each other and joining the free ribosome pool. The initiation factors implicated in the release of post-termination ribosomal subunits from the mRNA are eIF3, eIF1 and eIF1A. eIF3 is a large multimeric initiation factor containing up to 13 subunits (eIF3a-m) and has a mass of ~ 800 kD (Damoc *et al.*, 2007). Cryo-EM modeling of eIF3 bound to the 40S ribosomal subunit demonstrated that binding occurs at the solvent face of the 40S subunit but that an 'arm' may disrupt contacts between the 40S and 60S subunits (Siridechadilok *et al.*, 2005). eIF1 is the smallest initiation factor at 12 kDa, and binds the 40S subunit preventing some contacts of the 60S subunit with the interdomain bridges and eIF3c (Lomakin *et al.*, 2003). eIF1A is a 22 kDa protein homologous to the prokaryotic IF1 which blocks the ribosomal A-site and causes the movement of the domains of the small ribosomal subunit (Battiste *et al.*, 2000; Carter *et al.*, 2001). Though capable of releasing and separating the ribosomal subunits at translation termination, these three IFs on their own cannot dissociate translationally inactive 80S ribosomes or prevent their formation (Chaudhuri *et al.*, 1999; Kolupaeva *et al.*, 2005). In addition, either RNA or a ternary complex consisting of eIF2-GTP.Met-tRNA$_i^{Met}$ is required, which directly couples the dissociation of free ribosomal subunits with 43S pre-initiation complex formation (Chaudhuri *et al.*, 1999; Kolupaeva *et al.*, 2005)(see below).

1.10.1 Formation of the 43S pre-initiation complex

Following ribosomal subunit dissociation, eIF1, eIF1A, eIF3 and eIF5 assist in the recruitment of a ternary complex which delivers charged initiator tRNA (Met-tRNA$_i^{Met}$) to the P-site of the 40S ribosomal subunit, forming the 43S pre-initiation complex (PIC) (Chaudhuri *et al.*, 1999; Asano *et al.*, 2000). The ternary complex contains eIF2 a heterotrimeric GTPase, consisting of small α and β subunits and a larger γ subunit (Benne *et al.*, 1976; Schreier *et al.*, 1977), the latter facilitates binding of Met-tRNA$_i^{Met}$ in a GTP dependent manner (Yatime *et al.*, 2006). The γ subunit binds GTP and cycles between a GTP bound state with a high affinity for Met-tRNA$_i^{Met}$ and a GDP-bound state that lowers this affinity (Kapp and Lorsch, 2004). eIF2γ is homologous to the elongation factor eEF1A which is responsible for delivering aminoacylated tRNAs to the translating ribosome (Schmitt *et al.*, 2002). Though structurally and functionally very similar, these two factors preferentially bind different methionyl tRNAs; eIF2γ binds Met-tRNA$_i^{Met}$ whereas eEF1A binds an elongator methionyl tRNA, Met-tRNA^{Met}. eIF2α also shares homology with eEF1B (Ito *et al.*, 2004). Initiator tRNA binding is also aided by eIF1 which discriminates against non-initiator Met-tRNA by recognising a specific GC repeat in the anticodon stem of Met-tRNA$_i^{Met}$ (Lomakin *et al.*, 2006).

eIF2 has its own GTPase activating protein (GAP), eIF5, and guanine nucleotide exchange factor (GEF), eIF2B, which stimulate the GTPase activity of eIF2γ or restore its activity by catalysing the replacement of GDP for GTP respectively (Chakrabarti and Maitra, 1991; Chaudhuri *et al.*, 1994; Chaudhuri *et al.*, 1999; Nika *et al.*, 2000; Paulin *et al.*, 2001; Williams *et al.*, 2001). Phosphorylation of the α subunit in response to a variety of cellular stresses converts eIF2 to a competitive inhibitor of eIF2B, and constitutes a major regulatory step of translation (Clemens *et al.*, 1982). Four eIF2α kinases have been characterised which are activated in response to a variety of stresses: PKR in response to dsRNA in viral infection (Farrell *et al.*, 1977; Galabru and Hovanessian, 1987; Meurs *et al.*, 1990); PERK in response to endoplasmic reticulum (ER) stress caused by the accumulation or aggregation of misfolded proteins (Harding *et al.*, 1999); GCN2 in response to uncharged tRNAs or amino acid deprivation (Dever

et al., 1992) and HRI (haem-regulated eIF2α kinase) in response to low heme levels (Farrell *et al.*, 1977; Gross and Mendelewski, 1977), heat shock (Ernst *et al.*, 1982) and nitric oxide (NO) (Uma *et al.*, 2001). All four kinases phosphorylate eIF2α on the same residue and therefore initiate the same 'integrated stress response' (ISR) that results in a decrease in ternary complex that reduces global translation levels. Recently, eIF5 has been shown to both contribute to the regeneration of ternary complex by acting as a GDP dissociation inhibitor (GDI), and also to inhibit eIF2B function in an eIF2α-phosphorylation dependent manner (Jennings and Pavitt, 2010). eIF2B is also phosphorylated on multiple residues by four different kinases, the casein kinases (CKs) I and II, the DYRK kinase and glycogen synthase kinase (GSK) 3 (Wang *et al.*, 2001; Woods *et al.*, 2001). Phosphorylation of Ser-540 by GSK-3 inhibits eIF2B activity, however this is prevented by the binding of GSK-3 by Akt, activated in response to insulin-stimulation (Wang *et al.*, 2001).

The binding of eIF1 and eIF1A to the 40S ribosomal subunit induces an 'open' conformational state which both increases the rate of ternary complex binding and permits scanning of an mRNA (Passmore *et al.*, 2007). Together with eIF3, they form the 43S PIC, which, though capable of binding an unstructured mRNA in a 5'-end dependent manner (Pestova and Kolupaeva, 2002), secondary structure proximal to the 5'-cap means that its recruitment to an mRNA must be assisted by the cap-binding complex, eIF4F.

1.10.2 Cap-recognition by eIF4F

The discovery that the 5' terminal methyl-guanosine cap is important in the translation of eukaryotic mRNAs (Muthukrishnan *et al.*, 1975) led to the development of techniques able to isolate cap-binding proteins. A complex, termed eIF4F, was identified, which contains three initiation factors: a 26 kDa protein, eIF4E; a 220 kDa protein, eIF4G and the 46 kDa protein, eIF4A (Sonenberg *et al.*, 1978; Edery *et al.*, 1983; Grifo *et al.*, 1983). eIF4F is thought to direct the helicase activity of eIF4A to 'melt' 5' cap-proximal structure and provide a landing platform for the ribosomal subunit (Ray *et al.*, 1985; Svitkin *et*

al., 2001). Two additional proteins, eIF4B and eIF4H, are associated with the cap-binding complex and stimulate eIF4A's RNA and ATP binding and helicase activity. eIF4F formation and binding to the cap is regulated by a number of pathways in response to many stimuli, which will be discussed in more detail later on in this introduction.

eIF4E is a highly regulated cap-binding protein which forms a concave tertiary structure that contacts the capped end of mRNAs (Tomoo *et al.*, 2002). eIF4E activity is suppressed by the 4E-binding proteins (4E-BPs), of which there are three isoforms. The 4E-BPs binding site on eIF4E overlaps eIF4G's binding site and prevents the formation of eIF4F. Hyper-phosphorylation of 4E-BPs by mTORC1 results in a loss of affinity for eIF4E allowing it to bind eIF4G as part of eIF4F and so promotes translation initiation.

The interaction between eIF4E and the 5' cap is greatly enhanced by eIF4G *in vitro* (Haghighat and Sonenberg, 1997). eIF4G is a large, multi-domain protein that acts as a molecular scaffold, binding a number of proteins linking the 5' cap and the polyA tail of the mRNA and the ribosome (see figure 1.6, A). eIF4G has two homologues, eIF4GI and eIF4GII which share 46% homology and can both function in eIF4F (figure 1.6 B) (Gradi *et al.*, 1998). eIF4G also binds the MAP kinase interacting protein Mnk1 which phosphorylates eIF4E on Ser209 (Waskiewicz *et al.*, 1997), however there are contrary reports as to the effect eIF4E phosphorylation has on translation initiation (Scheper and Proud, 2002). Transgenic mice with impaired Mnk function develop normally in the absence of eIF4E phosphorylation (Ueda *et al.*, 2004), whereas eIF4E phosphorylation was found to be important for translation in both a mouse lymphoma model (Wendel *et al.*, 2007) and a prostate cancer cell line (Bianchini *et al.*, 2008). eIF4E phosphorylation has also been implicated in the nucleocytoplasmic transport of cyclin D1 mRNA (Topisirovic *et al.*, 2004).

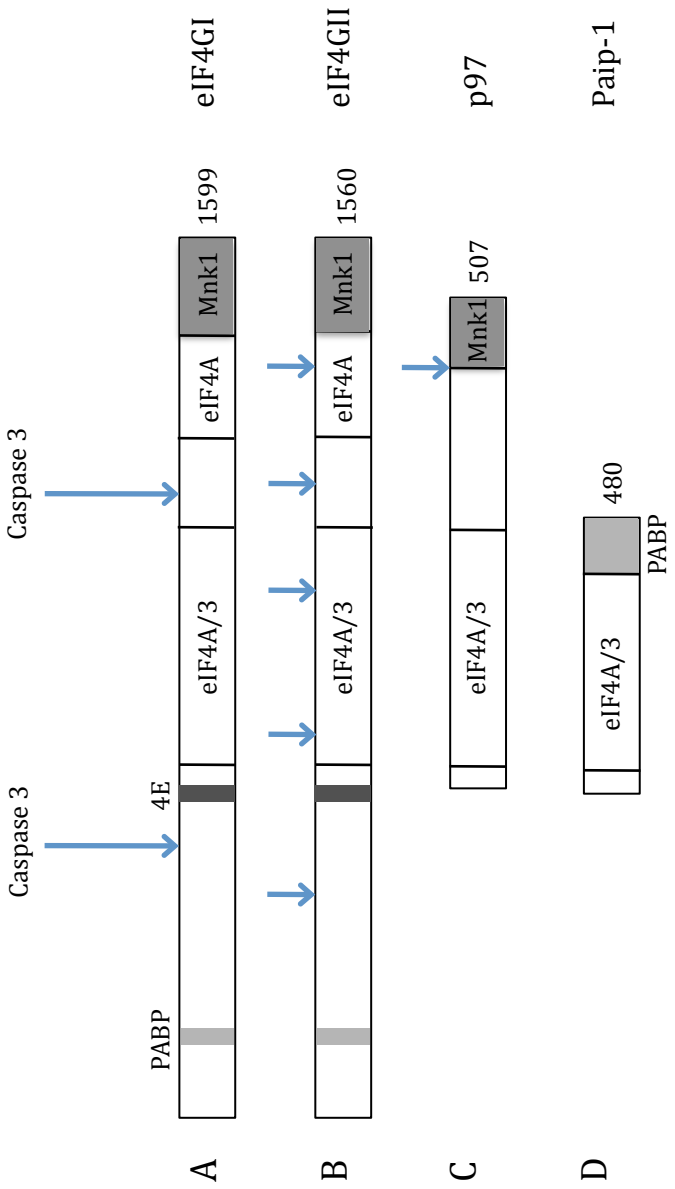

Figure 1.6. eIF4G homologues. Schematic diagram depicting the four eIF4G homologues. Binding regions for initiation factors and binding proteins are indicated by labeling or shading - PABP, eIF4E (4E), eIF4A, eIF3 and Mnk1. Caspase 3 cleavage sites are indicated by blue arrows. The amino acid length of the protein is indicated to the right of each diagram.

The cap and polyA tail of an mRNA synergistically enhance translational efficiency (Gallie, 1991). This effect is mediated by eIF4G, through binding eIF4E and the polyA binding protein PABP, which forms a closed loop complex that enhances translation initiation (Wells *et al.*, 1998) and functions as an assessment of mRNA integrity (Gallie, 2004). This closed loop complex is also thought to enable post termination ribosomes to be recycled to the 5' end of the mRNA. (figure 1.7) eIF4G contains three HEAT repeat domains, two of which, HEAT-1/MIF4G and HEAT-2/MA3, bind to eIF4A (Marcotrigiano *et al.*, 2001; Bellsolell *et al.*, 2006) and act as a 'soft-clamp' to stabilise its closed conformation (Pestova *et al.*, 1996b; Imataka and Sonenberg, 1997; Oberer *et al.*, 2005; Marintchev *et al.*, 2009). eIF3 also binds to the HEAT-1 domain in the middle of eIF4G, and does so in a cooperative manner with eIF4A (Korneeva *et al.*, 2000; Morino *et al.*, 2000).

eIF4G directs the recruitment of the 43S preinitiation complex to the 5' end of the mRNA by binding to eIF3 through eIF3e to form the 48S PIC (Lamphear *et al.*, 1995; Imataka and Sonenberg, 1997; Korneeva *et al.*, 2000; LeFebvre *et al.*, 2006). As mentioned above, the 43S PIC can associate with an mRNA in a 5'-end dependent manner, independent of eIF4F if no secondary structure is present proximal to the cap (Pestova and Kolupaeva, 2002). The introduction of secondary structure, however, minimally requires eIF4A and an eIF4G truncation, capable of binding eIF3 and eIF4A, for successful 48S PIC formation (Morino *et al.*, 2000; Pestova and Kolupaeva, 2002). Furthermore, a truncated version of eIF4G lacking eIF4E binding sites can support the translation of uncapped mRNAs in a rabbit reticulocyte lysate (RRL) translation system or capped mRNAs in a system depleted of eIF4F (De Gregorio *et al.*, 1998; Ali *et al.*, 2001). These findings support the conclusion that the interaction of eIF4E with the 5' cap primarily acts to enhance the action of eIF4F but is not crucial for the recruitment of the 43S PIC to the 5' end of an mRNA (Pestova and Kolupaeva, 2002).

1.10.3 Mechanism of 48S scanning to the start codon

In order to initiate protein synthesis, the 48S PIC must migrate along the 5' UTR, overcoming any stable secondary structure in its path until the 40S SSU recognises an initiation codon (AUG) in the correct consensus sequence. *In vitro* studies have demonstrated that the 43S PIC is able to migrate along an unstructured mRNA in the absence of ATP, eIF4F, eIF4A and eIF4B, though, if included, these factors increase the efficiency of this process (Pestova and Kolupaeva, 2002). Ribosomal scanning is inhibited by stable secondary structure formed in G:C rich 5' UTRs and is dependent upon ATP, eIF4A and eIF4F (Pelletier and Sonenberg, 1985; Kozak, 1986a; Koromilas *et al.*, 1992; Svitkin *et al.*, 2001; Pestova and Kolupaeva, 2002). Translational inhibition caused by structured 5' UTRs can be overcome by the overexpression of eIF4E, presumably through the recruitment of eIF4A to the mRNA as part of eIF4F (Koromilas *et al.*, 1992). Furthermore, increasing the secondary structure in a 5' UTR proportionally increases the requirement of eIF4A for successful translation initiation (Svitkin *et al.*, 2001). Although maximal translation rates require both eIF4A on its own and as part of eIF4F (Grifo *et al.*, 1983), it is likely that the free helicase is required to minimalise the effect of the fast dissociation rates of eIF4A from eIF4F rather than providing additional unwinding activity (Pause *et al.*, 1994; Korneeva *et al.*, 2001). A large body of evidence now corroborates the scanning hypothesis that 40S SSU translocation to the start codon is facilitated by eIF4F. It is worth noting though that unstructured mRNA still requires eIF4A and ATP for efficient translation suggesting some function in ribosomal recruitment (Blum *et al.*, 1989; Altmann *et al.*, 1990a; Altmann *et al.*, 1990b; Blum *et al.*, 1992).

eIF4A helicase activity is greatly stimulated by eIF4B and eIF4H and is increased 20-fold when part of eIF4F (Ray *et al.*, 1985; Rozen *et al.*, 1990; Jaramillo *et al.*, 1991; Rogers *et al.*, 2001b; Rozovsky *et al.*, 2008). In eIF4F, eIF4A interacts with the C-terminal HEAT-2/MA3 domain (Lamphear *et al.*, 1995) and the middle HEAT-1/MIF4G domain of eIF4G (Imataka and Sonenberg, 1997). Mutations to the residues implicated in eIF4A binding in HEAT-2 reduces the ribosome binding capabilities of eIF4G, and in HEAT-1

completely abolishes them (Morino *et al.*, 2000). This may give an indication as to why the middle region of eIF4G, containing HEAT-1, is required to facilitate ribosomal scanning *in vitro* (De Gregorio *et al.*, 1998; Ali *et al.*, 2001). HEAT-1 binds to eIF4A with a higher affinity than HEAT-2, but both regions are able to bind to both domains of eIF4A, acting like a 'soft-clamp' to maintain its closed conformation (Korneeva *et al.*, 2001; Oberer *et al.*, 2005; Schutz *et al.*, 2008; Marintchev *et al.*, 2009). Recent examination of eIF4G's interactions with eIF4A using surface plasma resonance (SPR) and nuclear magnetic resonance (NMR) chemical shift perturbation was able to detect differences between the affinity of HEAT-1 and HEAT-2 for each of eIF4A's domains (Marintchev *et al.*, 2009). Whereas HEAT-1 binds eIF4A's C-TD more strongly than its N-TD and ATP enhances this interaction and the ability of the complex to bind RNA, HEAT-2 is the opposite, binding eIF4A's N-TD more strongly than the C-TD and reducing this interaction and the complexes affinity for RNA in the presence of ATP (Marintchev *et al.*, 2009). Because of this, eIF4A could theoretically be bound to eIF4G at each stage of its nucleotide cycle, which provides a mechanism by which eIF4A can be retained in eIF4F after ATP hydrolysis. Though the central domain of eIF4G is highly conserved, the C-terminal domain is not, and therefore this mechanism may not apply to all eukaryotes (Keiper *et al.*, 1999).

Although the yeast crystal structure of eIF4G and eIF4A demonstrates that HEAT-1 domain is capable of holding eIF4A in its closed conformation, it lacks the C-terminal domain of human eIF4G (Schutz *et al.*, 2008). This may explain why two additional yeast helicases, Ded1 and its close homologue Dbp1, have also been implicated in unwinding 5' UTR secondary structure during translation in yeast (Chuang *et al.*, 1997; de la Cruz *et al.*, 1999; Berthelot *et al.*, 2004). The employment of additional helicases may compensate for eIF4A's fast dissociation rates from the eIF4F complex after each round of unwinding. DDX3/PL10, a mammalian homologue of Ded1, Vasa and DHX29 have all been implicated in translation initiation in higher eukaryotes, though their mechanism of action is not yet fully understood. DHX29, identified in RRL, promotes the assembly of the 48S PIC in RRL but displayed weaker helicase activity than eIF4A with eIF4B *in vitro* (Pisareva et al., 2008). DDX3 interacts

with eIF3 and is required for the translation of reporter constructs in both human and *Drosophila* cells (Lee *et al.*, 2008). The *Drosophila* helicase, Vasa, interacts with eIF5B and is crucial for normal development (Johnstone and Lasko, 2004).

Although the factors responsible for 48S PIC scanning to the initiation codon have been known for many years, the mechanism by which this is achieved is still largely unknown. This is mainly due to the large size of the complexes hindering any progress on their structural elucidation. In order to aid ribosomal scanning it is presumed that any useful helicase activity would occur in front of the ribosome. Modeling based on a cryo-electron microscopy reconstruction of eIF3, eIF4F, HCV viral mRNA and the 40S SSU, however placed eIF4F at the trailing edge of the scanning ribosomal subunit (Siridechadilok *et al.*, 2005). This led to the proposed model that eIF4A's activity was important for eIF4F binding and aided ribosomal scanning by ratcheting mRNA through the ribosomal mRNA binding channel. A second, rough topographical, model has recently been proposed of a minimal scanning complex of eIF4G, eIF4A and eIF4H (Marintchev *et al.*, 2009), which was created by combining data from mutational analysis with a higher order structure of eIF4G mapped to that of its evolutionary ancestor, CBP80 (Marintchev and Wagner, 2005). When fitted to the small ribosomal subunit, this model can place eIF4A both at the 5' or the 3' side of the 40S SSU, which the authors suggest may enable the helicase to switch back and forth between these positions, unwinding the secondary structure hindering scanning in front of the ribosomal subunit while keeping the RNA adjacent to the cap-bound eIF4E free of secondary structure allowing additional 43S PIC binding.

1.10.4 Identification of the start codon

The principal determinant in initiation codon recognition is its complementarity to the anticodon of Met-tRNA$_i^{Met}$ (Cigan *et al.*, 1988). Until an initiation codon is encountered, the 40S SSU adopts an 'open' conformation that positions the Met-tRNA$_i^{Met}$ in a way that is suitable for 48S PIC scanning (Pestova and Kolupaeva, 2002; Passmore *et al.*, 2007). Once the start codon has been recognised, the

release of inorganic phosphate (P_i) from the complex, irreversibly rearranges the PIC to the closed 'scanning-incompetent' conformation and commits the 40S ribosome to initiating translation at that position (Pestova *et al.*, 1998b; Pestova and Kolupaeva, 2002; Algire *et al.*, 2005; Maag *et al.*, 2005; Passmore *et al.*, 2007). In order to prevent this occurring at incorrect codons eIF1 and eIF1A work together in an antagonistic way that is crucial to start codon identification and the fidelity of protein synthesis (for review see (Mitchell and Lorsch, 2008)). Whereas eIF1A is responsible for recognising start codons in the correct context, eIF1 may destabilise unfavourable codon/anticodon pairings, and facilitate the dissociation of prematurely formed ribosomes (Pestova *et al.*, 1998b; Pestova and Kolupaeva, 2002; Lomakin *et al.*, 2006). The GTPase activating protein eIF5 specifically enhances eIF2's GTPase activity and is inhibited by eIF1 partially blocking a specific interaction between eIF5 and eIF2 (Paulin *et al.*, 2001; Algire *et al.*, 2005; Conte *et al.*, 2006; Nanda *et al.*, 2009). Start codon recognition causes conformational change within the PIC which results in the release of eIF1, allowing eIF5 to interact with eIF2 unhindered (Maag *et al.*, 2005; Cheung *et al.*, 2007b; Nanda *et al.*, 2009) and prompts an interaction between eIF1A and eIF5 which may induce the closed, 'scanning-incompetent' conformation of the PIC (Maag *et al.*, 2006) and ultimately ends with P_i release from the complex (Algire *et al.*, 2005; Maag *et al.*, 2005). eIF2-GDP release is enhanced by the recruitment of the ribosome-dependent GTPase eIF5B (Pisarev *et al.*, 2006) which is accelerated by its interactions with eIF1A (Acker *et al.*, 2009). Together, eIF5B and eIF1A recruit the large 60S ribosomal subunit and the formation of the complete 80S ribosome stimulates the GTPase activity of eIF5B, which accelerates eIF1A's and causes its own release from the complex (Acker *et al.*, 2006; Acker *et al.*, 2009). This leaves the A-site of the 80S ribosome available to accept an aminoacylated-tRNA and begin the second, elongational phase of translation.

1.11 Alternative mechanisms of translation initiation

The majority of mRNAs are translated by a cap-dependent scanning mechanism starting from the first initiation codon encountered by the ribosome (Kozak,

1983). During nutrient deprivation and cellular stress, cap-dependent translation is reduced or shut-down by targeted modification and proteolysis of components of the initiation complex. This down-regulation affects both the activity and integrity of the eIF2-ternary complex or eIF4F, resulting in a general reduction in the translational activity of the cell. Cellular stress also induces the formation of stable mRNA and mRNP aggregates, termed stress granules (SGs), that are induced in either an eIF2α-phosphorylation dependent or independent manner and act as storage sites for mRNAs and the translational machinery until the cell recovers (Anderson and Kedersha, 2006). eIF2α-phosphorylation independent formation of SGs can be brought about by drugs that affect either eIF4A's or eIF4G's activity (Low *et al.*, 2005; Mazroui *et al.*, 2006; Kim *et al.*, 2007) or depletion of cellular levels of eIF4B, eIF4H or PABP but not eIF4E (Mokas *et al.*, 2009). The mRNAs that are recruited to SGs appear to be selected as some remain within the cytoplasm, however which mRNAs and a full understanding of their mechanism of selection has yet to be discovered. Stress granules remain static within the cell, but are dynamic and interact with other cytoplasmic proteins and processing bodies (PBs). PBs contain the apparatus responsible for mRNA decay, and are presumed to 'sort' mRNA content according cellular requirement (Kedersha *et al.*, 2005) (for review see (Anderson and Kedersha, 2008).

Translational reduction via eIF4F can affect those mRNAs which are reliant on cap-dependent scanning in two ways: by inhibiting binding of the cap-structure to the mRNA, or inhibiting the scanning progress of the 48S PIC. The introduction of secondary structure to an mRNA increases the requirement of eIF4A and eIF4F for translation initiation. Logically therefore the decreased abundance or activity of these factors is likely to preferentially inhibit the translation of mRNAs with long and/or structured 5' UTRs when compared to unstructured messages (Svitkin *et al.*, 2001). The 5' UTRs of highly regulated genes, such as those involved in transcription or cell cycle control, are generally longer and more structured than those of housekeeping genes (Kozak, 1987, 1991; Davuluri *et al.*, 2000). Regulating the activity of eIF4A and eIF4F therefore offers the cell a mechanism by which it can selectively control the

expression of these genes. Indeed the overexpression of eIF4E has been shown to increase the translation of a reporter construct with inhibitory structure in its 5' UTR (Koromilas *et al.*, 1992), and the aberrant expression of eIF4E (reviewed in (De Benedetti and Graff, 2004)), eIF4A (Eberle *et al.*, 1997; Eberle *et al.*, 2002) and eIF4G (Bauer *et al.*, 2002; Comtesse *et al.*, 2007; Silvera *et al.*, 2009; Tu *et al.*, 2010) has been associated with tumourigenesis (for review see (Hagner *et al.*, 2010).

When a cell responds to harsh environments by impairing cap-dependent translation, a subset of mRNAs responsible for the maintenance of cellular homeostasis or the determination of the cell's fate must evade or take advantage of these conditions so expression may occur. Translation of these genes is able to proceed in conditions where global translation is inhibited, via mechanisms that take advantage of elements within the UTRs of these mRNAs. Some elements, which under normal conditions are inhibitory to the translation of the physiological open reading frame (ORF), become advantageous under such conditions. Others direct the initiation of translation via a cap-independent process that can occur with, or is enhanced by, post-translationally modified or even absent initiation factors.

1.11.1 Alternative start codons

Although in the majority of cases translation initiation occurs principally from the first AUG codon encountered by the scanning 48S PIC, some mRNAs contain upstream start codons (uAUGs) or upstream (u)ORFs before the coding sequence (CDS). Initial analyses of vertebrate mRNA sequences indicate that, although present in less than 10% of all mRNAs analysed, 5' leader sequences containing uAUGs are commonly found in protooncogenes and genes involved in cell growth (Kozak, 1987, 1991). The presence of an uAUG or uORF can inhibit the translation of the CDS due to the 48S PIC stalling at the uAUG or failing to reinitiate at the physiological AUG after the translation of the uORF.

Some cellular environmental conditions require the inhibitory action of the uORFs to be overcome. A well-documented example of this is the response of yeast cells to amino acid deprivation. Under these conditions, non-acylated tRNAs trigger GCN2 to phosphorylate eIF2α, causing the reduction in ternary complex which downregulates global protein synthesis. The downstream effect of this is that the translation of the transcription factor Gcn4p, which is usually hindered by four short uORFs in its mRNAs 5' leader sequence, is enhanced. Under optimal conditions, after translating the first uORF of *GCN4*, about 50 % of 40S SSUs continue scanning the mRNA and, after binding fresh ternary complex, resume translation at uORFs 2 - 4. During conditions where the amount of ternary complex is diminished, about 50 % of the scanning 40S SSUs will reach the start codon of uORF4 before binding ternary complex. Ribosomal subunits are therefore able to proceed to the start codon of *GCN4* and, if bound to a ternary complex, reinitiate translation here. An example of this process in mammalian cells is that of the mRNA *ATF4* (activating transcription factor 4), which contains two uORFs, but the initiation of its third ORF, encoding the ATF4 transcription factor, is inhibited due to its location within the second uORFs coding sequence. As with *GCN4*, during times of limited ternary complex, ATF4 expression is increased. One of the transcriptional targets of ATF4 is GADD34 (growth arrest and DNA-damage inducible protein 34), which forms part of a phosphatase complex that targets eIF2α, providing a feedback loop.

1.11.2 Ribosomal shunting

Ribosomal shunting is a rare mechanism by which the scanning 48S PIC is able to circumvent inhibitory secondary structure or uAUGs/uORFs in the 5' leader sequence of an mRNA in order to initiate translation from the physiological AUG. This mechanism has been primarily characterised in viral mRNAs such as cauliflower mosaic virus (CaMV) (Futterer *et al.*, 1993) and, though not completely understood is thought to be coordinated between an interaction with the 18S rRNA of the SSU and two mRNA shunt sites, a donor and acceptor, between which the SSU is able to translocate, avoiding any inhibitory structure inbetween (Yueh and Schneider, 2000; Chappell *et al.*, 2006). Shunting is not

well characterised in eukaryotic mRNAs but heat shock protein (Hsp) 70, under heatshock conditions employs a shunting mechanism to coordinate translation, whereas under normal conditions it is translated by a cap-dependent mechanism (Yueh and Schneider, 2000). The cellular inhibitor of apoptosis (cIAP) 2 transcript contains a long (2.83 kb) 5' UTR that contains 64 uORFs and stable secondary structure and therefore presents a formidable obstruction to cap-dependent scanning by the 48S PIC. Translation of cIAP2 is mediated by a shunting mechanism, which, after the translation of the first uORF, allows the SSU to bypass a stable hairpin containing 62 of the uORFs to position it close to the actual start codon of cIAP2 (Sherrill and Lloyd, 2008). Due to these findings it is suspected that more cellular mRNAs with 5' UTRs that would present strong barriers for cap-dependent scanning may be translated by a shunting mechanism.

1.11.3 Internal Ribosomal Entry

Under conditions of compromised cap-dependent translation, such as viral infection, apoptosis, heatshock or hypoxia, a subset of mRNAs are able to initiate translation independently of the 5' cap, via secondary structure within their 5' UTR called an internal ribosomal entry site (IRES). IRESs are able to recruit the ribosome directly to, or in close proximity of, the start codon and coordinate translation initiation with a limited set of initiation factors and trans-acting factors (ITAFs). Many viral RNAs contain IRESs which mediate their translation after viral infection causes the shutoff of host cell translation, as the viral RNA often encodes proteases that cleave initiation factors, and dsRNA triggers eIF2α phosphorylation by PKR. The translation of viral IRESs differ in their requirement of the canonical initiation factor, for instance the EMCV (encephalomyocarditis virus) IRES minimally requires eIF4A and the central domain of eIF4GI, eIF2, eIF3 and eIF4B (Pestova *et al.*, 1996a; Pestova *et al.*, 1996b) whereas HCV (hepatitis C virus) IRES only requires eIF2 (Pestova *et al.*, 1998a). Many mRNAs of highly regulated eukaryotic proteins are also found to contain IRES elements that are found to stimulate translation in the absence of a 5' cap. Such elements have been reported in mRNAs that are translated

when cap-dependent translation is silenced in response to apoptosis (Stoneley *et al.*, 2000; Bushell *et al.*, 2006), viral infection (Johannes *et al.*, 1999) and genotoxic stress (Subkhankulova *et al.*, 2001). Many of these mRNAs encode proto-oncogenes and therefore their IRES could possibly contribute to their deregulation in cancer (for review see (Stoneley and Willis, 2004).

1.11.4 5' terminal oligopyrimidine tracts (TOPs)

Many proteins associated with the translational apparatus are selectively expressed or repressed at the level of translation in a growth dependent manner. The mRNAs of these proteins were found to contain a cytosine residue at their 5' cap followed by a string of 4 - 14 pyrimidine residues or terminal oligopyrimidine tract (TOP). The 5' TOP acts as a cis-regulatory element that rapidly switches on or off the translation of these mRNAs in response to growth stimuli or nutrient deprivation. The MTORC1 signaling cascade has been implicated in the coordination of this activity, though the downstream effectors of this signaling have yet to be fully characterised. Initial studies indicated that phosphorylation of RpS6 by S6 kinase increases the translation of 5' TOP containing mRNAs (Jefferies *et al.*, 1997), however subsequent studies have demonstrated that translational control of 5' TOP messages by MTORC1 is independent of S6 kinase activity (Tang *et al.*, 2001; Pende *et al.*, 2004; Reiter *et al.*, 2008). The actual mechanism by which translation is selectively regulated via the 5' TOP is yet to be clarified.

1.11.5 Regulation of translation initiation via 3' UTR elements

The regulation of translation can also be directed by sequence elements in an mRNAs 3' UTR in response to changes in the cellular environment. Under certain conditions the cell can utilise response elements within an mRNAs 3' UTR to coordinate the expression of proteins which will maintain its homeostasis, e.g. in order to maintain cellular iron concentrations a number of transcripts, including ferritin and transferrin, that are involved in iron storage or influx respectively, contain iron response elements (IREs) that bind to iron response proteins (IRPs) when iron concentrations are low. This has the effect of either repressing the translation of the mRNA, as is the case for ferritin,

which contains one IRE in its 5' UTR, or increases the stability of the mRNA, as in the case for transferrin, which has several IREs in its 3' UTR. Together, this results in the reduction of iron storage and the increase of iron influx into the cell. Several other response elements are involved in translational regulation but will not be described further as this thesis focuses primarily on translational control coordinated by the 5' UTR.

Translational control is also mediated by a mechanism called RNA silencing in which short RNA molecules recruit a RNA-induced silencing complex (RISC) to complementary regions in the 3' UTRs of mRNAs. These short RNA molecules are generally referred to as silencing (si)RNAs or micro (mi)RNAs, though additional subsets have also been described. siRNAs and miRNAs are generated from double stranded (ds)RNA by a multimeric complex termed Dicer that facilitates their cleavage from their precursor dsRNA and the displacement of their complementary strand by the recruitment of a member of the argonaute family of endonucleases. The siRNA or miRNA produced remains associated with argonaute as part of the RISC complex and acts as a guide strand that, when bound to a complementary region in the 3' UTR of an mRNA, directs gene silencing according to how well it matches the mRNA sequence. This silencing is thought to occur via mRNA cleavage, de-capping or translational repression through reduced mRNA stability caused by miRNA coordinated deadenylation (Guo *et al.*, 2010).

Poly(A) tail length is also an important mechanism of control of translation initiation during development, particularly in growing oocytes and early embryos of animals. mRNAs with short poly(A) tails (20 - 50 A residues) are generally poorly translated, however the increased polyadenylation of these mRNAs (to 80 - 500 A residues) activates their translation and thereby acts as a translational switch. Cytoplasmic polyadenylation of mRNAs is directed by cytoplasmic polyadenylation elements (CPEs) that recruit CPE binding protein (CPEB) that leads to the recruitment of poly(A) polymerase (PAP) through cleavage and polyadenylation specificity factor (CPSF) and the elongation of the poly(A) tail. Deadenylation of poly(A) tails in somatic cells leads to the mRNA's

degradation, however this is not the case in oocytes and early embryos, where shortening of the poly(A) tail does not necessarily lead to the destabilisation of the mRNA but reduces its translation. Again, elements in the 3' UTR are thought to direct deadenylation, however the mechanism of this control has not yet been fully described (for review see (de Moor *et al.*, 2005).

1.12 eIF4A specific regulation.

As described above, members of the DEAD box family of proteins generally have domains flanking their minimal, highly conserved helicase core, which are thought to influence the position and efficiency of their helicase activity. eIF4A, however, does not possess an N- or C-TD and therefore has been used to represent the DEAD-box helicase core in kinetic assays. It is well documented, however, that eIF4A is able to bind to several proteins, the majority of which are thought to aid its function in translation initiation. Furthermore, several small molecule inhibitors of eIF4A have been isolated or designed and the current understanding of these and eIF4A binding proteins will be the focus of the final part of this introduction.

1.13 eIF4G and homologues

As described above, eIF4GI acts as a scaffold protein in translation initiation, mediating the recruitment of a number of initiation factors and the 40S SSU to the 5' cap of mRNAs. eIF4GI is thought to act as a 'soft-clamp', holding the two domains of eIF4A together in a closed formation capable of helicase activity. Recent structural mapping of the DEAD-box helicase YxiN placed its C-terminal RNA-binding domain (RBD) in a position relative to that of eIF4GI bound to eIF4A (Karow and Klostermeier, 2010). The authors postulate that this position may represent a conserved interface that facilitates an interaction between the DEAD-box helicase core and its flanking domains, or interacting proteins, and perhaps therefore contributes to the control of helicase activity. Indeed a number of proteins are able to interact with eIF4A at this position and are able to regulate its activity.

Four mammalian homologues of eIF4G have been described: eIF4G I and II, p97/DAP5 (death associated protein 5) and Paip1 (PABP-interacting protein 1). Figure 1.6 demonstrates the domain differences between each homologue. eIF4G I and II display 46 % total amino-acid sequence similarity which is distributed mainly in the central- and carboxy-terminal domains (Gradi *et al.*, 1998). Both contain two eIF4A binding domains in their middle and C-terminal regions, the first of which is highly conserved but the second, though conserved in *Arabidopsis* and *Drosophila*, is absent in yeast. Recent data has indicated that the two eIF4A binding domains in eIF4GI may preferentially bind eIF4A at different stages of its nucleotide cycle which may help it to remain associated with the mRNA during repeated rounds of unwinding (Marintchev *et al.*, 2009). eIF4G I and II can functionally interchange in eIF4F *in vitro* (Gradi et al., 1998), but it has been suggested that they coordinate the translation of different sets of mRNAs, as siRNA knockdown of either eIF4GI or II has demonstrated (Ramírez-Valle *et al.*, 2008). eIF4GI silenced cells display a phenotype typical of serum starvation, but this is not the case for eIF4GII knockdown (Ramírez-Valle *et al.*, 2008). These differences may possibly be attributed to variations in the posttranslational modification of each homologue in response to the cellular environment. The 'hinge' region between the eIF3/eIF4A and eIF4A/Mnk binding sites of eIF4GI/II shares only 17 % homology and is variably phosphorylated in response to different stimuli. eIF4GI is phosphorylated on numerous residues in its hinge region in response to serum stimulation via the mTOR pathway, which possibly coincides with an increase in eIF4F formation (Raught *et al.*, 2000; Vary and Lynch, 2006; Vary *et al.*, 2007). In response to hyper-osmolarity or contact-inhibition (Roig *et al.*, 2000; Ling *et al.*, 2005), Pak2/γ-PAK (p21-activated protein kinases 2) is able to bind eIF4GI in eIF4E's binding site (Orton *et al.*, 2004) and phosphorylate eIF4GI in the middle of its eIF3/eIF4A binding site on residue Ser-896 (Ling *et al.*, 2005). It is not known whether Pak2 elicits translational inhibition through the physical inhibition of the eIF4E:eIF4G interaction or its kinase activity, and it is yet to be demonstrated whether phosphorylation on Ser-896 has any influence on eIF3/eIF4A binding to eIF4GI (Ling *et al.*, 2005). eIF4GII phosphorylation, unlike eIF4GI, does not occur in response to hormonal or serum stimulation

and is not a known target of mTOR signaling, rather it is one of the few known targets of calcium/ calmodulin-dependent protein kinase I (CaMKI) (Qin *et al.*, 2003). CaMKI phosphorylates eIF4GII on its hinge region though the effect that this has on translation initiation is unknown (Qin *et al.*, 2003). eIF4GII and not eIF4GI is recruited to the 5' cap of mRNAs at the onset of cell differentiation and is thought to stimulate translation by effecting the strong, lasting phosphorylation of eIF4E (Caron *et al.*, 2004). Therefore, although they are structurally similar and their functions are interchangeable, eIF4GI and eIF4GII have evolved to respond to different stimuli at different stages of the cell's life cycle, possibly via targeting the translation of particular mRNAs (Caron *et al.*, 2004).

eIF4GI and II are also subject to proteolysis after picornaviral infection and during apoptosis. A number of viral proteases have been shown to target members of the translational machinery, including eIF4GI/II, resulting in the shutdown of global cap-dependent translation initiation. Picornavirus 2A protease differentially cleaves eIF4GI/II at a position just downstream of the eIF4E binding site, effectively separating the N-terminal eIF4E/PABP binding domains from the C-terminal eIF3/eIF4A binding domains (Etchison *et al.*, 1982; Lamphear *et al.*, 1995; Gradi *et al.*, 1998). Though the C-terminal fragment can still support some cap-dependent translation it is thought to preferentially be used in the translation of viral mRNAs through their IRES in concert with eIF4A and eIF3 (Pestova *et al.*, 1996a; Pestova *et al.*, 1996b; Lomakin *et al.*, 2000; Ali *et al.*, 2001). During apoptosis eIF4GI is cleaved by caspase-3 in two places to produce three fragments of apoptotic cleavage of eIF4G: N-FAG, M-FAG and C-FAG (see figure 1.6 A) (Clemens *et al.*, 1998; Bushell *et al.*, 2000). M-FAG contains the eIF4E, eIF3 and first eIF4A binding sites and is able to substitute for eIF4G in eIF4F in apoptosing cells and possibly maintain some of its function in both cap-dependent and independent translation initiation (De Gregorio *et al.*, 1998; Morino *et al.*, 2000). The first eIF4A binding site in eIF4GI/II has been shown to be essential for translation initiation whereas the second is thought to be modulatory. Considering the role of eIF4A in the process of translation initiation and the recent evidence that suggests

both eIF4A binding domains in eIF4GI/II are required to retain eIF4A on an mRNA's 5' UTR, one might assume that messages affected by the caspase-3 cleavage of eIF4GI would possess longer 5' UTRs (Morino *et al.*, 2000; Marintchev *et al.*, 2009). eIF4GII is also cleaved by caspase 3 during apoptosis at five different sites which disrupts all of its functional domains and is thought to inhibit its translational activity (Marissen *et al.*, 2000). Retaining at least one eIF4A binding site may therefore be an important regulatory feature in the cell's response to different environments through eIF4GI or II.

Dap5/p97 was identified as a positive regulator of interferon-γ (IFN-γ) mediated cell death that shares homology with the middle domain of eIF4GI/II, able to bind eIF4A and eIF3 but not eIF4E therefore resembling the C-terminal picornavirus cleavage product described above (Imataka *et al.*, 1997; Imataka and Sonenberg, 1997; Levy-Strumpf *et al.*, 1997). Dap5/p97 and eIF4GI/II also contain AA (aromatic/aliphatic and acidic residues) box motifs in their C-terminal domain which facilitate binding to Mnk1 and eIF2β in the case of Dap5/p97 (Bellsolell *et al.*, 2006; Lee and McCormick, 2006). Initial research demonstrated that Dap5/p97 is inhibitory to cap-dependent translation initiation and cap-independent initiation (Imataka *et al.*, 1997), however, though not fully understood, Dap5/p97 is polysome associated in non-stressed cells and moves to stress granules in stressed, non-apoptotic cells indicating its involvement in steady-state translation initiation (Nousch *et al.*, 2007). During apoptosis p97 is also cleaved at one site generating a fragment termed Dap5/p86 that shares 32% sequence similarity with M-FAG/p76 (Henis-Korenblit *et al.*, 2000). This cleavage fragment has been shown to act as a switch during apoptosis, controlling the translation of a number of pro- and anti-apoptotic mRNAs via their IRES elements, including its own (for review see (Marash and Kimchi, 2005). Full-length Dap5/p97 has more recently been shown to facilitate cap-independent translation of pro-survival genes Bcl-2 and CDK1 (Marash *et al.*, 2008) in non-stressed HeLa cells promoting cell survival during mitosis (Liberman *et al.*, 2009) and supports translation during ER stress in both a caspase-dependent and independent manner (Lewis *et al.*, 2008). DAP5 knockdown by siRNA had a similar effect to eIF4GI knockdown,

preventing the cell's recovery from serum-starvation and inducing autophagy (Ramírez-Valle *et al.*, 2008). This indicates that, though they are not physically interchangeable, eIF4GI and Dap5/p97 may contribute to common pathways in cellular control.

A fourth eIF4G homologue Paip1 was identified initially as a PABP binding protein that shares 39% similarity with the middle third of eIF4GI (see figure 1.6) (Craig *et al.*, 1998). In addition to two PABP binding domains (Roy *et al.*, 2002), Paip1 is also able to bind eIF4A (Craig *et al.*, 1998) and eIF3 (Martineau *et al.*, 2008) through eIF3g which is different to eIF4GI, and therefore both proteins can bind eIF3 at the same time. Paip1 is seen to have a stimulatory effect on translation initiation and this is thought to occur through the stabilisation of the closed-loop complex and allowing eIF3 to interact with PABP (Martineau *et al.*, 2008). The extent of eIF4A's collaboration with the eIF4G homologues and whether it has an active or passive role in the situations outlined above is yet to be explored fully.

1.14 Other MIF4G/MA3 domain containing proteins/eIF4G competitors

1.14.1 Programmed cell death 4

Programmed cell death 4 (Pdcd4) was identified as a protein upregulated during apoptosis (Shibahara *et al.*, 1995). This protein contains two MA3 domains in its middle and C-terminal regions, termed MA3-m and MA3-c respectively. Pdcd4 is able to bind to eIF4A through these domains and recent crystallographic data has demonstrated that both domains bind eIF4A in the interface between its two domains, preventing domain closure and blocking the RNA binding cleft (Göke *et al.*, 2002; Chang *et al.*, 2009; Loh *et al.*, 2009). It is through this interaction that Pdcd4 is thought to exert its inhibitory effect on translation by blocking eIF4A's helicase activity and preventing its association with eIF4G in eIF4F (Yang *et al.*, 2004; Suzuki *et al.*, 2008; Chang *et al.*, 2009). Though both MA3 domains act synergistically to bind eIF4A with higher affinity, its MA3-c domain alone has been shown to compete with eIF4G for eIF4A binding (Yang *et al.*, 2004; LaRonde-LeBlanc *et al.*, 2007) though this has

recently been disputed (Loh *et al.*, 2009). The MA3-c domain can also bind to an additional eIF4A molecule, though the effect that this has on the cell is unclear as mutations that block this interaction do not alter Pdcd4's inhibitory effect on translation (Loh *et al.*, 2009). Furthermore, Pdcd4 can bind both eIF4G and RNA which further complicates its role in translation initiation (Kang *et al.*, 2002; Böhm *et al.*, 2003).

The regulation of Pdcd4's own expression is highly complex, being effected at the transcriptional, translational and post translational level. A full description of this control is beyond the scope of this introduction but has been recently reviewed in (Lankat-Buttgereit and Göke, 2009). Of note is its phosphorylation by S6 kinase through the mTOR pathway in response to growth factors which targets Pdcd4 for ubiquitination, leading to its degradation by the proteasome, thus relieving eIF4A inhibition (Dorrello *et al.*, 2006). Analysis of the downstream effects of Pdcd4 mediated inhibition of translation has often been contradictory which may be explained by the observation that its actions may be cell-type specific (Lankat-Buttgereit *et al.*, 2008). Despite this, research directed towards understanding the activity of Pdcd4 is an exciting area of cancer research as *in vivo* models utilising its tumour suppressor activity have demonstrated remarkable anti-neoplastic activity (Jansen *et al.*, 2005; Hilliard *et al.*, 2006; Jin *et al.*, 2006; Hwang *et al.*, 2007). Pdcd4 expression has been shown to downregulate the c-jun activating kinase MAP4K1/ hematopoietic progenitor kinase 1 and therefore AP-1-dependent transcription, and this effect was demonstrated to be anti-tumourigenic in human carcinoma cells (Yang *et al.*, 2006). Furthermore, Pdcd4 deficient mice, though susceptible to lymphoma formation, were resistant to inflammatory diseases possibly through the selective increase in expression of anti-inflammatory cytokines IL-4, IL-10 and IFNγ (Hilliard *et al.*, 2006). The authors observe that the mRNAs of these cytokines all contain structured 5' UTRs which may contribute to this selectivity. Translational control of inflammation and the implications for regulating eIF4A activity will be discussed in more detail in Chapter 5.

1.14.2 Nucleolar MIF4G-containing protein (NOM1)

Nucleolar MIF4G-containing protein 1 (NOM1) was identified as a gene that lies in close proximity to the chromosome 7q36 breakpoint located in patients with a form of paediatric acute myeloid leukaemia (AML) characterised by a 7;12 chromosomal translocation (Simmons *et al.*, 2002; Simmons *et al.*, 2005). NOM1 shares the conserved MIF4G and MA3 domains with eIF4GI/II and has been shown to bind all three isoforms of eIF4A (Simmons *et al.*, 2005) though the impact that this may have on translation initiation is yet to be ascertained. More recently NOM1 has been shown to interact directly with protein phosphatase 1 (PP1), an essential serine/threonine phosphatase involved in a number of cellular processes (Ceulemans and Bollen, 2004; Gunawardena *et al.*, 2008). PP1 usually displays a nuclear distribution and is excluded from the nucleolus but NOM1 targets it to the nucleolus (Gunawardena *et al.*, 2008).

1.14.3 15-deoxy-delta(12,14)-prostaglandin J_2

Microbial infection or tissue damage results in the host mediating a localised inflammatory response that attracts cells of the immune system to the site of infection/damage. One of the main actions of these cells is to engulf any foreign or damaged material by phagocytosis and degrade this in their phagolysosomes. The unintentional release of the phagolysosomal contents into the surrounding tissue propagates the inflammatory response and causes additional cellular damage. To counteract this, a pro-resolution response is instigated shortly after the pro-inflammation response which begins to facilitate the apoptosis of the cells of the immune system once the initial insult has been dealt with. These responses prevent the perpetuation of damage caused by acute inflammation and restore homeostasis. Both responses are in part coordinated by a group of lipid signaling molecules termed eicosanoids of which there are four families: the prostaglandins, the leukotrienes, the prostacyclins and the thromboxanes. The prostaglandins are formed by the sequential oxidation of arachidonic acid or other fatty acids by cyclooxygenase (COX) 1 and 2. A number of prostaglandins have demonstrated anti-inflammatory or pro-resolution activities including the cyclopentenones PGJ_2 and its derivative 15-deoxy-

delta(12,14)-prostaglandin J_2 (15d-PGJ_2) (Straus and Glass, 2001). PGJ_2 and its derivatives have been recognised as having both anti-proliferative and anti-tumourigenic effects and much work has been done to understand the cellular pathways that they are involved in (Fukushima, 1990). The actions of 15d-PGJ_2 were originally disputed as being physiologically irrelevant as it was difficult to assess whether *in vivo* quantities were sufficient to elicit a biological response. It has now been established, however, that levels of 15d-PGJ_2 increase during an inflammatory response and it is now recognised as an important mediator during inflammation resolution, providing a natural feedback loop (Gilroy *et al.*, 1999; Straus and Glass, 2001).

15d-PGJ_2 mediates some anti-inflammatory activity by acting as an agonist of the transcription factor PPARγ (peroxisome proliferator-activated response-γ) which represses the transcription of pro-inflammatory mRNAs (Forman *et al.*, 1995; Kliewer *et al.*, 1995; Jiang *et al.*, 1998; Ricote *et al.*, 1998). 15d-PGJ_2 also blocks the pro-inflammatory signaling cascade of NF-κB independent of PPAR-γ (Straus *et al.*, 2000) and covalently modifies c-jun, inhibiting AP-1 dependent signaling (Pérez-Sala *et al.*, 2003). More recently 15d-PGJ_2 was recognised as a natural inhibitor of translation after the observation that it induced stress granule formation in the absence of eIF2α phosphorylation (Kim *et al.*, 2007). 15d-PGJ_2 is able to interact directly with eIF4AI through cysteine residue 264 and this interaction prevents eIF4AI's association with eIF4GI (Kim *et al.*, 2007). The physiological relevance of translational inhibition caused by 15d-PGJ_2 inhibition of eIF4AI activity is yet to be ascertained. It is likely that translational inhibition will produce an immediate cellular response before the effects of PPAR-γ agonism are realised, however, whether translation initiation is affected in general or whether pro- or anti-inflammatory mRNAs are particularly targeted remains to be determined.

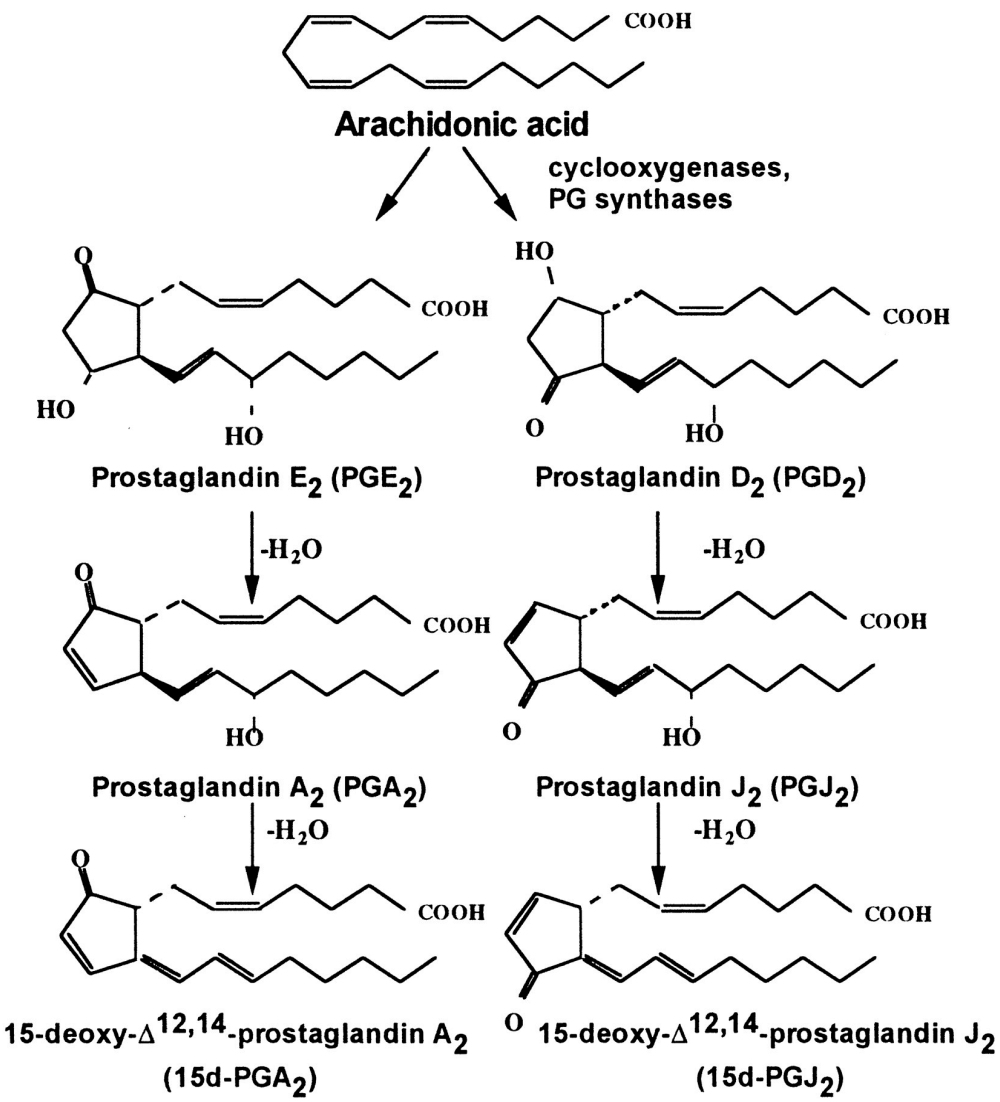

Figure 1.7 15d-PGJ_2 synthesis pathway
Diagramatic representation of the synthesis pathway of 15d-PGJ_2 from Arachidonic acid, taken from Petrova *et al.*1999.

1.15 eIF4B

eIF4B is an 80 kD dimeric protein that was initially isolated with the cap-binding complex and has been shown to increase both eIF4A's affinity for RNA and its helicase activity (Ray *et al.*, 1985; Abramson *et al.*, 1988; Rogers *et al.*, 1999). A yeast strain expressing a mutated variant of TIF3, eIF4B's homologue in yeast, inhibited the translation of mRNAs containing secondary structure in their 5' leader sequences indicating its stimulatory effect on helicase activity (Altmann *et al.*, 1993). eIF4B contains two regions capable of binding RNA: an arginine-rich region in its C-terminus which binds RNA with high affinity in a non-specific manner (Méthot *et al.*, 1994; Naranda *et al.*, 1994), and a second RRM near its N-terminus (Milburn *et al.*, 1990) which binds specifically to the 18s rRNA of the 40S SSU (Methot *et al.*, 1996a), thus explaining the observed requirement of eIF4B for ribosome recruitment to an mRNA (Trachsel *et al.*, 1977; Benne and Hershey, 1978). In addition, eIF4B also displays RNA annealing activity that is ATP and Mg^{2+} independent (Altmann *et al.*, 1995). Furthermore human eIF4B has been shown to bind PABP through its N-terminus (Bushell *et al.*, 2001) and interacts with eIF3a through its DRYG domain (Methot *et al.*, 1996b). Like eIF4G, eIF4B is subject to post-translational modifications in response to mTOR signaling and cellular stress that alter its activity in the cell. eIF4B is thought to be phosphorylated on a number of residues, but the only characterised modification is by S6 kinase on Ser-422 (Raught *et al.*, 2004). This results in the enhancement of translation and increased binding of eIF3a (Raught *et al.*, 2004; Holz *et al.*, 2005; Shahbazian *et al.*, 2006; Kroczynska *et al.*, 2009). During apoptosis eIF4B is cleaved near its N-terminus both in a caspase-3 dependent (Bushell *et al.*, 2000) and independent manner (Jeffrey *et al.*, 2002). The effect that this cleavage has on translation initiation is unclear, as though it prevents its association with PABP, cleaved eIF4B is still able to associate with eIF4F (Bushell *et al.*, 2000).

1.16 eIF4H

eIF4H is 25 kD protein homologous to eIF4B over its entire sequence, though eIF4B contains additional N- and C-TDs (Richter-Cook *et al.*, 1998). eIF4H also

contains an RRM which is 45% identical to that of eIF4B and has also been shown to enhance the helicase activity of eIF4A (Rogers *et al.*, 1999; Rogers *et al.*, 2001b). Though it is suspected that the stimulation of eIF4A by eIF4B or eIF4H occurs through a direct interaction, it has been difficult to establish this experimentally. This lack of available evidence is perhaps due to the weakness of the interaction or that a particular conformation of eIF4A's domains is required, and no crystal structures of either eIF4B or eIF4H in complex with eIF4A have been resolved. The formation of stable complexes in the presence of AMPNP and RNA have been described (Rozovsky *et al.*, 2008) and a yeast-two hybrid screen of eIF4H binding proteins positively identified eIF4AII (Feng *et al.*, 2005). By performing GST-pulldown assays with truncated versions of eIF4H, Feng and coworkers were also able to establish that reductions of as little as 37 amino acids to the C-terminal end of eIF4H resulted in the abolition of eIF4AII binding (Feng *et al.*, 2005). Recently NMR analysis established that eIF4H contacts eIF4AI on its C-TD and that the C-terminal 72 amino-acid residues of eIF4H were sufficient to demonstrate this binding, though a weaker interaction between eIF4H's N-TD and eIF4AI's C-TD was also observed (Marintchev *et al.*, 2009). Marintchev and coworkers also observed that the interaction between eIF4AI and eIF4H was too weak to observe using SPR, however, after the addition of ATP or ADP a complex could be observed which displayed differential dissociation rates dependent on the nucleotide substrate; a slow dissociation of the complex was seen in the presence of ATP but not ADP (Marintchev *et al.*, 2009). In conclusion, the authors predicted that eIF4H may bind behind eIF4AI and therefore aid helicase activity by stabilising the single stranded mRNA that it has previously unwound, preventing it from reannealing (Marintchev *et al.*, 2009).

eIF4H has also been implicated in mediating the specific degradation of mRNAs after herpes simplex viral (HSV) infection by binding to the virion host shutoff (Vhs) protein (Feng *et al.*, 2001). Vhs is an endoribonuclease that is released after the uncoating of the infecting virion and acts to selectively destabilise the host's mRNA to thereby favour the synthesis of the virion's own proteins (Fenwick and McMenamin, 1984; Schek and Bachenheimer, 1985; Strom and

Frenkel, 1987; Smibert *et al.*, 1992). Vhs activity was shown to be dependent on eIF4H (Feng *et al.*, 2001) and later research demonstrated that eIF4AII also formed part of the degradative complex through an eIF4H-independent interaction with Vhs (Feng *et al.*, 2005). No binding between eIF4AI and Vhs was established by a far-western blotting technique, which may reflect a genuine difference in complex requirements of Vhs, though the technique doesn't establish whether an interaction could occur if eIF4AI was native (Doepker *et al.*, 2004). The role that eIF4AI/II has to play in this behaviour, whether passive or active, is yet to be determined. eIF4B has also been shown to bind Vhs (Doepker *et al.*, 2004) and it will be interesting to ascertain whether the additional domains of eIF4B target the degradation of alternative mRNAs than the eIF4H complex.

1.17 Other eIF4A binding proteins

1.17.1 RBM4

RNA binding motif 4 (RBM4), known as Lark in *Drosophila*, is an RNA binding protein that is associated with several post-transcriptional cellular processes including translation initiation. RBM4 is a nucleo-cytoplasmic shuttling protein (Lai *et al.*, 2003) that is phosphorylated in response to cellular stress on serine residue 309 by the MAPK-p38 signaling pathway (Lin *et al.*, 2007). Phosphorylation targets RBM4 to stress granules, however, under these conditions it is also able to stimulate the cap-independent translation of some IRES-containing mRNAs, possibly through an interaction with eIF4A (Lin *et al.*, 2007). RBM4 has also been shown to interact with two members of the argonaute protein family, Ago1 and Ago2, and this association is thought to influence miRNA-mediated cleavage of mRNAs (Höck *et al.*, 2007).

1.17.2 HuD

The Hu family (also known as ELAV (embryonic lethal abnormal vision)) are classical RNA binding proteins that contain three RRMs that are 90 % homologous between the four vertebrate members (Okano and Darnell, 1997).

Three members of the family, HuB, HuC and HuD are specifically expressed in neurons and are essential for neuronal development, whereas HuR (HuA) is constitutively expressed (reviewed by (Hinman and Lou, 2008). The most documented function of the Hu family of proteins is the regulation of mRNA stability, however they have also been linked with the regulation of translation. Recent advances in the understanding of the mechanism by which HuD mediates translational control has demonstrated an ability to bind both eIF4A and the poly(A) tail and this synergistically enhances cap-dependent translation (Fukao *et al.*, 2009). In this manner it is very similar to Paip1, although HuD does not interact with PABP but the poly(A) tail, and may therefore affect the translation of a similar set of mRNAs. This may occur through an increased stability of the closed-loop complex, enhancing ribosomal reinitiation, or through the stimulation of eIF4A. The ability of HuD to induce neurite outgrowth is dependent on both its ability to interact with the cap-binding complex and the presence of active eIF4AI (Fukao *et al.*, 2009). It is likely that eIF4AI's helicase activity is required for some of HuDs cellular roles but further research is required to understand the mechanism through which HuD influences translation.

1.17.3 *Drosophila* Mad/Medea

Decapentaplegic (dpp) in *Drosophila* is a member of the TGF-β (transforming growth factor-β) family of signaling molecules and is crucial for the correct development of the *Drosophila* embryo. A genetic screen established to identify maternal suppressors of *dpp* haploinsufficiency detected a role for eIF4A (Li *et al.*, 2005). It was later established that the control of this pathway of control is directed by the helicase. This occurs through the physical association of eIF4A with two of the signaling molecules in this pathway, Mad and Medea, eIF4A is able to target their degradation and thus inhibit dpp signaling (Li and Li, 2006). This indicates that eIF4A may serve additional roles within the cell which is outside of the realms of translation initiation.

1.17.4 Cyclin dependent kinase (CDK) 4

A possible mechanism linking cell proliferation and translation has been proposed by Hutchins *et al.* following the discovery of a novel protein-protein interaction between eIF4A and cyclin dependent kinase A (CDKA) in *Arabidopsis*. CDKs are a family of serine/threonine kinases involved in cell cycle control and progression: the isolation of the eIF4A-CDKA complex from cells that were actively proliferating may indicate that eIF4A has another chaperone role within the cell that targets CDKA to the translation machinery (Hutchins *et al.*, 2004).

1.17.5 Plakophilin 1

The plakophilins (PKPs) 1-3 are desmosomal plaque proteins involved in cellular adhesion but have recently been linked to translational control. Both PKP1 and 3 associate with stress granules in response to cellular stress (Hofmann *et al.*, 2006) and this observation led to the discovery that PKP1 is a novel stimulator of eIF4AI activity (Wolf *et al.*, 2010). PKP1 associates with eIF4AI via its N-terminal head domain and stimulates its ATPase activity and also the recruitment of eIF4AI and eIF4B to the 5' cap of mRNAs (Wolf *et al.*, 2010). Knockdown of PKP1 was also associated with a reduction in cell size and a decrease in cellular proliferation, which is indicative of a role of PKP1 in cell growth (Wolf *et al.*, 2010). Indeed PKP1 overexpression has been observed in some cancers, such as Ewing's sarcoma (Cheung *et al.*, 2007a) and some head and neck carcinomas (Villaret *et al.*, 2000) leading to the hypothesis that its role in stimulating translation may be contributory to tumourigenesis (Wolf *et al.*, 2010). Ablation of PKP1 is also the cause of an autosomal recessive disease called ectodermal dysplasia/skin fragility (EDSF) syndrome (McGrath *et al.*, 1997) therefore a further understanding of its role in translation initiation may help to identify it as a potential therapeutic target.

1.18 Non-protein specific modulators of eIF4A activity

1.18.1 BC1 non-protein-coding RNA

BC1 is a non-protein-coding (npc), dendritic RNA (Tiedge *et al.*, 1991) that is targeted to dendrites (Muslimov *et al.*, 1997; Muslimov *et al.*, 2006) and enriched at the synapses (Chicurel *et al.*, 1993) and suppresses translation initiation by targeting the activity of eIF4AI and PABP (Wang *et al.*, 2002; Kondrashov *et al.*, 2005; Wang *et al.*, 2005). Both BC1 and BC200, BC1's mouse homologue (Tiedge *et al.*, 1993), are able to bind to eIF4AI and prevent its helicase activity whilst stimulating ATPase activity, thereby uncoupling these two processes (Lin *et al.*, 2008). In this manner BC1/200 is able to inhibit eIF4AI dependent translation initiation.

An *in vitro* RNA selection method termed SELEX (Systematic Evolution of Ligands by Exponential Enrichment) (Ellington and Szostak, 1990; Tuerk and Gold, 1990) was used to identify RNA molecules that are able to bind eIF4AI (Oguro *et al.*, 2003). Of those selected, aptamer 21 stood out for its ability to alter eIF4AI activity by inhibiting its ATPase activity and thus suppressing translation initiation *in vitro* (Oguro et al., 2003). Aptamer 21 is an 87 nt, highly structured artificial RNA molecule that contains a core 58 nt region responsible for its interaction with eIF4AI (Oguro *et al.*, 2003). The same laboratory has also identified RNA aptamers that inhibit eIF4GI and eIF4E (Mochizuki *et al.*, 2005; Miyakawa *et al.*, 2006). Due to the ease and low cost of their manufacture, aptamers offer a financially viable way of targeting specific proteins both for research and therapeutic intervention.

1.19 Natural small molecule modulators of eIF4A activity

1.19.1 Hippuristanol

Hippuristanol was first isolated from the gorgonian *Isis hippuris* (Shen et al., 2001) and later identified as a specific inhibitor of eIF4A (Bordeleau *et al.*, 2006b). Hippuristanol interacts with the C-TD of eIF4AI and inhibits its ATPase activity, its RNA binding activity and its helicase activity in a dose dependent

manner (Bordeleau *et al.*, 2006b). Other members of the DExD/H extended family of proteins are not affected by hippuristanol due to amino acid sequence differences in its binding site (Bordeleau *et al.*, 2006b; Lindqvist *et al.*, 2008). eIF4AI and II share considerable sequence homology in their hippuristanol binding site and are inhibited to a similar extent (Lindqvist *et al.*, 2008). There are seven differences, however, in the equivalent amino acids in eIF4AIII and a 10 X increase in hippuristanol is required to achieve an inhibitory effect similar to that observed for eIF4AI/II (Lindqvist *et al.*, 2008). Recently the protocol to chemically synthesise hippuristanol from hydrocortisone has been described (Li *et al.*, 2009) and the exact chemical groups that contribute its anti-proliferative properties are being researched (Li *et al.*, 2010).

1.19.2 Pateamine A

Pateamine A is an antiproliferative and proapoptotic marine product isolated from the marine sponge *Mycale* sp (Northcote *et al.*, 1991; Hood *et al.*, 2001). Pateamine A appears to exert its cellular effects by binding and stimulating eIF4A activity (Bordeleau *et al.*, 2005; Low *et al.*, 2005; Bordeleau *et al.*, 2006a; Low *et al.*, 2007). Low *et al.* observed that pateamine A inhibited the association of eIF4A with eIF4F but enhanced its binding to eIF4B and that both of these proteins isolated to stress granules after treatment (Low *et al.*, 2005). The increased interaction between eIF4AI and eIF4B was later found to be an indirect effect of pateamine A inducing the stable binding of RNA by eIF4AI (Bordeleau *et al.*, 2006a), which was proposed to sequester it from the initiation complex. Mutational analysis of eIF4AI located pateamine A's interaction to its inter-domain linker region and initial data from limited proteolysis studies suggested that, in the presence of AMPNP (ATP) and RNA, pateamine A induced the closed conformation of eIF4AI (Low *et al.*, 2007). In addition to its inhibition of translation, by interacting with eIF4AIII, which forms part of the exon junction complex, pateamine A is also able to inhibit nonsense mediated decay (Dang *et al.*, 2009). Further research is required to understand how pateamine is able to both stimulate eIF4A activity and inhibit translation initiation.

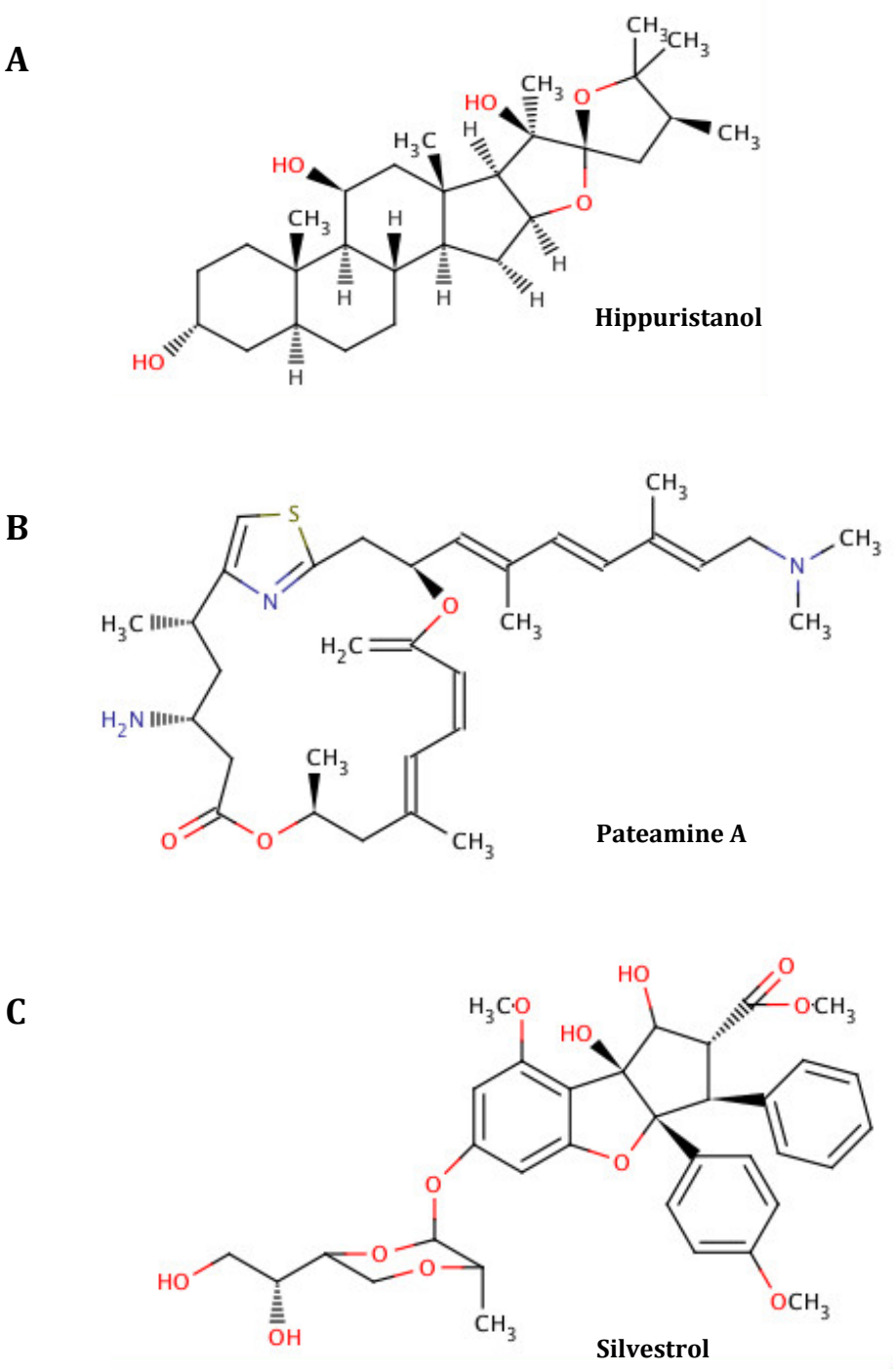

Figure 1.8. Chemical structures of small molecule inhibitors of eIF4A **(A)** Hippuristanol; **(B)** Pateamine A and **(C)** Silvestrol. Images drawn with MarvinSketch V. 5.3.8.

1.20 Silvestrol

Silvestrol was first isolated from *Aglaia silvestris* and found to have potent anti-proliferative activity (Hwang *et al.*, 2004). It was one of a number of cyclopenta[*b*]benzofuran flavaglines (CBFs) isolated from the *Aglaia* genus of Meliaceae plant family that have been identified as novel inhibitors of translation (Ohse *et al.*, 1996; Lee *et al.*, 1998; Bordeleau *et al.*, 2008). Silvestrol is able to inhibit translation in a manner similar to pateamine A by interacting directly with eIF4A and increasing its affinity for RNA (Bordeleau *et al.*, 2008) and inhibiting the formation of eIF4F, thereby reducing ribosomal recruitment (Cencic *et al.*, 2009). Silvestrol has been shown to work in synergy with the standard cytotoxic reagents (daunorubicin, etoposide, cytarabine) used for the treatment of AML and could therefore be potentially used as an adjuvant therapy in the treatment of malignancies (Cencic *et al.*, 2010).

1.21 Aims of this project

eIF4A is an integral member of the translation initiation machinery and is thought to unwind secondary structure in the 5' leader sequences of mRNAs aiding ribosomal recruitment and scanning to the start codon. It has also been implicated in a number of other cellular pathways and its deregulation is associated with several diseases. Therefore a thorough understanding of eIF4A's role within the cell and whether targeting its activity preferentially affects the translation of a specific subset of mRNAs with long and/or highly structured 5' leader sequences is required. This knowledge may potentially lead to new therapeutic opportunities. Elucidating eIF4A's mechanism of action will also allow a further insight into the mechanics of the other members of the DEAD-box family. The aims of this PhD project are therefore to investigate eIF4AI's helicase activity with the aid of eIF4A inhibitors hippuristanol and 15d-PGJ_2. To this effect a single molecule assay will be developed to allow the investigation of eIF4AI's helicase activity at a resolution greater than that achievable by bulk studies. This study will also enable the further characterisation of 15d-PGJ_2's inhibitory effect. The synthesis of the molecules to be used in these assays will be optimised and then the helicase activity of

recombinant human eIF4AI, with eIF4B, will be analysed in the presence of these inhibitors. Additionally, a further insight into the mechanism by which eIF4A inhibition, specifically by 15d-PGJ_2, targets the translation of subsets of mRNAs will be explored using polysome profiling and microarray studies. The structural differences between the population of mRNAs whose translation is selectively downregulated after eIF4A inhibition will be compared to those whose translation is upregulated or maintained. In this manner different inhibitors of eIF4A that differentially effect eIF4A activity can be compared

2 Materials and Methods

2.1 General reagents

2.1.1 Reagent and equipment suppliers

Invitrogen Ltd. 3 Fountain Drive, Inchinnan Business Park, Paisley, UK. PA4 9RF

Sigma-Aldrich Company Ltd. The Old Brickyard, New Road, Gillingham, Dorset. SP8 4XT

Roche Products Limited. 6 Falcon Way, Shire Park, Welwyn Garden City. AL7 1TW

New England Biolabs (NEB). 75 - 77 Knowl Piece, Wilbury Way, Hitchin, Herts. SG4 0TY

Fisher-Scientific. Bishop Meadow Road, Loughborough, Leicestershire. LE11 5RG

GE Healthcare (Amersham). GE Healthcare Life Sciences, Amersham Place, Little Chalfont, Buckinghamshire. HP7 9NA

2.1.2 Antibodies

Cell Signaling. Supplier - NEB

2.2 Tissue culture techniques

2.2.1 Solutions and reagents

Phosphate buffered saline (PBS): 4.3 mM Na_2HPO_4, 1.5 mM KH_2PO_4, 137 mM NaCl, 2.7 mM KCl, pH 7.4. (OXOID)

Dulbecco's Modified Eagles Medium (DMEM) (PAA)

Schneider's *Drosophila* medium (Gibco)

Express-5 medium (Gibco)

Foetal calf serum (FCS) heat-inactivated (PAA)

Foetal horse serum (FHS) heat-inactivated (PAA)

2 x HEPES-buffered Saline (HBS): 50 mM HEPES, 1.5 mM Na_2HPO_4, 280 mM NaCl, pH 7.1.

2.2.2 Cell lines and maintenance

Cell line	Origins	Description
HeLa	Human cervical epithelial carcinoma	Adherent cell line maintained in DMEM supplemented with 10% FCS and 2mM L-glutamine
SH-SY5Y	Human neuroblastoma	Adherent cell line maintained in DMEM supplemented with 10 % FCS, 1 % FHS and 2 mM L-glutamine
Hek293	Human embryonic kidney 293	Adherent cell line maintained in DMEM supplemented with 10 % FCS and 2 mM L-glutamine
S2	Drosophila Schneider (S) 2	Semi-adherent cell line maintained in Schneiders Drosophila medium supplemented with 10 % FCS

All cells were cultured in gamma sterilised, tissue culture treated plasticware (TPP)

Human cell lines were maintained at 37 ˚C, under a humidified atmosphere containing 5 % CO_2. Cells were grown to near confluence in 150 cm^2 flasks and then sub-cultured by removing the old media, washing with PBS, and treating with 1 x trypsin-0.5mM EDTA (PAA) solution to disassociate them from the flask/dish. Cells were diluted in fresh medium which had been preheated to 37 ˚C and seeded at 4 x 10^6 cells/150 cm^2 flask.

Drosophila S2 cells were maintained at 28 ˚C under atmospheric conditions. S2 cells are a semi-adherent cell line and are therefore easily passaged when they reach a density of ~ 20 x 10^6 cells/ml by resuspending them in their media by tapping the flask several times, and then sub-culturing at a density of ~ 1 x 10^6 cells/ml (never lower than 0.5 x 10^6 cells/ml) in complete medium. To assist

with cell growth, some conditioned medium (previously had cells growing in it) was carried through with the sub-culturing.

2.2.3 Isolation of total RNA

Total RNA was isolated from various human cell lines in order to use as a template for cDNA synthesis. Human cell lines were grown to confluency in a 10 cm dish and after removal of the medium, lysed in 1 ml of Tri Reagent (Sigma), using a cell scraper to ensure full lysis. The lysate was left at room temperature for 5 minutes then mixed vigorously with 0.2 ml chloroform and centrifuged at 4 ˚C, at 12,000 *g* for 15 minutes to allow the RNA, DNA and proteins to separate into the aqueous, inter- and organic phases respectively. The aqueous phase was isolated and mixed with 0.5 ml isopropanol and incubated at room temperature for 10 minutes to precipitate the RNA, which was pelleted by centrifugation at 4 ˚C, at 12,000 *g* for 10 minutes. The supernatant was removed and the RNA pellet washed in 1 ml 75 % ethanol (vortex) and centrifuged at 4 ˚C, at 7,500 *g* for 5 minutes. The supernatant was removed and the pellet was allowed to dry at room temperature before being resuspended in 50 µl RNase-free water.

2.2.4 Transient and stable transfections of S2 cells

Overexpression of post-translationally modified recombinant proteins was achieved using the *Drosophila* Expression System (DES) developed by Invitrogen and outlined in the Invitrogen manual "*Drosophila* Expression System. For the stable expression and purification of heterologous proteins in Schneider 2 cells. Version H. February 28 2003. 25-0191". The main points of the protocols are described below.

2.2.4.1 Transient transfection of S2 cells

The protein of choice was cloned into the plasmid pMT/V5-His A (Invitrogen) that allows high-level, metal inducible expression of recombinant proteins from the *Drosophila* metallothionein (MT) promoter in S2 cells. Plasmid DNA was

prepared on a large scale using maxi-prep kits (see method 2.4.5.1.3) and used as a stock for all transfections.

S2 cells were seeded at a density of 1 x 10^6 S2 cells/ml (3 ml total) in complete Schneider's *Drosophila* medium and grown at 28 °C until they reached a density of 2 - 4 x 10^6 cells/ml.

The recombinant DNA vector was transfected into the cells using the classical calcium phosphate method; a 300 μl solution containing 36 μl 2 M $CaCl_2$ and 19 μg recombinant DNA was added dropwise to 300 μl 2 X HEPES-Buffered Saline (HBS) with continual mixing and incubated for 30 minutes to allow a fine co-precipitate of DNA-$Ca_3(PO_4)_2$ to form. This mixture was added slowly to the cells, swirling the media in between each drop and the cells then incubated for 16 hours at 28 °C. The transfected cells were collected by centrifugation at 1000 *g* for 10 minutes, washed twice in complete medium and replated in 3 ml complete medium, then allowed to recover from the transfection for 2 - 3 days (until the cell count reached 2 - 4 x 10^6 cells/ml). Expression of the recombinant protein was induced with 500 μM $CuSO_4$ and the cells incubated for a further 5 days at 28˚C. To test for expression of the recombinant protein, 200 μl cell samples were taken before, and each day after, induction, pelleted and lysed in 50 μl 1 x lysis buffer (50 mM Tris, pH 7.8; 150 mM NaCl; 1 % Nonidet P-40), separated by SDS-PAGE and analysed by Coomassie Blue staining or western blotting as described in 2.4.27-28.

2.2.4.2 Stable transfection of S2 cells

In order to generate a stable cell line capable of expressing a recombinant protein of choice the transient transfection protocol was followed as above with the addition of 1 μg pCoBlast plasmid DNA (Invitrogen) which allows positive selection of successful transfectants in the presence of the antibiotic blasticidin. After cells were washed and allowed to recover from the transfection for two days they were replated in fresh medium containing 25 μg/ml Blasticidin (Invitrogen). The selective medium was replaced every 4 - 5 days until resistant

colonies appeared (this generally took 1 week). Resistant cells were replated into larger vessels when they reached a density of 6 – 20 x 10^6 cells/ml in order to expand the population. Once the culture was more that 200 ml the cells were transferred to a Nalgene sterile filter bottle and grown in a shaking incubator (110 rpm, 28 °C). To avoid clumping of cells before induction, serum-free Express-5 medium was added to reduce the cell density until a volume of 500 ml was reached (never reducing the cell count below 1 x 10^6 cells/ml). Blasticidin was no longer added to the medium as stable S2 cell lines can lose their resistance in serum free medium, however, Invitrogen note that they have maintained Blasticidin-resistant S2 cells for up to a week without selective medium. After 5 days, or when the cell density reached ~8 x 10^6 cells/ml, protein expression was induced by adding 500 μM $CuSO_4$. Cells were harvested 4 days after induction, pelleted by centrifugation for 30 minutes at 1000 *g*, and stored at - 80 °C.

2.3 Bacterial methods

2.3.1 Solutions and reagents

Lysogeny Broth (LB) medium: 10 g Bactotryptone (OXOID); 5 g Bacto-yeast extract (OXOID); 10 g NaCl in 1 l; pH 7 (adjusted with NaOH); autoclaved.
LB agar: As above with the addition of 15 g bacto agar before autoclaving.

2.3.2 Bacterial strains used

TOP10 (Invitrogen) – F- *mcr*A Δ(*mrr-hsd*RMS-*mcr*BC) φ80*lac*ZΔM15 Δ*lac*X74 *rec*A1 *ara*D139 Δ(*ara- leu*)7697 *gal*U *gal*K *rps*L (StrR) *end*A1 *nup*G. Prepared using the method described in 2.3.3
DH5α (Promega) – *F' ϕ80dlacZΔM15 Δ(lacZYA-argF) U169 deoR recA1 endA1 hsdR17 phoA supE44 λ- thi-1 gyrA96 reA1.* Prepared by L. Cobbold using the method as specified in the Promega handbook.
Nova blue (Novagen) – *endA1 hsdR17* (r_{k12}^- m_{k12}^+) *supE44 thi-1 recA1 gyrA96 relA1 lac F'*[*proA*$^+$*B*$^+$*lacI*^{q}*ZΔM15::*T*n10*] (Tet^R). Prepared by H. Dobbyn using the method as specified in the Promega handbook.

BL21 (DE3) (Novagen) – F^- *ompT hsdS*$_B$ (r_B, m_B) *dcm gal λ(DE3).* Prepared by H. Booden using the method as specified in the Promega handbook.

2.3.3 Preparation of chemically competent *E. coli*

E. coli cells, made chemically competent through a series of washes in salt solutions, readily uptake plasmid DNA during a brief period of heat-shock at 42 ˚C. The downstream efficiency of transformation is greatly decreased by allowing the cells to warm up to temperatures greater than 4 ˚C, therefore all solutions and pipettes are chilled prior to use, and cells are kept on ice at all times during their preparation.

To make the cells a 500 ml LB culture was inoculated with a 5 ml starter culture (prepared the previous night from a fresh *E. coli* colony) and grown at 37 ˚C in a shaking incubator (220 rpm) until the absorbance at 560 nm (A_{560}) reached ~ 0.5 (3 - 4 hours) in the absence of antibiotic. The culture was then cooled on ice, decanted into sterile 50 ml falcon tubes and the cells pelleted by centrifugation at 4000 rpm (3200 *g*) at 4 ˚C for 10 minutes. The cell pellets were resuspended in 50 ml (total) ice-cold 0.1 M $MgCl_2$ by swirling gently, decanted into 2 x 50 ml falcon tubes and then pelleted again by centrifugation as described above. The cell pellets were then resuspended in 50 ml (total) ice-cold 0.1 M $CaCl_2$ by swirling and incubated on ice for at least 20 minutes. After pelleting again (using the centrifugation procedure as described above), the cells were resuspended in 14.3 ml ice-cold 0.1 M $CaCl_2$ and 2.3 ml glycerol and then aliquoted into sterile ependorfs and snap-frozen in liquid nitrogen. Cells were stored at – 80 ˚C.

2.3.4 Transformation of chemically competent cells

50 µl of competent cells were thawed on ice and added to 10 ng of plasmid DNA or ligation products and incubated on ice for 15-20 minutes. Cells were heat shocked at 42 ˚C for 1 minute and incubated on ice for a further 2 minutes before adding 400 µl of LB medium. Cells were incubated at 37 ˚C in a shaking incubator (220 rpm) for 40 minutes to allow them to acquire antibiotic

resistance before plating them on an LB agar plate containing either 1 x ampicillin (100 μg/ml) or 1 x kanamycin (30 μg/ml) depending on the resistance of the vector. Plates were incubated overnight at 37 ˚C.

2.3.5 Overexpression of recombinant proteins

Using protocol 2.3.3, a bacterial expression vector containing the recombinant protein of choice was transformed into the expression *E. Coli* cell line BL21 (DE3) and colonies were allowed to grow overnight. A single colony was inoculated into a 5 ml culture (LB plus 1 x antibiotic) and grown overnight at 37 °C with shaking (220 rpm). This starter culture was used to inoculate 500 ml LB + 1 x antibiotic, which was grown until it reached an A_{560} of ~ 0.5 (3 - 4 hours). Protein expression was induced by the addition of 1 mM isopropyl β-D-1-thiogalactopyranoside (IPTG) and the culture grown for 2 - 16 hours (see below). Cells were pelleted by centrifugation at 7000 rpm (~ 10,000 *g*) for 15 minutes at 4 °C and stored at – 80 °C.

To determine the time required for sufficient expression of the recombinant protein, initially a trial expression was performed using a smaller culture volume (10 ml). The steps described above were performed and 1 ml culture samples taken before and at time-points after (e.g. 2, 4, 8, 16 hours) induction with 1 mM IPTG. At each time-point the A_{560} was recorded. Samples were pelleted by centrifugation for 5 minutes at maximum speed (13,400 rpm, 17,000 *g*) and stored at – 20 °C. Once all samples had been taken, cell pellets were resuspended according to their A_{560} reading (A_{560}: 1 = 100μl dH_20), and lysed by sonication (Bioruptor, Diagenode; 60 % power; setting H (High) 320 W; 4 x 10 seconds). Insoluble proteins were pelleted by centrifugation at maximum speed for 1 minute. The supernatant containing soluble proteins was placed into a fresh 1.5 ml ependorf tube and the insoluble fraction resuspended in an equal volume of dH_2O. 20 μl of each lysate sample was separated by SDS-PAGE and visualised by Coomassie Blue staining, as described in 2.4.26-28. These gels were used to identify the optimum time required for induction of expression to allow the maximum yield of soluble recombinant protein.

2.4 Molecular biology techniques

2.4.1 Buffers and solutions

TE: 10 mM Tris-HCl, pH 7.5; 1 mM EDTA.

1 x TAE: 40 mM Tris; 40 mM acetic acid; 1 mM EDTA; pH 8.0.

1 x TBE: 89 mM Tris base; 89 mM boric acid; 2.5 mM EDTA; pH 8.0.

6 x TAE loading buffer: 30 % (v/v) glycerol; 0.25 % (w/v) bromophenol blue; 0.25 % (w/v) xylene cyanol.

5 x MOPS: 0.1 M MOPS, pH 7.0; 10 mM sodium acetate; 5 mM EDTA, pH 8.0; pH 7.0.

RNA loading dye: 50 % (v/v) glycerol; 1 mM EDTA, pH 8.0; 0.25 % (w/v) bromophenol blue; 0.25 % (w/v) xylene cyanol.

UREA loading dye: 8 M UREA; 20 mM Tris, pH 8.0; 1 mM EDTA, pH 8.0; 0.05 % (w/v) bromophenol blue.

Hybridisation buffer: 80 % formamide; 0.4 M NaCl; 40 mM Pipes, pH 6.4; 1 mM EDTA.

20 X SSC: 3 M NaCl, 0.3 M sodium citrate, pH 7.

Church Gilbert's: 14.4 mM Na_2HPO_4, 5.6 mM NaH_2PO_4, 1 mM EDTA, 1 % SDS

2.4.2 Oligonucleotide sequences

ODC hairpin sequence (overlapping oligonucleotides for hybridisation)

atgacgattcgtcagtccctgcagccgccgccgccggccgcct ODC hp1 F2

gccgccgccgccggccgccttcagtcagcagctcggcgccacctccggtcggcga ODC hp1 F1

cgccccgtcagccgcctcgtcgagcccgccgcagtcgccgaccggaggtggcgc ODC hp1 R1

tcgatggatccgtcttcccgccgccgccccgtcagccgcctcg ODC hp1 R2

2.4.3 Primer sequences

ODC hairpin construct primers

TAATACGACTCACTATAGGGAGCCGAAAAGTGCCACCTGACG, pGEM4Z T7 2242F

GGCCTTTTTACGGTTCCTGG, pGEM4Z 493 R

ATAAACAAATAGGGGaTCCGCGCACATTTCC, pGEM4Z 2218 EcoRI F

TAAATCCAATTCACTGGCCG, pGEM4Z 2733 R

GCAACGCGGCCTTTTTACGG, pGEM4Z Thiol 500 R

TCTAGAGTCGACCTGCAGGC, pGEM4Z 33F (plus a version phosphorylated at the 5' end)

eIF4A cloning primers

GGGGGATCCATGTCTGCGAGC, F eIF4A1 pGAT2 Bam HI

AGTCAAGCTTTCAGATGAGGTC, R eIF4AI pGAT2 Hind III

eIF4B cloning primers (*Drosophila*)

GATATACGGTACCATGGCGGCCTCAGC, eIF4B KpnI pMT/V5-His B F

CCGGGCCCTCTTCGGCATAATCTTC, eIF4B ApaI pMT/V5-His B R

2.4.4 Purification of nucleic acids

2.4.4.1 Extraction of DNA from cell cultures

Two main methods were used for the extraction and purification of plasmid DNA from transformed *E. coli* depending on the downstream use of the plasmid DNA. Colonies screened for cloned plasmids were purified from mini-cultures of 700 µl-1 ml cultures using the crude mini-prep method. Plasmid DNA purified for all other applications was extracted and purified from *E. coli* cultures using either the SV Wizard Mini-prep Kits (Promega) for 5 – 10 ml cultures, or the Nucleobond Xtra Maxi kit (Macherey-Nagel) for 300 ml cultures.

2.4.4.1.1 Crude DNA extraction for colony screening

Single *E. coli* colonies were inoculated into 700 µl LB medium containing antibiotic and incubated at 37 ˚C overnight in a shaking incubator. Cells were pelleted by centrifugation at 13,400 rpm (~17,000 *g*) for 5 minutes and the pellet resuspended in 100 µl TE. Cells were lysed by adding 200 µl of solution II (0.2 M NaOH, 1 % (w/v) SDS) and mixed gently prior to incubation at room temperature for 5 minutes. Proteins were precipitated by adding 150 µl of 7.5 M ammonium acetate, pH 7.6, and pelleted by centrifugation at 13,400 rpm for

10 minutes. The supernatant was transferred to a fresh ependorf containing 900 µl 100% ethanol and plasmid DNA precipitated by centrifugation at 13,400 rpm for 30 minutes. The DNA pellet was allowed to dry at room temperature before being resuspended in 20 µl of sterile water. 3 µl of prepared plasmid DNA was used in diagnostic restriction digests including RNase A to identify successful clones.

2.4.4.1.2 Preparation by SV Wizard Mini-prep kits

To produce plasmid DNA at a standard suitable for transfection Wizard® *Plus* Minipreps DNA Purification System (Promega) was used according to the manufacturer's instructions to produce up to 25 µg plasmid DNA.

2.4.4.1.3 Preparation by Maxiprep kits

To produce large amounts of plasmid DNA at a standard suitable for transfection Nucleobond Xtra Maxi kit (Macherey-Nagel) was used according to the manufacturer's instructions.

2.4.5 Agarose gel electrophoresis

Nucleic acids were separated according to their molecular weight by electrophoresis through agarose gels. In general 1 % (w/v) agarose was melted in 1 x TAE and cast in a gel tray after the addition of 2 µl 10 mg/ml ethidium bromide. DNA samples were mixed with 6 x loading buffer and loaded into the gel. Gels were submerged in 1 x TAE buffer in a horizontal electrophoresis tank and electrophoresed at approximately 120 V for 20 – 40 minutes. DNA was visualised with a UV transilluminator.

2.4.6 Purification of DNA from agarose gel

2.4.6.1 Using Wizard columns

DNA fragments were cut from agarose gels and purified using the Wizard® SV Gel and PCR Clean-Up System (Promega) as specified by the manufacturer. DNA was typically eluted in 50 µl sterile water.

2.4.6.2 Using Qiagen columns

DNA fragments were cut from agarose gels and purified using the Qiaquick spin columns (Qiagen) as specified by the manufacturer. DNA was typically eluted in 50 µl sterile water.

2.4.6.3 Using glass wool

The excised gel fragment was centrifuged at 13,000 rpm (~ 17,000 g) for 10 minutes through a glass wool column, packed into a 0.5 ml ependorf which had been pierced at the bottom with a needle. DNA was purified and precipitated as in 2.4.5.4 and 2.4.5.5.

2.4.6.4 Using liquid nitrogen

The excised gel fragment was snap frozen in liquid nitrogen to make the gel matrix brittle before vortexing for 1 minute and centrifuging at 13,000 rpm (~ 17,000 g) for 10 minutes. Liquid liberated from the gel slice was transferred to a fresh ependorf and the process repeated three times. Any remaining liquid contained in the gel slice was freed by following the glass wool method above (2.4.5.3.3). DNA was purified and precipitated as in 2.4.5.4 and 2.4.5.5.

2.4.7 Phenol: chloroform extraction

Phenol: chloroform extraction was performed to remove any contaminating proteins from DNA samples. An equal volume of phenol: chloroform was added to the nucleic acid solution and mixed by vortexing until an emulsion formed. The aqueous and organic layers were separated by centrifugation at 13,400 rpm (~ 17,000 g) for 1 minute at room temperature. The aqueous phase was transferred to a fresh ependorf and an equal volume of chloroform added. The solution was mixed and separated as above and the aqueous layer transferred to a fresh ependorf prior to DNA precipitation.

2.4.8 DNA precipitation

DNA was precipitated by adding 0.1 % (v/v) 3 M NaOAc, pH 5.2 and 300 % (v/v) 100% ethanol incubating the solution at – 20 ˚C for 20 minutes. The precipitate was pelleted by centrifugation at 13,400 rpm (~ 17,000 g) for 30

minutes at 4 ˚C. The pellet was washed with 75 % ethanol to remove excess salt and allowed to dry for 5 - 10 minutes before being resuspended in 20 - 50 µl sterile water.

2.4.9 Determination of nucleic acid concentrations

The concentrations of DNA and RNA were determined spectrophotometrically by measuring the absorbance at 260 nm (A_{260}).

2.4.10 cDNA first strand synthesis

cDNA was synthesised from total mRNA extracted from cell monolayers and used as a template for PCR reactions. 5 µg total RNA, isolated using the protocol 2.1.4., in a total 12 µl reaction mixture with 1µl 10 mM dNTPs and 1µl 0.5 µg/µl oligo$(dT)_{15}$, was denatured at 65 ˚C for 5 minutes. The reaction mixture was placed on ice for 1 minute before adding 4 µl 5 x reverse transcriptase buffer (with 25 mM $MgCl_2$), 2µl 0.1 M Dithiothreitol (DTT) and 1 µl RNase inhibitor and incubating at 42 ˚C for 2 minutes to allow the primers to anneal. To start the polymerase reaction 1 µl (200 units) of SuperScript II reverse transcriptase (Invitrogen) was added to the reaction mixture and the solution incubated at 42 ˚C for a further 50 minutes. The reaction was terminated by incubating the mixture at 70 ˚C for 15 minutes, and the cDNA was then stored at – 20 ˚C.

2.4.11 Polymerase chain reaction

DNA was amplified using the polymerase chain reaction (PCR) from cDNA or vector templates and used in downstream applications such as cloning and northern blotting. PCRs were performed using Phusion DNA polymerase (Finnzymes) or Taq DNA polymerase (Roche) according to the manufacturer's instructions. In brief, approximately 10 - 50 ng vector or 100 - 200 ng cDNA template DNA was added to a Phusion 50 µl reaction mixture containing 1 x Phusion HF Buffer (Finnzymes), 200 µM dNTPs, 100 ng of each primer, 5 % DMSO and 1 unit of Phusion DNA polymerase; or a Taq 50 µl reaction mixture containing 1 x Taq polymerase buffer + $MgCl_2$, 200 µM dNTPs, 200 ng of each

primer, 5 % DMSO and 1.25 unit of Taq DNA polymerase. Reactions were performed in a Techne TC-512 gradient PCR machine. DNA was first denatured at 98 ˚C (Phusion) or 94 °C (Taq) for 2 minutes before entering a cycle of denaturation at 98/94 ˚C for 30 seconds, annealing at 50 – 65 ˚C for 30 - 45 seconds and extension at 72 ˚C for 1 minute. After a total of 35 cycles the reaction entered a final extension phase at 72 ˚C for 5 minutes. Products were cooled and then analysed by agarose gel electrophoresis.

2.4.12 Restriction enzyme digestion

Restriction digests of DNA were performed with restriction enzymes using the buffers recommended by the manufacturer. The reaction volume was typically 50 µl and the reaction was incubated at the recommended temperature for 1 - 2 hours. Digests that used two different enzymes that required different buffers were performed sequentially; after the required incubation period the first enzyme was denatured at 65 ˚C for 10 minutes and the DNA extracted and purified using an SV mini column as described in 2.4.6.1 and incubated with the second enzyme. After heat denaturation of the enzyme as before, restriction products were either dephosphorylated (see 2.4.13) or subjected to electrophoresis in agarose gels and purified using the protocol outlined in 2.4.6.

2.4.13 Alkaline phosphatase treatment

The 5'- phosphate ends created by the restriction digestion of plasmid DNA were dephosphorylated in order to reduce self-ligation of vectors during cloning. After restriction digestion, linearised plasmid DNA was de-phosphorylated with calf intestinal alkaline phosphatase (CIAP) by adding 1 unit of enzyme (Invitrogen) directly to the previously denatured reaction mixture. The reaction was then incubated at 37 °C at 5 minutes for 5' overhangs and 50 °C for 5' recessed and blunt ends. DNA products were then separated by agarose gel electrophoresis as described above.

2.4.14 Ligations

Vector DNA and insert DNA amplified by PCR, which has been restriction digested to produce complementary sticky-ends, were ligated together using T4 DNA ligase (Promega) using the protocol outlined by the manufacturer. To calculate the amount of insert DNA to use in each ligation the following equation was used:

$$\frac{(\text{ng of vector} \times \text{kb size of insert})}{\text{kb size of vector}} \times \text{molar ratio of } \frac{\text{insert}}{\text{vector}} = \text{ng of insert}$$

when 50 - 100 ng vector DNA was used. In general 10 μl ligation reactions containing 1 x T4 ligase buffer and 1 unit T4 DNA ligase were incubated at room temperature for 4 hours or 4 °C overnight and then 5 μl of this reaction mixture used to transform competent *E. coli.*

2.4.15 End-Labelling of DNA using Klenow fragment

To functionalise the 5' end of the RNA:DNA construct used in the single molecule experiments, before hybridisation, the 5' DNA handle was restriction digested with EcoRI to leave a 5' overhang which was then filled in with biotin-dATP using Klenow fragment. 0.5 mM biotin-14-dATP (Invitrogen), 0.5 mM dTTP and 5 units Klenow Fragment (exo-) (Fermentas)/ μg DNA were added to the 50 μl digestion reaction and incubated at room temperature for 10 minutes and then denatured at 65 ˚C for 10 minutes.

2.4.16 Biotinylation band shift

A simple band shift assay that took advantage of the near-covalent strength of the biotin– streptavidin interaction, was used to detect the efficiency of the biotinylation reaction. Biotinylated DNA was incubated with streptavidin-conjugated horseradish peroxidase (HRP), which, if the DNA had two biotin-dATP moities present, would cause a bandshift of approximately 200 bp. 100 ng DNA was incubated with 1.5 % glycerol, 1 x TBS and 250 μg streptavidin-HRP in a total reaction volume of 10 μl at room temperature for 15 minutes. Reaction

products were separated by electrophoresis on 1.5 % TAE gel in the absence of ethidium bromide. DNA was visualised using UV trans-illuminator after being soaked in 1 x TAE containing 0.5 μg/ml ethidium bromide for 45 minutes at room temperature, followed by destaining in dH_2O for 20 minutes.

2.4.17 *In Vitro* transcription

DNA was PCR amplified using the appropriate primers to produce linear DNA templates with T7 RNA polymerase promoter site at their 5' end for the synthesis of RNA using either of the following protocols.

2.4.17.1 General transcription method

1 μg of linear DNA template was added to a reaction mixture containing 1 x T7 transcription buffer (Promega), 1 mM each rNTP (Roche) and 20 units of RNaseOUT recombinant ribonuclease inhibitor (Invitrogen) at room temperature. 1 μl T7 RNA polymerase (20 U/μl) (Promega) was added to the mixture prior to incubation at 37 ˚C for 1 hour at which another 1 μl T7 RNA polymerase was added and the mixture again incubated for another hour at 37 ˚C. The DNA template was removed and the transcription products cleaned up using the protocols described below.

2.4.17.2 RiboMAX™ large scale RNA production system

Typically 10 μl reactions were performed using 1 μg template DNA. All reagents were thawed and brought up to room temperature before use, except the enzyme mix. Each 10 μl reaction contained 1 x T7 transcription buffer, 7.5 mM rNTP mix, 1 μg DNA template and 1 μl T7 Enzyme Mix. Reactions were incubated at 37 °C for between 2 - 4 hours according to how long the transcript was, then cleaned up using the procedures outlined below.

2.4.17.3 DNase treatment

50 μl transcription reactions were incubated with 1 unit of RQ1 RNase-free DNase 1 (Promega) at 37 ˚C for 15 minutes immediately after termination of the transcription reaction to digest the DNA template.

2.4.17.4 Removal of unincorporated rNTPs

Unincorporated rNTPs were removed by filtration though sephadex G-50 columns (Roche). Column buffer was removed from the column by centrifugation at 1100 *g* for 2 minutes and any residual buffer removed by repeating this process. The transcription reaction mixture was applied to the central column bed and centrifuged as above to elute the RNA whilst retaining any unincorporated nucleotides.

2.4.17.5 Phenol: chloroform purification of RNA

As for DNA in method 2.4.5.4, but using acid phenol, pH 4.5.

2.4.18 Hybridisation of single molecule construct

Equimolar concentrations of ODC hp RNA, 3' DNA handle and 5' DNA handle were mixed (approximately 3.5 μg of each DNA handle and 4 μg of RNA) and precipitated in 0.1 x NaAc and 3 x 100 % ethanol as described above. The nucleic acids were pelleted by centrifugation at maximum speed for 30 minutes at 4 °C, then the pellet was washed in 75 % ethanol and resuspended in 30 μl hybridisation buffer (70 % formamide; 40 mM Pipes, pH 6.4; 0.4 M NaCl; 1 mM EDTA) and denatured at 95 ˚C for 10 minutes and then placed in a beaker of water at ~95 °C which is then allowed to cool gradually to 55 °C in a 55 °C water bath. Reactions were hybridised overnight (~ 16 hours) at 55 °C and then cooled to room temperature. The hybridisation products were made up to 100 μl with ddH_2O then ethanol precipitated as described above. Products were resuspended in 30 μl ddH_2O and 1 μl samples mixed with UREA loading buffer separated by electrophoresis through a 2 % agarose gel buffered in 1 x TBE. Products were stored at - 80 °C. All solutions used were RNase-free.

2.4.19 Acrylamide gel electrophoresis of RNA

For the separation and purification of small RNA molecules (10 - 100 nt) acrylamide gels were preferentially used. Both the non-denaturing and denaturing gels use acrylamide solutions at the ratio 19:1 acrylamide:bisacrylamide.

2.4.19.1 Non-Denaturing

Typically 15% polyacrylamide gels were made by combining 1 ml 5 x TBE with 3.75 ml 30 % acrylamide (19:1 acylamide:bisacrylamide, Accugel, National Diagnostics) and making the solution up to 10 ml with ddH_2O, then adding 100 µl 25 % ammonium persulfate (APS) and 15 µl *N*, *N*, *N*', *N*',- tetramethylethylene diamine (TEMED) to catalyse the polymerisation of the gel. Gels were cast using Bio-Rad vertical mini-gel equipment, which had previously been cleaned thoroughly with RNaseZap (Invitrogen) and ethanol. After the gel had set, the wells were cleaned out using a needle small enough to fit between the glass plates. Gels were pre-run at 150 V for 30 minutes in 0.5 x TBE, before loading RNA samples containing 1 x RNA loading buffer. Samples were electrophoresed at between 150 - 200 V for ~ 30 minutes at room temperature or ~ 1 - 1.5 hours at 4°C until the lowest dye front had migrated ½ - ¾ down the gels length.

2.4.19.2 Denaturing

Denaturing gels were cast as for non-denaturing gels apart from the addition of 7 M UREA to the gel mix. Samples were denatured before electrophoresis in 1 x UREA loading buffer at 65 °C for 10 minutes and electrophoresed as described above (2.4.15.1).

2.4.19.3 Ethidium bromide staining and visualisation of RNA

After electrophoretic separation, RNA migration in polyacrylamide gels was visualised by immersing the gel in an RNase-free solution of 0.5 µg/ml EtBr in 0.5 x TBE for 5 minutes, then destained in ddH_2O for 2 minutes before viewing using a UV trans-illuminator.

2.4.19.4 Elution from gel slice

RNA products identified by ethidium bromide staining were excised from the gel using a scapel and eluted overnight by immersing the gel slice in enough buffer (typically TE with or without 100 mM KCl) overnight at 4 °C.

2.4.20 Agarose gel electrophoresis of RNA

To view large transcription products (> 100 nt) electrophoresis through agarose gels was used.

2.4.20.1 Non-Denaturing

To view transcription products quickly after transcription non-denaturing TBE-agarose gels were used in the same manner as for electrophoresis of DNA samples (see method 2.4.5.2). In general, 2 % agarose was melted in 1 x TBE and cast in a gel tray after the addition of 2 µl of 10 mg/ml ethidium bromide. RNA samples were mixed with 6 x loading buffer and loaded into the gel. Gels were submerged in 1 x TBE buffer in a horizontal electrophoresis tank and electrophoresed at approximately 120 V. RNA was visualised with a UV trans-illuminator.

2.4.20.2 Denaturing

RNA products were checked for integrity and purity on RNA denaturing gels. 1 g of RNase-free agarose was melted in 75 ml RNase-free H_2O until fully dissolved and allowed to cool slightly before adding 10 ml 10 x MOPS and 17.5 ml formaldehyde (99 %) and casting into an RNase-free gel tray. RNA samples were denatured at 65 °C for 15 minutes in a solution containing 5-10 µl RNA, 2 µl 5 x MOPS, 3.5 µl formaldehyde and 10 µl formamide and then immediately cooled on ice for 2 minutes. 2 µl of RNA loading dye and 1 µl ethidium bromide (260 mM) was added before loading each sample into a well of the gel. Products were electrophoresed at 80 V in 1 x MOPS for 1 - 2 hours and visualised using a UV trans-illuminator.

2.4.20.3 Electroelution of RNA using an electroelutor

After electrophoresis, transcribed RNAs were electroeluted from gel slices using the S&S Elutrap Electro-Separation System (Schleicher and Schuell). RNA bands, visualised with EtBr staining, were excised from the gel with a clean scalpel and then loaded into the elution chamber fitted with the appropriate membranes according to the manufacturers instructions. The chambers were filled with enough 1 x TBE to cover the gel slice and 200 V applied to the system for 1 – 2 hours until all the RNA had been eluted. The polarity was reversed for 20 seconds at 200 V to release any material attached to the membrane and the contents of the trapping chamber removed and precipitated as described in 2.4.8.

2.4.20.4 Electroelution within the gel

An alternative method to electroelute RNA after agarose gel electrophoresis is to perform it within the gel by cutting a well out of the gel directly below the RNA band. The well was filled with 1 x TBE and a piece of BT1 membrane from the Elutrap kit, which is impermeable to nucleic acids, was inserted at the end of the well. The gel was placed into an electrophoresis tank filled with 1 x TBE and the buffer volume adjusted so it was level with the top of the gel. RNA was electroeluted into the well by applying a current at 150 V for 20 minutes. The polarity of the current was reversed for 1 minute to release any material attached to the membrane and then the contents of the well removed with a pipette and precipitated as described in 2.4.8.

2.4.21 Northern blotting

2.4.21.1 Northern blotting by capillary action and membrane fixation

After separation by denaturing agarose gel electrophoresis, the distribution of individual mRNAs within gradient fractions was detected by northern blotting. RNA molecules were transferred to a positively charged membrane by capillary action using a salt gradient. A piece of filter paper (3MM, Whatman) was soaked in 20 x SSC and used as a salt-wick by placing it over a glass plate resting on a

tub containing a reservoir of 20 x SSC so that both ends of the paper reach the salt solution. Any bubbles trapped between the filter paper and the glass plate were removed using a clean, RNase-free pipette. The denaturing agarose gel was placed on top of this so that the loaded side of the gel was face down, and again, any air bubbles trapped in between the gel and the filter paper were removed. Any exposed areas of filter paper were covered with a layer of Parafilm to ensure that any capillary action is via the gel, rather than straight from the wick itself. A gel-sized piece of transfer membrane (ZetaProbe, BioRad) was wet in ddH_2O and then washed in 20 x SSC before placing on top of the gel, and two gel-sized pieces of filter paper, soaked in ddH_2O, were placed on top of this, again ensuring no air bubbles were trapped between layers. A stack of paper towels (5 - 8 cm) were placed on top of this and a weight placed on top of these to promote capillary action. RNA molecules were left to transfer for 6 - 18 hours.

RNA molecules were fixed to the membrane by UV crosslinking at 254 nm with 120,000 μJ/cm^2 using a UV CrossLinker (CX2000, UVP). The membrane was then baked for 1 hour at 80 °C. The 18 S and 28 S ribosomal RNA bands were stained by soaking the membrane in a methylene blue solution (0.02 % (w/v) methylene blue, 0.3 M NaOAc (pH 5.2)) for 30 seconds and then visualised by rinsing the membrane in ddH_2O. The positions of these bands were marked on the membranes using a pencil, so that their size could be used as an estimation of molecular weight when probing. The stain was removed by washing the membrane in a solution of 1 x SSC, 1 % SDS, several times for no longer than 15 minutes. The blots were then washed twice in water before storing them dry.

2.4.21.2 Probe labelling and membrane hybridisation

Target RNA molecules were visualised by hybridisation to a complementary radio-labelled DNA fragment. DNA fragments of about 500 - 1000 nt in length were either amplified by PCR from a cDNA template, or restriction digested out of cloning vectors and then separated by agarose gel electrophoresis and extracted and purified using the methods described above. Single-stranded

DNA probes were amplified with Klenow fragment (Fermantas), by denaturing 25 - 30 ng DNA template in a total volume of 15 μl at 95 °C for 3 minutes, then adding 5 μl labelling buffer (1 x) (Promega), 1 μl nuclease-free BSA (1 x) (NEB), 0.5 μl 25mM dNTP mix (0.5 mM), 1 μl Klenow fragment (10 U/μl) (Fermentas) on ice. To this 2.5 μl α^{32}P-dCTP (10 μCi/μl was added and the reaction incubated at 37°C for 1 hour. Unincorporated nucleotides were removed by filtering the reaction through one or two g-50 sephadex columns for 5 minutes at 4000 rpm. Probes were stored at – 20 °C in Perspex blocks or used straight away.

Membranes were pre-hybridised in 5 ml warmed Church Gilbert's solution in a rotating hybridisation oven at 65 °C for 30 minutes. Labelled probes were denatured at 95 °C for 3 minutes then chilled on ice for 5 minutes. The pre-hybridisation solution was replaced with fresh Church Gilbert's solution (5 ml) before carefully adding the denatured probe. The probe was hybridised overnight in a rotating oven at 65 °C.

Membranes were washed twice for 15 minutes in a series of three wash solutions (wash 1 - 2 x SSC, 0.1 % SDS; wash 2 – 0.5 x SSC, 0.1 % SDS; wash 3 – 0.1 x SSC, 0.1 % SDS). The first wash was performed at 65 °C and the rest at room temperature. After washing, the blots were wrapped in clingfilm and exposed to a phosphorimager screen (FujiFilm) overnight.

To strip hybridised probes from the blots so they could be re-probed, membranes were washed with gentle agitation in a hot solution (~ 80 – 90 °C) of 0.5 % SDS in ddH_2O for 30 minutes, until the solution cooled. This process was repeated until no signal was detected on the blots with a Geiger counter (usually 1 – 2 times). The blots were then rinsed in ddH_2O and stored in clingfilm, or re-probed directly.

2.4.22 Sucrose density gradient polysome profiling

2.4.22.1 Gradient preparation

Sucrose solutions containing 10 – 50 % sucrose and 1 x Gradient Buffer (10 x stock: 3 M NaCl; 150 mM $MgCl_2$; 150 mM Tris-HCl, pH 7.5; 1 mg/ml cycloheximide; 10 mg/ml heparin) were layered in Sorvall PA 12ml tubes by carefully adding 2.1 ml of sucrose solution and freezing at - 80 °C before the subsequent addition of the next layer. Layers were added with decreasing density so that the bottom layer was 50 % sucrose and each additional layer decreased in density by 10 % (5 layers in total). The gradients were covered in foil and stored at – 80 °C until required.

2.4.22.2 Treatment and lysis of cells

For the downstream application of microarray analysis after polysome gradient fractionation, two 15 cm plates of HeLa cells at 80 % confluency were used for each treatment. For northern analysis after polysome gradient fractionation, one 15 cm plate of HeLa cells at 80 % confluency was used per treatment. Fresh media was added to the cells 1.5 hours prior to harvest to ensure that the cells would be actively synthesising proteins. Individual treatments will be described in chapter 5. After treatment, 100 ng/ml cycloheximide was added to the media and the cells incubated for a further 2 minutes at 37 °C. Cells were then immediately put on ice, the media was removed and cells were washed twice with 5 ml ice-cold PBS containing 100 ng/ml cycloheximide. Cells were harvested by scraping twice into 3 ml ice-cold PBS containing 100 ng/ml cycloheximide and pelleted by centrifugation at 1000 rpm (200 g) at 4 °C for 10 minutes. The supernatant was removed and 0.5 ml ice-cold lysis buffer (1 x Gradient Buffer; 1% Triton X 100) was added and complete lysis ensured by pipetting the cells in the lysis buffer several times. The cell lysate was transferred to a 1.5 ml ependorf and centrifuged at maximum speed (13,400 rpm, ~ 17,000 g) for 1 minute at 4 °C to clear the lysate of cell debris. The supernatant was then layered carefully onto a sucrose gradient, which had been allowed to equilibrate overnight at 4 °C. mRNAs were separated according to

polysomal association by centrifugation of the lysate through the sucrose density gradient at 38,000 rpm for 2 hours at 4 °C. The centrifuge used was a Sorvall Discovery 100SE and the bucket and rotor Sorvall TH-641. Both were pre-chilled to 4 °C prior to use.

2.4.22.3 Fractionation of mRNA

Gradients were fractionated using a UV/Vis detector (UA-6, Teledyne ISCO), constant flow rate was achieved using a motorised pump (KD Scientific). Prior to use the gradient machine was cleaned through with ddH_2O, 70 % ethanol and ddH_2O at a flow rate of 5 ml/min. A blue 65 % sucrose solution (made as for the gradient sucrose solutions but with the addition of 0.25 % Bromophenol Blue) was pumped into the bottom of the sucrose gradient sample at a flow rate of 1 ml/min, pushing the sample through the gradient machine least-dense fraction first. The optical absorbance of the solution was read at 254 nm and recorded both directly onto a trace and also using PeakTrak Software V. 1.1. 1 ml fractions were collected directly into 3 ml 7.7 M Guanidine HCl. 4 ml ethanol was added and samples mixed thoroughly and stored a - 20 °C to precipitate overnight. The machine was rinsed thoroughly with ddH_2O between each sample.

2.4.23 Microarray profiling

2.4.23.1 Purification of fractionated mRNA

Fractionated mRNA precipitates were pelleted by centrifugation at 4 °C, at 4000 rpm for 50 minutes. Pellets were aspirated dry and resuspended in 400 μl ddH_2O, and then re-precipitated as in 2.4.8 overnight. The mRNA precipitate was pelleted by centrifugation at 13,400 rpm (17,000 *g*) for 30 minutes at 4 °C, then washed in 800 μl 75 % ethanol by agitation on a mixer for 10 minutes at room temperature. mRNA was pelleted again by centrifugation for 5 minutes at maximum speed, and the pellet dried for 5 minutes after removal of the supernatant. When dry each pellet was resuspended in 50 μl ddH_2O.

2.4.23.2 Preparation of RNA and cDNA for chips

mRNA fractions were pooled according to their subpolysomal or polysomal association which was identified by northern analysis of the distribution of PABP and Actin mRNAs within each gradient sample set. 35 μl of each fraction were combined together (fractions 1 - 5 – subpolysomes; fractions 6 - 11 – polysomes) and made up to 500 μl with ddH_2O. After the addition of 500 μl 5 M LiCl the pooled mRNA was precipitated overnight at -20°C and then pelleted by centrifugation at 13,400 rpm (17,000 *g*) 4°C for 30 min. The pellet was aspirated dry and then resuspended in 300 μl ddH_2O before precipitating again using the method described in 2.4.8. The precipitate was pelleted once more by centrifugation at 13,400 rpm (17,000 *g*) 4 °C for 30 minutes and then washed twice in 75 % ice-cold ethanol for 10 minutes on a mixer and centrifuged for 5 minutes at maximum speed to collect the pellet. The pellet was dried for 5 minutes after aspirating off the ethanol, and then resuspended in 15 μl ddH_2O. The concentration of each subpolysomal or polysomal sample was quantified by reading the optical absorbance of the solution at 260 nm.

2.4.23.3 Reverse transcription of aminoallyl cDNA

mRNA, pooled and purified as described above, was reverse transcribed into aminoallyl cDNA which can then be fluorescently labelled and hybridised onto cDNA microarrays. 5 μg of pooled RNA was added to a primer mix containing 3 μg denatured random hexamers (Invitrogen) and 5 μg $oligo(dT)_{25}$ and made up to a total volume of 14.5 μl with ddH_2O. The primer mix was annealed by heating at 70 °C for 10 minutes and then snap cooling on ice for 5 min before adding 14 μl labelling mix (final concentration: 1 mM dATP; 1 mM dCTP; 1 mM dGTP; 0.06 mM dTTP; 0.3 mM aadUTP (Ambion); 1 X first-strand buffer; 20 mM DTT) and 1 μl Superscript III (200 U/μl) (Invitrogen). The reaction was incubated at 50 °C for 1 hour before adding another 1 μl Superscript III and incubating for a further 2 hours. RNA was then hydrolysed by adding 10 μl 0.5 M EDTA and then 10 μl 1 M NaOH and incubating for a further 15 minutes at 65 °C, and the reaction quenched by adding 25 μl 1 M HEPES-KOH, pH 7.

Aminoacyl cDNA was purified using Microcon-30 columns (MW cut-off – 30,000 Da) (Millipore) by first adding 400 μl ddH_2O to the column, and then the sample. The columns were placed in a collection tube and then centrifuged at 12,000 rpm for 7 minutes. The flow-through was discarded and an additional 450 μl ddH_2O added. The centrifugation process was repeated until the filtrate volume reached ~ 20 μl and the sample collected by inverting the column in a fresh collection tube and centrifuging at 1000 *g* for 5 minutes. The concentration of the cDNA was quantified by reading the optical absorbance of the solution at 260 nm, and the solution stored at - 20 °C.

2.4.23.4 Fluorescent coupling of NHS-functionalised Cy dye to aa-cDNA

NHS-functionalised Cy dyes will covalently cross-link with the primary amine group of aminoallyl-dUTP at a pH of 8.5 - 9.0. These dyes are prone to degradation when exposed to light so every care was taken to minimise exposure of the dyes before and after coupling to the aa-cDNA. Cy mono NHS-ester dye (Ambion) was resuspended in excess according to manufacturer's instructions in a solution of aa-cDNA prepared in 2.4.18.4 buffered with sodium carbonate solution, pH 9, to a final concentration of 0.1 M, and the reaction mixture incubated at room temperature, in the dark, for 1 hour. Subpolysomal aa-cDNA was cross-linked to Cy5 mono NHS-ester dye (fluoresces red - emits at 635 nm), and polysomal aa-cDNA was cross-linked to Cy3 mono NHS-ester dye (fluoresces green – emits at 532 nm). The reaction was quenched by the introduction of free 1° amine to the mixture (4.5 μl 4 M hydroxylamine) and incubated for a further 15 minutes in the dark.

The subpolysomal and polysomal fluorescently labelled aa-cDNA for each treatment / control sample were then combined and any unincorporated dye removed, and the buffer exchanged to 10 mM Tris, pH 7.4 with 0.02% sodium azide, by filtering through a Biospin 6 Tris column (BioRad) using the manufacturers protocol. The cDNA yield was quantified by reading the optical

absorbance of the solution at 260 nm, and the dye incorporation quantified at 550 nm and 650 nm for Cy3 and Cy5 dyes respectively.

The coupling efficiency was calculated using the following equations;

To correct for the contribution of the dye on the absorbance at 260 nm:

$$A_{base} = A_{260} - (A_{dye} \times CF_{260})$$

To calculate the coupling efficiency:

$$\text{Dye:base} = \frac{(A_{base} \times \varepsilon_{dye})}{(A_{dye} \times \varepsilon_{base})}$$

Where:

CF_{260} is correction factor for each dye (Cy3 = 0.04, Cy5 = 0.00)

ε_{dye} is the extinction coefficient for the dye (Cy3 = 150,000 $cm^{-1}.M^{-1}$, Cy5 = 239,000 $cm^{-1}.M^{-1}$)

and ε_{base} is the extinction coefficient for ssDNA = 8919 $cm^{-1}.M^{-1}$

1 dye for every 100 or less bases = good labelling, 1 dye for every 50 or less bases = very good labelling.

2.4.23.5 Preparation of arrays

The microarrays used were 30,000 gene probe pan human Array (MWG Biotech, now taken on by Ocimum Biotechnologies) printed by the Post-Genomics Laboratory (University of Nottingham, approximate failed spot rate < 5 %) on Schott Nexterion A+ (gamma APS coated) single slides. The microarrays were prepared for hybridisation by denaturing the oligo probes by heating the slide at 100 °C for 2 minutes, fixing the probes by baking at 80 °C for 2 hours and then putting the slides through a series of washes as follows:

Wash 1 – 3.75 X SSC, 0.25 % SDS (kept at 65 °C until use to prevent precipitation of SDS), 5 minutes;

Wash 2 - ddH_2O, 5 minutes;

Wash 3 - fresh solution of 1 g $NaBH_4$ in 300 ml PBS and 100 ml 95 % ethanol, 20 minutes. This wash was performed in a fumehood as the reaction produces hydrogen gas. The slides were agitated every few minutes to release any bubbles stuck to their surface.
Wash 4 - 0.2 % SDS, 2 minutes;
Wash 5 - 1 % BSA, 0.2 % SDS, 5 X SSC, 10 minutes;
Wash 6 - ddH_2O, 2 minutes, (twice).
The slides were then dried completely before hybridisation of the fluorescently labelled cDNA.

2.4.23.6 Hybridisation of probe to chips

To reduce background annealing to the array 1 μg Poly(A), 10 μg human Cot1 DNA, 4 μg tRNA were added to each cDNA probe. To this, 380 μl ddH_2O was added before filtering each solution through a Microcon-30 (Millipore) for ~ 7 minutes at 12,000 rpm until the volume was reduced to 10 – 20 μl. Samples were collected by inverting each column in a collection tube and centrifuging at 1000 *g* for 5 minutes. The samples were dried completely using a vacuum drier (DyNaVap, Labmet) and then resuspended in 50 μl hybridisation buffer (Genisphere, Hatfield, PA, USA). The labeled probe hybridisation mixture was pipetted on to the array and a clean 22 mm by 64 mm coverslip gently lowered on top to cover the printed area of the array, ensuring no air bubbles got trapped in the process. The probes were left to hybridise to their targets at 50 °C overnight in a sealed hybridisation chamber (Genetix) that had a little water in the bottom of it to prevent evaporation of the hybridisation solution from in between the coverslip and the slide.

A number of washes were performed for each array to wash off the hybridisation solution and minimise background fluorescence:
Wash 1 – 2 X SSC, 0.1 % SDS, 5 minutes;
Wash 2 – 1 X SSC, 0.1 % SDS, 5 minutes;
Wash 3 – 0.1 X SSC, 0.2 % SDS, 5 minutes;
Wash 4 – 0.1 X SSC, 5 minutes, twice.

Each wash solution was freshly prepared and changed once during each wash. The slides were then dried by centrifugation for 2 minutes and stored in the dark until they were scanned.

2.4.23.7 Scanning chips and gridding

Arrays were scanned using a GenePix Professional 4200A Scanner and the GenepixPro v. 6 software. Each array was first scanned quickly using the 40-micron preview setting to adjust the levels of red and green fluorescence so that they were at a ratio of ~ 1 and then scanned at either a 5 or 10 micron resolution. Images were saved as Tiff files and manipulated using GenepixPro V. 6, firstly by fitting a grid to the arrays from a GAL file to identify each spot, and secondly to flag any spots which were considered anomalous in order to omit them from downstream analysis.

2.4.24 Protein purification

2.4.24.1 Nickel affinity chromatography

Over-expressed histidine-tagged recombinant proteins were affinity-purified using nickel-coated agarose resin under native conditions. Recombinant proteins overexpressed using an *E. coli* expression system (see method 2.3.5) were stored as a cell pellet overnight at - 20 °C to aid lysis. After thawing on ice, cells were resuspended in 5 ml lysis buffer (50 mM Tris-HCl, 150 mM NaCl, 2 mM $MgCl_2$, 10 mM imidazole, pH 7.5) and lysed by sonication (15 reps of 10 seconds at 60 % power using the SonoPlus sonicator, Bandelin) with 10 seconds cooling between each repetition) on ice. 1 x protease inhibitor cocktail (Roche) was added to the lysate before pelleting the cell debris at 17,000 rpm (34541 *g*) for 30 minutes at 4°C. A 1 ml affinity column was prepared by loading 2 ml 50 % Ni-NTA agarose slurry (Qiagen) into a column and washing it with 10 ml lysis buffer. The cleared lysate was then applied directly to the column and the flow-through collected for SDS-PAGE analysis. The column was washed twice with 5 ml wash buffer (same as lysis buffer but with 40 mM imidazole) and the flow-through collected. Proteins were eluted from the column by adding 5 – 10 ml

elution buffer (same as lysis buffer but with 250 mM imidazole) and collected in 1 ml fractions. 10 μl samples of each flow-through sample or collected fraction was analysed by SDS-PAGE as described in 2.4.26 to determine whether the purification had been successful and which fractions contained the bulk of the purified protein. These fractions were combined and the imidazole removed from the solution by dialysis overnight at 4 °C in lysis buffer without imidazole using SnakeSkin Dialysis Tubing (Thermo Scientific). Protein concentration was determined by measuring its optical absorbance at 280 nm before adding 10 % glycerol to the solution and snap-freezing 50 - 100 μl aliquots in liquid nitrogen. Samples were stored at - 80 °C.

2.4.24.2 Amylose affinity chromatography

Over-expressed maltose binding protein (MBP)-tagged recombinant proteins were affinity-purified using amylose-coated agarose resin under native conditions. Recombinant proteins were overexpressed using an *E. coli* expression system as described previously with the addition of glucose to the LB medium to prevent the amylase activity during the purification procedure (see method 2.3.5). *E. coli* were stored as a cell pellet overnight at - 20 °C to aid lysis. After thawing on ice, cells were resuspended in 5 ml lysis buffer (20 mM Tris-HCl, pH 7.5; 200 mM NaCl; 1 mM EDTA) and as described above (2.4.24.1). A 2.5 ml affinity column was prepared by loading 5 ml 50 % amylose resin (NEB) into a column and washing it with 10 ml lysis buffer. The cleared lysate was then applied directly to the column and the flow-through collected for SDS-PAGE analysis. The column was washed twice with 10 x column volume (25 ml) lysis buffer as described in 2.4.24.1 and the recombinant protein eluted with in lysis buffer supplemented with 10 mM maltose. Fractions were collected and analysed as described in 2.4.24.1. Protein fractions were dialysed as described in 2.4.24.1 in preparation for cleavage of the fusion protein with tobacco etch viral (TEV) protease.

2.4.24.3 TEV protease cleavage

Eluted protein fractions were dialysed into a TEV cleavage buffer (50 mM Tris, pH 8.0; 0.5 mM EDTA; 1mM DTT) as described in 2.4.24.1 for 3 hours at 4 °C, changing the buffer every hour. Recombinant fusion protein was cleaved overnight at room temperature with an approximate OD_{280} ratio of 1 : 2 TEV protease (recombinant protein, gift from P. McEwan, University of Nottingham): eIF4AI-MBP.

2.4.24.4 Heparin affinity chromatography

Separation of recombinant eIF4AI and MBP-tag proteins was attempted by taking advantage of eIF4AI RNA binding activity by using heparin affinity chromatography. TEV cleaved proteins were dialysed overnight into 10 mM sodium phosphate, pH 7 as described in 2.4.24.1. Dialysed proteins were loaded onto a pre-packed heparin column (1 ml, Hi Trap Heparin, GE Healthcare), washed with 10 ml sodium phosphate buffer, pH 7, and eluted in 3 ml fractions of increasing KCl concentration (0.5, 1, 2 M). Fractions were analysed for protein content by SD PAGE and coomassie blue staining. No proteins were observed in the wash fractions demonstrating that MBP-tag protein is able to non-specifically bind to recombinant eIF4AI or the heparin-coated agarose resin.

2.4.25 Quantification of protein

2.4.25.1 Bradford assay

To determine the concentration of proteins in order to ensure equal loading of SDS-polyacrylamide gels used in western blot analysis, the Bradford colorimetric assay was used. Typically 1 - 2 μl cell lysate in lysis buffer was mixed with 50 - 200 μl 1 x Bradford Reagent (Bio-Rad), incubated for 5 - 10 minutes at room temperature and their optical absorbance read at 595 nm. Sample absorption could be compared to a BSA protein standard to estimate the concentration of each sample or the samples were diluted relative to each other.

2.4.25.2 Nanodrop

To determine the concentration of overexpressed and purified recombinant proteins, the optical absorbance of the protein solution was read at 280 nm using the Nanodrop and the concentration calculated using the extinction coefficient and molecular weight of the protein, as calculated using ExPaSy tool 'ProtParam'.

2.4.26 SDS polyacrylamide electrophoresis

Proteins were separated according to their size by SDS polyacrylamide gel electrophoresis using Bio-Rad vertical mini-gel equipment. Typically 10% polyacrylamide gels were made by combining 1.25 ml Resolving Buffer (1.5 M Tris-HCl, 1 % SDS, pH 8.8) with 1.67 ml 40 % acrylamide (37.5:1 acrylamide:bis) (Protogel) and making the solution up to 5 ml with ddH_2O, then adding 50 μl 25 % ammonium persulfate (APS) and 10 μl TEMED to catalyse the polymerisation of the gel. The resolving gel was poured so that there was space between the glass plates to pour a layer of stacking gel and add the comb to make the wells. Water-saturated butanol was layered on top of the resolving gel and poured off once it had set. A stacking gel, consisting of 2.5 ml stacking buffer (0.25 M Tris-HCl, 1 % SDS, pH 6.8) and 0.67 ml 40 % acrylamide, made up to 5 ml with ddH_2O and polymerised as for the resolving gel, was then poured on top and a comb added to make the wells. Protein samples were denatured in 1 x SDS loading buffer (100 mM Tris-HCl, pH 6.8; 20 % glycerol; 8 % SDS; 20 % β-mercaptoethanol; 2 mM EDTA; 0.2 % Bromophenol blue) at 95 °C for 5 minutes, centrifuged briefly and then put on ice until loaded into the gel. Gels were run in 1 x SDS-PAGE running buffer (25 mM Tris-HCl; 192 mM glycine; 0.1 % SDS, pH 8.3) at 120 V for 1 - 2 hours according to the separation required.

2.4.27 Western blotting

After separation by SDS-PAGE, proteins were transferred to membranes using an electroblotter (TransBlot SemiDry, BioRad) by layering three gel-sized pieces of filter paper (3MM, Whatman) soaked in blotting buffer (50 mM Tris, 192 mM glycine, 20 % methanol); a gel-sized piece of PVDF membrane (Hybond-P,

Amersham, GE Healthcare), soaked in methanol and then blotting buffer; the gel, soaked in blotting buffer, stacking gel removed; and three more pieces of filter paper soaked in blotting buffer. Any bubbles between layers were removed with a clean pipette. Proteins were transferred for 1 hour at 10 V. Transferred proteins were visualised by soaking the membrane in Ponceau stain (0.5 % (w/v) Ponceau, 5 % (w/v) trichloroacetic acid (TCA)) and rinsing in ddH_2O until bands appeared.

Membranes were blocked for 1 hour with either 5 % milk (Marvel) or 5 % BSA in TBST (10 mM Tris-HCl, pH 8, 0.9 % (w/v) NaCl, 0.1 % (v/v) Tween) at room temperature with gentle shaking and then incubated overnight at 4 °C in fresh blocking solution with a selected primary antibody at a concentration specified by the manufacturer. Membranes were then washed three times in TBST for 15 minutes before incubating with the appropriate secondary antibody for 1 hour at room temperature. Membranes were washed three times again for 15 minutes in TBST before visualising the antibody-bound-proteins by chemiluminescence.

2.4.28 Coomassie staining

To assess the success of recombinant protein overexpression, sample bacterial cell lysates were subjected to SDS-PAGE and then proteins viewed directly in the gel by staining with Coomassie Blue stain (40 % (v/v) methanol, 10 % (v/v) glacial acetic acid, 0.05 % (w/v) Coomassie Blue R-250) for 1 hour at room temperature, and then destaining in the same solution without the dye.

2.4.29 Helicase assay

Helicase assays were performed to assess the activity of purified recombinant eIF4A1 with eIF4B. The basic method followed is described in (Rogers *et al.*, 1999). RNA oligonucleotides (11mer - gcuuuacggug; 44mer - gggagaaaaacaaaacaaaacaaaacuagcaccguaaagcacgc) were synthesised by Dhamacon and resuspended to a concentration of 100 pmol/µl in ddH_2O. The shorter RNA oligomer was end-labelled with ^{32}P-γ-ATP using T4 polynucleotide kinase (PNK) in a reaction containing 1 x T4 PNK buffer; 5 pmol/µl 11mer; 2µl

^{32}P-γ-ATP (10 μCi/μl); 2 μl T4 PNK (10 U/μl) (NEB), for 1 hour at 37°C. An equal quantity of the longer RNA oligomer (44mer) was added to the labelling reaction in 30 μl annealing buffer (TE, 100mM KCl) and the reaction heated at 95 °C for 5 minutes before allowing to cool to room temperature slowly in a beaker of heated water (2 - 3 hours) to allow the labelled RNA duplex to anneal. An equal volume of 2 x RNA loading dye was added to the sample and the duplex separated from any non-hybridised RNA oligomers by non-denaturing 15 % TBE-polyacrylamide gel electrophoresis at 4 °C as described in 2.4.19.1. The gel was stained with EtBr and the duplex excised from the gel with a clean scalpel and eluted overnight as described in 2.4.19.4. The yield of eluted duplex was quantified by reading the optical absorbance at 260 nm and aliquoted and stored in a Perspex block at - 20 °C until required.

Helicase assays were set up on ice and contained 25 mM Tris-HCl pH 7.5; 75 mM NaCl; 1 mM $MgCl_2$; 2 mM DTT; 1 mg/ml UltraPure BSA (Ambion); 0.5 μl RNaseOUT recombinant ribonuclease inhibitor (Invitrogen); 1 mM ATP, 0.25 - 1 μM recombinant eIF4A1; 0.125 - 0.5 μM recombinant eIF4B and 9 pg/μl duplex (~ 500 pM). Typically 50 μl total reactions were made up and a 7.5 μl sample taken off to act as a control before adding ATP. After the addition of ATP, reactions were incubated at 37 °C for 15 minutes and 7.5 μl samples were taken off at 5 minute intervals (including 0) and immediately mixed with an equal volume of stop buffer (50mM Tris-HCl, pH 6.8; 2 % (w/v) SDS; 100 mM DTT; 10 % (v/v) glycerol and 0.1 % (w/v) bromophenol blue) and kept on ice. The no-ATP control was also incubated at 37 °C for 15 minutes and then mixed with an equal volume of stop buffer and kept on ice. Samples were separated by non-denaturing 15 % TBE-polyacrylamide gel electrophoresis at 4 °C as described in 2.4.19.4 for 1 - 1.5 hours. The gels were dried in between a wet sheet of filter paper (3MM, Whatman) and a piece of clingfilm by heating to 80 °C under vacuum for 45 minutes and then exposed to a phosphorimager screen overnight. Images were viewed using QuantityOne software (v. 4.6.5, BioRad) ad quantified using ImageJ (v. 1.43, National Institute of Health, USA).

2.4.30 ^{35}S Methionine labelling of protein

The rate of translation in HeLa cells, with or without eIF4A1 inhibition, was measured by quantifying radiolabelled methionine incorporation in newly synthesised proteins. HeLa cells were seeded in 6 well plates at a density of 0.15 x 10^6 cells/well and grown overnight so they reached ~ 70 % confluency the next day. Fresh media was applied to the cells 1 - 1.5 hours before treatment with the inhibitory agent/control for a chosen time, in complete DMEM. Cells were then washed twice in pre-warmed PBS before applying 0.5 ml methionine free DMEM medium containing 10 % (v/v) dialysed FCS and 2 mM L-glut and 2 µl ^{35}S methionine (10 Ci/µl) and incubated at 37 °C for 20 minutes. The cells were then placed on ice, washed three times with and then scraped into 1 ml ice-cold PBS containing 4 mg/ml methionine. Cells were pelleted at 1500 rpm (200 *g*) for 10 minutes at 4 °C and then lysed on ice in 50 µl lysis buffer (15 mM Tris-HCl, pH 7.5; 300 mM NaCl; 15 mM $MgCl_2$ and 1 % (v/v) triton X-100). Cell debris was pelleted by centrifugation at maximum speed for 1 minute and the cleared lysate diluted in 200 µl lysis buffer without 1 % triton. A 20 µl sample was removed at this point for quantification using the Bradford assay in case normalisation was required later. The proteins in the remaining cell lysate were precipitated on ice for 30 minutes by adding TCA solution to a final concentration of 10 % (v/v). Precipitated proteins were applied to Whatman GF/A filter papers using a vacuum manifold and washed twice with 70 % IMS and 100 % acetone. Filters were dried in an oven at 40 °C for ~ 10 minutes and their radioactivity calculated by adding 2 ml Ecoscint scintillation fluid (National Diagnostics) and counting the activity using a liquid scintillation counter (1409, WALLAC).

2.5 Biophysical techniques

2.5.1 Atomic Force Microscopy

2.5.1.1 Cantilevers, instruments and software

All AFM imaging was performed using a Multimode Nanoscope IIIa AFM (Veeco Instruments, Santa Barbara, USA) using Nanosensor N-CL silicon cantilevers

with nominal spring constants between 40 N/m and 55 N/m and a resonant frequency of around 200 kHz. Images were scanned at a line frequency of 1.97 Hz at 512 x 512 pixel resolution, with an amplitude set point of 0.9 - 1 V, and a drive frequency at or just below the resonance frequency. Images were flattened and analysed using Nanoscope software v. 5.13r3.

2.5.1.2 Sample Preparation for AFM imaging in air

5 - 10 μl of diluted construct (0.5 - 10 ng/μl) or recombinant eIF4AI-MBP (5 - 10 pg/μl) were deposited onto freshly cleaved mica surfaces (Agar Scientific) and incubated for 5 - 10 minutes. The surface was washed gently with 50 μl ddH_2O and then dried under a gentle flow of nitrogen gas.

2.5.2 Molecular Force Probe

2.5.2.1 Cantilevers, instruments and software

AFM force microscopy was performed using a 1D molecular force probe (MFP) (Asylum Research, Santa Barbara, USA) operated with Igor Pro software (Wavemetrics, Oregon, USA) using the largest triangle lever on the 6-levered MLCT cantilever (Veeco) with a nominal spring constant of 0.01 N/m. The resonant frequency of the cantilever was determined prior to, and after, force experiments from a power spectral density (PSD) curve recorded by the instrument software using the thermal noise method (Butt and Jaschke, 1995).

2.5.2.2 Cantilever tip functionalisation

Silicon nitride cantilevers (MLCT, Veeco) were cleaned in a 'piranha' solution (30 % hydrogen peroxide (w/v) in concentrated sulphuric acid) for two minutes with gentle agitation, washed three times in dH_2O and dried at 80 °C for 1 hour in a glass petri dish. Dried cantilevers were silanised for two hours using 50 μl 3-aminopropyledimethylepoxysilane (3-APDES) (Fluorochem), washed twice in methanol and biotinylated by incubation in 1 mM NHS-biotin (Sigma) in dimethyl sulphoxide (DMSO) for three hours. After rinsing twice in DMSO and

once in dH_2O, the cantilevers were stored for up to one month at 4 °C in PBS until required for use. Thirty minutes prior to use, the cantilevers were incubated in a solution of 1 mg/ml streptavidin and then rinsed twice in PBS.

2.5.2.3 Preparation of gold coated surfaces

Small pieces of silicon wafer (~ 1 cm^2) were cleaned with 'piranha' solution, rinsed in dH_2O and dried at 80 °C as described above. The cleaned surfaces were then coated in a thin layer of gold and then glued, gold side down, to small pieces of cleaned glass slide (~ 1.5 cm^2) using epoxy-glue. The day prior to the experiment the silicon wafer was chipped off the glass side to reveal a clean, flat gold surface ready for molecule attachment.

2.5.2.4 Attachment of labeled molecules to gold surfaces

The day prior to the experiment, 50 μl of labelled DNA (~ 150 ng/μl) or ODC hp construct (~ 500 ng/μl for 100 % efficient hybridisation and recovery) in TE-NaCl buffer (10 mM Tris-HCl, pH 7.5; 1 mM EDTA and 150 mM NaCl) was deposited onto a fresh gold surface and left in a sealed humid petri dish at room temperature overnight (~ 16 - 20 hours). The surface was then washed with 100 μl TE-NaCl and the surface was coated in a solution of 1 mM mercaptohexanol (MCH) for one hour to reduce non-specific interactions of the DNA with the surface. The sample was rinsed prior to use in force experiments with 100 μl TE-NaCl.

2.5.3 Optical Tweezers

2.5.3.1 Bead functionalisation

200 μl (~ 10 mg) NH_2-functionalised green-yellow fluorescent (excitation - 488 nm) 1 and 2 μm polystyrene microspheres (Invitrogen) were collected by centrifugation at 6500 rpm and then washed twice in PBS prior to incubation in 500 μl 10 mM sulfo-GMBS (Pierce) in PBS at room temperature for 30 minutes with gentle agitation to add a maleimide group which will covalently bind to the

thiol moiety of the ODC hp construct. After functionalisation, beads were washed three times in PBS and then stored in PBS, in the dark at 4 °C until required.

Streptavidin-coated 3 μm silica microspheres were purchased from Bangs Laboratories, distributed by Park Scientific, UK.

2.5.3.2 Attaching molecules to beads

Maleimide functionalised beads (5 μl, 250 ng) were incubated with varying amounts of ODC hp construct (ranging from 1:1000 to 1: 320000 bead to construct ratio) in a total volume of 100 μl PBS at room temperature or one hour with gentle agitation. Beads were collected by centrifugation at 6500 rpm, washed three times in PBS then resuspended in 200 μl PBS. 25 μl of ODC hp construct bound beads were mixed with the equivalent number of streptavidin beads (1.5 μl, 2 % solids) immediately prior to addition to the microscope cell.

2.5.3.3 Instrument

Optical tweezer experiments were performed with a NanoTracker optical tweezers platform mounted on a Zeiss Axio Observer inverted optical microscope (JPK Instruments, Berlin, Germany). Dual optical traps are created by the focusing of two lasers via separate pathways that allow both lateral and axial movement of each trap. Both traps also have two individual detection units to detect movement on the x and y axis separately from that on the z axis, increasing the sensitivity of the instrument. The instrument is controlled by Nanotracker software that also performs online trap calibration using a power spectrum fitted by a Lorentzian curve method (Berg-Sorensen and Flyvbjerg, 2004). Analysis software was developed by J. Mamaren (JPK, Berlin) written in LabVIEW and was used to correct the measured distance by accounting for the displacement of the bead out of the trap.

3 Recombinant eIF4AI has *in vitro* helicase activity that is inhibited by 15d-PGJ$_2$ and hippuristanol

3.1 Investigating helicases *in vitro*

Helicases are enzymes capable of unwinding nucleotide duplexes, in a NTP hydrolysis dependent manner. As described in chapter 1, helicases are categorised into superfamilies and families according to their sequence, their substrate specificity, their directionality, whether they are passive or active helicases, their step-size and their rate of activity. A number of *in vitro* assays have been devised which allow the researcher to investigate the NTPase and helicase activity of a protein under different buffer conditions, with and without cofactors. A simple assay, developed to investigate the bacteriophage T7 DNA helicase, measures the displacement of DNA duplexes made with DNA oligomers of different lengths, one of which is radiolabeled, by observing the separation of the single labeled oligomer from that incorporated in the duplex by gel electrophoresis (Venkatesan *et al.*, 1982; Matson *et al.*, 1983). This assay can be altered in a number of ways, e.g. oligomer length, nucleotide content or composition (i.e. DNA, RNA, G:C rich), in order to investigate the helicases activity, efficiency, directionality and specificity. In combination these data can afford a detailed description of a helicase activity *in vitro*.

eIF4A is the prototypical member of the DEAD-box family of helicases and plays a prominent role in translation initiation. Due to its lack of N- and C-terminal domains eIF4A is comprised of the minimal two-domain 'helicase core' and is therefore representative of the conserved motifs of the DEAD-box family. As such the many studies undertaken to analyse the activity of eIF4A and its role in translation initiation also shed light on the DEAD-box helicase family at large. The functional properties of many the DEAD-box conserved motifs was discovered by the mutational analysis of eIF4AI (Pause and Sonenberg, 1992; Pause *et al.*, 1993) and the same researchers identified that eIF4AI was vital for translation initiation (Pause *et al.*, 1994). eIF4AI was shown to have bidirectional helicase activity (Rozen *et al.*, 1990), but this activity was at first

thought to be dependent upon it being complexed in eIF4F and on the presence of eIF4B (Lawson *et al.*, 1989; Rozen *et al.*, 1990; Pause and Sonenberg, 1992; Pause *et al.*, 1993). This contradicted previous data which had shown that eIF4AI/II purified from rabbit reticulocyte lysate made reoviral mRNA more susceptible to nuclease cleavage in an ATP-dependent manner, presumably by altering its secondary and/or tertiary structure (Ray *et al.*, 1985). Subsequent kinetic analysis also demonstrated that eIF4AI was able to hydrolyse ATP and bind RNA independent of other initiation factors (Lorsch and Herschlag, 1998a) and limited proteolysis with bound ATP/RNA demonstrated changes in the conformation of eIF4AI during different stages of its nucleotide cycle (Lorsch and Herschlag, 1998b) indicative of eIF4AI containing independent helicase activity. Rogers *et al* demonstrated in a series of studies that eIF4AI displayed a non-processive helicase activity, independent of other initiation factors, that became less efficient as the substrate duplex it was unwinding became more stable (Rogers *et al.*, 1999). The same researchers were also able to show that eIF4AI is able to unwind blunt ended duplexes, though with less efficiency than a duplex with a single stranded leader region, and duplexes that only contained one strand of RNA (i.e. DNA:RNA hybrids) (Rogers *et al.*, 2001a), though eIF4AI as part of eIF4F was unable to unwind anything other than an RNA:RNA duplex (Rogers *et al.*, 2001b). eIF4B and eIF4H have been shown to stimulate the helicase activity of eIF4AI, both on its own and as a complex with eIF4F (Ray *et al.*, 1985; Lawson *et al.*, 1989; Rozen *et al.*, 1990; Rogers *et al.*, 2001b) so that it becomes a slightly more processive helicase (Rogers *et al.*, 2001b). The degree of stimulation that eIF4B or eIF4H has on the helicase activity of eIF4AI is also dependent upon the stability of the duplex substrate (Rogers *et al.*, 2001b). eIF4B's stimulation of eIF4AI was observed to be substrate dependent as together they were less active at unwinding RNA:DNA hybrids than eIF4AI was on its own, whereas eIF4H did not appear to discriminate between RNA:RNA or RNA:DNA duplexes (Rogers *et al.*, 2001b). This difference in activity may be as a consequence of eIF4B containing additional domains to eIF4H, including an extra RNA binding region (Richter-Cook *et al.*, 1998). Though it appears to be a weak interaction that may be dependent both on ATP (or its analogues) and

RNA, eIF4H and eIF4B are thought to interact with eIF4AI on the same binding surface as each other (Rozovsky *et al.*, 2008).

Despite this research, the mechanism of eIF4AI's helicase activity and how it is stimulated by eIF4B or eIF4H is still largely unknown, as is its role in translation initiation. Due to its overexpression in cancer (Eberle *et al.*, 1997; Eberle *et al.*, 2002) and being the target of the tumour suppressor protein, Pdcd4 (Göke *et al.*, 2002), an effort has been made to identify drugs that target eIF4AI (Bordeleau *et al.*, 2008; Lindqvist *et al.*, 2008; Cencic *et al.*, 2010). A number of natural and synthesised inhibitors of eIF4AI have already been documented and in addition to being researched as potential inhibitors of tumourigenesis, they can also be used to discover eIF4AI's role in cellular biology. Understanding the mechanics of eIF4AI's helicase activity is essential to designing drugs that can inhibit it. This first chapter will present data regarding the cloning and expression of eIF4AI and eIF4B and demonstrate that they are both active *in vitro*. In addition two inhibitors of eIF4A activity will be assessed for their effect on helicase activity.

3.2 Cloning and expression of recombinant eIF4AI

In order to produce human recombinant protein, the coding sequence of eIF4AI was first PCR amplified from HeLa cell cDNA using primers that added the *Bam*HI or *Hin*dIII restriction sites to the 5' and 3' ends respectively. The amplified product was cloned, in frame, into the bacterial expression vector pGAT2 (EMBL laboratories, Heidelberg, Germany), which adds an N-terminal histidine tag to be used for purification purposes (figure 3.1). Successful cloning was verified by sequencing (Geneservice, Cambridge/Nottingham) and the vector transformed into BL21 (DE3) chemically competent *Escherichia coli*. Transformed *E. coli* were grown at 37 °C in a 500 ml culture until it reached an optical density, measured at 360 nm, of approximately 0.6. The expression of recombinant protein was then induced by the addition of 1 mM IPTG and the cells harvested after two hours. The optimal time for expression was determined by performing a trial expression that assessed the quantity of

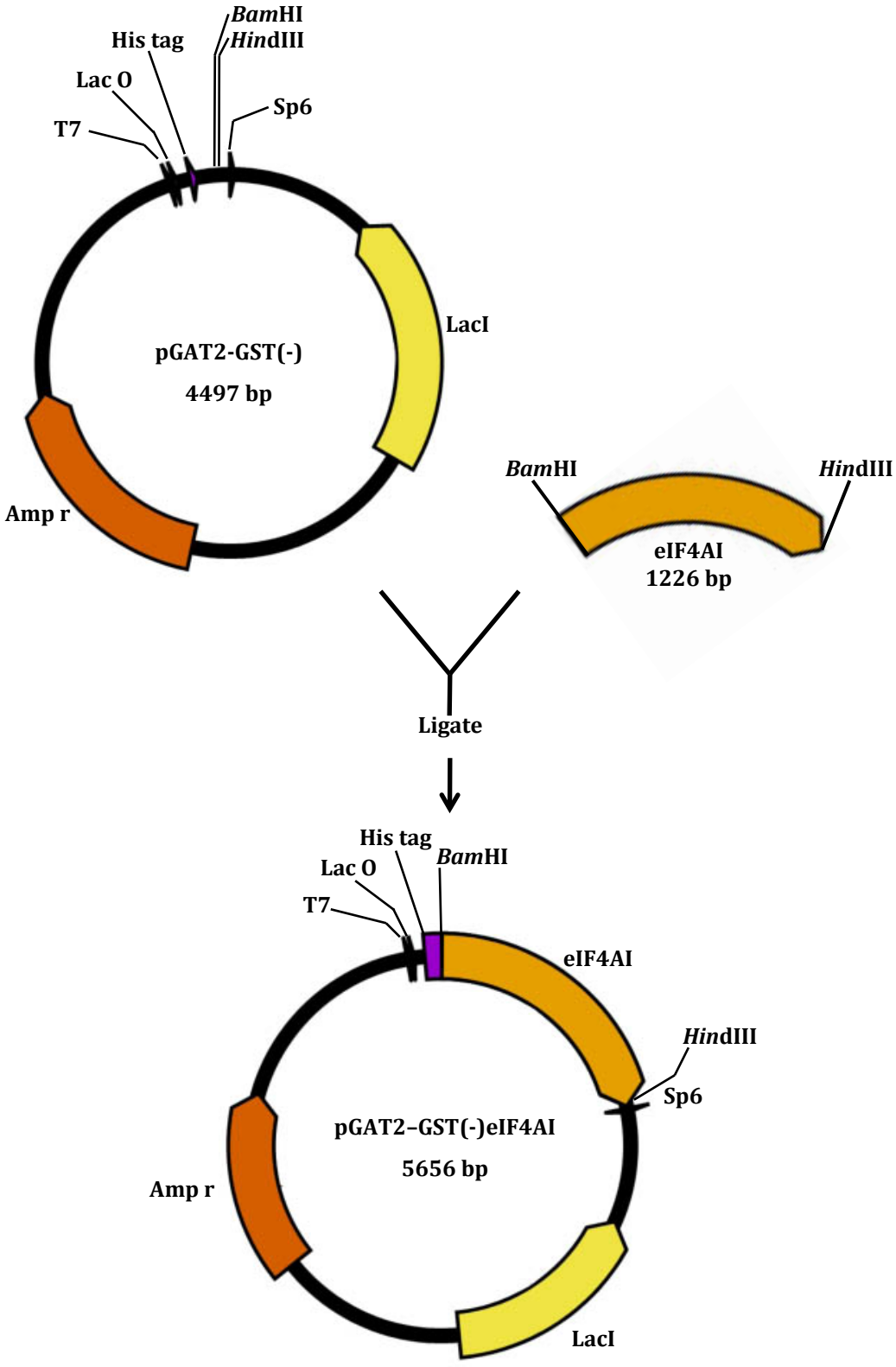

Figure 3.1 Cloning of eIF4AI into the bacterial expression vector pGAT2. Human eIF4AI was PCR amplified from HeLa cDNA and cloned into the bacterial expression vector pGAT2 (EMBL laboratories) using *Bam*HI and *Hin*dIII restriction sites. Amp r – Ampicillin resistance gene; T7 – T7 promoter; Lac O – Lac operator; His tag – histidine tag; Sp6 – promoter; LacI – Lac repressor

A

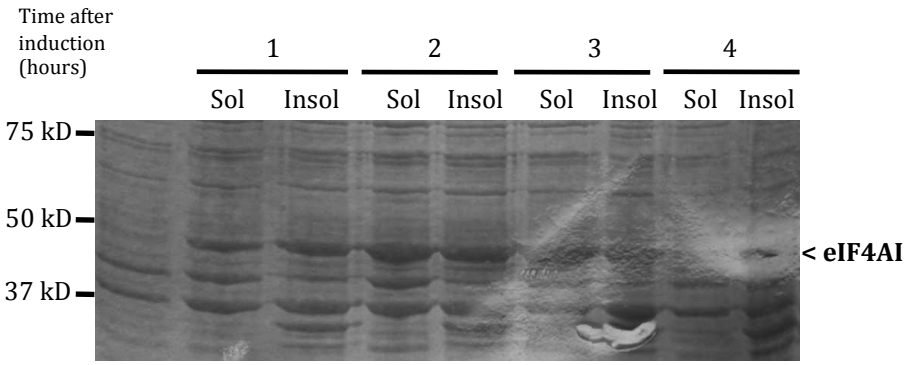

B

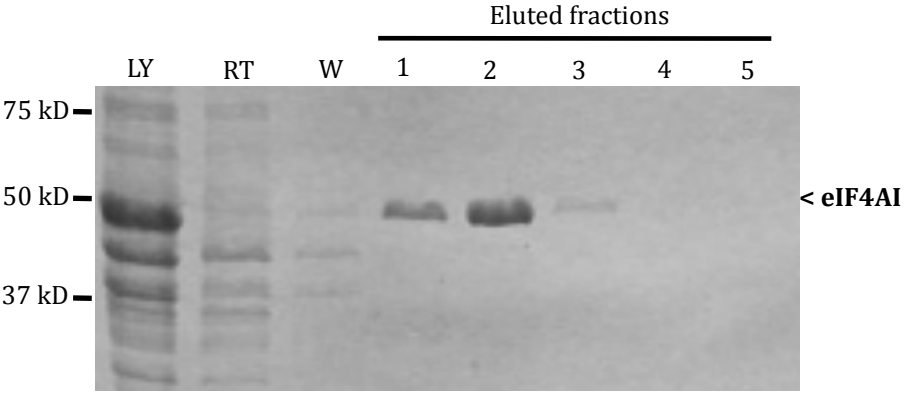

Figure 3.2 Bacterial expression and purification of recombinant eIF4AI. After the verification of the successful cloning of pGAT2-GST(-) eIF4AI by sequence analysis the expression vector was transformed into competent BL21 *E. coli*. Overexpression of the recombinant protein was induced with 1 mM IPTG and the optimal conditions for expression (A) and purification by affinity chromatography using nickel-coated agarose (B) were visualised by PAGE and coomassie blue staining. **A.** Sol – soluble fraction; Insol – Insoluble fraction. **B.** LY – cleared lysate; RT – Run through; W – Wash, 40 mM imidazole.

soluble and insoluble recombinant eIF4AI at different timepoints after induction (see figure 3.2, A). Recombinant eIF4AI was purified through a column packed with nickel-coated agarose and eluted in a buffer containing (50 mM Tris-HCl, pH 7.5; 150 mM NaCl; 2 mM $MgCl_2$) containing 250 mM imidazole in 1 ml fractions. The fraction(s) that contained the protein and the success of the purification procedure was determined by SDS-PAGE and coomassie blue staining (see figure 3.2, B), and the chosen fractions combined and diluted to approximately 0.1 - 0.2 mg/ml to avoid aggregation. The imidazole was removed by dialysis overnight in the buffer described above at 4 °C. The concentration of expressed eIF4AI was determined by reading the optical absorbance of the solution at 280 nm and it was then mixed with 10 % glycerol and stored in 50 μl aliquots at - 80 °C after snap-freezing in liquid nitrogen. The total amount of recombinant eIF4AI recovered after purification from a 500 ml culture was approximately 1 mg which is a low yield considering the quantity present in the crude lysate, however some loss occurred during the dialysis step where the protein in contact with the dialysis membrane appeared to come out of the solution. This was minimised by diluting the protein solution in imidazole-free buffer prior to dialysis.

3.3 Cloning and expression of recombinant eIF4B

In response to mTOR signaling eIF4B is thought to be phosphorylated on a number of residues, however the only modification characterised to date is by S6 kinase on serine residue 422 (Ser422) (Raught *et al.*, 2004). This phosphorylation event enhances translation through the increased binding of eIF3a (Raught *et al.*, 2004; Holz *et al.*, 2005; Shahbazian *et al.*, 2006; Kroczynska *et al.*, 2009). The influence that eIF4B post-translational modification has on eIF4AI/II, however, is unknown. A *Drosophila* expression system was therefore used initially to produce post-translationally modified recombinant eIF4B. To this end the coding sequence of human eIF4B was PCR amplified from HeLa cell cDNA using eIF4B specific primers that added the *Kpn*1 and *Apa*1 restriction sites to 5' and 3' ends respectively. The amplified product was cloned, in frame, into the *Drosophila* expression vector pMT/V5-HisB (Invitrogen), which adds a

C-terminal histidine tag and a V5-epitope that may be used for purification purposes (figure 3.3). Successful cloning was verified by sequencing (Geneservice, Cambridge/Nottingham) and the vector transfected into Schneider S2 *Drosophila* cells using a calcium phosphate transfection procedure. After the cells had recovered from the transfection a trial expression was performed by inducing the expression of recombinant protein with the addition of 500 μM copper sulphate and taking off 100 μl samples over the proceeding five days. The induction of expression was difficult to visualise by coomassie blue staining due to the low expression level of recombinant eIF4B and the *Drosophila* S2 cells expressing a protein that migrated to the same position as eIF4B and appearing as a prominent band. Western blot analysis was therefore employed to detect recombinant eIF4B expression using an antibody raised against eIF4B and also specifically against residue Ser422 of phosphorylated eIF4B. Figure 3.4, A and B, show that expression of eIF4B seems to have peaked at 4 days after its induction and that at least some of the expressed protein is phosphorylated on Ser422. Once eIF4B expression had been established for the *Drosophila* expression system, a stable cell line was generated by cotransfecting cells with the eIF4B expression vector and a selection vector, pCoBlast (Invitrogen) that positively selected for Blasticidin resistance. Stably selected S2 cells were sub-cultured for approximately three weeks until they reached a density of approximately eight million cells/ml in a 500 ml culture volume. The expression of recombinant eIF4B was then induced by the addition of 500 μM copper sulphate and the cells harvested on the fourth day after induction. Initial attempts to purify *Drosophila* expressed recombinant eIF4B were performed using a column packed with nickel-coated agarose as described above for bacterially expressed eIF4A, supplementing the lysis and elution buffer with phosphatase inhibitors. When examined by SDS-PAGE and coomassie blue staining this purification procedure produced a prominent, though weak band that migrated to about 100 kD, 20 kD larger than expected, and the eluted fractions also contained some contaminating proteins (see figure 3.4 C). In order to further purify the 100 kD band, the eluted fractions in which it was contained were passed through a heparin column and proteins eluted using increasing concentrations of KCl. The eluted fractions were visualised by SDS-

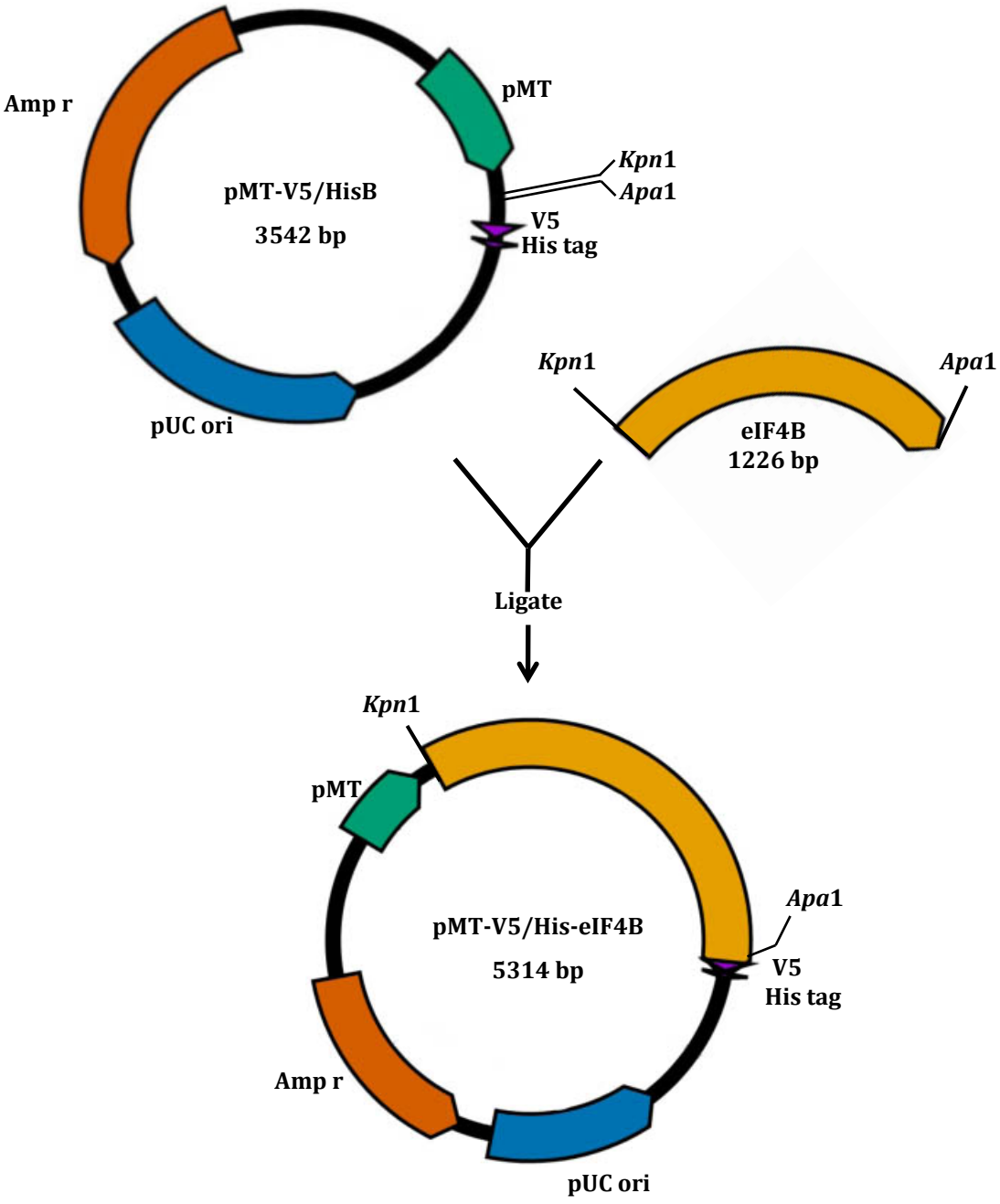

Figure 3.3 Cloning of eIF4B into the *Drosophila* expression vector pMT-V5/HisB. Human eIF4B was PCR amplified from HeLa cDNA and cloned into the *drosophila* expression vector pMT-V5/HisB (Invitrogen) using *Kpn*1 and *Apa*1 restriction sites. Amp r – Ampicillin resistance gene; pUC ori – pUC origin of replication; His tag – histidine tag; V5 – V5 epitope tag; pMT – metallothionein promoter.

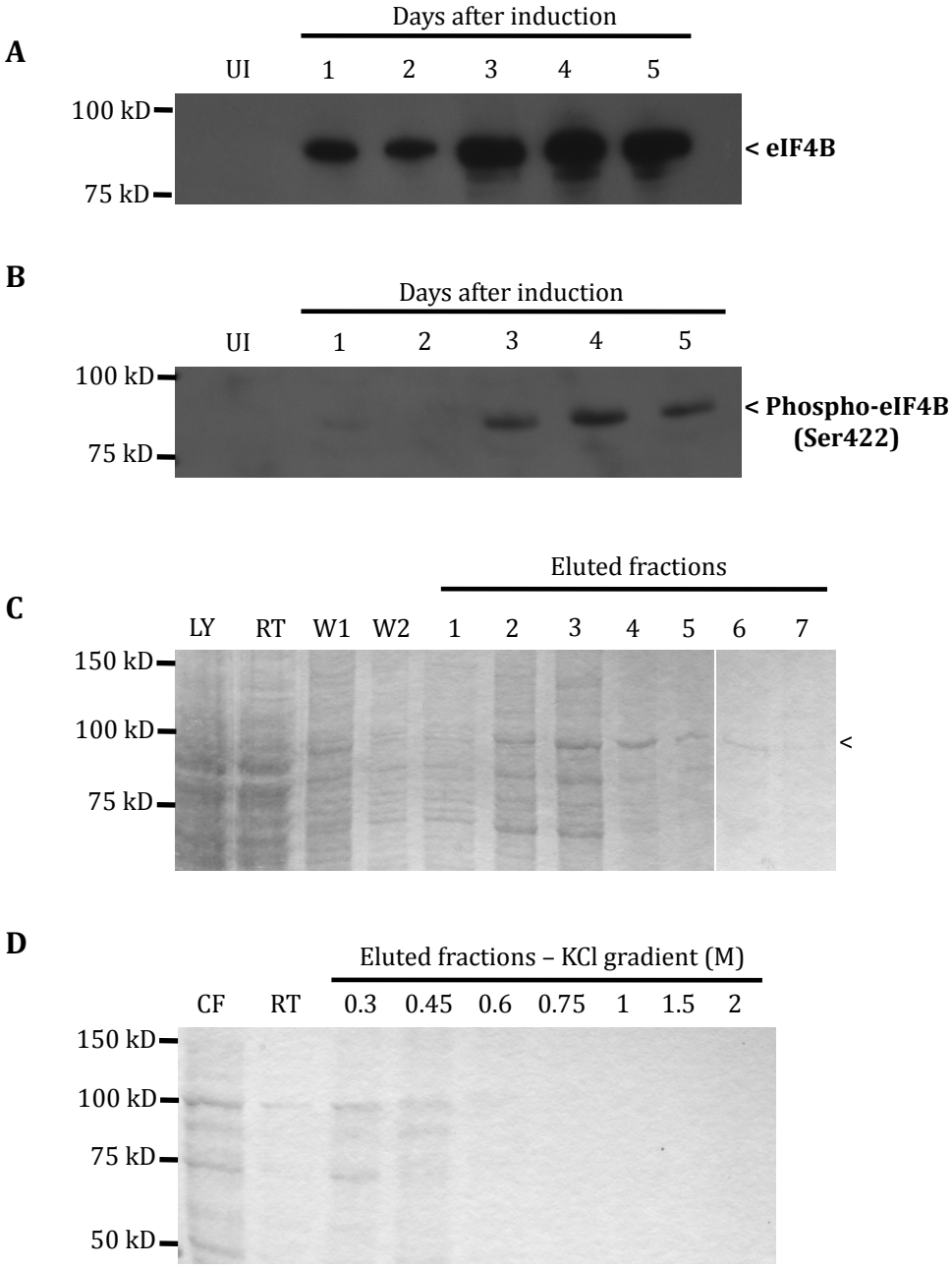

Figure 3.4 *Drosophila* expression of recombinant eIF4B. The successful cloning of pMT-V5/HisB-eIF4B was verified by sequence analysis and then transfected into Schneider S2 drosophila cells using the protocol outlined in the *Drosophila* Expression System (DES) (Invitrogen). Overexpression of the recombinant protein was induced with 500 μM copper sulphate and the number of days required for optimal expression assessed by the detection of expressed protein by PAGE and western blot analysis using: (A) eIF4B antibody (gift from J. W. B. Hershey, Davis, USA) and (B) Phospho-eIF4B (Ser 422) (Cell Signaling). Purification was carried out using affinity chromatography with nickel-coated agarose (C) and heparin-coated agarose (D) and samples analysed by SDS-PAGE and coomassie blue staining.

PAGE and coomassie blue staining but all of the proteins were eluted at relatively low concentrations of KCl (300 - 450 mM), demonstrating that they were not retained on the heparin column, which possibly meant that they did not have RNA binding activity (see figure 3.4, D). Western blot analysis using an eIF4B specific antibody then revealed that none of the purified fractions contained eIF4B. A further attempt to overexpress recombinant eIF4B using the stably transfected S2 cell line was made, however, before purification it was determined by western blotting that eIF4B overexpression was not detectable. Due to this a bacterial expression scheme was designed as detailed below.

In order to produce recombinant eIF4B using a bacterial expression system, the coding sequence of the protein was PCR amplified from HeLa cell cDNA using primers that added the *Bam*HI or *Hin*dIII restriction sites to the 5' and 3' ends respectively. The amplified product was then cloned into the bacterial expression vector pGAT2 (see figure 3.5) and expressed and purified as described above for recombinant eIF4AI. The eluted fractions were assessed for recombinant eIF4B content by SDS-PAGE and coomassie blue staining (see figure 3.6). Protein containing fractions were combined and dialysed overnight to remove the imidazole from the buffer as described above for eIF4A. The concentration of recombinant eIF4B was determined by reading the optical absorbance of the solution at 280 nm and it was then mixed with 10 % glycerol and stored in 100 μl aliquots at - 80 °C after snap-freezing in liquid nitrogen. The total amount of recombinant eIF4B recovered after purification from a 500 ml culture was approximately 3.6 mg. The purity of eIF4B is estimated to be approximately 85 - 90 %.

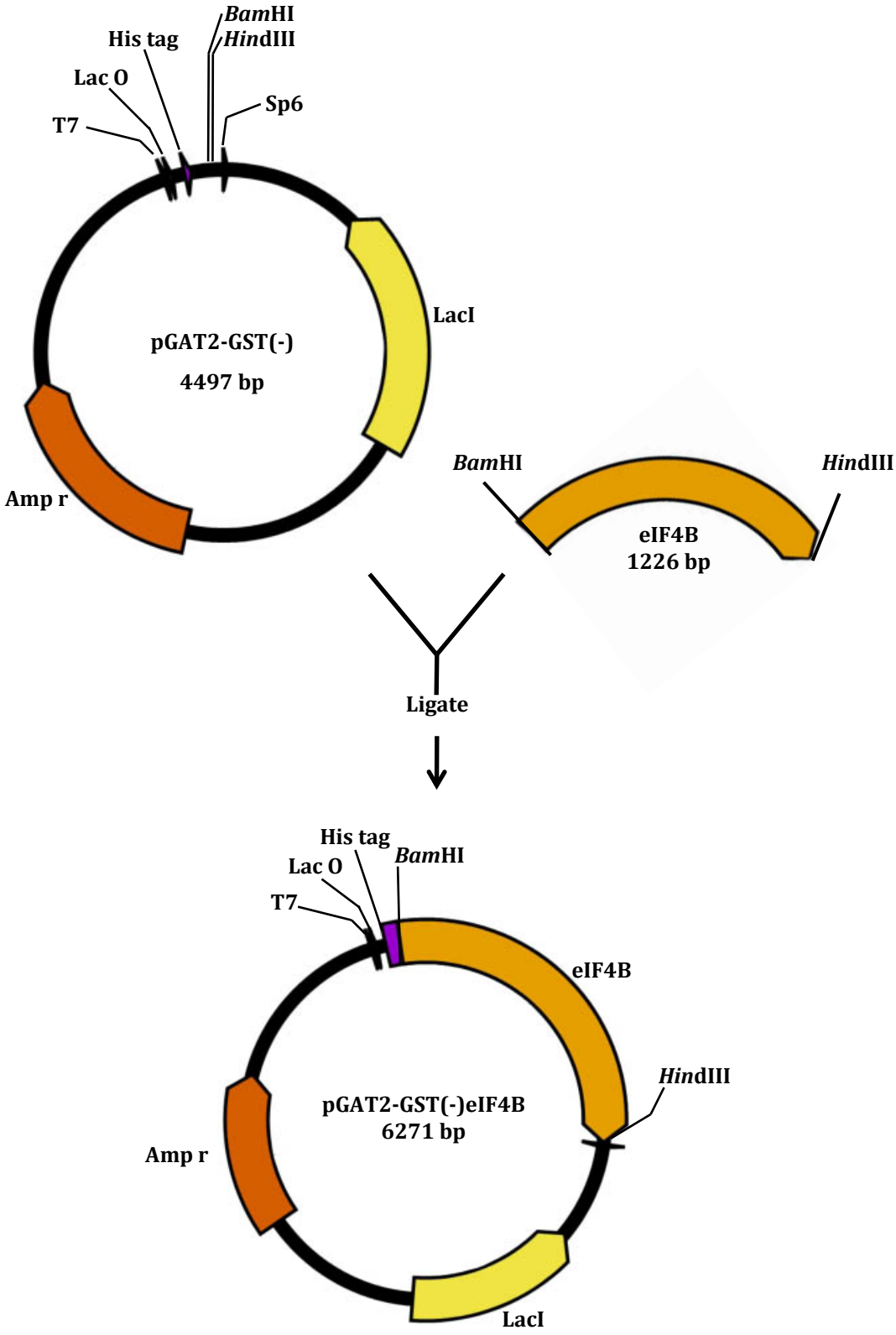

Figure 3.5 Cloning of eIF4B into the bacterial expression vector pGAT2. Human eIF4B was PCR amplified from HeLa cDNA and cloned into the bacterial expression vector pGAT2 (EMBL laboratories) using *Bam*HI and *Hin*dIII restriction sites. Amp r – Ampicillin resistance gene; T7 – T7 promoter; Lac O – Lac operator; His tag – histidine tag; Sp6 – promoter; LacI – Lac repressor

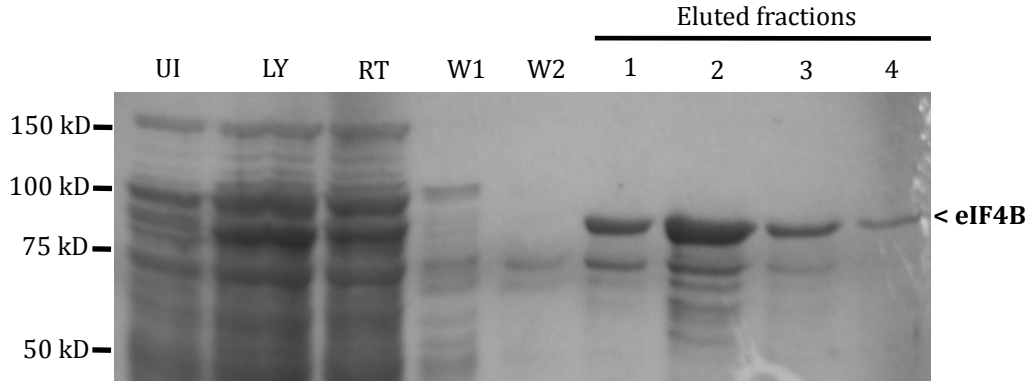

Figure 3.6 Bacterial expression and purification of recombinant eIF4B. The successful cloning of pGAT2-GST(-)eIF4B was verified by sequence analysis and the expression vector then transformed into competent BL21 *E. coli*. Overexpression of the recombinant protein was induced with 1mM IPTG for two hours and purified using nickel agarose columns. Proteins were visualised by PAGE and coomassie blue staining. UI – Uninduced; LY – cleared lysate; RT – Run through; W1 – Wash 1, 40 mM imidazole; W2 – Wash 2, 40 mM imidazole.

3.4 eIF4AI displays helicase activity *in vitro*

A number of assays have been developed to examine different aspects of helicase related activity, such as NTP hydrolysis and nucleic acid binding affinity. To measure helicase activity directly, a simple assay, first developed to investigate the bacteriophage T7 DNA helicase (Venkatesan *et al.*, 1982; Matson *et al.*, 1983), can be modified to investigate RNA helicases. An RNA duplex, radiolabeled at the terminus of one strand, is incubated with the putative helicase in the presence of ATP and any displacement of the duplex caused by unwinding activity is measured by separating the intact duplex and the displaced radiolabeled strand by PAGE (see figure 3.7, B). This procedure has been used a number of times to assess eIF4AI activity, on its own and in complex with eIF4G and eIF4E as eIF4F, and with eIF4B and eIF4H (Lawson *et al.*, 1989; Rozen *et al.*, 1990; Pause and Sonenberg, 1992; Pause *et al.*, 1993; Rogers *et al.*, 1999; Rogers *et al.*, 2001a; Rogers *et al.*, 2001b). Initially eIF4AI was seen to only have helicase activity in the presence of eIF4B or in complex as eIF4F (Lawson *et al.*, 1989; Rozen *et al.*, 1990; Pause and Sonenberg, 1992; Pause *et al.*, 1993), but later research demonstrated that it could unwind duplexes in an ATP dependent manner (Rogers *et al.*, 1999). The discrepancy in helicase activity could be caused by differences in the activities of bacterially expressed recombinant eIF4AI and that purified from rabbit reticulocyte lysate (RRL), or, as Rogers *et al* note, by the low concentration of RNA duplex used in the initial experiments which was later shown to be below that required for ATPase activation (Lorsch and Herschlag, 1998a).

In order to assess whether bacterially expressed recombinant eIF4AI had *in vitro* helicase activity a helicase assay was developed using a modified version of the protocols outlined in (Rogers *et al.*, 1999; Rogers *et al.*, 2001a). In the second study the authors use a series of RNA duplexes of increasing stability to analyse the effectiveness of eIF4AI. The duplex "R-44/R-11" was comprised of a 44-mer and a 5'-^{32}P-labeled 11-mer and has a stability of -17.9 ΔG (measured in kcal/mol and calculated by Rogers *et al* using the nearest neighbour method described in (Sugimoto *et al.*, 1995) at 35 °C (Rogers *et al.*, 2001a)). This duplex

was selected for use in the helicase assay due to its relatively low stability, which will allow eIF4AI activity to be monitored without the secondary structure acting as an inhibitor. In addition, Rogers *et al* noted that this duplex, amongst a number tested of different lengths and stabilities, produced the largest difference between eIF4AI catalysed unwinding and background thermal melting (Rogers *et al.*, 1999) meaning that an accurate estimation of the initial rate of unwinding should be achievable. Initially the RNA molecules were synthesised by *in vitro* transcription using DNA oligomers with 5' T7 polymerase promoters as templates and adding α-^{32}P-CTP to the transcription mix of the 11-mer. The purification of the 11-mer, however, was difficult and therefore the hybridised duplex was contaminated with an excess of radiolabeled nucleotide, even after its excision and elution from the gel. Synthesised RNA oligonucleotides were therefore purchased and the 11-mer was end labeled using γ-^{32}P-ATP and polynucleotide kinase as depicted in figure 3.7, A. A series of helicase assays were carried out in total volumes of 50 μl, using 0.5 nM duplex, 1 mM ATP and 0.125 μM - 1μM recombinant eIF4AI in a reaction buffer consisting of 25 mM Tris-HCl, pH7.5; 75 mM NaCl and 1 mM $MgCl_2$. The reaction components were kept on ice at all times prior to the initiation of the reaction by the addition of ATP. The order at which ATP, eIF4AI or RNA duplex was added was previously determined to have no influence on the outcome of the reaction (Rogers *et al.*, 1999). At five-minute intervals 7.5 μl samples were taken from the main reaction and mixed with 7.5 μl stop solution on ice. An ATP-free control reaction that was incubated at 37 °C for the duration of the experiment was used to assess the level of background thermal duplex displacement and whether there was any noticeable nuclease activity. Reaction products were separated by 15 % PAGE buffered in 0.5 x TBE at 150 V for approximately 1 hour at 4 °C, and the gel was then dried and exposed to a phosphorimager screen overnight. Images were visualised using QuantityOne software (v. 4.6.5, BioRad) and the area and intensity of each band quantified using ImageJ (v. 1.43, National Institute of Health, USA) (figure 3.8, A). The initial rate of unwinding was determined by first calculating the percentage of intact duplex at each timepoint to allow for any pipetting or gel loading errors.

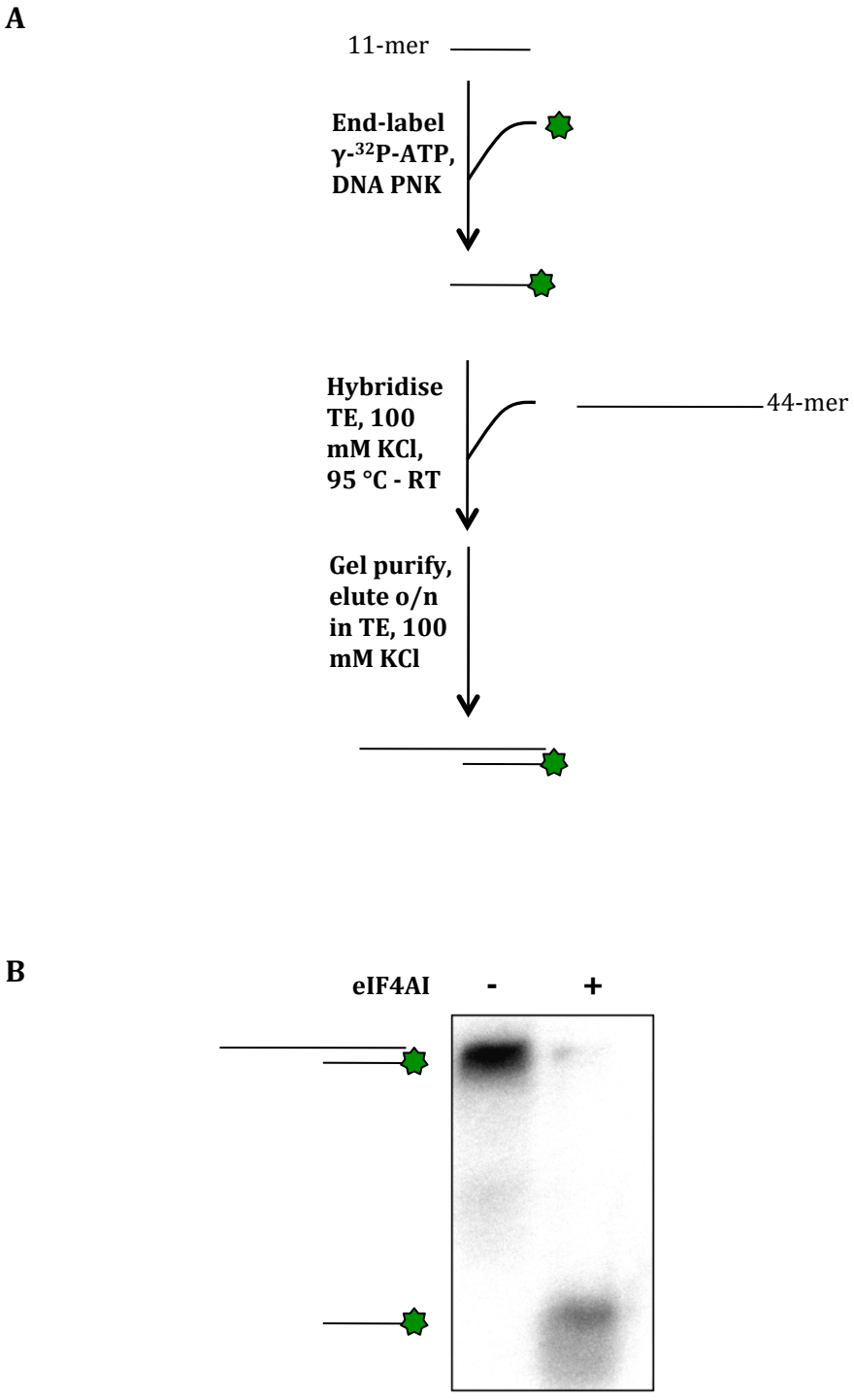

Figure 3.7 Helicase assay principle. **A.** Schematic diagram representing the method used to prepare the radiolabeled duplex used in the helicase assay as described in 2.4.29. **B.** Example of the displacement of the duplex RNA in the presence of eIF4AI.

These data were then normalised to the first sample taken at the start of the reaction (0 minutes) to allow comparison between each set of reactions and plotted using Prism (v. 5, GraphPad) fitting each data set with an exponential decay model (figure 3.9, A). The initial rate was calculated using Excel (Microsoft Office) by drawing a tangent to each curve between zero and one minute and the results are displayed as percentage unwound/minute in figure 3.9, B.

As expected, increasing the concentration of eIF4AI in the reaction increases the total amount of duplex unwound at 30 minutes and also increases the initial rate of unwinding. As observed in (Rogers *et al.*, 1999) the R-44/R-11 duplex displayed very little background thermal melting and no noticeable RNase activity was noted. The rate of unwinding was less than that observed by Rogers *et al*, who demonstrated that 0.8 μM eIF4AI unwound 91 % duplex RNA at 15 minutes compared to 82 % at 15 minutes with 1 μM recombinant eIF4AI (figure 3.8) (Rogers *et al.*, 2001a). Rogers *et al* used eIF4AI purified from RRL, however, which may account for this difference in activity. By doubling the concentration of eIF4AI, the initial rate of unwinding would also be to increase in a linear manner as previously observed (Rogers *et al.*, 1999), however this was not seen to be the case (figure 3.9, B) as each increase in concentration stimulated a ~ 1.55, 1.44 and 1.25 fold increase in unwinding rate respectively. This may be due to the reaction completing its linear phase prior to the first time point taken at five minutes, which would therefore cause an underestimate of the initial rate calculation. The diffuseness of the lower band may also cause an underestimate in the amount of unwound duplex RNA detected. It is also noted that the concentration of RNA duplex used was four times lower than that used by Rogers *et al*, which perhaps would become limiting during the course of the reaction, however this would not influence the initial rate. This initial analysis of bacterially expressed recombinant eIF4AI demonstrates that it displays helicase activity *in vitro*.

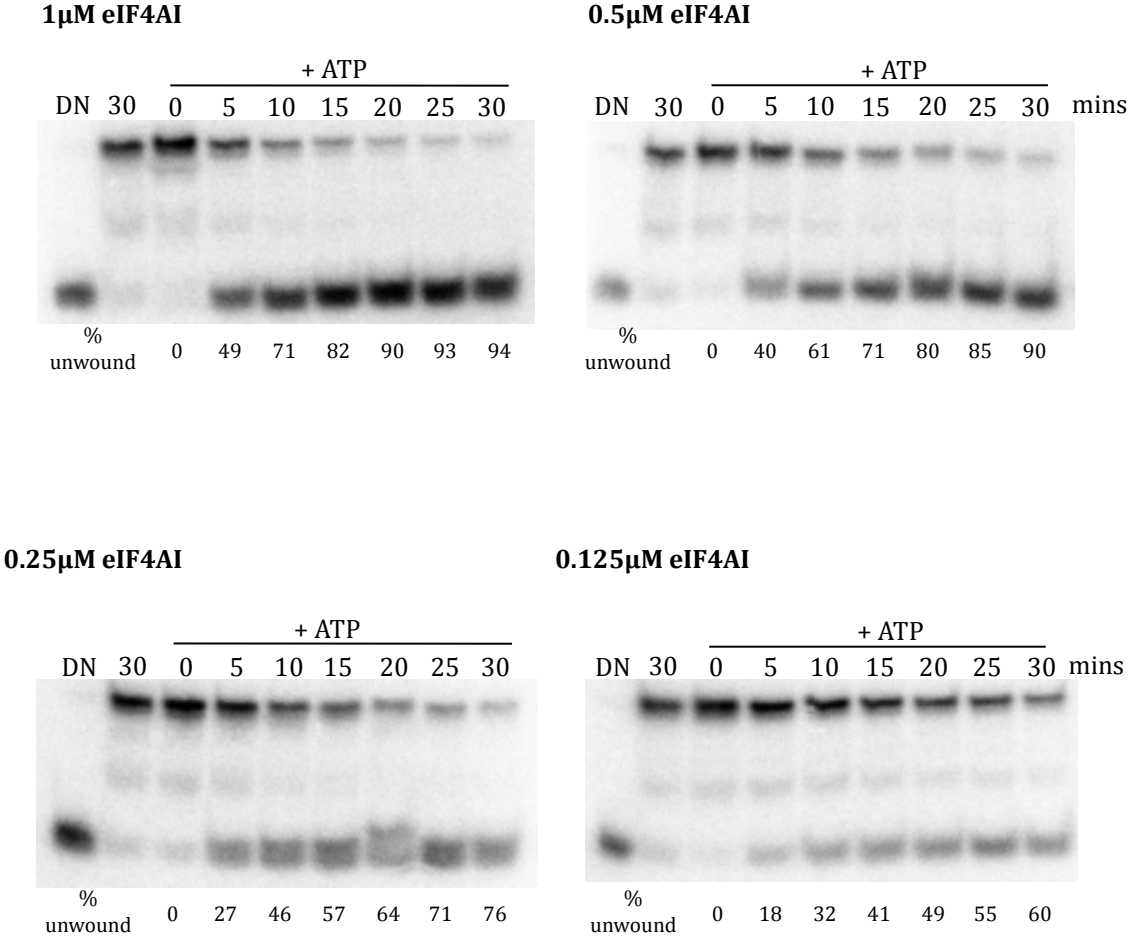

Figure 3.8 Helicase activity of recombinant eIF4AI. Recombinant eIF4AI helicase activity was examined *in vitro* by measuring the displacement of a radiolabeled RNA oligomer duplex at fixed timepoints using different concentrations of eIF4AI (as indicated above each image). Each experiment contained a control denatured at 95 °C for 5 minutes (DN – lane 1), and a control omitting ATP which was incubated at 37 °C for the duration of the experiment (30 minutes – lane 2). After the addition of 1 mM ATP, each reaction was incubated at 37 °C and 7.5 µl samples taken off and mixed with 7.5 µl stop solution. The samples were separated by PAGE through a 15 % acrylamide gel buffered in 0.5 x TBE at 4 °C for approximately one hour at 150 V. The gel was then vacuum dried and exposed to a phosphorimager screen overnight. Images were scanned using QuantityOne software (v. 4.6.5, BioRad) and quantified using ImageJ (v. 1.43, National Institute of Health, USA). Average values of % unwound displayed under each lane, calculated as described in figure 3.9. n=3.

A

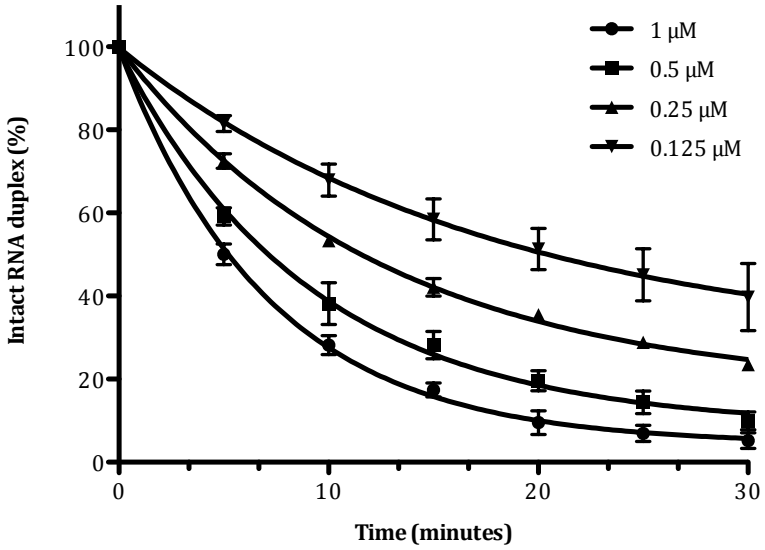

B

Concentration of eIF4AI (μM)	Initial rate of unwinding (% unwound/minute)
0.125	4.0
0.25	6.2
0.5	8.9
1	11.1

Figure 3.9 Rate of recombinant eIF4AI *in* vitro helicase activity. The rate of unwinding was calculated for each enzyme concentration using ImageJ (v. 1.43, National Institute of Health, USA) to quantify the area and intensity (AI) of each band representing intact duplex RNA (upper band) or unwound 11-mer RNA (lower band) for each timepoint. The amount (%) of intact duplex remaining was calculated using the following equation:- (AI upper band/(AI upper band + AI lower band)) X 100. n = 3 **A.** Graphs were produced using Prism (v. 5, GraphPad) using an exponential decay fit. Concentration of eIF4AI as indicated. Error bars indicate standard error of the mean (SEM) **B.** The initial rate of reaction was calculated for each enzyme concentration using Excel (Microsoft Office) by drawing a tangent of the initial slope (0 - 1 minute) using the line equation determined (% unwound/minute).

3.5 eIF4B stimulates the helicase activity of eIF4AI *in vitro*

It is well established that eIF4B and eIF4H are able to stimulate eIF4AI or eIF4F activity *in vitro* in a mutually exclusive fashion as they are thought to compete for binding to the same site on eIF4AI (Ray *et al.*, 1985; Lawson *et al.*, 1989; Rogers *et al.*, 2001b; Rozovsky *et al.*, 2008). eIF4B increases the affinity of eIF4AI for ATP and RNA (Rozen *et al.*, 1990; Pause and Sonenberg, 1992), however, the mechanism by which eIF4B can stimulate eIF4AI helicase activity in translation initiation has not been clarified. Recent modeling of a limited translation initiation complex comprised of eIF4AI, eIF4GI and eIF4H placed eIF4H 5' to eIF4AI and eIF4H was therefore proposed to stabilise newly unwound ssRNA regions, which would help prevent secondary structure reannealing (Marintchev *et al.*, 2009). Due to their homology it is thought that eIF4B may fulfill a similar role, however due to its larger N- and C-terminal domains which confer additional binding capabilities it is also likely that it performs further functions during translation initiation (Milburn *et al.*, 1990; Altmann *et al.*, 1995; Methot *et al.*, 1996a; Methot *et al.*, 1996b; Bushell *et al.*, 2000).

To investigate the extent of recombinant eIF4B stimulation of recombinant eIF4AI *in vitro*, the helicase assay described above was repeated using different concentrations of eIF4B. As the initial rate was deemed the most relevant and accurate form of comparison between the experiments the timecourse was shortened to 15 minutes. The data gained from the experiments described above were used to determine the optimum concentration of eIF4AI, which would allow an accurate estimation of the initial rate of reaction (0.25 μM eIF4AI achieved ~ 57 % unwinding at 15 minutes). After initially assessing that recombinant eIF4B did not display any helicase activity in the presence and absence of ATP, four separate experiments were performed using four different concentrations of eIF4B: 0, 0.0625, 0.125 and 0.25 μM to generate eIF4AI:eIF4B ratios of 1:0, 1:0.25, 1:0.5 and 1:1 respectively. Reactions were performed and analysed as described above and the results are displayed in figures 3.10 and 3.11.

Figures 3.10 and 3.11 show that recombinant eIF4B stimulates eIF4AI activity *in vitro*. Previous studies had demonstrated that eIF4B stimulation of eIF4AI was maximal at an equimolar concentration (Rogers *et al.*, 2001b), causing an approximately 3.4-fold stimulation of helicase activity (7.9 % unwound/minute, 0.2 μM eIF4AI; 27 % unwound/minute, 0.2 μM eIF4AI and eIF4B). The initial rate of unwinding recorded in our experiments demonstrated that eIF4B achieved a maximal 1.6-fold stimulation of eIF4AI activity at an equimolar concentration of eIF4AI:eIF4B. This is 2.4-fold lower than that previously recorded by Rogers *et al.* (Rogers *et al.*, 1999; Rogers *et al.*, 2001b). As with the above experiments investigating the independent helicase activity of eIF4AI the difference between the results recorded in this study and the published literature may be due to a number of factors including if the RNA concentration became limiting during the first five minutes of the experiment so that the first timepoint misses the linear phase of the reaction or errors in the quantification of the bands. Furthermore, if there were inaccuracies in the quantification of the protein then this would mean the molar ratios between the two proteins would be incorrect. As purified recombinant eIF4B was less pure than eIF4AI (~ 85 - 90 % as opposed to ~ 99 % - see figures 3.6 and 3.2 B respectively) it is likely that the quantification of eIF4B would be an underestimate rather than an overestimate, which may result in a reduced activity than that predicted. The quantification procedure also assumes that the protein population in each sample is homogenously active, if this is not the case then this would be reflected as an unknown difference between the ratios of the two proteins. Further experiments that could be performed in order to rule out any or all of these possibilities will be discussed below.

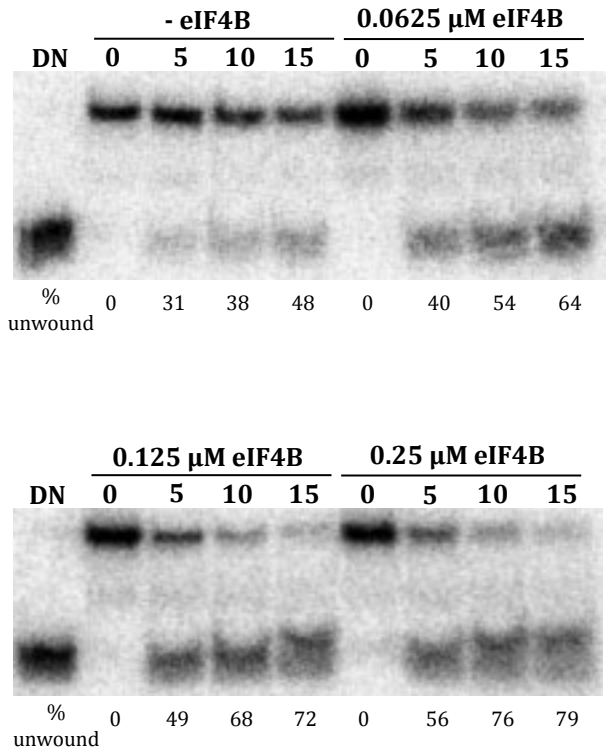

Figure 3.10 Stimulatory effect of recombinant eIF4B on recombinant eIF4AI's *in vitro* helicase activity. The stimulatory effect of recombinant eIF4B on recombinant eIF4AI helicase activity was examined *in vitro* by measuring the displacement of a radiolabeled RNA oligomer duplex at fixed timepoints using different concentrations of eIF4B (as indicated above each image). In each experiment 0.25 µM eIF4AI was used. Initial studies were conducted which determined that eIF4B contained negligible helicase activity in the presence and absence of ATP. Each experiment contained a control denatured at 95 °C for 5 minutes (DN – lane 1). Reactions were carried out and visualised as described in figures 3.8 and 3.9. Average values of % unwound displayed under each lane, calculated as described in figure 3.9. n=3.

A

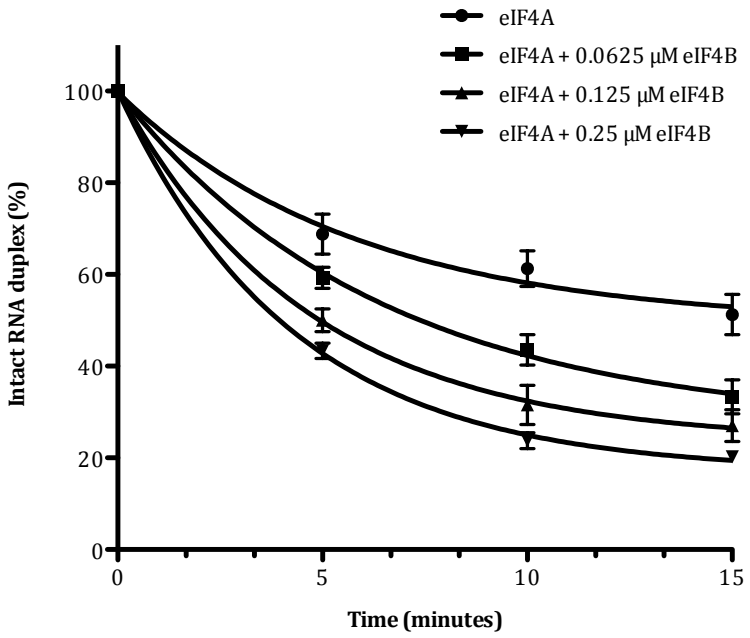

B

Concentration of eIF4B (μM)	Ratio eIF4AI:eIF4B	Initial rate of unwinding (% unwound/minute)
0	1:0	9.4019
0.625	1:0.25	11.337
0.125	1:0.5	13.359
0.25	1:1	15.303

Figure 3.11 Rate of recombinant eIF4B stimulated *in* vitro helicase activity. The rate of unwinding was calculated for each enzyme concentration using ImageJ (v. 1.43, National Institute of Health, USA) to quantify the area and intensity (AI) of each band representing intact duplex RNA (upper band) or unwound 11-mer RNA (lower band) for each timepoint. The amount (%) of intact duplex remaining was calculated using the following equation:- (AI upper band/(AI upper band + AI lower band)) X 100. n = 3 **A.** Graphs were produced using Prism (v. 5, GraphPad) using an exponential decay fit. Error bars indicate standard error of the mean (SEM) **B.** The initial rate of reaction was calculated for each enzyme concentration using Excel (Microsoft Office) by drawing a tangent of the initial slope (0 - 1 minute) using the line equation determined (% unwound/minute).

3.6 Inhibition of eIF4AI's helicase activity by hippuristanol and 15d-PGJ_2

A number of modulators of eIF4AI activity have been described that can inhibit translation initiation by targeting different aspects of eIF4AI function. Hippuristanol is a well-characterised inhibitor of eIF4AI and II and to a lesser extent eIF4AIII (Lindqvist *et al.*, 2008), that is isolated from the gorgonian *Isis hippuris* (Shen et al., 2001). By binding to the C-TD of eIF4A hippuristanol inhibits the ATPase, RNA binding and helicase activity of the enzyme and exerts an anti-proliferative activity (Shen *et al.*, 2001; Bordeleau *et al.*, 2006b). The cyclopentenone 15-deoxy-delta(12,14)-prostaglandin J_2 (15d-PGJ_2) is a derivative of PGD_2 expressed during acute inflammation as part of the host's pro-resolution response (Gilroy *et al.*, 1999). It has recently been established that one of the many mechanisms by which 15d-PGJ_2 exerts its anti-inflammatory activity is via an interaction with eIF4AI that prevents its association with eIF4GI, and thereby eIF4F (Kim *et al.*, 2007). Whether this interaction also inhibits the helicase activity of eIF4AI has not been examined.

To assess whether hippuristanol and 15d-PGJ_2 could inhibit recombinant eIF4AI activity *in vitro*, the helicase assay described above was repeated using an eIF4AI concentration of 0.5 μM and varying concentrations of inhibitors. Initial experiments to assess whether the inhibitors or DMSO caused any duplex dissociation independent of eIF4AI activity were negative. As with the eIF4B experiments, an experimental duration of 15 minutes was used to obtain an activity profile of eIF4AI helicase activity in the presence of either of the inhibitors or a DMSO control. A smaller sample size of 5 μl was used to conserve recombinant eIF4AI stocks so that all the helicase assay experiments were performed with the same batch of protein. The experiments and analysis of the results were carried out as described above with the exception of BSA being omitted from the reactions with 15d-PGJ_2 as albumin is known to bind and sequester the prostaglandin (Person *et al.*, 2001). The results are shown in figures 3.12 and 3.13 for hippuristanol and 3.14 and 3.15 for 15d-PGJ_2 respectively.

50 µM hippuristanol

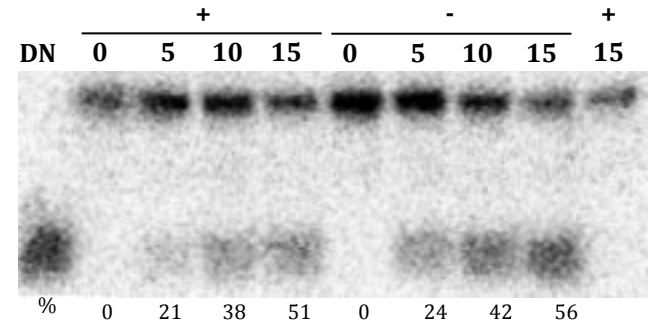

100 µM hippuristanol

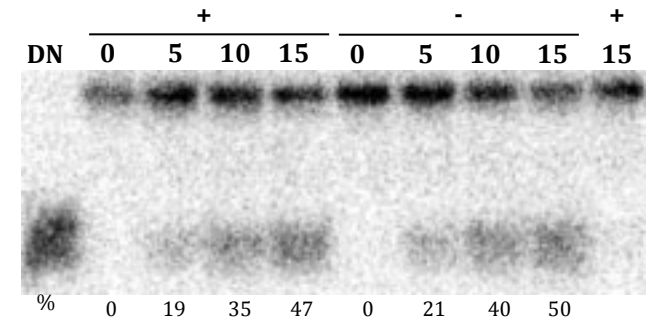

Figure 3.12 Effect of hippuristanol on recombinant eIF4AI's *in vitro* helicase activity. The inhibitory effect of hippuristanol on recombinant eIF4AI helicase activity was examined *in vitro* by measuring the displacement of a radiolabeled RNA oligomer duplex at fixed timepoints using different concentrations of hippuristanol or a DMSO equivalent control (as indicated above each image, (+) with hippuristanol; (-) with DMSO). In each experiment 0.5 µM eIF4AI was used. Each experiment contained a control denatured at 95 °C for 5 minutes (DN – lane 1) and an ATP-free control that was incubated for the duration of the experiment at 37 °C (lane 10). Reactions were carried out and visualised as described in figures 3.8 and 3.9. Average values of % unwound displayed under each lane, calculated as described in figure 3.9. n=2.

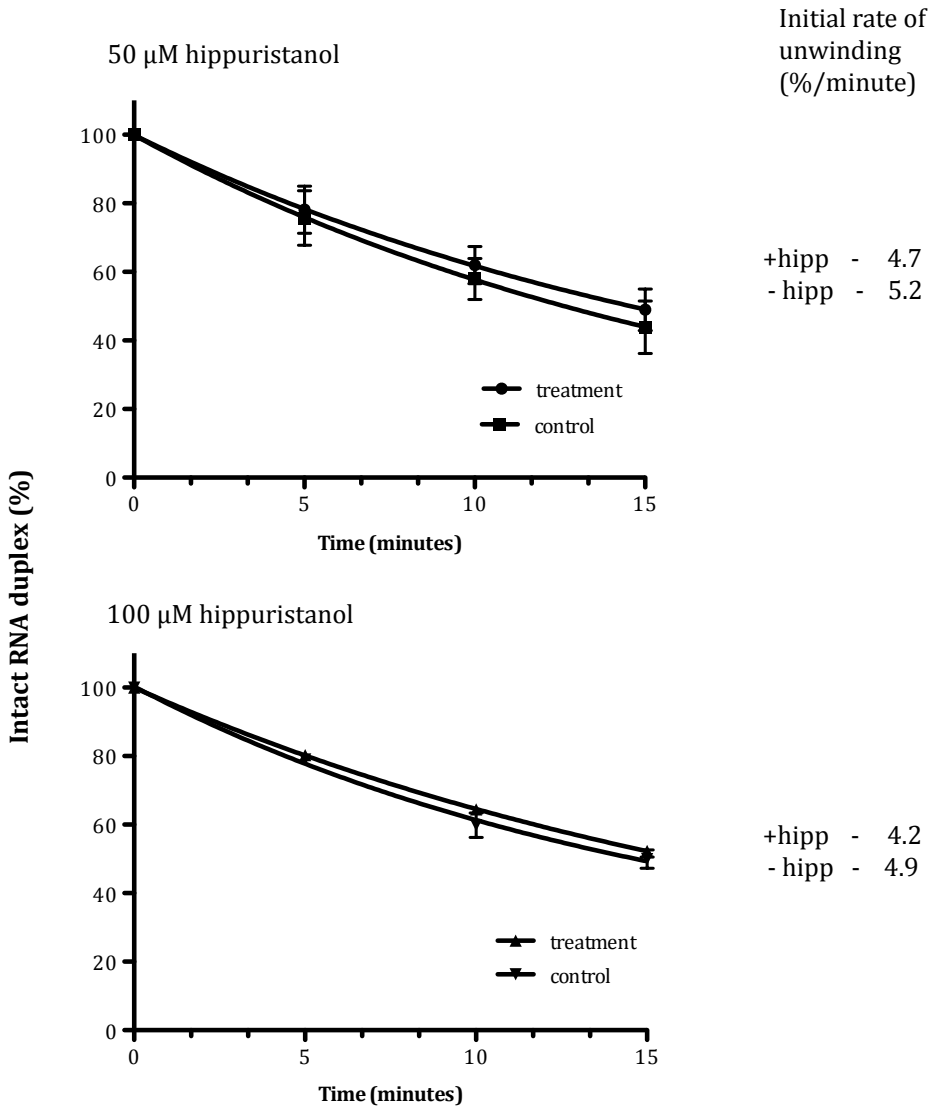

Figure 3.13 Rate of hippuristanol inhibited recombinant eIF4AI *in vitro* helicase activity. The rate of unwinding was calculated for each enzyme concentration using ImageJ (v. 1.43, National Institute of Health, USA) to quantify the area and intensity (AI) of each band representing intact duplex RNA (upper band) or unwound 11-mer RNA (lower band) for each timepoint. The amount (%) of intact duplex remaining was calculated using the following equation:- (AI upper band/(AI upper band + AI lower band)) X 100. n = 2 **A.** Graphs were produced using Prism (v. 5, GraphPad) using an exponential decay fit. Error bars indicate standard error of the mean (SEM) **B.** The initial rate of reaction was calculated for each enzyme concentration using Excel (Microsoft Office) by drawing a tangent of the initial slope (0 - 1 minute) using the line equation determined (% unwound/minute).

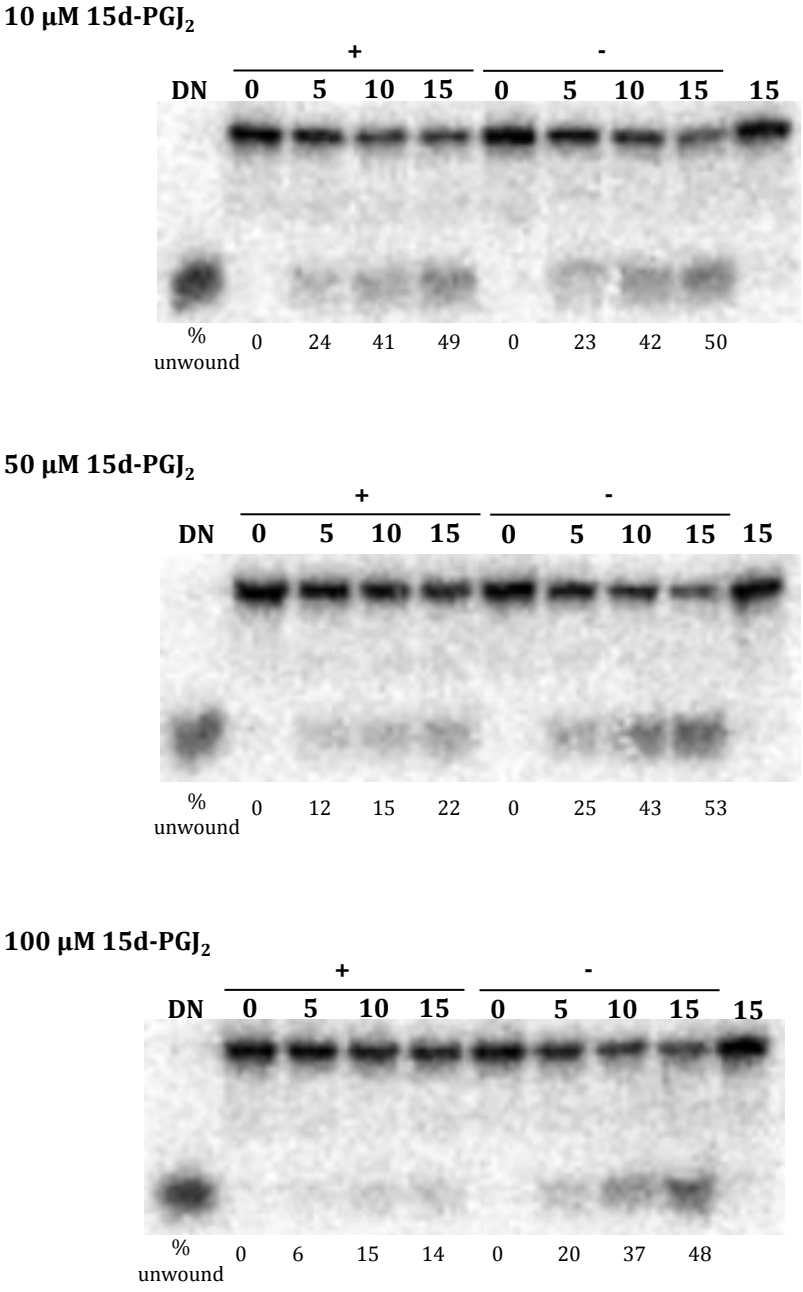

Figure 3.14 Inhibitory effect of 15d-PGJ_2 on recombinant eIF4AI's *in vitro* helicase activity. The inhibitory effect of 15d-PGJ_2 on recombinant eIF4AI's helicase activity was examined *in vitro* by measuring the displacement of a radiolabeled RNA oligomer duplex at fixed timepoints using different concentrations of 15d-PGJ_2 or a DMSO equivalent control (as indicated above each image, (+) with hippuristanol; (-) with DMSO). In each experiment 0.5 µM eIF4AI was used. Each experiment contained a control denatured at 95 °C for 5 minutes (DN – lane 1) and an ATP-free control that was incubated for the duration of the experiment at 37 °C (lane 10). Reactions were carried out and visualised as described in figures 3.8 and 3.9. Average values of % unwound displayed under each lane, calculated as described in figure 3.9. n=3.

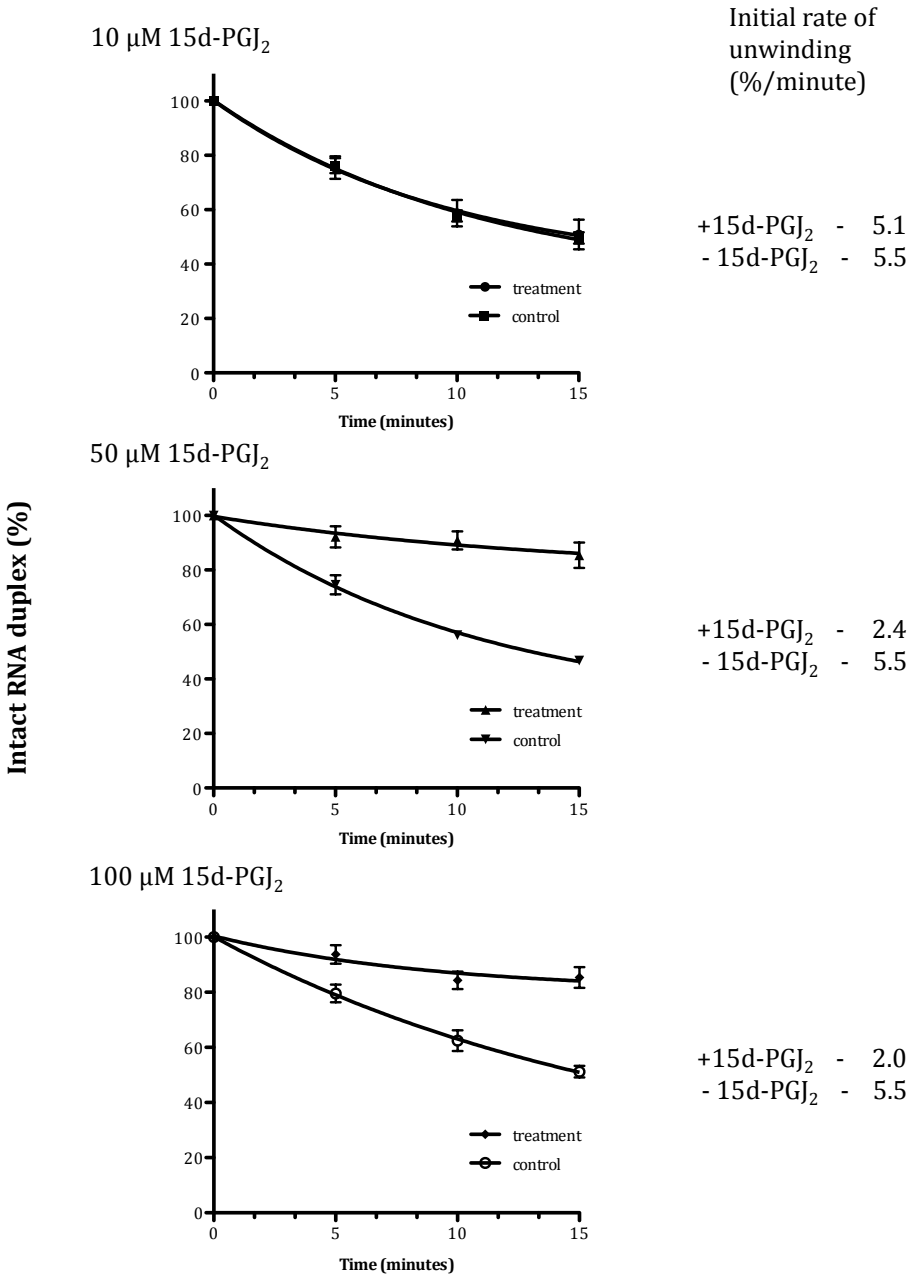

Figure 3.15 Rate of 15d-PGJ$_2$ inhibited recombinant eIF4AI's *in vitro* helicase activity. The rate of unwinding was calculated for each enzyme concentration using ImageJ (v. 1.43, National Institute of Health, USA) to quantify the area and intensity (AI) of each band representing intact duplex RNA (upper band) or unwound 11-mer RNA (lower band) for each timepoint. The amount (%) of intact duplex remaining was calculated using the following equation:- (AI upper band/(AI upper band + AI lower band)) X 100. n = 3 **A.** Graphs were produced using Prism (v. 5, GraphPad) using an exponential decay fit. Error bars indicate standard error of the mean (SEM) **B.** The initial rate of reaction was calculated for each enzyme concentration using Excel (Microsoft Office) by drawing a tangent of the initial slope (0 - 1 minute) using the line equation determined (% unwound/minute).

As displayed in figure 3.13, the initial rate of unwinding of eIF4AI in the presence of 50 μM or 100 μM hippuristanol or its DMSO equivalent demonstrates that little or no inhibition of eIF4AI activity is taking place. Conversely, figures 3.14 and 3.15 demonstrate that 15d-PGJ_2 is able to inhibit eIF4AI helicase activity by approximately 57 % and 74 % when used at a concentration of 50 μM or 100 μM respectively, though has little effect at 10 μM (8 %). The initial rate of unwinding between the two sets of control experiments is similar between the two sets of experiments (hippuristanol experiments - 5.2 and 4.9 % unwound/minute for 50 and 100μM respectively; 15d-PGJ_2 experiments - 5.5 % unwound/minute for 10, 50 and 100 μM respectively). This indicates that hippuristanol displays a greatly reduced inhibitory effect on eIF4AI activity in these experiments than that previously recorded (Bordeleau *et al.*, 2006b).

3.7 Discussion

The methods and results presented here demonstrate a successful regime for the cloning and bacterial expression of recombinant eIF4AI and eIF4B and the demonstration that these proteins display a helicase or helicase stimulatory activity *in vitro*. Recombinant eIF4AI was shown to unwind duplex dsRNA with a Gibbs free energy of -17.9 ΔG in a concentration dependent manner. Unlike that reported in (Rogers *et al.*, 1999) the unwinding reaction did not proceed linearly and a 2.8-fold increase in helicase concentration resulted in a 1.2 - 1.5-fold increase in activity. In order to assess whether this is an accurate measurement of eIF4AI activity, future experiments should increase the concentration of RNA used to ensure steady state kinetics are being observed, and reduce the time that the initial sample is taken from the helicase assay to two minutes in order to observe the linear phase of the reaction.

The addition of eIF4B to the eIF4AI helicase reaction (1:1 ratio of eIF4B:eIF4AI) resulted in a 1.6-fold stimulation of helicase activity compared to eIF4AI on its own. To establish whether the results described here are an accurate representation of recombinant eIF4B stimulation of recombinant eIF4AI the

concentration of RNA duplex used in the assay should be increased to ensure steady state kinetics and the initial timepoint taken reduced to two minutes. Further purification steps in recombinant eIF4B production could be added to reduce the level of contaminating peptides, which in turn will increase the accuracy in the quantification of the protein and should reduce nuclease activity. This could be achieved using heparin-conjugated agarose affinity purification.

Differences in the results from the published literature could also be due to the source of initiation factors as Rogers *et al* obtained eIF4A and eIF4B from RRL and therefore these proteins may be more active than those bacterially expressed. Attempts to express a post-translationally modified form of eIF4B using a *Drosophila* expression system (Invitrogen) that would produce a protein more representative of human eIF4B *in vivo* were unsuccessful due to low expression levels and a high level of histidine-rich *Drosophila* proteins that contaminated the purification step. Overexpression of recombinant eIF4B was detected successfully using immunoblotting, however quantification of this by coomassie blue staining after SDS-PAGE was difficult due to the S2 cell lysate containing proteins that co-migrated with eIF4B. In order to increase the level of expression of recombinant eIF4B the amount of expression vector transfected into the S2 cells could be optimised. In addition, performing ion exchange chromatography prior to the affinity chromatography purification step with nickel-coated agarose, may help to reduce the number of contaminating proteins and concentrate the sample therefore making recombinant eIF4B more easily detectable at later stages.

The modulation of eIF4AI activity by two small molecule inhibitors, hippuristanol and 15d-PGJ_2 was also assessed. 15d-PGJ_2 has been previously shown to bind specifically to eIF4AI and prevent eIF4GI binding (Kim *et al.*, 2007) thus inhibiting cap-dependent translation initiation. The ability of 15d-PGJ_2 to affect eIF4AI helicase activity directly has not yet been assessed. Data presented in this chapter demonstrates that 15d-PGJ_2 can inhibit the helicase activity of eIF4AI directly *in vitro*, which may contribute to its anti-inflammatory

and pro-apoptotic roles *in vivo*. Data presented here, however, showed little or no inhibition of eIF4AI helicase activity in the presence of 50 and 100 μM hippuristanol. Previous studies have demonstrated a convincing inhibition of helicase activity using 50 μM hippuristanol on 0.4 μM eIF4AI and very similar assay conditions (Bordeleau *et al.*, 2006b). As there is no inhibitory activity displayed in these experiments it is likely that the aliquot of hippuristanol used has been degraded or inactivated by oxidation. Repeating these experiments using a fresh aliquot of hippuristanol at higher concentrations will determine whether it can inhibit the helicase activity of recombinant eIF4AI.

Though the helicase assay used in this chapter demonstrates that bacterially expressed recombinant eIF4AI and eIF4B are active *in vitro*, using this method to obtain detailed information regarding its rate kinetics will always be affected by a high level of error due to experimental variability and inaccuracies in the quantification of the results. In the next chapter a new approach to analysing eIF4AI activity *in vitro* using a single molecule technique designed to investigate the hepatitis C viral (HCV) helicase, NS3 (Dumont *et al.*, 2006), will be described that should afford a much more detailed picture of eIF4AI unwinding kinetics.

4 Single molecule investigations of eIF4AI

4.1 Investigating helicases using single molecule experiments

DNA and RNA helicases are a large, diverse family of molecular motors, which convert the chemical energy from nucleoside triphosphates (NTPs) into the mechanical unwinding of DNA or RNA duplexes. Present in bacteria, eukaryotes and viruses, these ubiquitous enzymes can be categorised into one of six superfamilies based on conserved sequence motifs and common biological properties (Gorbalenya and Koonin, 1993; Singleton *et al.*, 2007). Helicases can vary according to substrate preference, directionality, translocation and unwinding rate, and step-size in addition to acting as monomers, dimers or oligomers, which creates enormous variety within each superfamily (Tuteja and Tuteja, 2004; Singleton *et al.*, 2007). Helicases are required in many aspects of RNA and DNA metabolism, including transcription and translation, repair, replication and recombination and have also been associated with several diseases, emphasising the importance of understanding the mechanisms by which they work (Ellis, 1997; Singleton *et al.*, 2007).

There are a number of methods that can be used to analyse the activity of helicases *in vitro*. Bulk assays, such as the helicase assay described in chapter 3, and ATPase and nucleic acid binding assays can demonstrate the substrate specificity of the enzyme and define steady state kinetic parameters. Combined with mutational analysis, these assays can aid in the assignment of particular functions to the conserved sequence motifs of the helicase. Pre-steady state kinetic parameters can be established by using stopped-flow techniques to measure the unwinding activity of a helicase under single ATP turnover conditions. In addition, the helicase can be analysed on a single molecule level using a number of techniques including fluorescence resonance energy transfer (FRET), atomic force microscopy (AFM) and optical or magnetic trapping. In the last ten years these techniques have been widely developed and have allowed the exploration of a number of helicases and motor proteins at a resolution that cannot be achieved by bulk experiments. Unlike ensemble methods of assaying helicase activity, single molecule experiments can

demonstrate the heterogeneity amongst a protein population. Due to the greater resolution of the data capturing methods, researchers using these techniques are able to observe helicase activity in real time to determine the reaction dynamics, step-size and force-dependence of the enzyme.

A number of helicases have been investigated by single molecule methods including several DEAD-box helicases. Klostermeier and colleagues were able to address the ATP and RNA dependence of the inter-domain conformation of *Bacillus subtilis* DEAD-box helicase, YxiN, by using a single molecule FRET study (Theissen *et al.*, 2008). As is common with all members of SFII, YxiN contains two RecA-like domains with a number of the conserved motifs common to the DEAD-box helicases and responsible for the ATPase and helicase activity of the enzyme positioned between the inter-domain cleft (Linder *et al.*, 1989; Hall and Matson, 1999; Caruthers and McKay, 2002). By placing a donor or acceptor fluorophore on either side of the inter-domain cleft, changes in YxiN conformation in the presence of different substrates could be monitored as a change in FRET. When only ATP or RNA was present, moderate FRET levels were detected, indicating an open conformation of the helicase, however, in the presence of ATP and RNA, an increase of FRET was observed, indicating inter-domain closure (Theissen *et al.*, 2008). Single molecule FRET studies can therefore offer a real-time alternative method by which the substrate dependence of inter-domain conformation can be determined.

In addition to measuring conformational and spatial rearrangements of domains single molecule experiments can also measure the forces involved in unfolding nucleic acid structure. The yeast translational DEAD-box helicases TIF1/eIF4A and ded1 have been investigated by single molecule AFM/scanning force microscopy experiments. Marsden *et al* developed a force experiment in which an RNA molecule containing a 25 base pair (bp) hairpin from the 5' untranslated region (UTR) of *GCN4* was tethered between an AFM cantilever and microscope slide using streptavidin:biotin and thiol:gold chemistry respectively (see figure 4.1, A). By moving the cantilever away from the surface

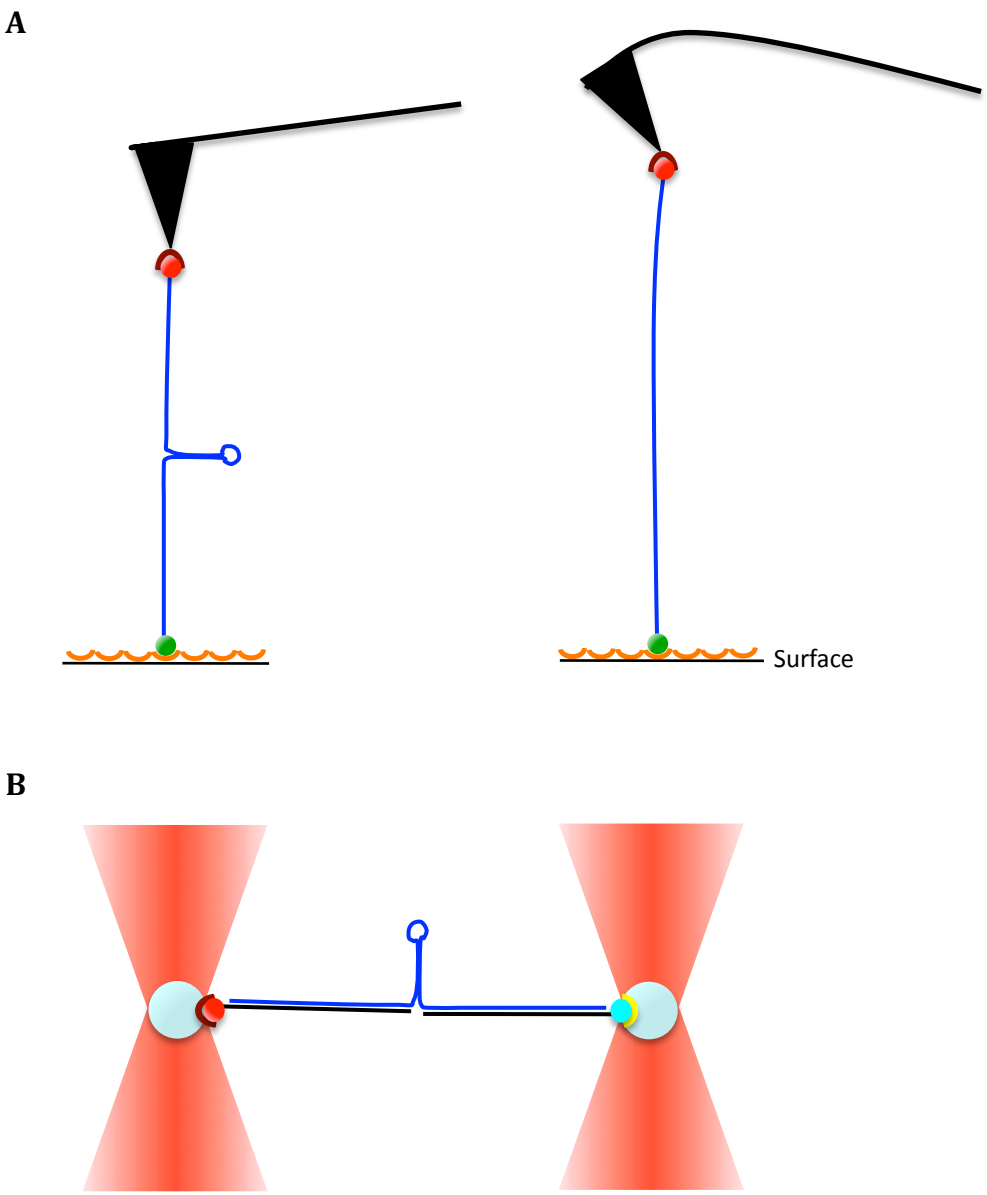

Figure 4.1 Force experiments using atomic force microscopy and optical tweezers. A. Experimental setup of Marsden *et al*. An RNA molecule (blue) containing a 25 base pair (bp) hairpin is tethered between a gold coated slide (orange) and a streptavidin-functionalised cantilever (black and dark red) via a thiol group (green circle) or biotin group (red circle) in solution. The application of force to the RNA molecule via the raising of the cantilever results in the opening of the hairpin. **B.** Experimental setup as described in Dumont *et al*. An RNA molecule (blue) containing a 60 bp hairpin is hybridised to two DNA handles (black), a 5' handle biotinylated on one termini (red circle) and a 3' handle labeled on one termini with digoxygenin (DIG) (cyan circle). The construct is attached to two polystyrene beads (light blue large spheres) functionalised with streptavidin (dark red – 5' handle) or anti-DIG (yellow, 3' handle) respectively. The beads are held in dual optical traps (red) in solution.

a force can be applied to stretch the RNA molecule and unwind the secondary structure. A series of force experiments were conducted to observe how the addition of varying concentrations of either TIF1/eIF4A, with or without eIF4B, or Ded1, affected the force required to open the hairpin. A ~ 35 pN reduction in the force required to open the hairpin occurred upon the addition of TIF1/eIF4A or Ded1, though the latter only required a third of the concentration to induce the same effect as TIF1/eIF4A, indicating a stronger helicase activity (Marsden *et al.*, 2006). The mean forces required to cause hairpin unwinding in these experiments were unusually high, even after the addition of helicase, and showed highly varied standard deviations (relative forces of hairpin unwinding; no enzyme - 151.3 pN ± 29.75; 0.4 μM eIF4A - 135.2 pN ± 32.98; 0.4 μM eIF4A/eIF4B 114.1 pN ± 34.12; 0.4 μM ded1 - 94.6 pN ± 23.3). Alternative methods of single molecule force experiments can yield results at a greater resolution and a much lower force thereby allowing a more detailed analysis of helicase activity than that gained with atomic force microscopy.

Dumont *et al.* developed a single molecule assay to measure NS3 helicase function that uses optical tweezers to measure force-extension changes of a structured RNA molecule during helicase activity (Dumont *et al.*, 2006). The hepatitis C virus (HCV) multifunctional helicase NS3 unwinds RNA secondary structure in a 3' to 5' direction in an ATP-dependent manner to facilitate viral RNA replication in conjunction with NS5B polymerase and other proteins (Pang *et al.*, 2002; Dimitrova *et al.*, 2003). The design for the construct used by Bustamante and coworkers differs to that used by Marsden *et al.* as it contains only a short stretch of ssRNA encoding a 60 base pair (bp) RNA hairpin and a short helicase landing-pad and the remaining RNA is hybridised to 5' and 3' DNA handles (see figure 4.1, B), which limits the amount of alternative secondary structures that the molecule can form. The 5' and 3' DNA flanking arms were end-labeled prior to hybridisation with the RNA molecule and then tethered to beads via DIG/anti-dig or biotin/streptavidin interactions respectively. The two beaded ends of the construct were caught in optical traps allowing the hairpin to be unzipped by the application of force. By using dual beam optical tweezers, the experimental setup is completely decoupled from

the experimental machinery, which reduces the signal to noise ratio in comparison to experimental setups where one or both ends of the construct are attached to a micropipette, cantilever or slide surface. The high sensitivity of the experiment meant that it was possible to observe the step and sub-step size of NS3 to base pair resolution (Dumont *et al.*, 2006) and the enzyme was observed to pause at sequence barriers in an ATP-dependent manner (Cheng *et al.*, 2007). Although NS3's step size was unaffected by the application of force, the enzyme's processivity was seen to increase with increasing force, independent of ATP concentration. From these results, Dumont *et al.* were able to conclude that the rate of the enzyme was limited by translocation rather than unwinding activity. This was further corroborated by a study using single molecule FRET which showed that helicase unwinding was preceded by a series of tension building one-nucleotide (nt) long translocations (Myong *et al.*, 2007).

Further investigation of eIF4AI using single molecule experiments may yet reveal a more detailed analysis of its behaviour. This chapter will present the cloning strategy and construction protocol of an RNA:DNA hybridised construct based on that used in (Dumont *et al.*, 2006) and its characterisation by AFM imaging. A small study will be shown which analyses the behaviour of dsDNA during overstretching by AFM and will be used to ascertain the suitability of AFM to look at RNA structure. Finally the initial optimisation of a single molecule experiment using dual-trap optical tweezers will be presented and the technical difficulties of the approach discussed.

4.2 Construct design and synthesis strategy

The construct was based on a design used to investigate the NS3 HCV helicase (Dumont *et al.*, 2006), which consisted of a ~ 1000 nt RNA molecule with a single 60 bp stem-loop hairpin located at its centre and two DNA handles, chemically functionalised at opposite ends, hybridised to the flanking RNA strands to either side of this (figure 4.1, B). The hairpin used in these experiments is encoded by the 5' UTR of ornithine decarboxylase (ODC), the rate-limiting enzyme in the synthesis of polyamines, which are essential for cell

growth and proliferation. ODC is strictly regulated and levels of the protein are altered in response to a variety of stimuli including tumour promoters and carcinogens and deregulation of ODC synthesis is often reported in neoplastic transformation (Pegg, 1988). *ODC* mRNA contains a long and highly structured 5' UTR which regulates translation of the protein in two respects; firstly an inhibitory hairpin (referred herein as ODC hp) in the first exon of the 5' UTR of *ODC* prevents cap-dependent translation initiation and secondly exon 2 and part of exon 3 contain an IRES element which promotes cap-independent translation initiation (figure 4.2) (Wen *et al.*, 1989; Pyronnet *et al.*, 2000). Translational repression caused by the first hairpin sequence is thought to be partially overcome by interactions with the 3' UTR (Grens and Scheffler, 1990) however it is still likely that eIF4A is required in some manner to unwind the structure, and recently silencing of eIF4B induced a selective reduction in ODC translation, which the authors propose is to do with eIF4AI inhibition, though it could be due to the stabilisation of the translation initiation complex (Shahbazian *et al.*, 2010).

In brief, the synthesis of the construct, as outlined in (Dumont *et al.*, 2006) is as follows. The 60 bp ODC hp DNA was cloned into the DNA plasmid pGEM4Z and used as the template in a series of PCR reactions to amplify (i) a DNA template with a 5' T7 RNA polymerase promoter added by primer extension for the *in vitro* transcription of the hairpin containing RNA molecule; (ii) a 5' labeled DNA handle with an *Eco*RI site added by the sense primer which, after restriction digestion with *Eco*RI, can be biotinylated by the DNA polymerase activity of Klenow fragment with biotinylated-dATP; (iii) a 3' labeled DNA handle with a 5' thiol group added by the anti-sense primer (for a schematic diagram of the synthesis regime see figure 4.3). The construct is then hybridised under optimised conditions and used as the RNA substrate in single molecule experiments.

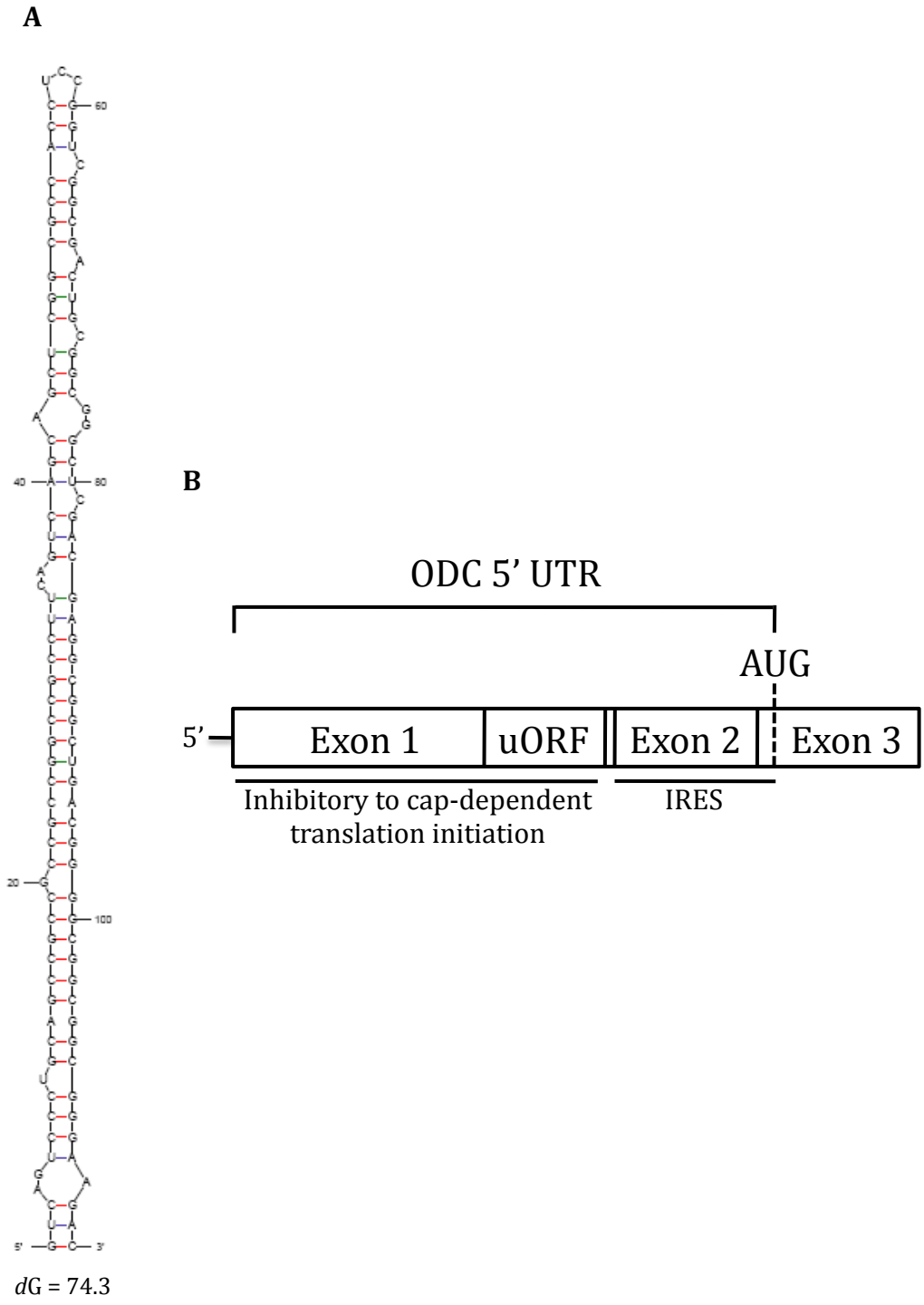

Figure 4.2 Ornithine Decarboxylase (ODC) 5' UTR and hairpin structure. A. Secondary structure prediction of the first hairpin encoded by the first exon of the *ODC* mRNA 5' UTR as predicted using *mfold* (Zuker, 2003) **B.** Schematic diagram representing the ODC 5' UTR.

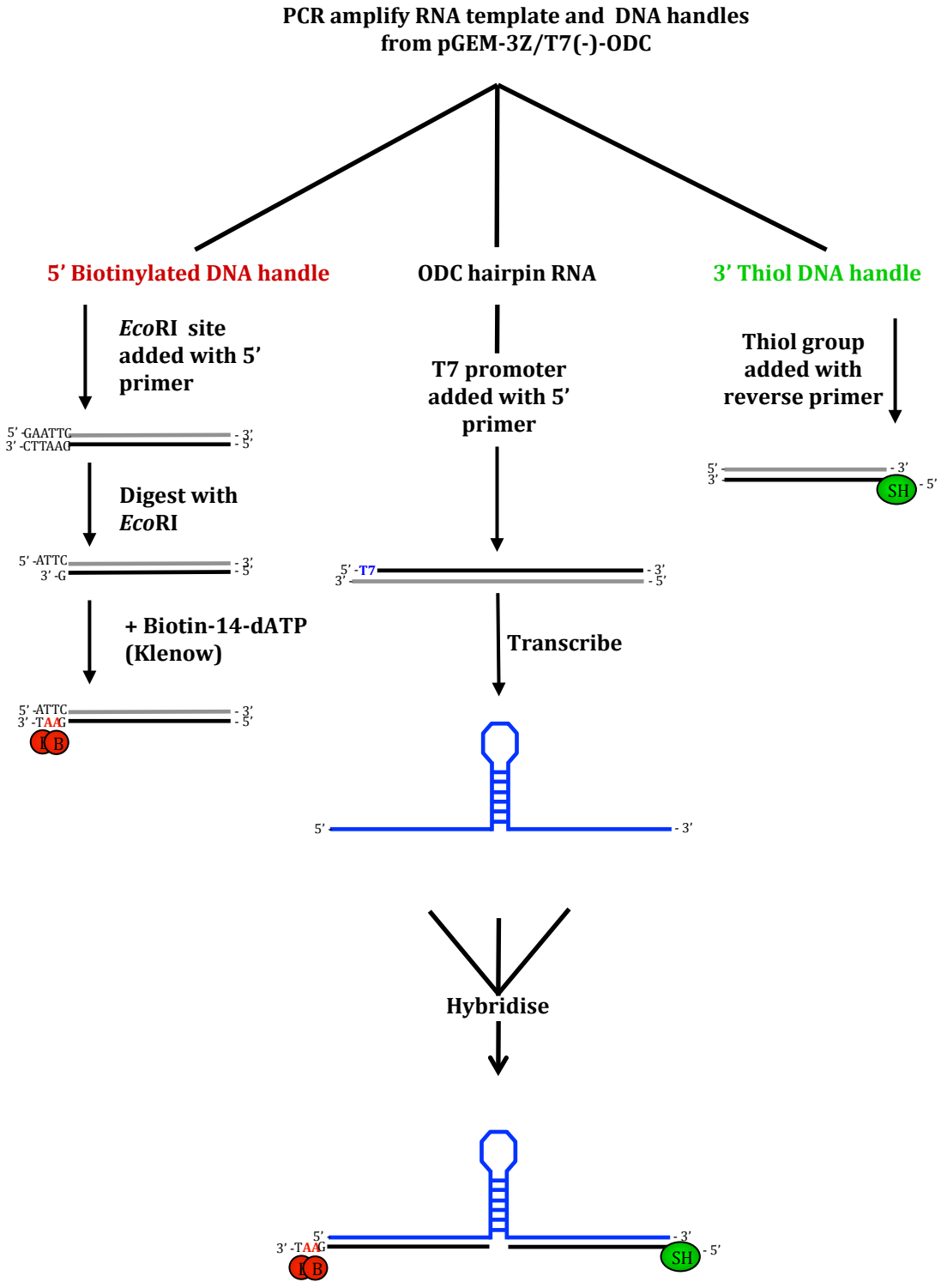

Figure 4.3 Schematic diagram representing the protocol for the synthesis and hybridisation of ODC hairpin construct. Black and grey lines – DNA, blue line **–** RNA; red circle - biotin group; green circle – thiol group.

4.3 Cloning and subcloning of the ODC hairpin

Overlapping oligonucleotides sequences encoding the ODC hp were annealed together by heating to 100 °C in 100 mM KCl and used as a template for PCR amplification using primers that added the *Eco*RI or *Bam*HI restriction sites to the 5' and 3' ends respectively. The amplified product was cloned into the vector pGEM-4Z (Promega) (figure 4.4). As a later PCR amplification step involved the addition of a T7 RNA polymerase promoter to create the transcription template DNA, the T7 promoter in pGEM-4Z had to be removed. pGEM-3Z is identical to pGEM-4Z, except the multiple-cloning site and SP6 and T7 RNA polymerase promoter sites are reversed, therefore a fragment of pGEM-4Z-ODC was subcloned into pGEM-3Z using the *Nde*I and *Hind*III restriction sites, which omits the T7 RNA polymerase site from the final vector, pGEM3Z/T7(-)-ODChp (figure 4.5). Successful cloning was verified by sequencing (Geneservice, Cambridge/Nottingham) and the vector used as a template for the synthesis of the RNA and DNA components of the construct as described above and depicted in figure 4.3. To create a control construct the ODC hp was restriction digested out of the vector using *Eco*RI and *Bam*HI enzymes, the 5' and 3' overhangs filled in using Klenow fragment and the vector re-ligated to produce pGEM3Z/T7(-).

4.4 Biotinylation of 5' handle and electromobility shift assay

As the success of the single molecule experiments will, in part, depend on the efficiency of the biotinylation of the 5' DNA handle, an electromobility shift assay was developed which took advantage of the high affinity of biotin for streptavidin. After the purification of the 5' DNA handle subsequent to restriction digestion and biotinylation by Klenow fragment 5' recessed end filling-in, a sample of biotinylated and non-biotinylated DNA was incubated in the presence or absence of streptavidin conjugated horseradish peroxidise (strep-HRP). By subjecting the samples to electrophoresis through a 1.5 % agarose gel buffered in 1 x TBE, successfully biotinylated DNA will migrate slower than non-labeled DNA as it will be bound to two molecules of strep-HRP, which appears as a 200 bp increase in size (figure 4.6). If the labeling efficiency

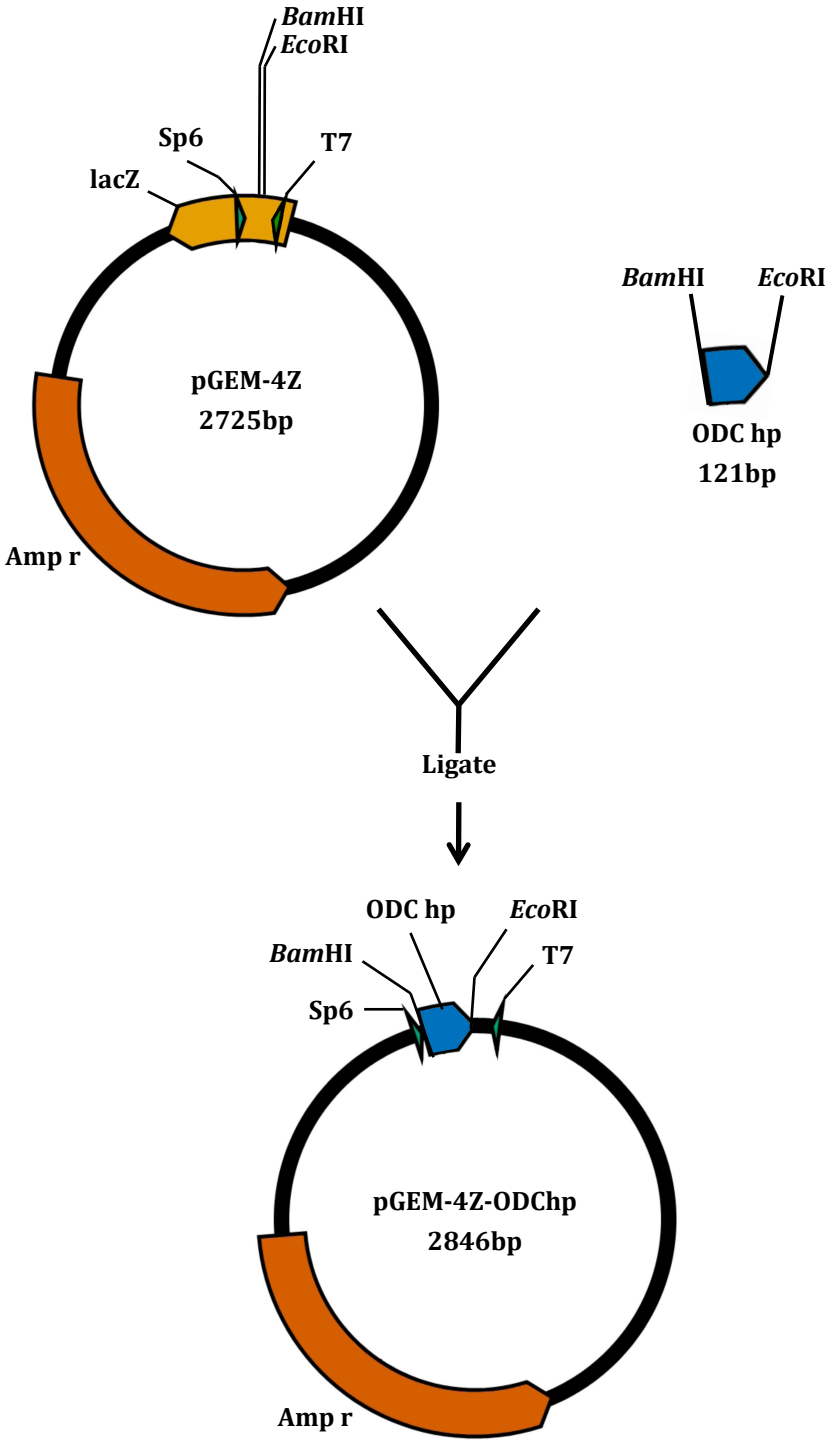

Figure 4.4 Cloning of ODC hairpin into pGEM-4Z. The first hairpin encoded by the 5' 'UTR of ornithine decarboxylase (ODC) mRNA was PCR amplified from an oligomer template and cloned into pGEM-4Z (Promega) using *Bam*HI and *Eco*RI restriction sites. Amp r – Ampicillin resistance gene; T7 – T7 RNA polymerase promoter; Sp6 – Sp6 RNA polymerase promotor; LacZ – LacZ gene. Vector maps drawn with PlasmaDNA (v. 1.4.2)

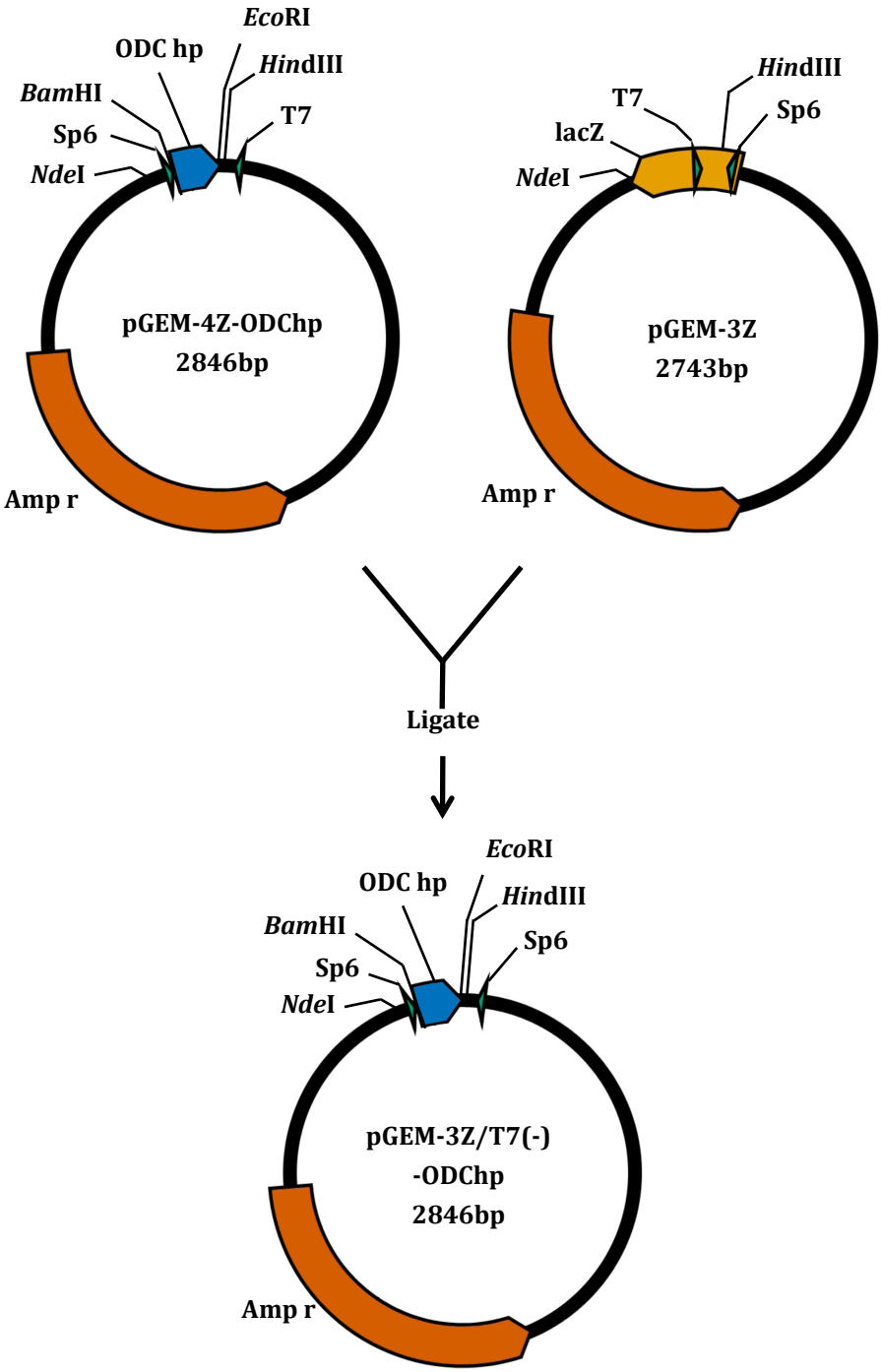

Figure 4.5 Subcloning of pGEM-4Z-ODC into pGEM-3Z. In order to remove the T7 promoter from the vector, pGEM4Z-ODC was subcloned into pGEM-3Z (Promega) using the using *Nde*I and *Hin*dIII restriction sites. Amp r – Ampicillin resistance gene; T7 – T7 promoter; Sp6 – Sp6 promotor; LacZ – LacZ gene. Vector maps drawn with PlasmaDNA (v. 1.4.2)

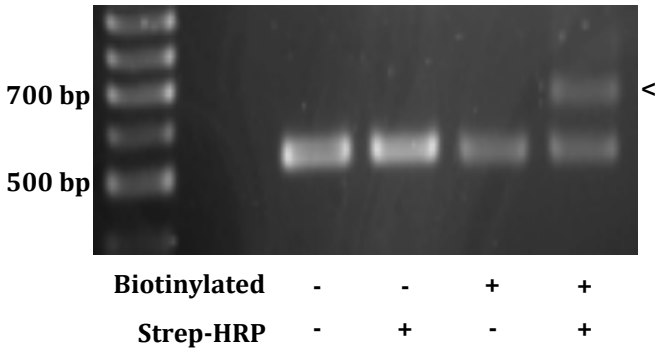

Figure 4.6 Biotinylation DNA electromobility shift assay. Biotinylated DNA was incubated with streptavidin conjugated horseradish peroxidase (Strep-HRP) and electrophoresed through a 1.5 % agarose gel to separate unlabeled DNA and labeled biotinylated DNA bound to strep-HRP.

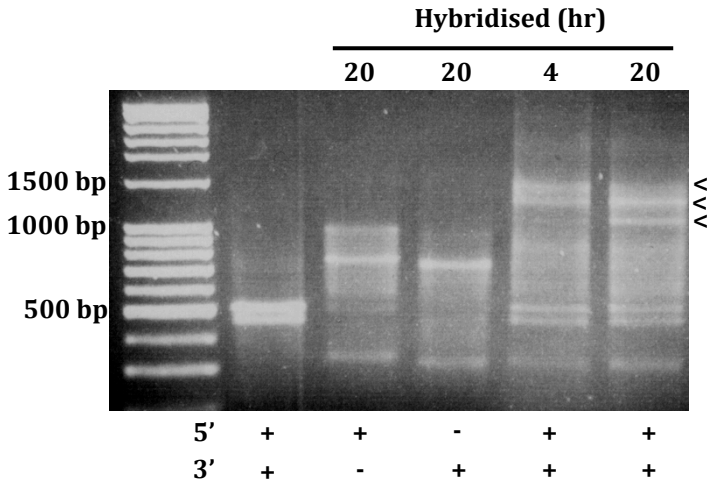

Figure 4.7 Hybridisation of construct. Equimolar concentrations (1 pmol) of RNA , 5' DNA handle and 3' DNA handle were denatured at 95 °C for 5 minutes in 70 % formamide hybridisation buffer then allowed to cool to 55 °C and hybridised for the time specified. Each reaction contains 1 pmol RNA. Lane 1 - not hybridised.

was approximately 75 % successful the DNA was used in the hybridisation protocol.

4.5 Hybridisation of the construct

It was initially desired that the hybridised construct population be as homogeneous as possible and therefore attempts were made to remove the unwanted sense strand from each DNA handle using two different methods: (i) The selective degradation of the sense strand of the 3' DNA handle was attempted by phosphorylating the 5' end of the sense strand through PCR amplification with a phosphorylated primer and then incubating this with λ exonuclease, which preferentially degrades phosphorylated DNA in a 5' - 3' manner. This reaction either proved unsuccessful or produced such low yields that the ssDNA was lost in subsequent purification steps. (ii) The method used to separate the biotinylated DNA strand took advantage of the high affinity bond between biotin and streptavidin. The labelled DNA was incubated with streptavidin-coated magnetic beads (Dynabeads, Invitrogen) and then subjected to repeated rounds of denaturing at 95 °C followed by the removal of the aqueous solution from the bead suspension to remove unlabeled ss or dsDNA. This method was also unsuccessful as no product was detected by subsequent agarose gel electrophoresis. Efforts were therefore addressed towards the optimisation of the hybridisation reaction and the successful visualisation of this.

RNA:DNA hybrids have a greater relative binding strength compared to DNA:DNA hybrids in a GC content dependent manner (Casey and Davidson, 1977). Unlike DNA:DNA hybrids, RNA:DNA polynucleotides are relatively stable at high concentrations of formamide (Casey and Davidson, 1977), and therefore a high percentage formamide buffer was used to selectively destabilise DNA:DNA hybrids in preference for RNA:DNA hybrids. An equal molar ratio of RNA, 5' and 3' DNA were denatured in a 70 % formamide hybridisation buffer at 95 °C for five minutes and then hybridised at an optimised temperature of 55 °C for four or 20 hours. Figure 4.7 shows the products of a controlled series of

hybridisation reactions separated by electrophoresis through a 1.5 % agarose gel buffered in 1 x TBE. Three distinct product bands (indicated by <) migrated more slowly through the gel than those produced in the controls (lanes 2 and 3) which omitted one of the two DNA handles indicating that these are fully hybridised construct molecules. It is presumed that the three bands represent different folding states of the hairpin in the final product. The two lower bands appeared to become more defined after 20 hours of hybridisation, which may indicate that these are the more stable conformations of the product. These bands were excised from the gel and visualised by AFM.

4.6 Atomic Force Microscopy (AFM)

The atomic force microscope is a scanning probe microscope developed in the mid-1980s as an alternative to the scanning tunneling microscope (STM) that would be able to image non-conductive materials (Binnig *et al.*, 1986). The principal components of an AFM are shown in figure 4.8. In brief, a cantilever with a sharp tip surveys a sample surface to build an image of its topology. As the cantilever scans along the *x* and *y* planes of the sample surface, the attractive or repulsive forces experienced by the tip cause it to deflect in the *z* direction. These deflections generate a movement in a laser beam that is directed onto the back of the cantilever and then reflected onto a position-sensitive photodiode. This data is used to generate a two-dimensional relief map of the surface. In response to cantilever deflection, an electronic feedback mechanism causes the piezoelectric scanner to adjust the distance between the sample surface and the cantilever to maintain the force at which the sample is being scanned.

Three main modes of scanning are used to image sample surfaces: contact mode, in which the cantilever tip directly contacts the surface; non-contact mode, in which the tip is oscillated at resonance frequency but never contacts the surface and tapping mode, in which the cantilever is oscillated at, or near to, its resonance frequency and is allowed to gently tap the sample surface. Tapping mode is preferentially used to image soft biomolecules as contact mode

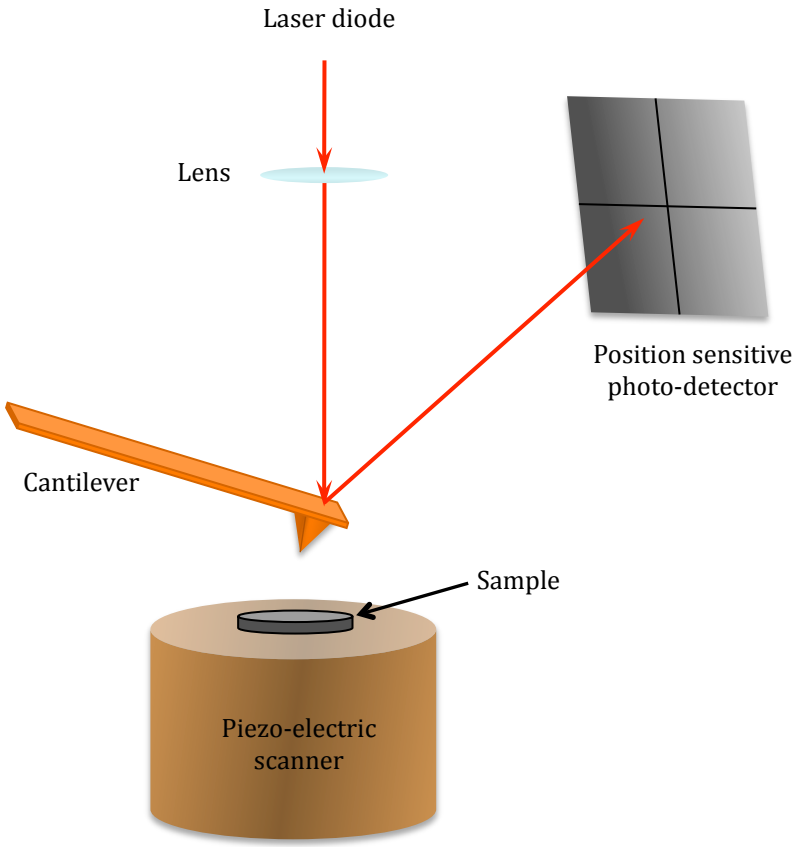

Figure 4.8 Principles of Atomic Force Microscopy (AFM). A schematic diagram showing the main components of AFM which can either be used to measure the topology or force-extension of a sample. The piezo-electric scanner can move the sample in all directions allowing the cantilever to scan the surface which results in its deflection. This deflection is measured as a change in position of a focussed laser beam that is reflected off of the back of a cantilever onto a photo-detector.

can 'sweep' the sample across the surface and non-contact mode gives a lower spatial resolution.

4.7 AFM imaging of helicase activity

The high resolution of AFM imaging has afforded a direct visualisation of helicase activity. The progress of an unwinding assay can be monitored by dry imaging samples at different timepoints during a reaction. Differences between the height of single stranded (ss) polynucleic-acids compared to double stranded (ds) can be used to estimate the degree of unwinding activity, and protein binding can be seen as 'blobs' attached to nucleic acid strands. In this manner the *Escherichia coli* DEAD-box helicase DbpA was visualised as binding dsRNA in the absence of ATP and helicase activity was detected by the formation of 'Y' shaped intermediates globular protein at the junction of the fork (Henn *et al.*, 2001). In addition, AFM imaging has been used to visualise intermediate stages of plasmid DNA unwinding catalysed by the helicase activity of PcrA stimulated by RepD (Zhang *et al.*, 2007). The next section will describe the AFM imaging of the hybridised construct and recombinant eIF4A.

4.8 AFM imaging of construct and eIF4AI-MBP

Gel purified hybridised construct was imaged by tapping mode AFM in air. 5 - 10 μl of sample (5 - 10 ng/μl) was deposited onto a freshly cleaved mica surface (~ 1 cm^2), washed off after 10 minutes incubation at room temperature with 100 μl ddH_2O and dried in a gentle flow of nitrogen gas.

Figure 4.9 shows a typical image of the sample population. Most molecules are linear in appearance, though there is some variation in their length and some globular structures are observed. Population heterogeneity may be the result of the mechanical disintegration of the structure or agarose contamination of the sample. The longest structures appear to be flexed near their centre, and this flexion is generally accompanied by an increase in the height of the molecule at this point as indicated by the arrows on figures 4.9, A. 1 - 4. This may be indicative of the 60-bp hairpin structure at the centre of the construct. dsRNA is

A

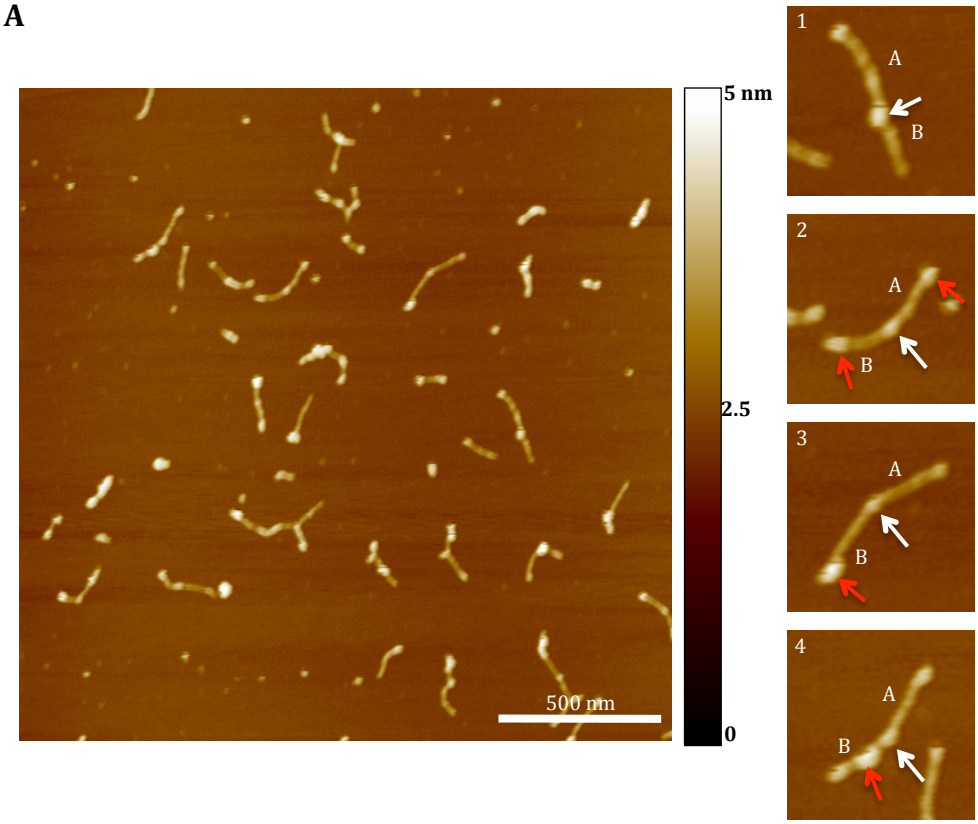

B

Figure		Length (nm)	Total (nm)
1	A	140	244
	B	104	
2	A	102	216
	B	114	
3	A	115	247
	B	132	
4	A	119	230
	B	111	

Figure 4.9 AFM images of ODC hairpin construct. Hybridised construct samples were purified after separation by electrophoresis and then imaged in air by AFM. **A.** Large image. Scan of population of hybridised molecules. Smaller images 1-4. Examples of molecules that display lengths within the range expected for the hybridised construct. White arrows indicate central flexion point. Red arrows indicate possible conformational abnormalities formed during sample preparation. **B.** Measurements of molecules shown in A, 1-4.

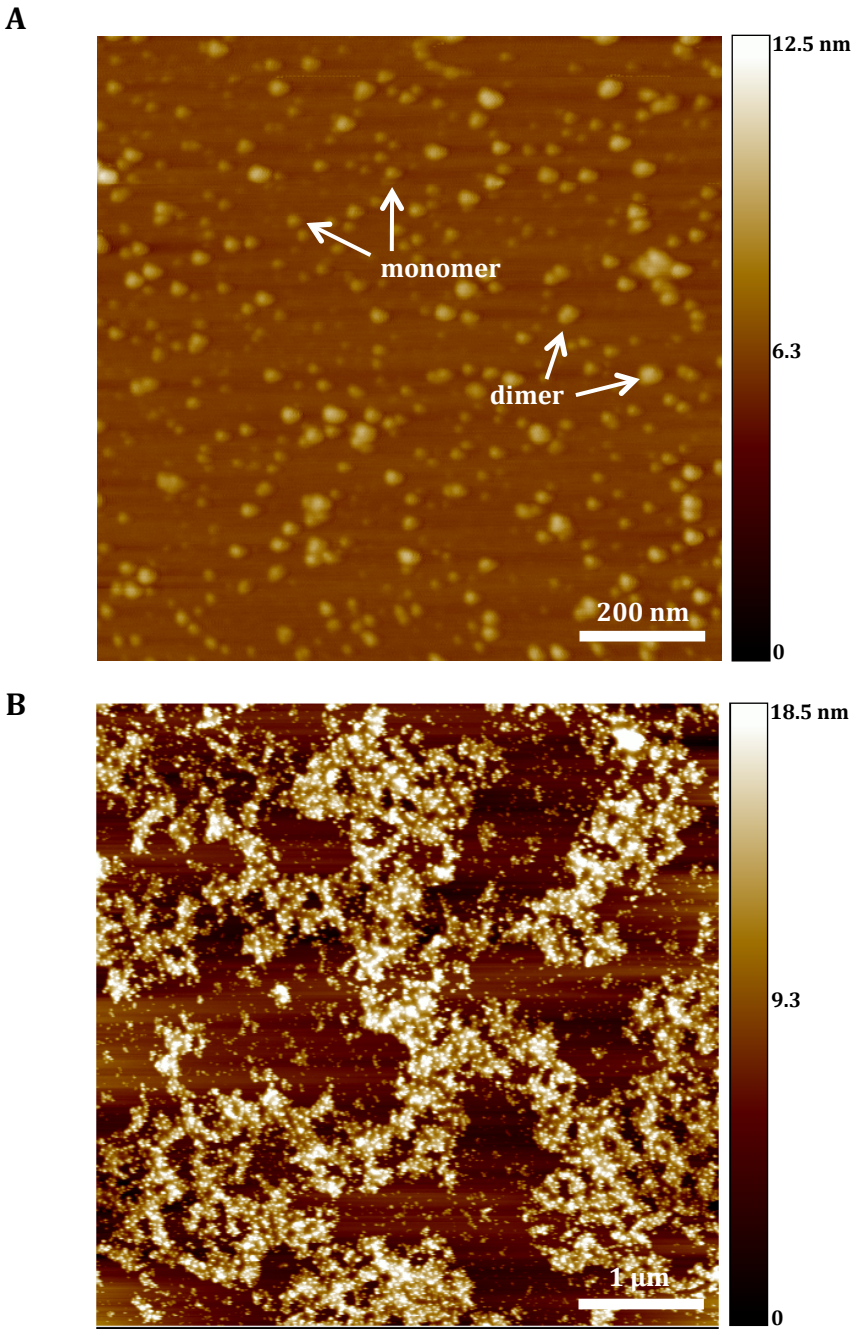

Figure 4.10 AFM images of eIF4A-MBP and hybridised construct. A. Image of eIF4A-MBP **B.** Aggregation observed after incubation of eIF4A-MBP with hybridised construct.

an A-form helix with a helical rise of 2.7 Å/bp which equates to ~ 16 nm for the ODC hairpin, however this is not observed in the centre of the molecules imaged which may be due to the sharpness of the tip or limitations in the image resolution or it may be due to the hairpin forming a globular structure. DNA:RNA hybrids are also A-form helices with a slightly larger helical rise to that of dsRNA (2.9 Å/bp (Conn *et al.*, 1999)) which equates to ~ 149 nm for the 5' biotinylated arm of the construct and ~ 135 nm for the 3' thiol-labeled arm. Of those molecules measured the lengths were generally smaller than those expected (figure 4.9 B). This discrepancy may be due to differences in the conformation of the molecule as it is dried, as demonstrated by the red arrows on figures 4.9 A,1 - 4.

eIF4AI-MBP (10 pg/μl) was imaged in air by tapping mode AFM as described above. As expected, the protein is globular and is represented mainly as monomers of 15 - 20 nm diameter. A significant proportion of the sample is larger than that expected (30 - 40 nm diameter) and is thought to represent protein dimers caused by the non-specific interaction between the MBP-tag and eIF4AI observed during the purification of the protein after TEV mediated cleavage (figure 4.10, A). Attempts to image the construct and protein together in the presence of non-hydrolysable ATP analogue, AMPNP, resulted in a high degree of sample aggregation that could not be resolved by altering buffer conditions (figure 4.10, B).

4.9 AFM as a tool to measure forces

In addition to being used as an imaging tool, AFM can also function as a molecular force probe to measure the interactions between a sample and a cantilever tip. The adhesive forces encountered by the tip as it is lowered and retracted from a sample surface are transduced by the deflection of the cantilever using the equation:

$$F = -k_{cant.} \cdot d$$

where F is the force, $k_{cant.}$ is the spring constant of the cantilever ($N.m^{-1}$) and d is the deflection of the cantilever. By measuring the oscillation of the cantilever in the sample buffer at ambient temperature, its spring constant can be calculated using the following equation:

$$k_{cant.} = k_B \, . \, T / \langle q^2 \rangle$$

where k_B is Boltzmann's constant, T is the temperature (K) and q is the displacement of the cantilever (Hutter and Bechhoefer, 1993). A force-distance curve is generated by plotting the distance moved by the cantilever against the force calculated from its deflection (figure 4.11).

A functionalised cantilever tip can be used to pick up labeled biomolecules attached to a sample surface in order to view the molecular extension profile upon the application of force. AFM cantilevers are typically functionalised with streptavidin and silicon surfaces coated with gold in order to tether biological molecules labeled at each end with a biotin or thiol moiety respectively, as is the design for the ODC hp construct described above (see methods section 2.5.2). Due to the low yields of hybridised construct initially produced for this project a labelled DNA molecule was first used in a series of AFM force experiments described below, in order to optimise the functionalisation of the surface and cantilever tip.

4.10 Force extension profile of dsDNA

A typical force extension profile of double stranded DNA is displayed in figure 4.12 and proceeds through four distinct phases: 1. a small force (~ 10 pN) is required to extend randomly coiled dsDNA to B-form; 2. the molecule can then be extended until forces of ~ 60 pN are reached; 3. when forces of ~ 70 pN are reached the molecule undergoes a transition to a second stable form, termed 'S', that has a contour length 1.7-fold larger than B-form; 4. beyond 70 pN much larger forces are required to extend the molecule further, rather they result in denaturation (Cluzel *et al.*, 1996; Smith *et al.*, 1996; Leger *et al.*, 1999).

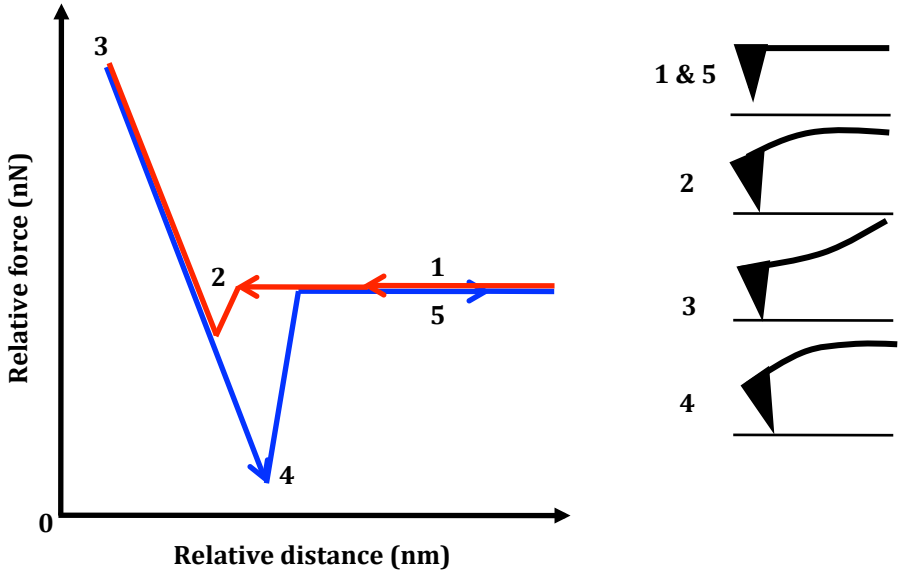

Figure 4.11 Typical force-extension curve displaying the deflection encountered by the cantilever. As the tip approaches the surface **(1)** it experiences long-range attractive van de waals forces **(2)** that cause it to 'jump to contact' resulting in its upwards deflection. After reaching the 'maximum load' (pre-defined by the user) **(3)** the tip disengages, or 'pulls off' from the surface **(4)** and returns to the start position, away from surface forces **(5)**. Red line is the approach trace, blue line is the retract trace.

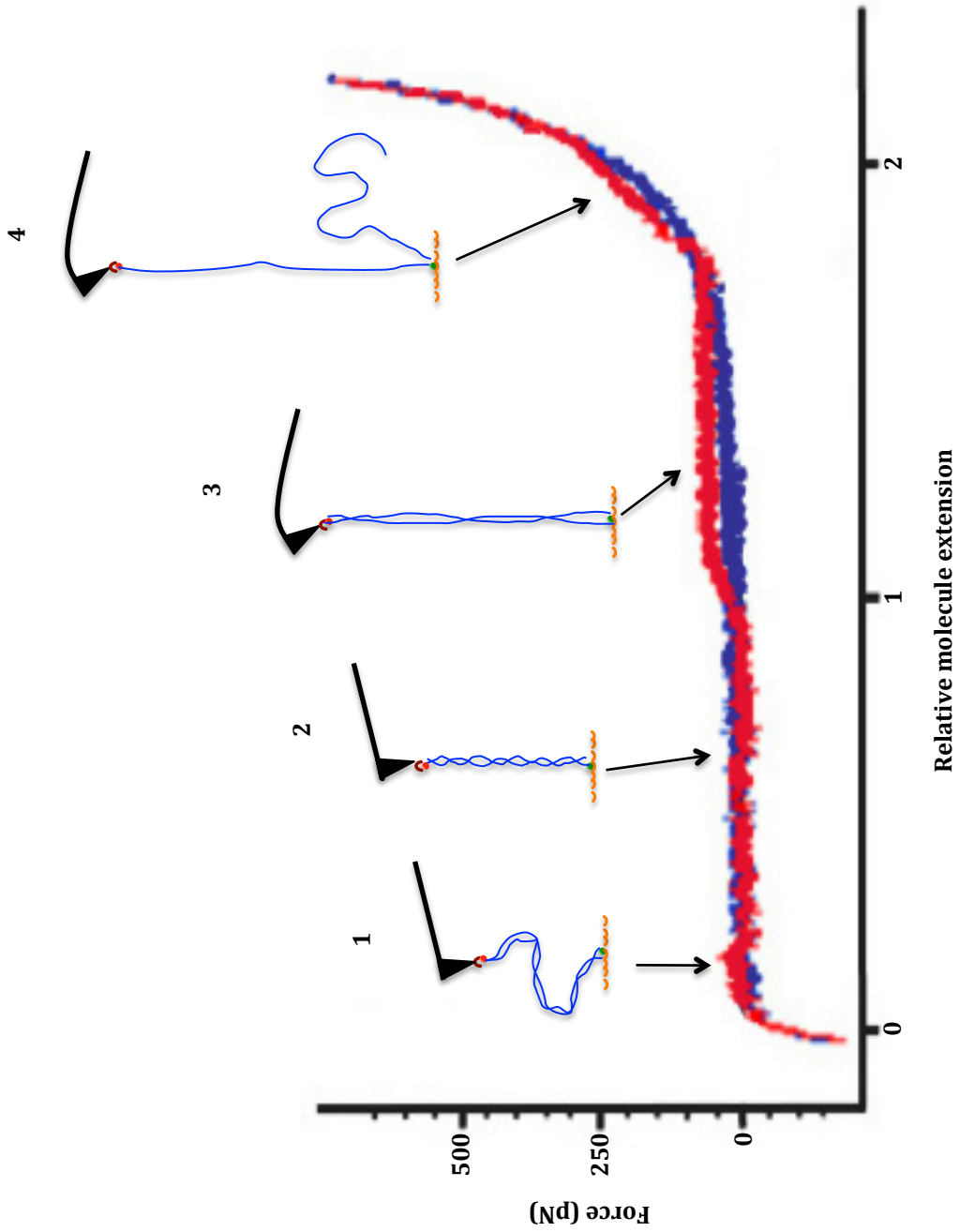

Figure 4.12 Force extension curve demonstrating the overstretching of dsDNA. Schematic diagram representing a typical DNA force extension curve and the different transition states of the DNA molecule as it is pulled (based on Rief *et al*, 1999). Red – pulling trace; blue – relaxation trace.

The relaxation trace shown in figure 4.12 (blue line) demonstrates some hysteresis as the effects of overstretching the molecule to a denatured state are reflected by its inability to fold back to B-form DNA (i.e. the relaxation trace does not follow the transitions of the stretching trace). If the extension does not proceed through the second transition state, the dsDNA molecule will reform B-form dsDNA, which is demonstrated by the relaxation trace following the transitions of the extension trace. There is some controversy surrounding the nature of the B-S form stretching transition (reviewed in (Chaurasiya *et al.*, 2010)); does S-form dsDNA, which is predicted to maintain base-pairing but not base-stacking, exist or does this transition result in the denaturation of the molecule? In the following experiment, the extension of a 2532 bp dsDNA molecule is recorded and the molecules integrity after the B-S-form transition monitored by the addition of single stranded binding (SSB) protein.

A dual-labeled (5' thiol, 5' biotin) 2532 bp dsDNA was prepared by W. Zhang using labeled primers in a PCR reaction as described in (Zhang *et al.*, 2005) and this substrate used in a series of AFM experiments in order to investigate the properties of dsDNA overstretching and establish initial parameters for our experiments on RNA unwinding. The labeled DNA was immobilised on a gold-coated silicon surface overnight and, after washing with ddH_2O, the surface was then coated in a solution of 1 mM mercaptohexanol (MCH) for one hour to reduce non-specific interactions of the DNA with the surface. The surface was washed and then probed in a solution of TE-NaCl buffer. After calculating its spring constant, a streptavidin functionalised cantilever was lowered to the surface and then repeatedly raised and lowered at an average rate of 1 μm/s to a distance between 500 and 800 nm. Caught molecules assumed a characteristic DNA force extension curve, going through a B-S form transition between ~ 60 and 70 pN (figure 4.13). Each molecule caught was not extended through to the last stage of the FEC in order to prevent forced denaturation. Once caught, molecules could usually be extended 10 - 20 times before the contact ruptured. Repeated extension of each molecule did not result in a deviance in the force extension profile.

To examine the structural integrity of the dsDNA when it is overstretched, 7.4 μM SSB protein (prepared by W. Zhang as described in (Zhang *et al.*, 2007)) was carefully added to the sample solution using a micro-syringe. Force extension curves obtained in the presence of SSB protein displayed hysteresis in the relaxation trace (blue) compared to the stretching trace (red) (figure 4.14) indicative of protein binding to the DNA. As SSB binds to single stranded regions of DNA, but not to dsDNA, this infers that during the B-S form transition, under the experimental conditions described herein, some regions of ssDNA are exposed.

These experiments were compared with those performed by W. Zhang and A. Orta to investigate the DNA binding ability of DnaD, a protein involved in replication and DNA remodelling and published in (Zhang *et al.*, 2008). DnaD is a protein of the *B. subtilis* primosome complex that functions to reinitiate DNA replication at stalled replication forks (Bruand *et al.*, 1995; Bruand *et al.*, 2001). Previous data using AFM imaging had demonstrated that the remodelling capability of DnaD was able to relax supercoiled plasmid DNA in a concentration dependent manner (Turner *et al.*, 2004). AFM force experiments showed that the hysteresis induced by the C-terminal domain of DnaD (Cd) was greater than that induced by a higher concentration of SSB (shown in figure 4.14), despite SSB displaying a 600-fold higher binding affinity for ssDNA (Zhang *et al.*, 2008). This indicates that the Cd is able to enhance dsDNA melting, perhaps through a helix untwisting activity (Zhang *et al.*, 2006).

4.11 Force extension profile of ODC hp construct using AFM

We repeated the dsDNA experiments described above using RNA in the form of labeled ODC hp construct. The yield from a typical hybridisation method was diluted in 30 μl TBE, which would give a concentration of approximately 500 ng/μl if the hybridisation reactions was 100 % successful and the precipitation steps resulted in no loss. The success of the hybridisation reaction could be estimated by separating a sample of the products by agarose gel electrophoresis assessing the fraction of hybridised; this varied between 50-60 %, and therefore

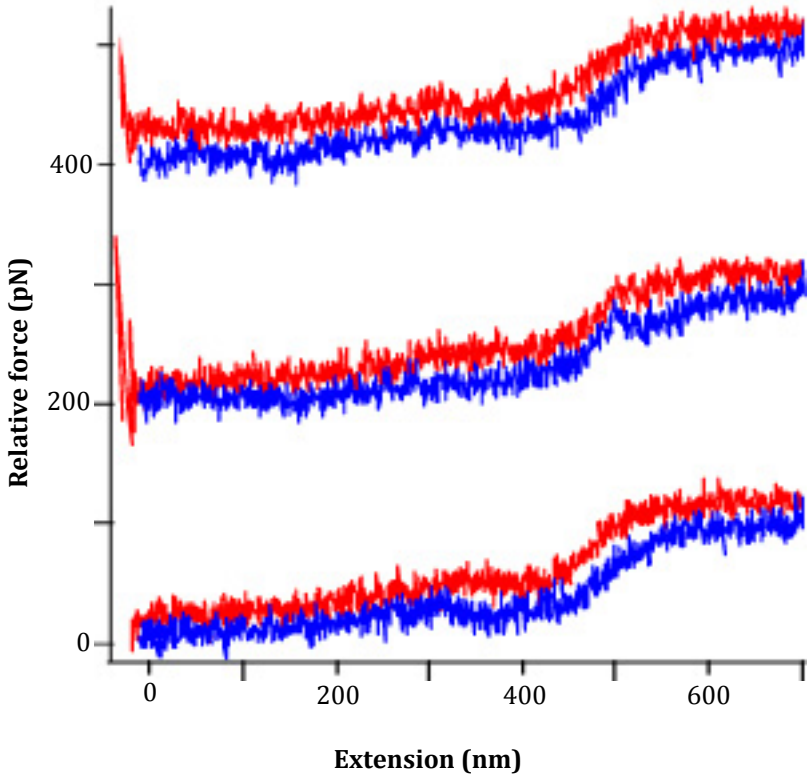

Figure 4.13 DNA force extension curves. Repeat force extension curves of a single dual-labeled (5' thiol, 5' biotin) 2532 bp dsDNA molecule in TE-NaCl. Red – pulling trace, blue – relaxing trace.

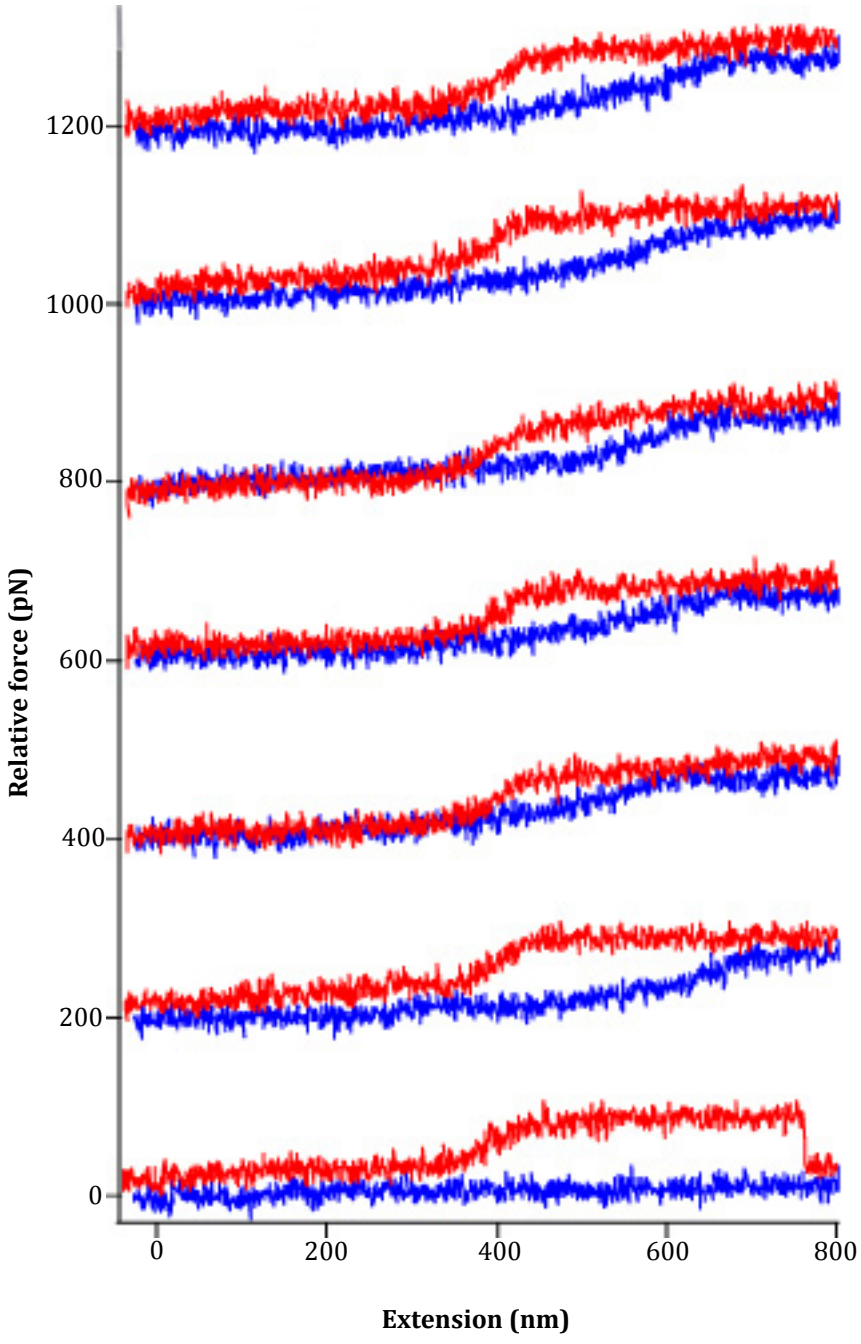

Figure 4.14 DNA force extension curves in the presence of single stranded binding protein. Repeat force extension curves of a single dual labeled (5' biotin, 5' thiol) 2532 bp dsDNA molecule in the presence of single stranded binding protein (SSB). Red – pulling trace, blue – retract trace. The molecule is dropped in the lowest puling trace.

it is estimated that the maximum concentration of hybridised construct used in these experiments was 300 ng/μl but after precipitation this may be as low as 150 ng/μl (if 25 % loss occurred during each precipitation). The hybridised sample (50 μl) was incubated overnight on a gold-coated glass surface. After washing, incubation in 1mM MCH and rinsing in TE-NaCl the sample was probed with a streptavidin-functionalised cantilever. Some surface interactions were observed, but no specific interactions were established as they were disrupted below the estimated total construct length of ~ 280 nm. This may be due to a low surface density of fully labeled molecules signifying that the yield of ODC hp construct molecules needs to be improved. As the concentration of molecules required for optical tweezer experiments is much smaller and the instrumentation used should be able to afford a much higher force resolution, it was decided that the AFM experiments would be optimised no further.

4.12 Optical tweezers

In the 1970s Arthur Ashkin first demonstrated that optical forces could be used to levitate dielectric particles in air and water (Ashkin, 1970) and 15 years later described the first single-beam laser optical trap (Ashkin *et al.*, 1986). Optical traps, or tweezers as they are now more commonly known, are formed by tightly focusing a laser beam through a lens with a high numerical aperture. The focus, or waist, of the beam is able to trap small transparent objects of a high refractive index. If an object is small enough, a beam of light will impart a force on it in the direction of its linear momentum. As the light passes into, and out of, a transparent object it is refracted according to the refractive index of the object and the surrounding solution. This refraction produces a reaction force that is equal and opposite to the linear momentum of light. At the centre of the focus the force caused by the momentum of light and the force caused by the refraction of light are balanced out, trapping the object. The focus of the laser is the centre of a three-dimensional (3-D) intensity gradient that can trap an object axially and laterally (see figures 4.15 A and B). The net reaction force that acts on the object is directly related to the intensity of light that refracts through it. As the trap forms a 3-D gradient of light intensity, the position of the

A. Axial trapping force

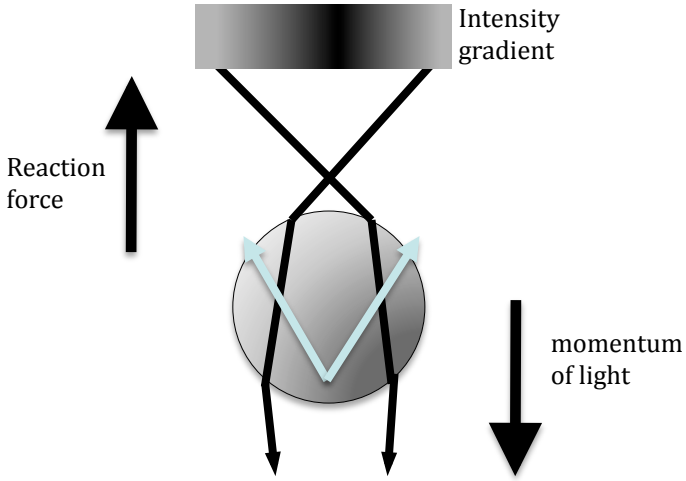

B. Lateral trapping force

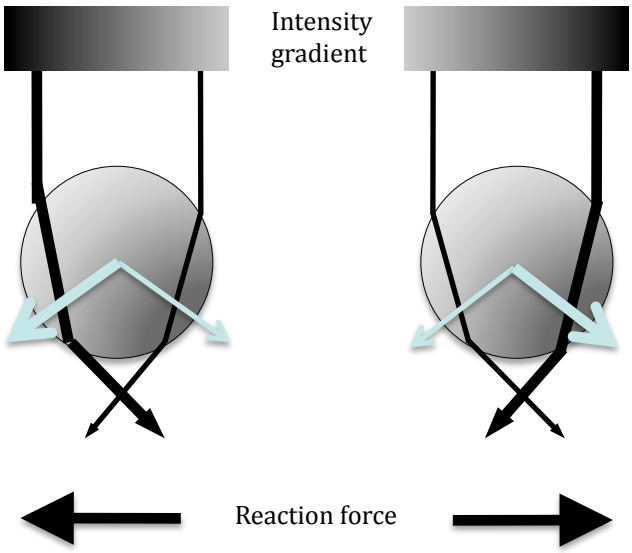

Figure 4.15 Particle trapping forces of optical tweezers. Focusing a beam of light produces a 3-dimesional intensity gradient that is most intense at the point of focus **A.** The refraction of a beam of light as it passes through a transparent bead results in a change in momentum which imparts a net force towards the beam focus. **B.** An intensity gradient of parallel light that increases from one side to the other. Two rays of different intensities are represented by two black arrows of different thicknesses. Though the refraction of each ray is at the same angle, the reaction force imparted on the bead is equal and opposite to the input momentum. Consequently the net reaction force will move the bead towards the highest intensity ray

object within the trap will correspond to the intensity of the light and therefore the reaction force it experiences. If the intensity is weaker on one side than the other, the refraction of the more intense light will cause a greater reactionary force than the weaker light, as demonstrated by figure 4.15 B. This will result in a net reaction force moving the object towards the more intense side of the light gradient. Moving the position of the focus will result in a change in the intensity of the light refracting through the object, which will produce a reactionary force that moves the object back towards the focus. Thereby a trapped object can be moved in 3-D. This is the basic premise behind optical trapping, for a more detailed review of the physics behind the instrumentation, please see (Molloy and Padgett, 2002; Neuman and Block, 2004).

Biomolecules can be indirectly investigated with optical tweezers through their attachment to functionalised μm-sized beads that are then caught in the optical trap. There are many experimental systems that can be used during optical trapping experiments with biomolecules. Three common methods that enable the researcher to investigate the forces required to unwind nucleic acid structure are shown in figure 4.16. The first method (A) uses laminar flow to stretch a nucleic acid molecule tethered at one end to a bead that is held in an optical trap. Bianco *et al* used this method to investigate *E. coli* RecBCD, a helicase/nuclease that preferentially unwinds and then degrades DNA from the 3' end and is required for recombinatorial repair (Bianco *et al.*, 2001). A long DNA molecule that was fluorescently labeled using YOYO-1 dye which intercalates to dsDNA and complexed with RecBCD, was tethered at one end to a bead held in an optical trap and stretched by laminar flow. By moving the trap into a flow stream containing ATP, RecBCD helicase and nuclease activity could be recorded by observing the decrease in fluorescence of the DNA molecule as it was unwound and cleaved using a CCD camera. Later experiments demonstrated that RecBCD unwinding progress was halted at by the introduction of χ (chi) sequences to the DNA, and resumption of activity after these sites continued at a 2-fold reduced rate (Spies *et al.*, 2003). By combining it with site-directed mutagenesis of the proteins in RecBCD, Spies *et al* were also

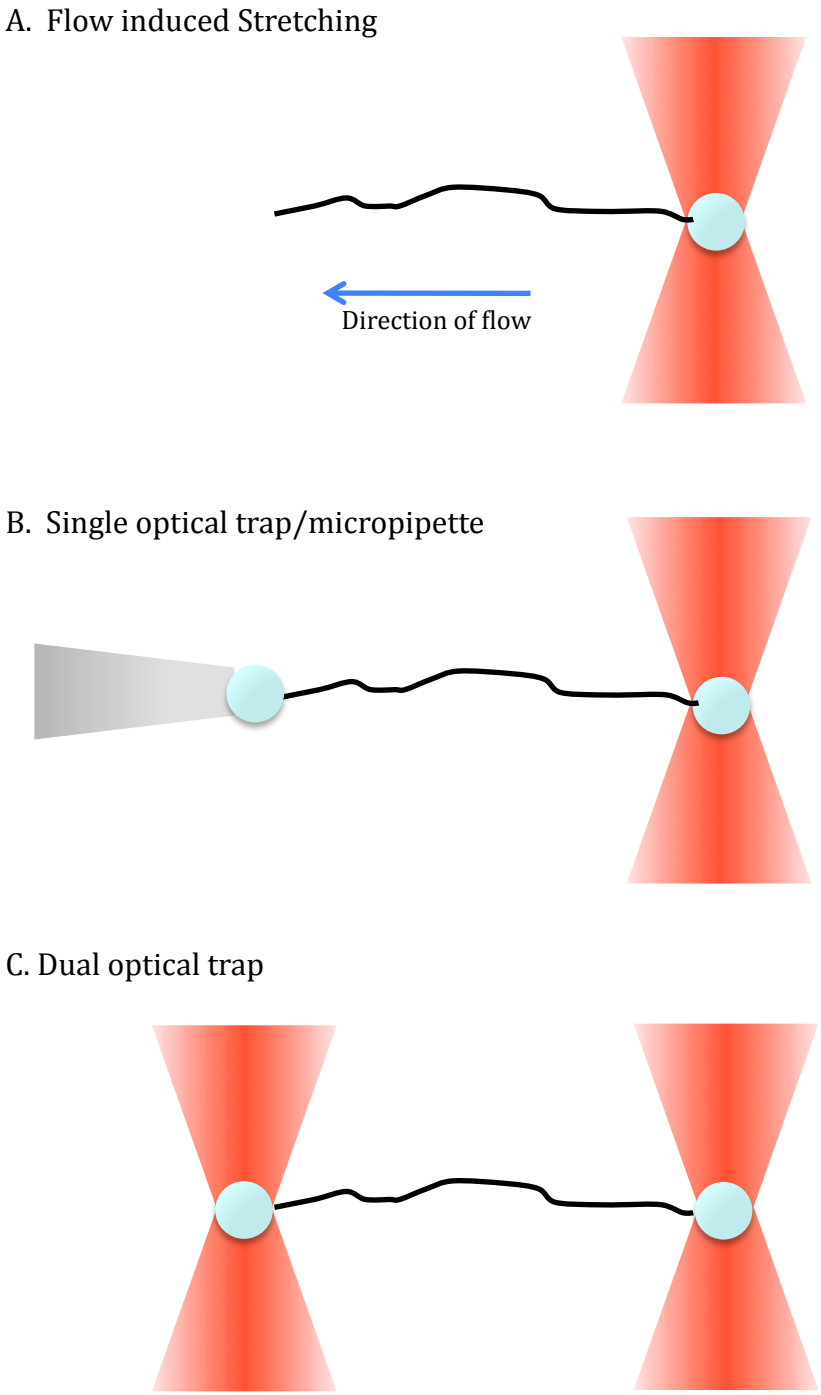

Figure 4.16 Optical tweezer experimental set up. Three main experimental designs are used with optical tweezers. **A.** The flow of buffer through a flow-cell is used to extend a nucleic acid molecule tethered at one end to a bead held in an optical trap. **B.** A nucleic acid is tethered between two spheres; one is held in a micropipette, the other in an optical trap. Moving the pipette changes the force experienced by the molecule. **C.** The molecule is tethered between two beads that are held in two separate optical traps, separating the experimental system from the experimental apparatus. Moving the position of one trap changes the force experienced by the molecule.

able to determine that the lead motor prior to χ sequence recognition was RecD and after was RecB (Spies *et al.*, 2007).

The second method (B) shows a nucleic acid tethered to two spheres; one is held in a micropipette, the other in an optical trap. The third method (C) utilises two optical traps, which separates the experimental system from the experimental apparatus, reducing the background thermal noise. Both of these methods have been employed by Bustamante and coworkers to investigate the forces required to unwind RNA molecules (Liphardt *et al.*, 2001; Dumont *et al.*, 2006; Wen *et al.*, 2008). In these systems one bead is held still, while the other, held by a pipette or an additional optical trap, is moved to place tension on the polynucleic acid in a controlled manner. Increases in the tension of the molecule as it is stretched beyond its contour length will result in a displacement of the bead, which is recorded by a position sensitive diode. If the trap stiffness is known, these displacements can be used to calculate the force imparted on the bead in the same way that the deflection of a cantilever in an AFM force experiment is used.

The use of optical tweezers to investigate nucleic acids can result in a spatial resolution of one base pair, providing a means by which the activity of helicases and translocases can be observed in intricate detail. This technique was recently applied to the process of translation where the translation of single mRNA hairpins by single bacterial ribosomes was tracked in real-time (Wen *et al.*, 2008). The authors stalled translating ribosomes on mRNA-hairpin constructs, similar to that described above (Dumont *et al.*, 2006) and then held them with dual-beam optical tweezers at a constant force just below that required to unzip the hairpin. Translation was reinitiated by the introduction of aminoacids and the progress of ribosome translocation observed by monitoring the changes in the end-to-end distance of a hairpin construct as it was unwound. The data showed that ribosomes translocate in three-bp step and revealed that translation is not a continuous process but is interrupted by ribosomal pausing of mixed duration between translocations (Wen *et al.*, 2008).

4.13 Force extension profile of ODC hp construct using optical tweezers

Initial optical tweezer work was performed with an in-house multiple trap optical tweezer system developed by A Orta (Orta, 2008), based on the setup used by the JE Molloy laboratory, MRC, London, UK (Veigel *et al.*, 1998). A system was developed and successfully used to catch DNA molecules (Orta, 2008), however, due to technical defects in this system a *Nanotracker* quantitative optical tweezer platform, manufactured by JPK Limited (Berlin, Germany), was used to perform initial experiments with the ODC hp construct. The *Nanotracker* contains two lasers that are steered, focused and detected by two separate pathways to produce two high-powered optical traps.

In order to manipulate the ODC hp construct in a dual trap optical tweezer system the molecule was tethered between a streptavidin-functionalised microsphere via the 5' biotin-labeled handle, and to a maleimide functionalised microsphere via the 3' thiol handle. Streptavidin-coated silica microspheres (3 μm) were purchased from Bangs Laboratories (Park Scientific, UK). The maleimide beads were functionalised from amine-coated polystyrene microspheres (1 and 2 μm) (Invitrogen) by incubation with an excess of sulfo-GMBS according to the reaction scheme depicted in figure 4.17. Prior to each experiment, 250 ng maleimide-functionalised beads were incubated with varying amounts of ODC hp construct in PBS for one hour at room temperature to allow the covalent linkage between the thiol group of the construct with the maleimide group of the bead. Ideally a ratio of one molecule of construct per bead would be used in order to avoid multiple binding of molecules between the differentially labeled beads during the experiment, however it is predicted that the functionalisation will not be 100 % efficient and therefore a concentration of 1:1000 bead:construct ratio was first used, and this was increased throughout the experiments to try and find an optimum ratio. Maleimide-ODC hp construct microspheres (31.25 ng) were then mixed 1:1 with streptavidin coated microspheres (~ 0.003 % beads total) in either TE-NaCl or helicase buffer without BSA (20 mM Hepes, pH 7.4, 70 mM KCl, 1 mM MgCl, 2 mM DTT) and immediately drawn into a ~ 10 μl channel of a flow cell using capillary action, which was then sealed with nail-varnish before being positioned in the

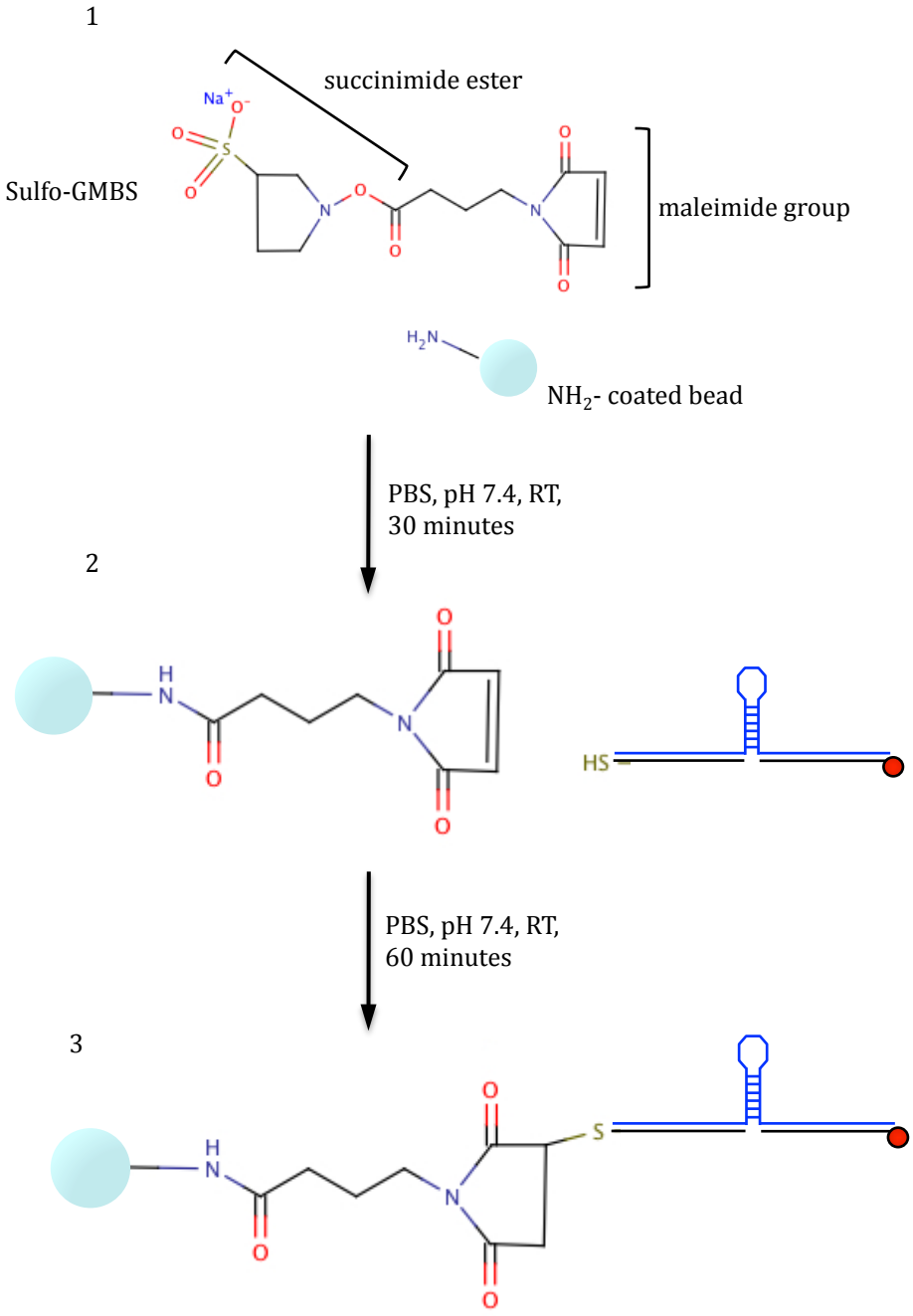

Figure 4.17 Functionalisation of amine-coated beads. Amine (NH_2) coated beads (light blue sphere) are functionalised with sulfo-GMBS. The sulfo group increases the solubility of the compound which allows the reaction to occur in aqueous conditions. 1. The *N*-hydroxysuccinimide (NHS) ester group rapidly reacts with the primary amine group coating the beads at room temperarure (RT). 2. The thiol group of the 3 ‘ DNA handle is reacted with the maleimide group at pH 7.4 (pH > 8 results in this group also reacting with primary amines). 3. The bead is covalently attached to the construct molecule and is ready for use in optical tweezer experiments.

microscope. A longer construct was manufactured in order to double the extended length of the ODC hp construct to allow a greater distance between the two optical traps in case an overlap occurred with the shorter molecule. This long ODC hp construct was manufactured in exactly the same way as the ODC hp construct but used different primers in the initial amplification process that had the effect of adding 500 bp to each arm.

The two types of beads used in these experiments were easily distinguishable due to the size difference and due to the smaller maleimide-functionalised beads fluorescing green/yellow when excited at a wavelength of 488 nm). After the successful capture of a different bead in each trap, the trap that held the larger streptavidin bead (trap 1) was slowly moved towards the maleimide-ODC hp construct bead in trap 2 and then gently pulled away. Near-contact was observed as a sharp increase in force as the repulsion between the two beads displaced each other in each trap (see figure 4.18 A). As the beads were slowly separated, caught molecules appeared as an increase in force as the molecular tether pulled the beads towards each other, thus displacing them from the trap. If the molecule remained tethered when trap 1 returned to its initial position, then trap 1 was slowly moved towards trap 2 without allowing the beads to make contact. Repeated round of extension and relaxation were then programmed, moving trap 1 away from trap 2 and back again at speeds between 2 - 1000 nm/s for increasing distances until the molecular tether ruptured. Data were collected between 100 - 1000 Hz.

Initial experiments determined that the flow cell needed to be blocked with BSA prior to the addition of the bead mix in order to prevent bead adherence to the glass surface. In addition, it was realised early on that both the 1 μm beads and the shorter construct reduced the success of molecule capture and therefore all further investigations were performed with 2 μm maleimide-functionalised beads and the longer ~2000 kb construct. Many short interactions between the beads were observed that ruptured at low forces (between 10 - 20 pN) (figure 4.18 A) at the initial ratio of 1:1000 bead:construct. Considering the maleimide -thiol linkage is covalent and that between biotin and streptavidin can

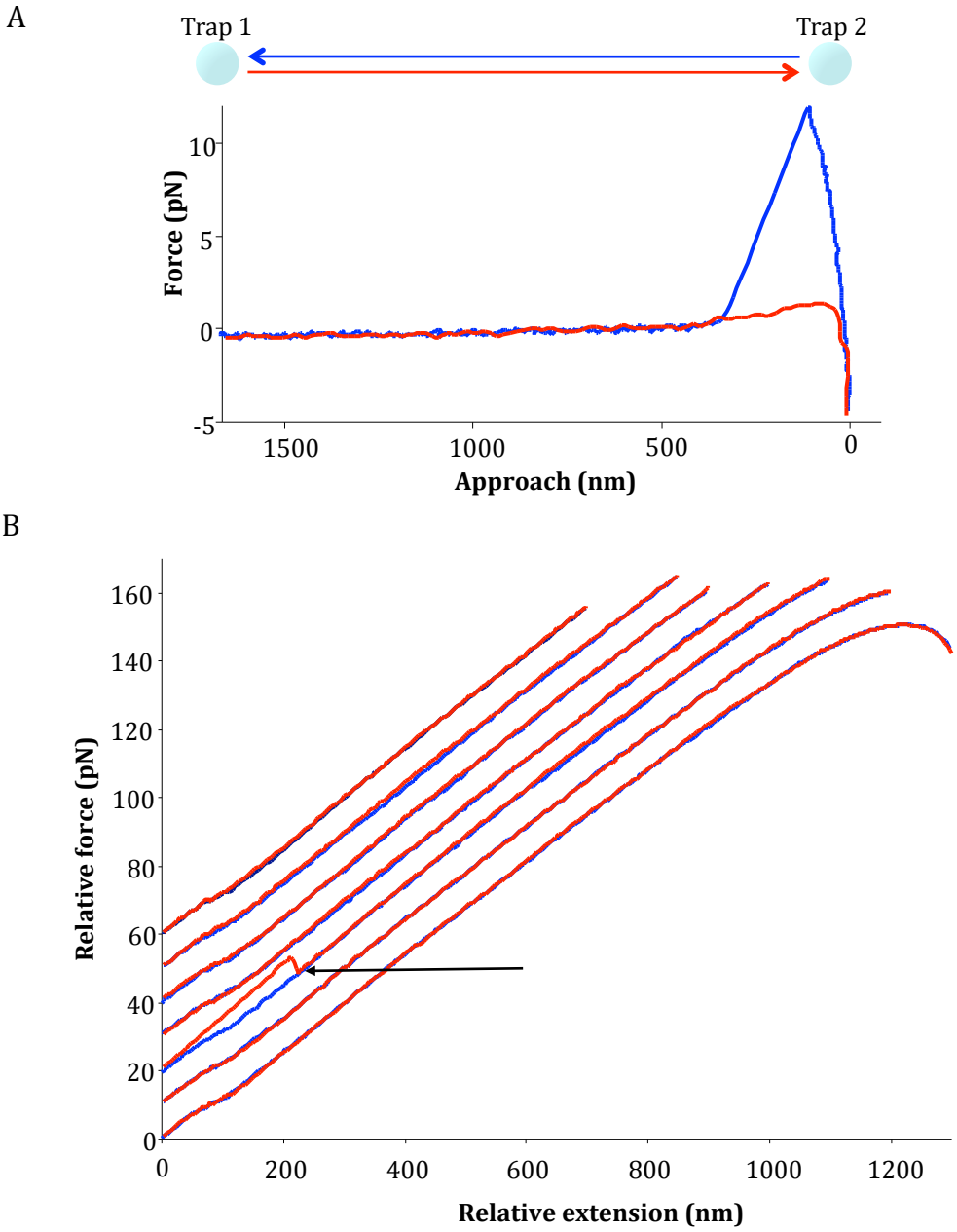

Figure 4.18 Non-specific low and high force bead interactions. A. Initial approach and retract trace. As trap 1, containing the smaller, maleimide-construct bead approaches trap 2, containing the streptavidin bead, (red trace) a repulsive force, shown as a reduction in force on this graph, occurs. Retraction of trap 1 (blue trace) causes a sharp increase in force indicating the 'capture' of a molecule that is held until ~ 12 pN before the contact is ruptured and the force returns to zero. **B.** Example curves caused by a non-specific molecular interaction between the beads. The highest curve is the first after capture and each successive curve increases the extension of the molecule until the decrease in extension at the end of the last curve demonstrates that the molecule is being pulled beyond the detection limits of the apparatus. Arrow marks an 'unwinding-like' event.

withstand up to 300 - 400 pN (Chilkoti *et al.*, 1995) these lower force ruptures were considered non-specific and disregarded. As no higher-force interactions were observed with the 1:1000 sample the ratio of bead to construct was successively raised to 1:4000 and 1:8000. These samples produced several interactions that could be pulled to forces between 60 - 70 pN, however no unfolding events were observed and the molecule could be extended over 600 nm further than the expected contour length of the long ODC hp construct (~ 570 nm zipped, 638 nm unzipped). Control experiments without the construct demonstrated that, after the maleimide group had been reacted with DTT in the buffer solution, a non-specific molecular interaction could occur (figure 4.18 B). This molecule could withstand forces larger than 70 pN and could be extended beyond the limitations of the detector, as demonstrated by the lowest curve of figure 4.18 B, and could be pulled at speeds of 1 μM/s.

The majority of molecules caught from beads from the 1:8000 sample resembled those of the non-specific molecule shown in figure 4.18 B. As seen in figure 4.18 B, occasionally discrete changes in force as would be expected of an unwinding event would occur with these molecules, however, these events were not followed by a refolding event, and were never reproduced between curves so they were disregarded. Only one molecule was caught at this concentration that showed specific, reproducible unwinding and refolding events. Figure 4.19 shows the force extension traces of this molecule, which was pulled at 50 nm/s, 11 successive times before rupture. Initially the molecule was extended over ~ 300 nm and this extension was gradually increased to ~ 450 nm, up to a force of ~ 50 pN (full extension not shown in figure). The change in length of the ODC hp construct that occurs after the hairpin is unzipped is estimated to be ~ 70 nm, as calculated from a predicted ssRNA contour length of 0.58 nm/base using the worm-like chain (WLC) model (Liphardt *et al.*, 2001). The unwinding/refolding events have been numbered 1 - 5 (figure 4.20 C) and the change in distance that occurred with each event was measured on the stretching and relaxation trace of each curve, the results of which are displayed as a histogram in figures 4.20 A and B respectively. The first event on each trace (1 - blue bars on histogram) occurs at ~ 10 pN and produces an average

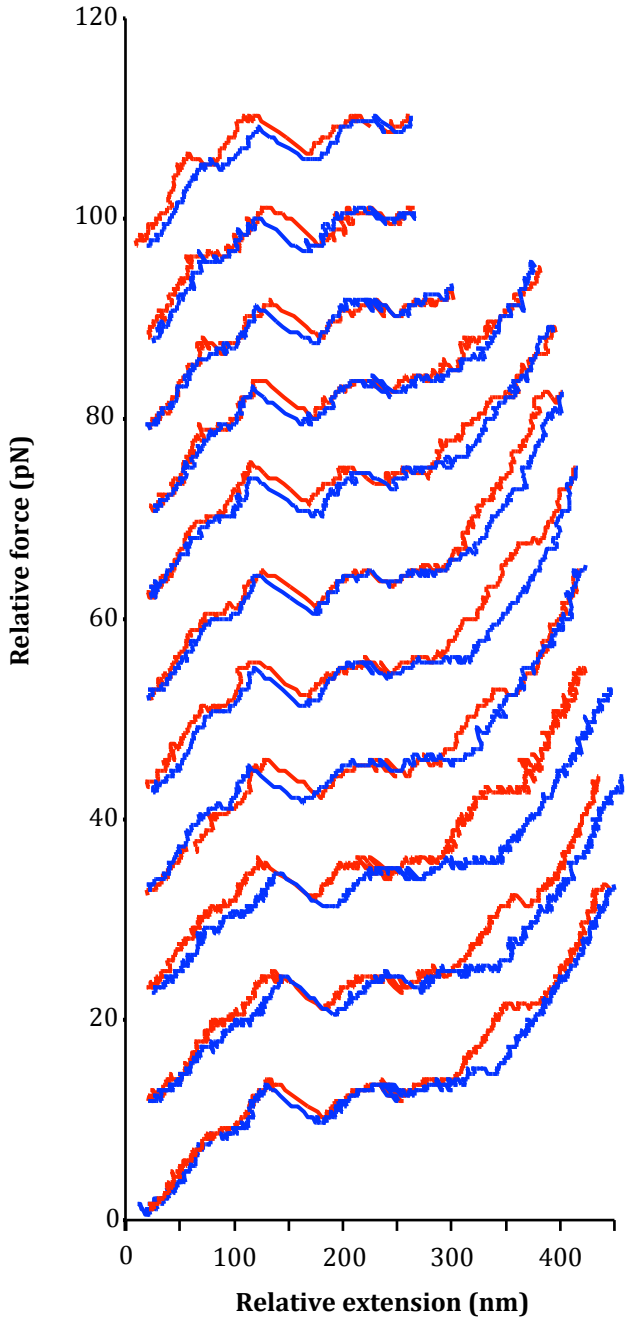

Figure 4.19 Stacked caught molecule traces. First caught molecule traces showing reproducible unwinding and refolding events. The top two curves are the first recorded with the molecule and each subsequent trace is stacked below. The extension of the molecule was increased from ~ 250 nm to ~ 450 nm by the lowest, final trace. Red trace - extend; blue trace - retract; trap speed - 50 nm/s; data collection - 1000 Hz.

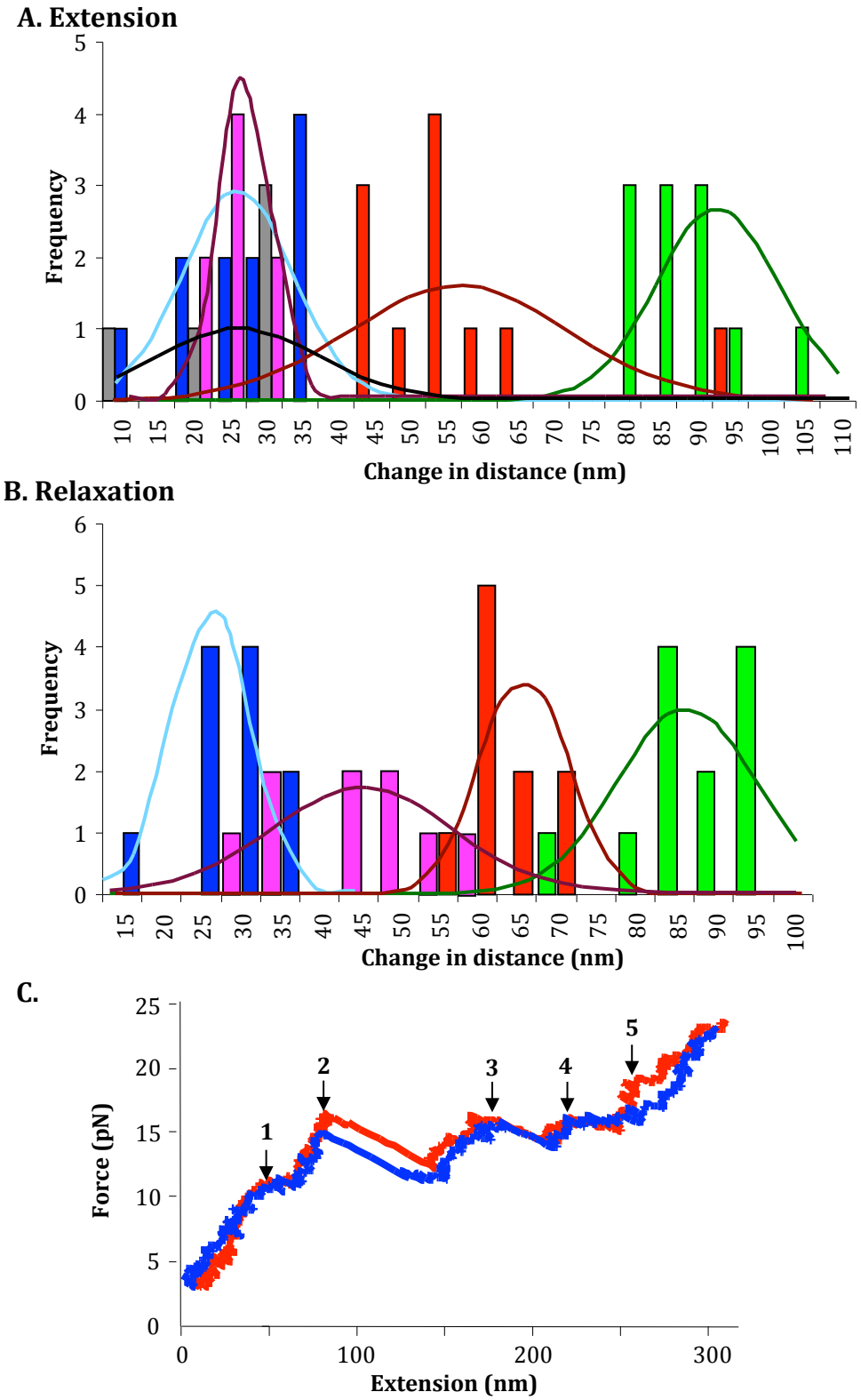

Figure 4.20 Distance and frequency of unwinding/refolding events. The distance change each unwinding/refolding event was measured using J. Mameren's programme written in LabView and catagorised into 5 nm bins to plot the frequency distribution of unwinding/refolding events from the curves displayed in figure 4.19. **A.** extension. **B.** relaxation. Colours relate to the position of each event numbered in curve **C.** 1. blue; 2. green; 3 - red; 4 - magenta; 5 - grey. Normal distribution of frequency displayed as a curve of corresponding colour. n=11

distance change of ~ 24.2 nm ± 2.2 on both the stretching and relaxation traces, which may be attributed to non-specific secondary and tertiary structures of the relaxed molecule being overcome. The second, third and fourth unwinding events all occur at 16.17 pN ± 0.61 and produce a total distance change of 162 nm ± 3.3 (mean distance for each event: 2 - 85.9 ± 2.9; 3 - 54.5 ± 4.4 and 4 -23.4 ± 1.6). As the molecule was extended further an extra unwinding event occurred (marked as 5, figure 4.20, C) of approximately 22.5 nm ± 4.3. Though the molecule demonstrated reproducible force-extension behaviour, none of the events correlated to that expected of the hairpin being opened and the total distance change of the molecule was more than double that expected if the only change was the 60 bp hairpin opening.

The bead to construct ratio was increased to 1:3200 and 1:32000 as the rate of molecule capture was low and the force curves obtained with each sample resembled that of the control (figure 4.18) and showed no reproducible unwinding events. A final experiment was performed using a ratio of 1:320,000 bead:construct that produced a much higher rate of molecule capture. Figure 4.21 shows the force extension curves obtained for one molecule, which stayed attached to the bead for 23 successful extensions. The molecule was extended at a rate of 100 nm/s over a distance of 350 - 450 nm. Reproducible unwinding and refolding events occurred at an average force of 49.8 pN ± 0.25 and the frequency of these events is displayed in figure 4.22. Initial curves displayed a single unwinding event of 33.9 nm ± 0.65. As the force was increased this first event was followed by a second, longer unwinding event of an average distance of 114.3 nm ± 5.5, producing a total distance change of approximately 148 nm. The relaxation traces of the molecules that had two unwinding events appeared to refold in a series of substeps as shown by the large range on distances measured in figure 4.22, B. Perhaps this difference in relaxation trace characteristics from the traces observed in figure 4.19 is due to the larger forces that this molecule is being held at. As with the force extension curves displayed in figure 4.19, there was no correlation between the distance change observed and that predicted for ODC hp opening, however the total distance unwound at ~ 16 pN and ~ 50 pN for each set of curves was quite similar (162 and 148 nm

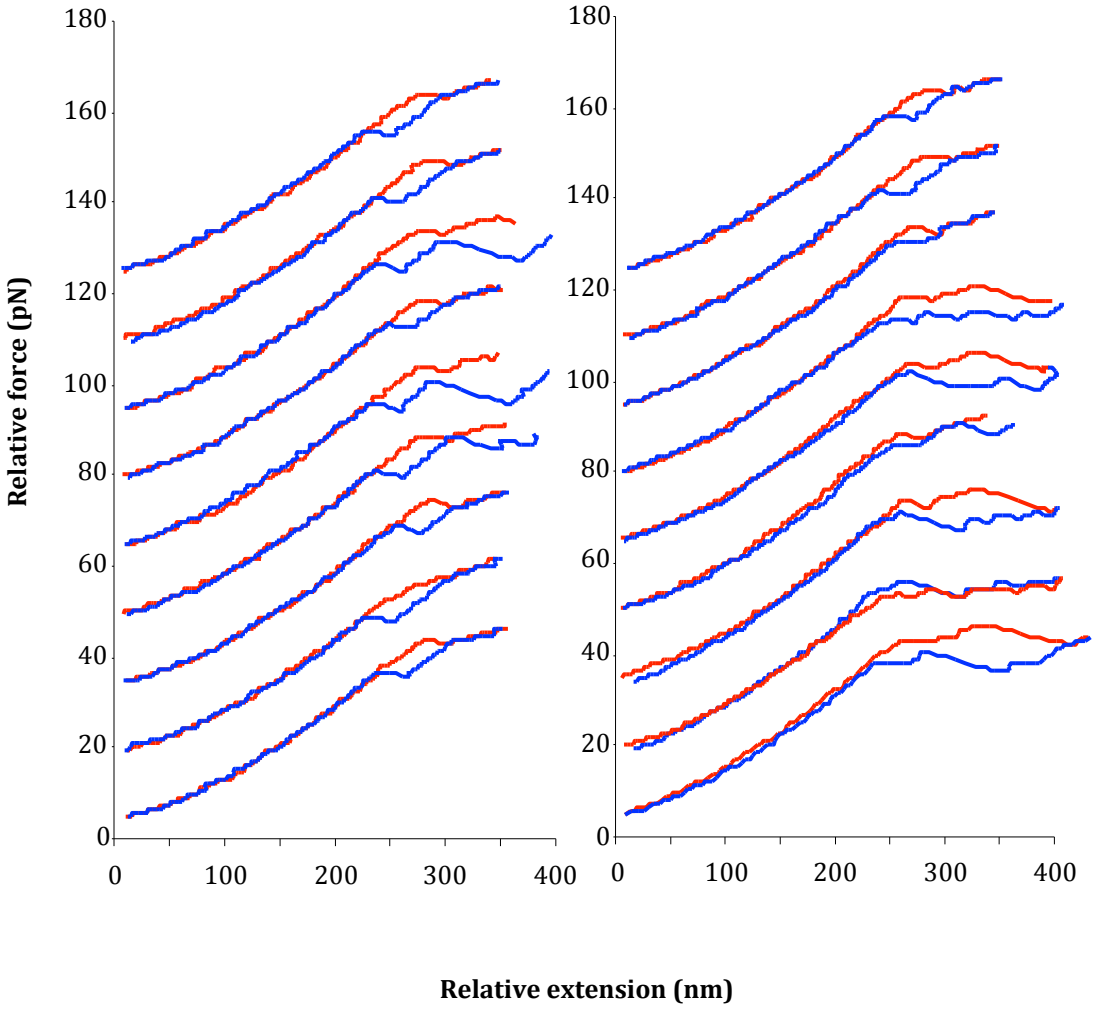

Figure 4.21 Stacked caught molecule traces. Caught molecule traces showing reproducible unwinding and refolding events. The first extension trace is the top left and each subsequent trace is stacked below until the last extension trace on the bottom, right. The extension of the molecule was increased from ~ 350 nm to ~ 450 nm by the lowest, final trace. Red trace - extend; blue trace - retract; trap speed - 100 nm/s; data collection - 500 Hz.

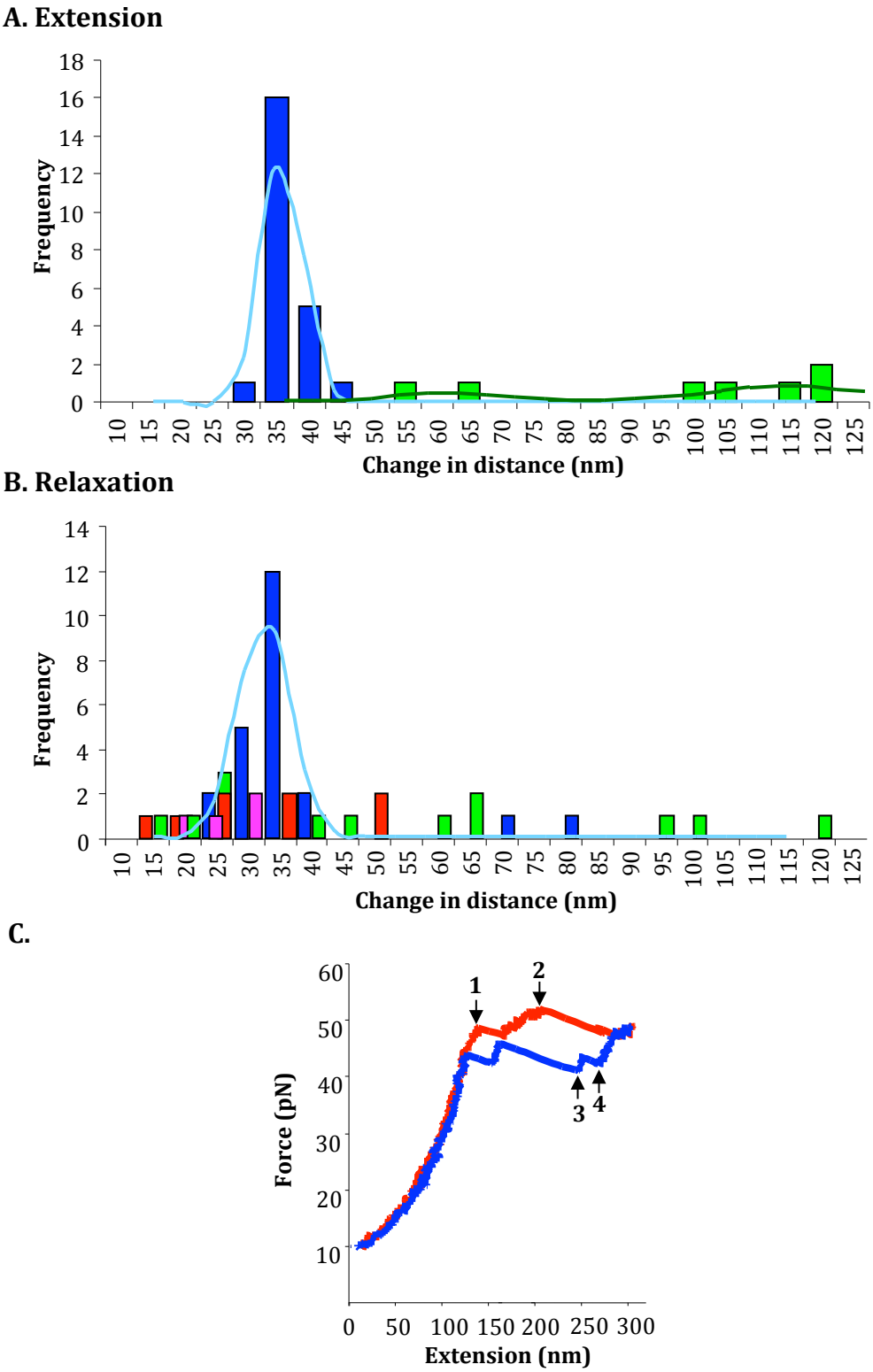

Figure 4.22 Distance and frequency of unwinding/refolding events. The distance change for each unwinding/refolding event from the curves displayed in figure 4.21 were measured using J. Mameren's programme written in LabView and catagorised into 5 nm bins to plot the frequency distribution of unwinding/refolding events. **A.** extension. **B.** relaxation. Colours relate to the position of each event numbered in curve **C.** 1. blue; 2. green; plus some relaxation traces displayed 3 - red; 4 – magenta. Normal distribution of frequency displayed as a curve of corresponding colour.

respectively) which may indicate that these force curves are generated from the same molecule.

4.14 Discussion

This chapter describes the design and initial optimisation of an experimental procedure to explore the activity of eIF4AI at a single molecule level. The methods and results demonstrated here show the successful cloning and manufacture of a RNA:DNA construct that contained a single region of secondary structure based on the first hairpin encoded by the ODC mRNA 5' UTR. This molecule was biotinylated on the 5' DNA handle and thiolated on the 3' DNA handle to produce functionalised termini that could be manipulated in single molecule experiments. AFM imaging of the construct demonstrated that it was within an expected size range for the molecule, however, attempts to visualise the construct bound to recombinant eIF4AI in the presence of the non-hydrolysable ATP analogue, AMPNP, resulted in large aggregates that could not be resolved.

AFM was also used to explore the force extension profile of dsDNA molecules in order to investigate the structural integrity of the molecule as it extended from B-form to S-form DNA. It was demonstrated that regions of ssDNA must be exposed during this transition as the addition of SSB protein resulted in hysteresis of the relaxation curve, indicative of protein binding (Zhang *et al.*, 2008). Although the experimental system was optimised, attempts to use it to pull the ODC hp construct were unsuccessful. This was thought to be due to a low yield of fully functionalised product, and because of this, and the limited force resolution achievable with AFM an alternative experimental system was pursued.

Dual trap optical tweezers have been widely used to explore biomolecules at a high force and spatial resolution. The demonstration model of JPK's dual-trap *Nanotracker* (Berlin, Germany) was used in a series of experiments, part-funded

by a travel award from the Korner Travelling Fellowship Fund (University of Sussex), to optimise the capture of the ODC hp construct molecules.

Initial experiments were used to determine the optimum ratio of bead to ODC hp construct required to catch molecules at an efficient rate without causing the binding of multiple molecules. At relatively low ratios (1:4000, 1:8000) a number of molecules were captured, however, they could be extended to high forces, beyond the contour length estimated for the ODC hp construct and were later determined to be caused by an unexpected, specific interaction between the maleimide and streptavidin functionalised beads used in these experiments. One molecule was captured that displayed reproducible unwinding and refolding events, however these did not equate to the change in extension expected to occur to the construct upon the unzipping of the ODC hairpin. Due to the low rate of non-background molecule capture the ratio of bead:construct ratio was increased to a final concentration of 1:320000 and this sample yielded a much higher rate of capture of molecules that displayed some unwinding behaviour. Analysis of the distances observed during each unwinding event demonstrated that, though reproducible, these distance changes were beyond that predicted for the ODC hp construct. The difference between the initial force required to cause unfolding events also varied considerably (15 pN - 50 pN), demonstrating that the molecules captured were not displaying homogeneous behaviour. Due to time and instrument limitations further experiments to characterise the ODC hp construct could not be performed.

In order to use this experimental system to investigate the helicase activity of eIF4AI the force extension behaviour of the ODC hp construct must first be characterised. A possible next step would be to use a hairpin-less construct to ascertain if the extension of the DNA handles displayed any anomalous behaviour that had not been anticipated. If a single unwinding event recorded with the ODC hp construct is different from that of the hairpin-less construct then this may be attributed to the unwinding of the hairpin. Only when a stable, reproducible force-extension behaviour can be ascribed to the unwinding of the hairpin can this molecule be used to explore the activity of eIF4AI. The most

effective way to measure helicase activity would be to hold the ODC hp construct at a steady force, also known as a force-clamp, just below the force required to unwind the hairpin. Any helicase activity that occurs upon the addition of eIF4AI, ATP, eIF4B or eIF4AI inhibitors will result in a lengthening of the construct, which in turn would result in a reduction of force. The force clamp acts to regulate and monitor this activity by increasing or decreasing the distance between the two traps resulting in a constant force being maintained. The movement of the traps can then be used to calculate the number of bases of the hairpin that have been unwound. Bustamante and coworkers have used this method to analyse the helicase and translocation activity of the HCV NS3 helicase and the bacterial ribosome at base-pair resolution (Dumont *et al.*, 2006; Cheng *et al.*, 2007; Wen *et al.*, 2008). Therefore continuation of the experiments described above will lead to a much greater understanding of eIF4AI activity.

5 Microarray analysis

5.1 Translational control during inflammation

The host's immune response to tissue injury or infection involves a complex coordination of gene expression at a transcriptional and post-transcriptional level to control the onset and resolution of inflammation. The initiation phase of acute inflammation stimulates the cells of the immune system to locate to the site of injury where they clear cellular debris and foreign material and repair damaged tissues. Prolonged or excessive production of the proteins and signaling molecules initially produced to promote the inflammatory response can negate these beneficial effects and become injurious to the host. To prevent the perpetuation of inflammation, the stimuli that trigger the initiation phase of inflammation simultaneously trigger a programmed response that resolves it. Due to this, drugs that target the initiation phase of inflammation to reduce the symptoms of acute inflammation, such as the non-steroidal anti-inflammatory drugs (NSAIDs) that target cyclooxygenase 2 (COX-2), can also prevent its resolution. Combining an anti-inflammatory drug with one that stimulates a pro-resolution response may provide a useful therapy for chronic inflammatory diseases. A greater understanding of the complicated network of cellular pathways that are involved in these responses is therefore an important area of research (Serhan *et al.*, 2008).

The induction of inflammation produces an immediate pulse of pro-inflammatory proteins that also stimulate signaling pathways that control the transcription of the genes that coordinate inflammation resolution. Resolution also requires that the expression of pro-inflammatory proteins be switched off, and this, in part, is controlled by post-transcriptional mechanisms. Translational control of inflammation is generally coordinated via the repression of specific mRNAs via 3' UTR sequences or structures that promote selective mRNA degradation or silencing. The release of the cytokine interferon-γ (IFN-γ) by T-cells is a well characterised example of this coupled control as it induces the expression of a number of pro-inflammatory proteins

but is also necessary for pro-resolution activity (Mühl and Pfeilschifter, 2003). IFN-γ controls the selective degradation of mRNAs via the formation of the IFN-γ-activated inhibitor of translation or GAIT complex that binds to GAIT sequences present in the 3' UTRs of some mRNAs. IFN-γ stimulates the phosphorylation and release of glutamyl-prolyl tRNA synthetase (EPRS) from the multisynthetase complex (MSC) and ribosomal protein L13A (RPL13A)) from the 60S ribosomal subunit (LSU). Together with heteronuclear ribonucleoprotein Q1 (HNRNPQ1) and glyceraldehyde 3 phosphate dehydrogenase (GAPDH) these proteins form the GAIT complex (Mazumder *et al.*, 2003; Arif *et al.*, 2009; Mukhopadhyay *et al.*, 2009), which binds to GAIT sequences in the 3' UTRs of target transcripts through EPRS. The translation of GAIT-bound transcripts is repressed by RPL13A binding to eIF4G, preventing its interaction with eIF3 and therefore the recruitment of the small ribosomal subunit to the RNA (Mazumder *et al.*, 2001; Kapasi *et al.*, 2007; Mukhopadhyay *et al.*, 2009). Due to the time it takes to form this complex, there is a delay of 14 - 16 hours after the initial stimulus before GAIT mediated translational repression comes into effect, which allows the initial pulse of protein synthesis at the onset of inflammation to occur (Mukhopadhyay *et al.*, 2009). Formation of the GAIT complex is also controlled by a temporal feedback loop as two proteins, death-associated protein kinase 1 (DAPK1) and zipper-interacting protein kinase (ZIPK), in the IFN-γ- stimulated kinase pathway that phosphorylate RPL13A also contain GAIT elements in their 3' UTRs (Mukhopadhyay *et al.*, 2008). It is thought that this feedback loop allows the restoration of normal expression of GAIT-containing mRNAs once inflammation has been resolved.

Many mRNAs that encode genes expressed during inflammation contain adenine- and cytosine-rich elements (AREs) in their 3' UTRs including several cytokines and chemokines (Bakheet *et al.*, 2006; Anderson, 2010). The fate of an ARE-containing mRNA is dependent upon the RNA binding protein that interacts with it. Tristetraprolin (TTP) coordinates the degradation of many ARE-containing mRNAs involved in immune function by recruiting the mRNA to the mRNA decay apparatus (Sandler and Stoecklin, 2008). TTP transcription is

induced by a number of inflammatory modulators, including tumour necrosis factor α (TNF-α) and IFN-γ, both of which contain AREs in their transcripts and are therefore subject to TTP coordinated decay (Carballo *et al.*, 1998; Sauer *et al.*, 2006). TTP activity is also regulated by phosphorylation that can reduce its affinity for ARE-containing mRNA or cause its association with the adaptor protein 14-3-3, which stabilises ARE-containing mRNAs and excludes them from stress granules (Stoecklin *et al.*, 2004; Hitti *et al.*, 2006; Tudor *et al.*, 2009). In addition, ARE-mediated control of translation can also be controlled through microRNA (miR) binding to result in both mRNA degradation and translational stimulation dependent on the cellular environment, transcript and miR (Vasudevan *et al.*, 2007; Lal *et al.*, 2009). MiRs are also widely associated with the translational control of mRNAs by the immune system (Baltimore *et al.*, 2008). It is apparent that translational control through 3' UTR elements in inflammation is both important and complicated. For a review that discusses the mechanism of translational control through elements in the 3' UTRs of transcripts involved in inflammation in greater detail please refer to (Anderson, 2010).

In addition to translational control during inflammation being dictated by 3' UTR elements, the initiation apparatus can also be directly affected. The induction of sepsis or an immune response by lipopolysaccharide (LPS) causes a reduction of translation initiation via the reduced activity of the mTOR signaling pathway that results in the activation of 4E-BP and the sequestration of eIF4E from eIF4F (Lang *et al.*, 2007). eIF4AI is also a regulatory target during inflammation through the activity of the tumour suppressor, programmed cell death 4 (Pdcd4) and the prostaglandin (PG) derivative, 15d-PGJ_2. Pdcd4 competes with eIF4GI for eIF4AI binding through two separate HEAT/MA3 domains positioned in the middle and C-terminal regions of the protein (Yang *et al.*, 2004; LaRonde-LeBlanc *et al.*, 2007). Structural data has also demonstrated that Pdcd4 inhibits eIF4AI activity directly by binding to the interface of the inter-domain cleft of the helicase (Göke *et al.*, 2002; Chang *et al.*, 2009; Loh *et al.*, 2009). In addition to displaying potent tumour suppressor activity, Pdcd4 has been shown to have pro-inflammatory activity (Jansen *et al.*, 2005; Hilliard *et*

al., 2006; Sheedy *et al.*, 2010). Pdcd4 -/- mice are resistant to the induction of inflammatory disease models and overexpress the anti-inflammatory cytokines IL-10 and IL-4 in a translation-dependent manner (Hilliard *et al.*, 2006; Sheedy *et al.*, 2010). It has recently been shown that LPS-triggered inflammation decreases the expression of Pdcd4 through miR-21 induced mRNA silencing, and through this activity the NF-κB pro-inflammatory signaling pathway is blocked (Sheedy *et al.*, 2010). Interestingly, the linoleic acid metabolite, (±)-13-hydroxy-10-oxo-*trans*-11-octadecenoic acid (13-HOA), suppresses the expression of pro-inflammatory genes but also induces the expression of Pdcd4 (Murakami *et al.*, 2005; Yasuda *et al.*, 2009). As in tumourigenesis, the role that Pdcd4 plays in inflammation is likely to be complicated by cell type specific behaviour (Lankat-Buttgereit *et al.*, 2008).

The cyclopentenone 15d-PGJ_2 is a dehydrated derivative of PGD_2 that exhibits anti-proliferative, pro-apoptotic and anti-inflammatory behaviour (Fukushima, 1990; Straus and Glass, 2001). The cyclopentenones are able to covalently bind to proteins through an unsaturated α, β - carbonyl group that readily reacts with free sulfhydryl groups, such as those contained in cysteine residues (Straus and Glass, 2001). 15d-PGJ_2 is expressed by T-cells, mast cells and macrophages that are recruited to the site of insult throughout the initiation phase of inflammation (Haberl *et al.*, 1998; Gilroy *et al.*, 1999). This results in an increase of 15d-PGJ_2 in the inflammatory milieu to levels that usurp pro-inflammatory PGE_2**,** signifying a switch to the resolution phase of inflammation (Gilroy *et al.*, 1999). 15d-PGJ_2 attenuates the transcription of many pro-inflammatory genes (Straus and Glass, 2001; Cuzzocrea *et al.*, 2002), however, it has also been shown to modulate the expression of genes that would favour inflammation (Zhang *et al.*, 2001). Like Pdcd4, 15d-PGJ_2 modulation of gene expression is likely to be cell-type specific according to the expression of its cellular targets (Straus and Glass, 2001). 15d-PGJ_2 was first identified as a potent peroxisome proliferator-activated response-γ (PPARγ) agonist that regulates the transcription of several anti-inflammatory genes (Jiang *et al.*, 1998; Ricote *et al.*, 1998; Straus and Glass, 2007). The anti-inflammatory activity of 15d-PGJ_2 is also mediated through a number of PPARγ-independent

pathways including the direct modulation of NF-κB, c-jun and H-Ras in addition to eIF4AI (Straus *et al.*, 2000; Oliva *et al.*, 2003; Pérez-Sala *et al.*, 2003; Kim *et al.*, 2007).

The observation that 15d-PGJ_2 induces stress granule formation, independent of eIF2α-phosphorylation, lead to the discovery that, in addition to modulating the transcriptome, 15d-PGJ_2 also functions through the inhibition of translation (Kim *et al.*, 2007). This inhibition was shown to be through the covalent binding of 15d-PGJ_2 to cysteine residue 264 of eIF4AI which prevented the association between eIF4AI and eIF4G, therefore preventing eIF4F formation (Kim *et al.*, 2007). Results presented in chapter 1 also demonstrated that 15d-PGJ_2 can also directly inhibit recombinant eIF4AI helicase activity *in vitro*. eIF4AI helicase activity is known to be required in proportion to the extent of secondary structure within the 5' UTR of an mRNA (Svitkin *et al.*, 2001). Whether 15d-PGJ_2 mediated inhibition of eIF4AI activity results in the general repression of protein synthesis, or whether it affects specific transcripts that contain a higher proportion of secondary structure in their 5' UTR is unknown. This latter hypothesis is supported by the observation that Pdcd4 -/- lymphocytes express a higher level of IL-4, IL-10 and IFN-γ than wild-type cells and the transcripts of these genes contain GC-rich 5' UTRs (Hilliard *et al.*, 2006). In this chapter cDNA microarrays were used to investigate the sequence and structural content of transcripts that have altered translational efficiency in response to 15d-PGJ_2.

5.2 Microarray analysis as a tool to investigate translational activity

The number of ribosomes attached to an mRNA at any one time can be regarded as a measure of translational efficiency, with a larger amount of ribosomes signifying a higher rate of protein synthesis. In order to separate transcripts according to their ribosomal association, cell lysates are applied to sucrose density gradients and then subjected to high-speed centrifugation. Highly translated mRNAs with numerous ribosomes attached will be 'heavier' and therefore migrate further through the gradient than mRNAs that are not translationally active and therefore are associated with fewer ribosomes (figure

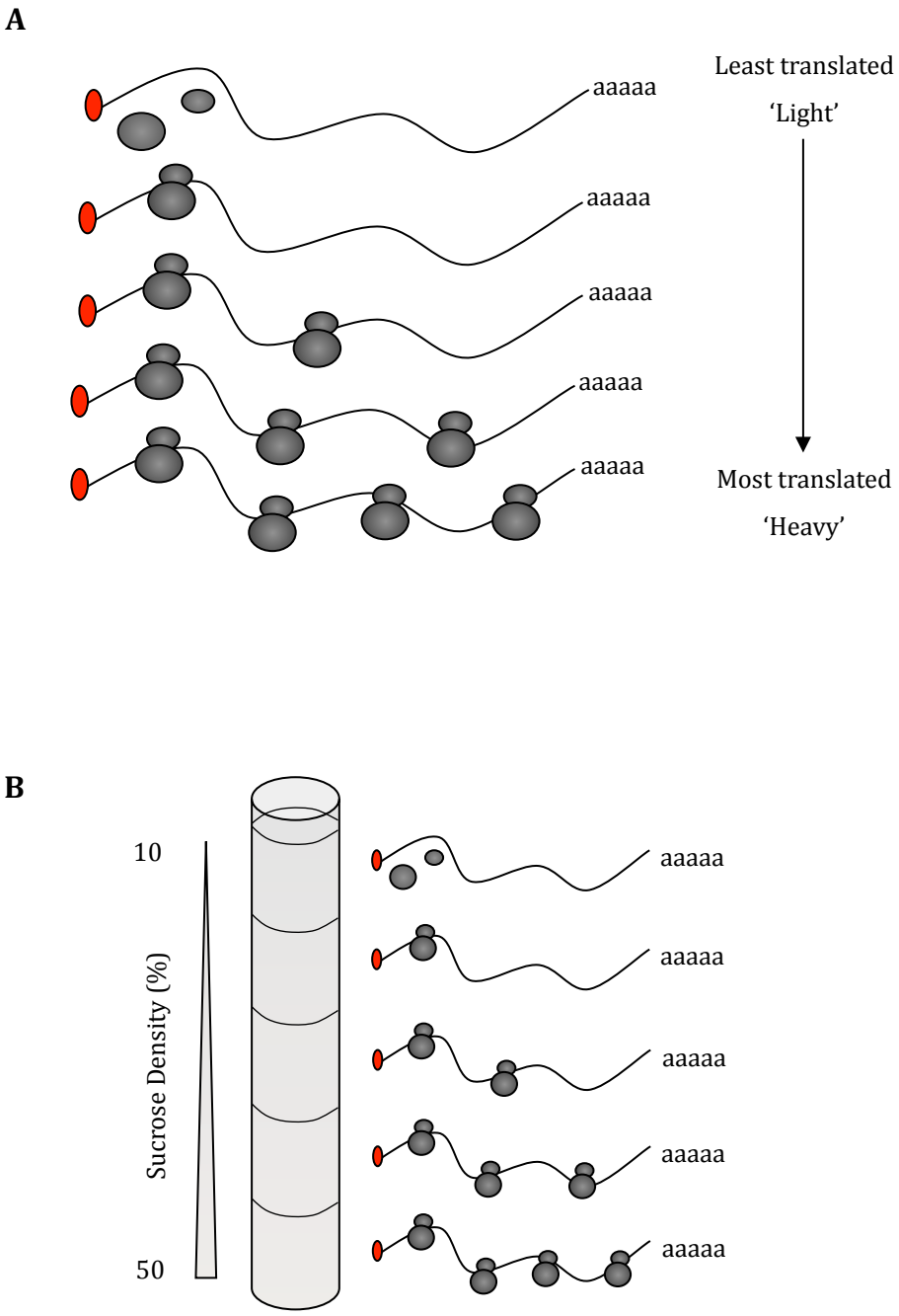

Figure 5.1 Sucrose density gradient centrifugation as a measurement of translational efficiency. The number of ribosomes associated with an mRNA can be used as a measure of translational efficiency (A). 'Heavy', ribosomally associated transcripts are separated from 'lighter' transcripts with few or no ribosomes attached by centrifugation through a 10 – 50 % sucrose density gradient (B).

5.1). Northern blotting analysis can be used to detect the distribution of transcripts throughout a fractionated gradient. Highly translated mRNAs associate with the heavier, denser fractions, or polysomes and untranslated mRNAs associate with the lighter sub-polysomal fractions. By observing changes to the polysomal distribution of a transcript, one is able to visualise the influence of the cellular environment on the translational efficiency of a gene.

By measuring the optical density (OD) of the sucrose fractions a 'polysome profile' can be drawn that plots the distribution of ribosomal subunits throughout the sucrose gradient (figure 5.2 A). The polysome profile, in combination with northern blot analysis of the polysomal distribution of β-actin and polyA-binding protein (PABP), can be used to divide the gradient into sub-polysomal and polysomal 'pools' of mRNAs. After reverse transcription and differential labeling with fluorescent dyes, the cDNA populations of each pool can be analysed using cDNA microarray (figure 5.2). Using mRNA isolated from the same cellular sample means that calculation of the subpolysomal/polysomal distribution of an mRNA between samples is relatively independent of the fluctuations in steady-state mRNA levels. Used in conjunction with transcriptional analysis, translational profiling by microarray allows the identification of genes that are differentially controlled by translational regulation under specific conditions. The following chapter will present data regarding the inhibition of translation in HeLa cells by 15d-PGJ_2. The transcripts that are differentially controlled by this inhibition will be detected using translation microarray profiling and the methods used to calculate the significance of these results will be discussed. Finally structural features of the mRNAs considered to be translationally activated, maintained or repressed will be compared.

5.3 15d-PGJ2 inhibits *de novo* protein synthesis

Due to the multiple cellular pathways that 15d-PGJ_2 effects a short treatment was preferred to reduce the influence that the deregulation of transcription had on the translational profile of HeLa cells after treatment. In order to establish

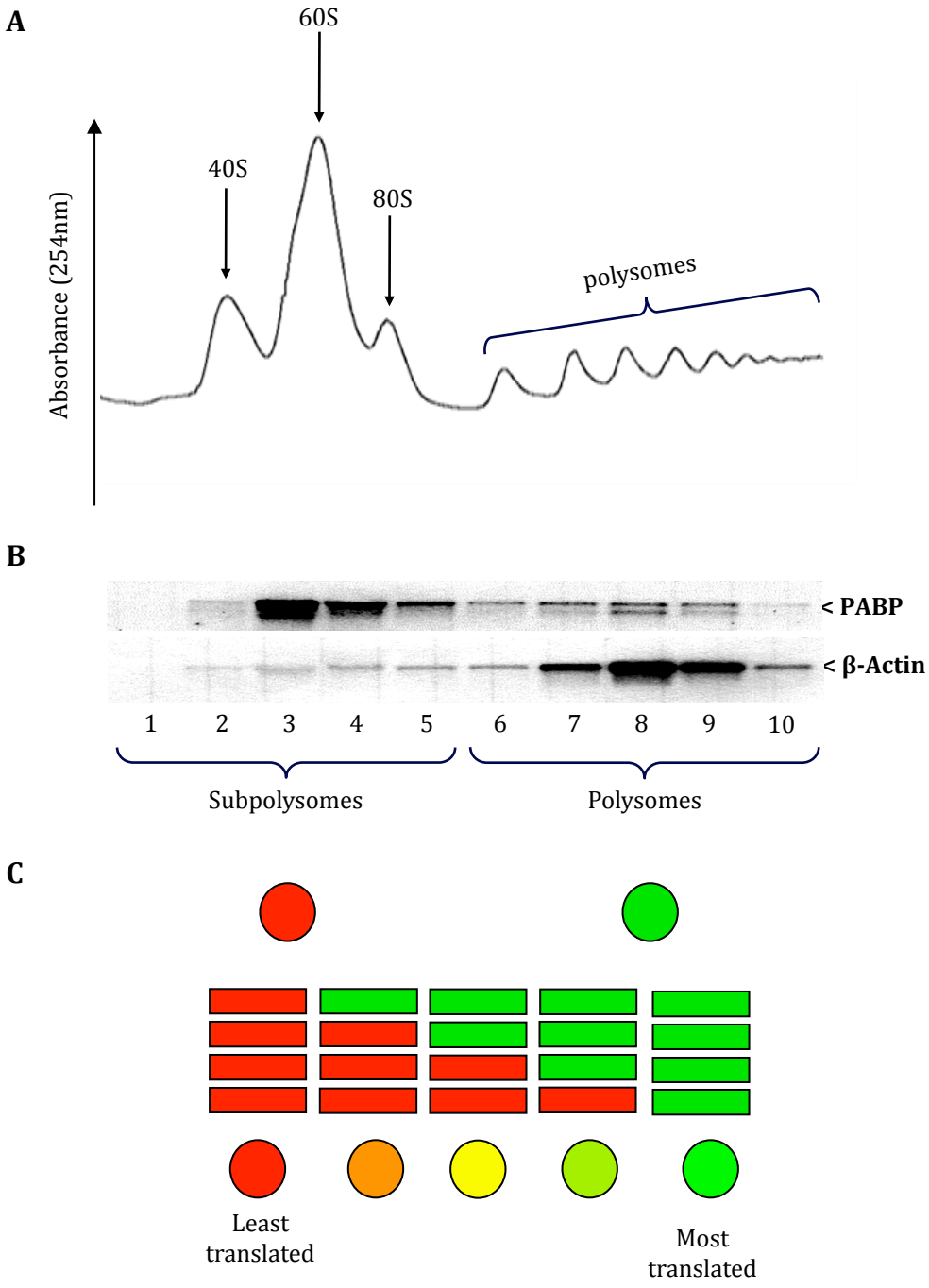

Figure 5.2 Polysome profiling and microarray analysis. Sucrose gradients are fractionated and the ribosomal content quantified by reading the optical density of each fraction at 254 nm and displayed in a polysome profile (A). The subpolysomal and polysomal fractions are pooled according to the distribution of PAPB and β-actin transcripts as analysed by northern blot (B). Each mRNA pool is reverse transcribed and the cDNA differentially labeled with Cy-5 (red –sub-polysomal pool) or Cy-3 (green - polysomal pool) dyes. The cDNA is hybridised to microarray chips (30,000 spots) and mRNAs whose polysomal association significantly changes between the inhibited sample and a negative control are further investigated.

the degree of translational inhibition that short treatments with 15d-PGJ_2 causes, *de novo* protein synthesis in HeLa cells was measured at 10 and 30 minutes after treatment. Kim *et al* had observed significant inhibition of protein synthesis (~ 80 %) in HeLa cells after 30 minutes of treatment with 90 μM 15d-PGJ_2 (Kim *et al.*, 2007), therefore a concentration of 100 μM was chosen for this study. HeLa cells, grown to ~ 80 % confluency, were treated with 100 μM 15d-PGJ_2 for a specified treatment time and then incubated with ^{35}S-methionine to pulse label newly synthesised proteins. After cell lysis, proteins were precipitated with 10 % trichloroacetic acid (TCA) and the quantity of newly synthesised labeled proteins calculated by scintillation counting. After normalisation of the detected counts per minute (cpm) to the total protein content of the cell lysates the data standardised to the cpm of mock treated cells (figure 5.3 A). After 10 minutes, 100 μM 15d-PGJ_2 causes a decrease in new protein synthesis of approximately 22 % and this inhibition is doubled at 30 minutes. This inhibition is lower than that reported by Kim *et al*, however, the same study reported that the same treatment for longer periods of time failed to achieve this degree of inhibition after six hours, which perhaps indicates some variation in their experimental technique. Furthermore, as changes to the amino-acid content of a cell can adversely affect translation, the pre-incubation in methionine-free medium that is a common step in ^{35}S-methionine *in vivo* labeling protocols was omitted from these experiments. Kim *et al*, however, did starve their cells of methionine prior to treatment with 15d-PGJ_2, which will likely contribute to the observed differences in inhibition.

In order to assess the comparative effectiveness of translational inhibition by 15d-PGJ_2, the above experiment was repeated with hippuristanol, a selective steroidal inhibitor of eIF4AI helicase activity. A 10 minute treatment with either 100 μM 15d-PGJ_2 or 10 μM hippuristanol prior to ^{35}S-methionine labeling was performed as described above and the results are presented in figure 5.3 B. Inhibition of new protein synthesis by hippuristanol was more effective than 15d-PGJ_2 in this assay (42 % in comparison to 26 %). These results may demonstrate a real difference in activity between the two inhibitors, which may be a reflection on differences between the rate of cellular uptake or in the mode

A

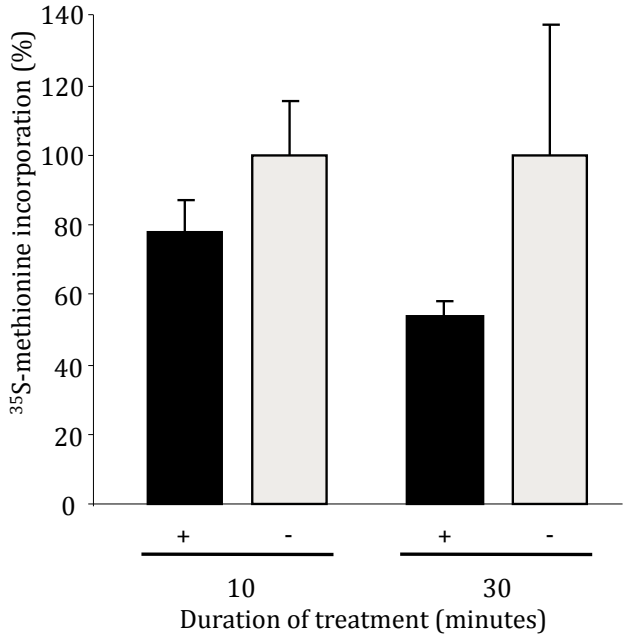

B

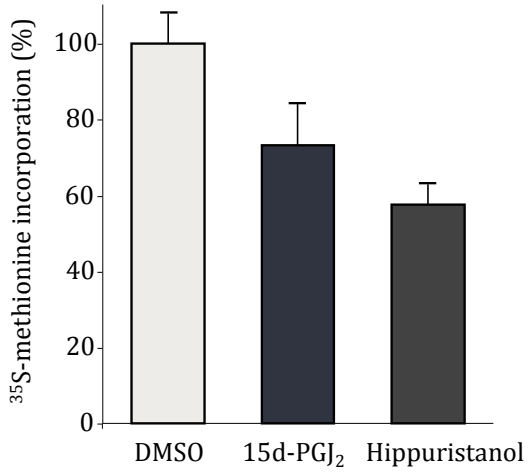

Figure 5.3 *de* novo translational inhibition by 15d-PGJ$_2$. The efficiency of 15d-PGJ$_2$ mediated translation inhibition was investigated by pulse labeling HeLa cells after treatment with ^{35}S-methionine. New protein synthesis was quantified by scintillation counting TCA protein precipitates. Results are displayed as percentage of mock treated cells (DMSO). **A.** HeLa cells were treated with 100 µM 15d-PGJ$_2$ for 10, 30 or 60 minutes prior to pulse labeling. **B.** HeLa cells were treated for 10 minutes with 100 µM 15d-PGJ2 or 10 µM hippuristanol. Results are displayed as a percentage of mock treated cells. Errors are standard deviation.

of translational inhibition. The high concentration of 15d-PGJ_2 required for a relatively small effect when compared to hippuristanol activity, however, may be due to the interaction of 15d-PGJ_2 with albumin (Person *et al.*, 2001). This would reduce the relative concentration of 15d-PGJ_2 available to interact with eIF4AI, therefore a direct comparison of the two inhibitors from these results may not accurately reflect their effectiveness. The data does show, however, that a 10 minute treatment of HeLa cells with 100 μM 15d-PGJ_2 is able to reduce translational activity by approximately 25 %.

5.4 Translational profiling of HeLa cells after 15d-PGJ_2 treatment

As described above, polysome profiling coupled to microarray analysis enables the detection of the differential translation of mRNAs between sample groups. In order to analyse changes in the translation profile of HeLa cells after treatment with 15d-PGJ_2 first the mRNAs must be separated according to ribosomal association by centrifugation through a sucrose density gradient. HeLa cells that had been grown to ~ 80 % confluency in 15 cm^3 plates were treated with 100 μM 15d-PGJ_2, or the equivalent amount of DMSO for 10 minutes at 37 °C. To ensure that cells were translationally active, one hour prior to treatment they were fed with fresh medium. To help maintain ribosomal attachment to transcripts, cells were treated with cycloheximide (100 ng/ml) for two minutes immediately after 15d-PGJ_2 treatment and then kept on ice for the duration of the experiment. Following cell lysis, cytosolic mRNAs were separated by centrifugation at 4 °C through 10 - 50 % sucrose density gradients. Polysome profiles of each sample were obtained by continuously reading the OD whilst each gradient was fractionated (figure 5.4, A). As expected if translation is inhibited at the initiation stage, treatment with 15d-PGJ_2 causes an increase of density in the lesser-translated sub-polysomal fractions. The distributions of β-actin and PABP transcripts throughout the gradient were analysed by northern blotting (figure 5.5 A and B) and used as a guide to pool the sub-polysomal fractions between 1 - 5 and the polysomal fractions between 6-11.

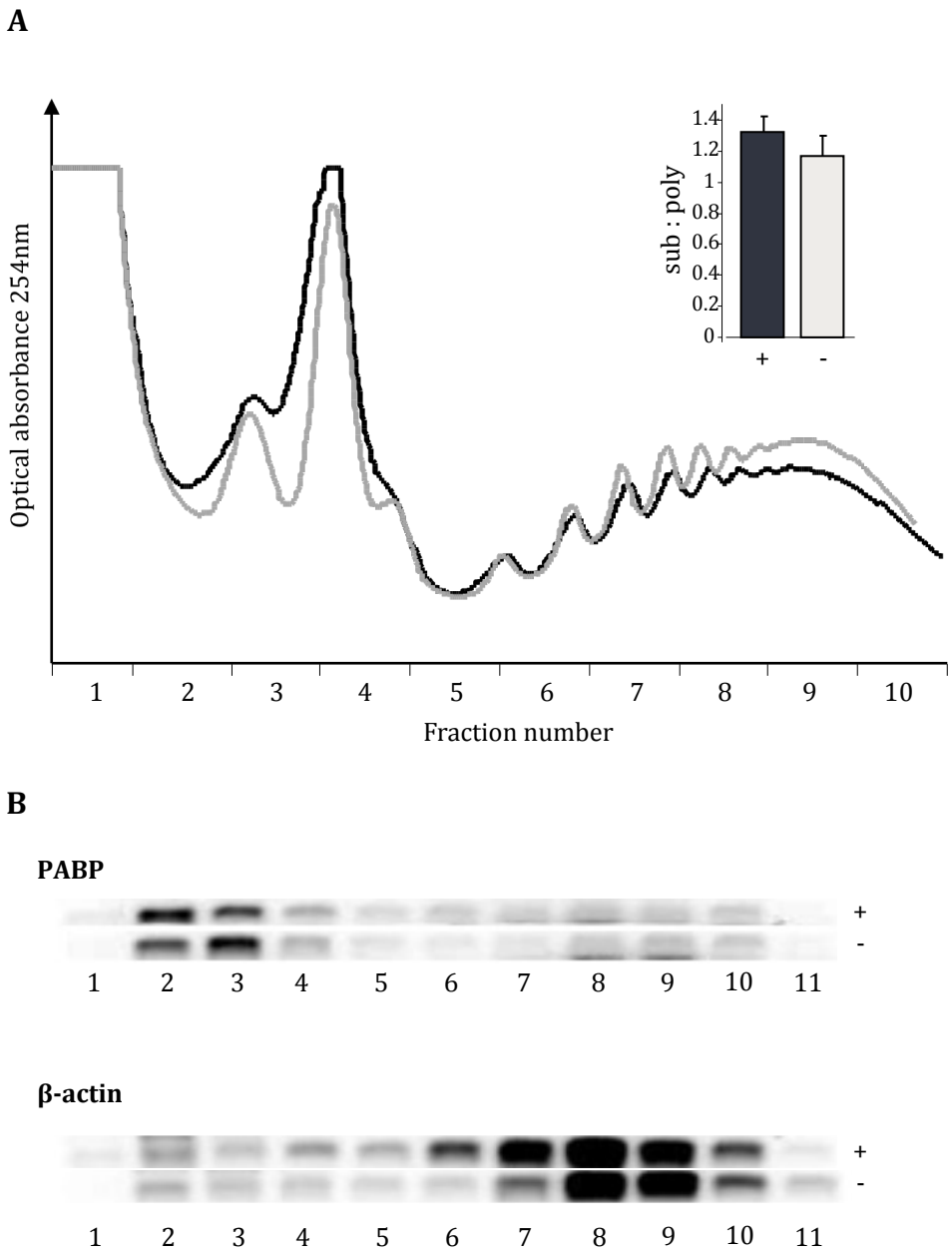

Figure 5.4 Polysome profiles of 15d-PGJ2 treated HeLa cells HeLa cells, grown to ~ 80 % confluency in 15 cm^3 plates, were treated with 100 μM 15d-PGJ_2, or the equivalent amount of DMSO for 10 minutes at 37 °C. 100 ng/ml cycloheximide was added to the medium for two minutes before the cells were lysed and applied to 10 – 50 % sucrose density gradients. Gradients were centrifuged at 38,000 rpm at 4 °C for 2 hours before being divided into 1 ml fractions be by a fractionator coupled to a UV spectrometer. The OD_{280} was read continuosly to obtain a polysome profile of the sample. **A.** Superimposed polysome profiles of 15d-PGJ_2 treatmed (black) compared to mock treated cells. Inset graph shows the relative sub:polysome ratio of each plot (+ = treated, - = untreated). **B.** Distribution of PABP and β-actin mRNAs across the polysome gradient, detected by northern blotting.

Pooled fractions were reverse transcribed and differentially labeled with fluorescent Cy dyes (sub-polysomal cDNA, Cy 5 - fluoresces red, emits at 635 nm; polysomal cDNA, Cy3 - fluoresces green, emits at 532 nm) and hybridised to oligonucleotide arrays (printed by the Post-Genomics Laboratory, University of Nottingham, UK using 30,000 gene probe pan human array, MWG Biotech, now Ocimum Biotechnologies). Equal amounts of RNA were used to synthesise the cDNA for each sample which will have the effect of enriching the polysomal fractions when the overall rate of translation is reduced (Carter *et al.*, 2000). Each array was washed in a series of high-stringency washes to reduce background and non-specific hybridisation and the dried chips scanned at a 5-10 μm resolution with a GenePix Professional 4200A Scanner using the GenepixPro software v. 6 to balance the overall fluorescence intensity of the two Cy dyes. Image files were fitted to an array grid and spot quality was manually assessed using GenepixPro v. 6. to assign a log intensity value of red and green fluorescence to each oligonucleotide spot. Four biological repeats of treated or control samples were reverse transcribed, fluorescently labelled, hybridised and scanned on the same day to reduce experimental error. Due to the method of normalisation used in these experiments which corrects for spot intensity, a dye swap was not deemed necessary (see below).

5.5 Normalisation and analysis of arrays

Array data is normalised to adjust for systematic error that is introduced because of variations in the experimental procedure or microarray technology that may bias observed differences between the samples. This involves the removal of background fluorescence from each spot intensity and normalisation within and between each array to reduce bias introduced by variations in spot intensity and location (Leung and Cavalieri, 2003). Both background subtraction and normalisation methods have been the subject of some debate as many software tools have been developed which focus on different aspects of array data (Yang *et al.*, 2002; Smyth and Speed, 2003; Ritchie *et al.*, 2007). After evaluating the available literature a background correction method termed *normexp+offset*, which adaptively adjusts the foreground intensity according to

the background intensity, was selected. This method avoids negative intensities, which can complicate downstream normalisation methods and is a more sensitive adjustment for lower intensity spots (Ritchie *et al.*, 2007). To normalise the data a print-tip loess method was employed to correct for spot intensity and spatial variation within each array and then the log intensities of each array were adjusted to allow inter-array comparison using the scale normalisation method (Yang *et al.*, 2002; Smyth and Speed, 2003). Background subtraction and normalisation was performed using the Bioconductor package *limma* in R (Smyth, 2005). The normalised list of genes was further modified by removing all genes with spot intensities lower than the background plus two standard deviations and all genes that did not appear on at least three of the four arrays for either the treatment or control. This produced a final list of 3687 genes for statistical analysis.

5.6 Statistical analysis of data

There are many statistical tests that can be applied to microarray data in order to identify differentially expressed genes, all of which generally result in different gene lists being generated (Jeffery *et al.*, 2006). Fold-change, calculated as either a ratio of, or the difference between, log-2 intensity ratios provides a reproducible means to compare the expression of particular genes between samples (Shi *et al.*, 2005; Guo *et al.*, 2006; Shi *et al.*, 2006). Small changes in expression, however, may be undermined by natural variations in steady-state expression levels and therefore go undetected using this method (Witten and Tibshirani, 2007). Another simple method of assessing differential expression is calculating the difference in position of a gene in the ranked lists of two different samples. This method has been seen to work well with small or noisy datasets and is more sensitive to small changes in gene expression (Jeffery *et al.*, 2006).

The translational profiling of HeLa cells after treatment with 15d-PGJ_2 resulted in a modest increase in the ratio of mRNAs located in the sub-polysomal fractions (0.2-fold) compared to a DMSO treated control. It is therefore

expected that, though there may be exceptions, only small differences in the intensity ratio between datasets will be observed. Due to this it was decided to analyse the data using a change in rank as the primary statistical tool and fold-change as a secondary tool to help interpret subsequent experiments. Two statistical tools were used to perform rank analysis: SAM (Statistical analysis of microarrays (Tusher *et al.*, 2001)) and RankProd (Breitling *et al.*, 2004). Both tools calculate the statistical significance that the ranked product of a gene, ranked according to its log intensity ratio, differs between sample types and display this as an estimated percentage of false positives prediction (pfp). As SAM produces an output which does not indicate the fold change, the list generated with this analysis was then supplemented with fold change ratios for each gene calculated using the empirical Bayes method in *limma* that improves the power of experiments with a small number of arrays (Smyth, 2004). Rankprod produces a list displaying both the fold change and the pfp. Each method generated a very similar list of genes, though a higher significance was generally observed using the SAM/*limma* method. The estimated percentage of false positives prediction (pfp) had to be raised to a threshold of 50 % to generate a list with a similar number of genes in RankProd in comparison to 14 % and 15 % for the positive and negative list generated by SAM. These differences may reflect a difference in the assumptions that each method uses, and the size of the experiment (Breitling *et al.*, 2004). The SAM/*limma* analysis was selected as the basis for further investigation to provide a comparison with chip data generated from polysome profiles of hippuristanol treated HeLa cells. This final list was reduced to all genes that had a calculated p value of < 0.2 and a fold change ($\log A/B = \log(A) - \log(B)$) greater than 0.5.

5.7 List validation

Genes from the positive and negative list were selected to validate the results of the SAM/*limma* statistical analysis and these are displayed in figure 5.5 and 5.6. Though a clear difference in the mean log intensity ratio between treated and untreated samples is observed (5.5, 5.6 B), corroborating the calculated fold change in the log intensity ratio calculated by *limma*, the standard deviation of

A

Name		FC	p value	pfp
STOML1	Stomatin-like protein 1	-1.329	0.052	0
VIM	Vimentin	-1.099	0.0018	8.15
CD52	CAMPATH-1 antigen Precursor	-1.009	0.0045	0
GM2A	Ganglioside GM2 activator Precursor	-1.054	0.0015	14.16
CAMK2G	Calcium/calmodulin-dependent protein kinase type II gamma	-1.030	0.0039	0
RCC2	RCC1-like protein	-1.004	0.0039	0
TRPV6	Transient receptor potential cation channel subfamily V member 6	-0.719	0.0041	0

B

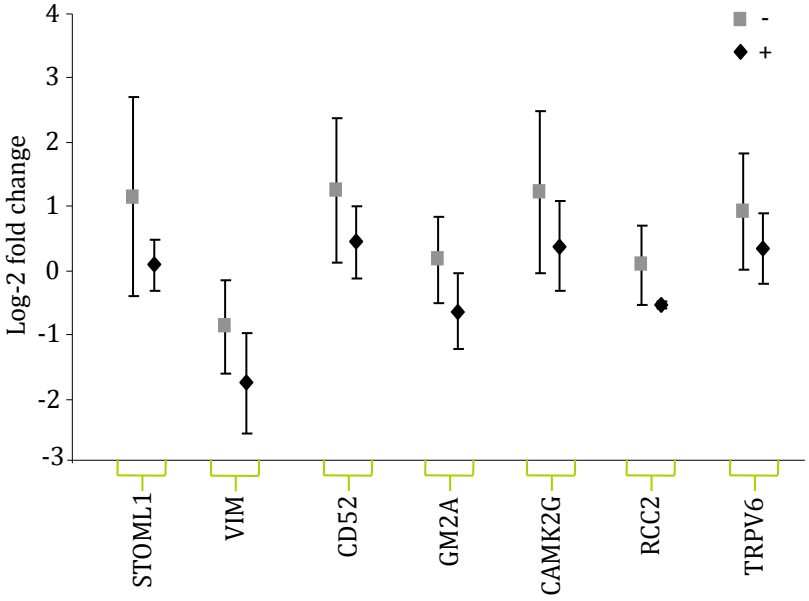

Figure 5.5 Selected mRNAs representative of the upregulated gene list. A. Statistical data obtained for selected genes using a combine SAM/ *limma* method. FC – log fold change in expression between treated and untreated samples; p-value – calculated for the statistical significance of FC (both using *limma*); pfp – percentage of false positive predictions that a change in rank is observed between the two datasets (calculated with SAM). **B.** Standard deviation in log intensity recorded for each gene spot (n = 4)

		FC	p-value	pfp
DNASE2	Deoxyribonuclease-2-alpha	2.208	0.0034	0
INPP5D	Phosphatidylinositol-3,4,5-trisphosphate 5-phosphatase 1	1.981	0.0051	15.27
BARHL1	BarH-like 1 homeobox protein	1.790	0.0027	0
KCNJ3	G protein-activated inward rectifier potassium channel 1	1.650	0.052	15.27
CASR	Extracellular calcium-sensing receptor Precursor	1.456	0.0087	0
GPX7	Glutathione peroxidase 7 Precursor	1.333	0.0072	0

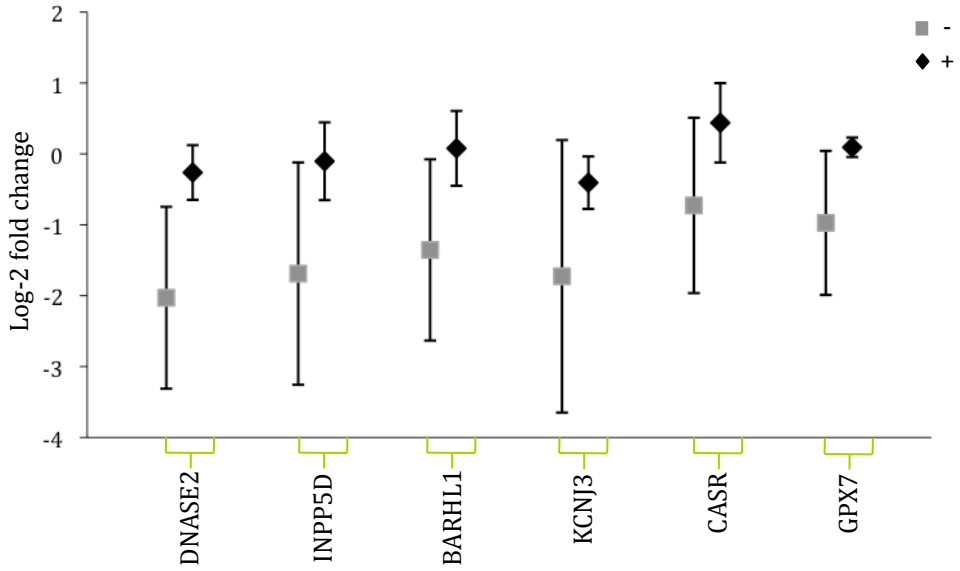

Figure 5.6 selected mRNAs representative of the downregulated gene list. A. Statistical data obtained for selected genes using a combine SAM/ *limma* method. FC – log fold change in expression between treated and untreated samples; p-value – calculated for the statistical significance of FC (both using *limma*); pfp – percentage of false positive predictions that a change in rank is observed between the two datasets (calculated with SAM). **B.** Standard deviation in log intensity recorded for each gene spot (n = 4)

the control sample demonstrates considerable variation between experimental repeats which is likely due to intensity differences between arrays that have not been removed by normalisation. This variance will contribute to a reduction in the statistical significance detected using the FC method, however the ranked change should be less affected as each array is ranked separately. The pfp calculated by SAM, which is completely based on change in rank and not fold change, indicates that the ranked position of these genes between arrays may be more similar than the variance in log ratio intensity. Detection of the mRNA distribution of each gene by northern blotting polysome profiles from treated and untreated cells will give an indication as to which method of analysis is right and whether the rest of the list should be researched further.

Of the genes selected only three were successfully probed for at the time of writing and each validates the list (figures 5.7 - 5.9). Calcium/calmodulin-dependent protein kinase type II gamma (CAM2KG) and vimentin (vim) both appeared on the positive or 'translationally maintained' list with a calculated fold change of approximately 1. The distribution of each transcript across a polysome gradient profile after treatment with 15d-PGJ_2 demonstrates that the efficiency of translation is maintained when there is an overall reduction in translation initiation (5.7 and 5.8). Deoxyribonuclease 2 (DNASE2) appears on the negative or 'translationally repressed' list with a fold change of approximately 2 calculated by *limma*. The *DNASE2* mRNA distribution across a polysome gradient profile after treatment with 15d-PGJ_2 demonstrates a reduction in the translational efficiency of this transcript (see fractions 5 and 6). As the subpolysomal and polysomal fractions were divided between fractions 5 and 6 this accounts for the identification of the DNASE2 as a differentially expressed gene in the array data. The translational profiles of each gene were verified by an additional independent repeat. The initial validation described above gives the first indication that the list may be an accurate reflection of the transcripts affected by 15d-PGJ_2 treatment, however to increase the certainty of this, additional genes will need to be verified and the relative total concentration of mRNA quantified in order to rule out transcriptional changes or increased mRNA degradation.

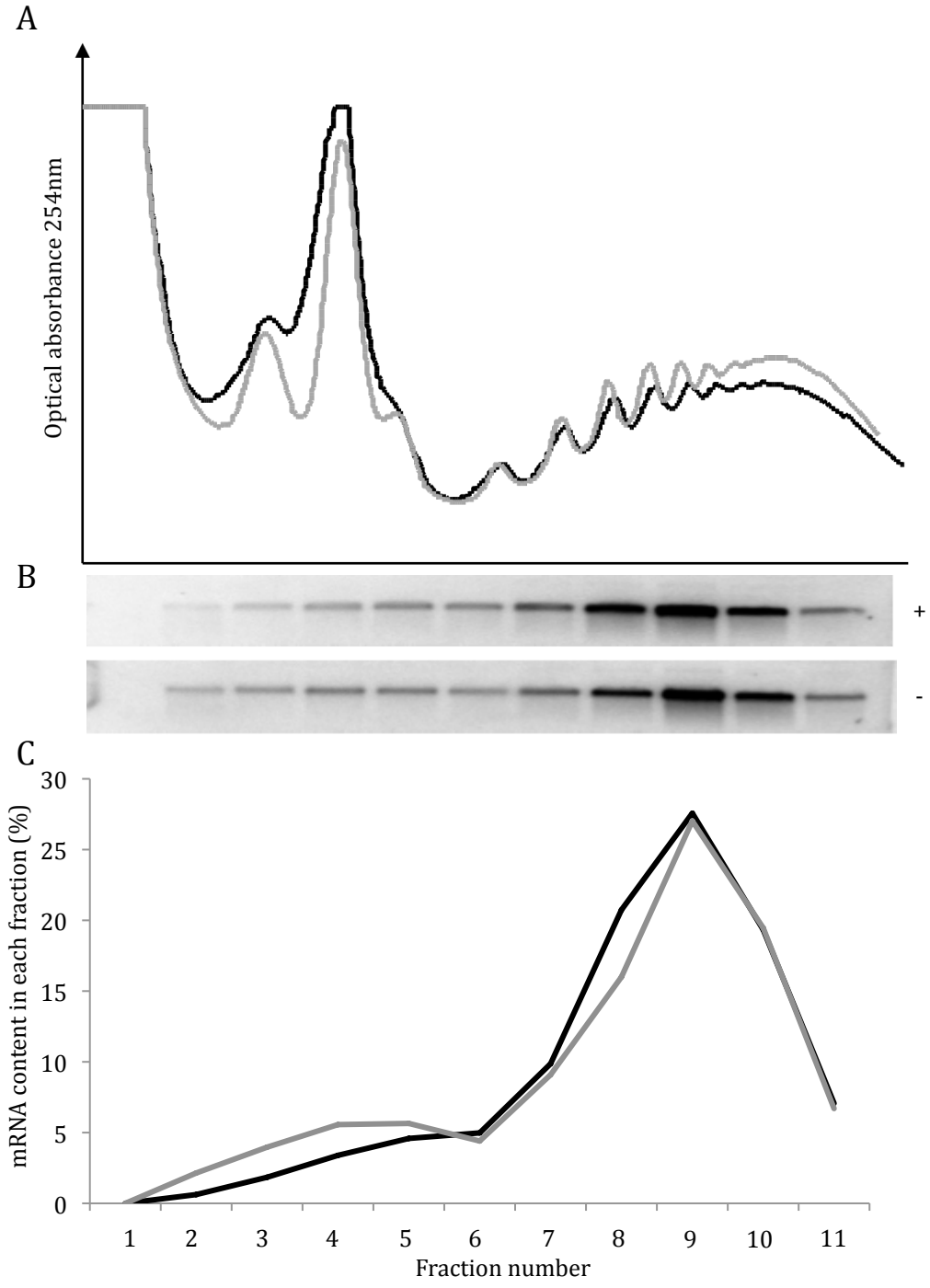

Figure 5.7 Translational maintenance of CAM2KG. A. Polysome profile of 15d-PGJ treated (+, black line) or mock treated (-, grey line) HeLa cells. **B.** The distribution of CAM2KG mRNA throughout polysome fractions as detected by northern blotting. **C.** Image quantification of northern blot performed using ImageJ and normalised to total quantity of mRNA calculated (colours as for polysome profile).

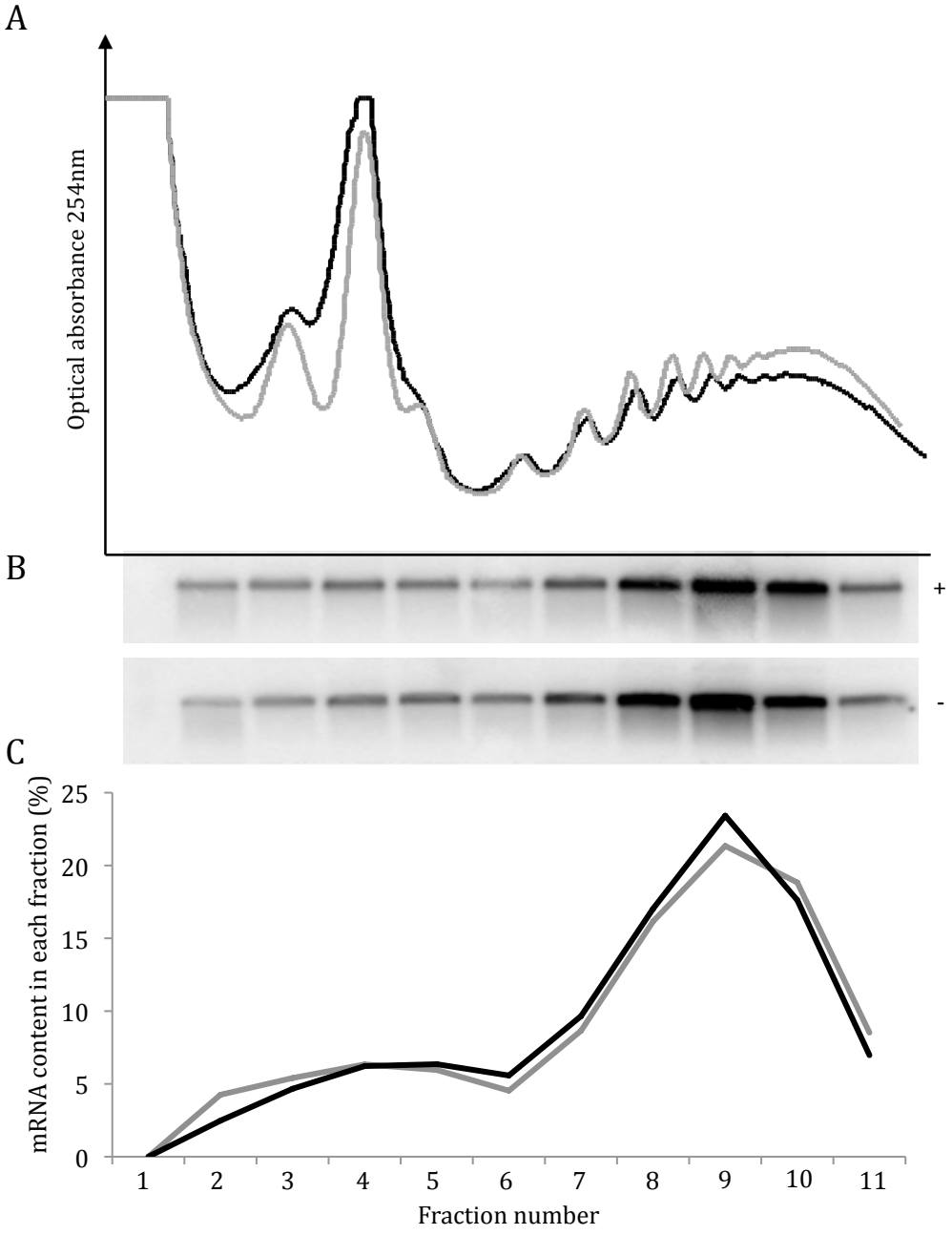

Figure 5.8 Translational maintenance of Vimentin. A. Polysome profile of 15d-PGJ treated (+, black line) or mock treated (-, grey line) HeLa cells. **B.** The distribution of Vimentin mRNA throughout polysome fractions as detected by northern blotting. **C.** Image quantification of northern blot performed using ImageJ and normalised to total quantity of mRNA calculated (colours as for polysome profile).

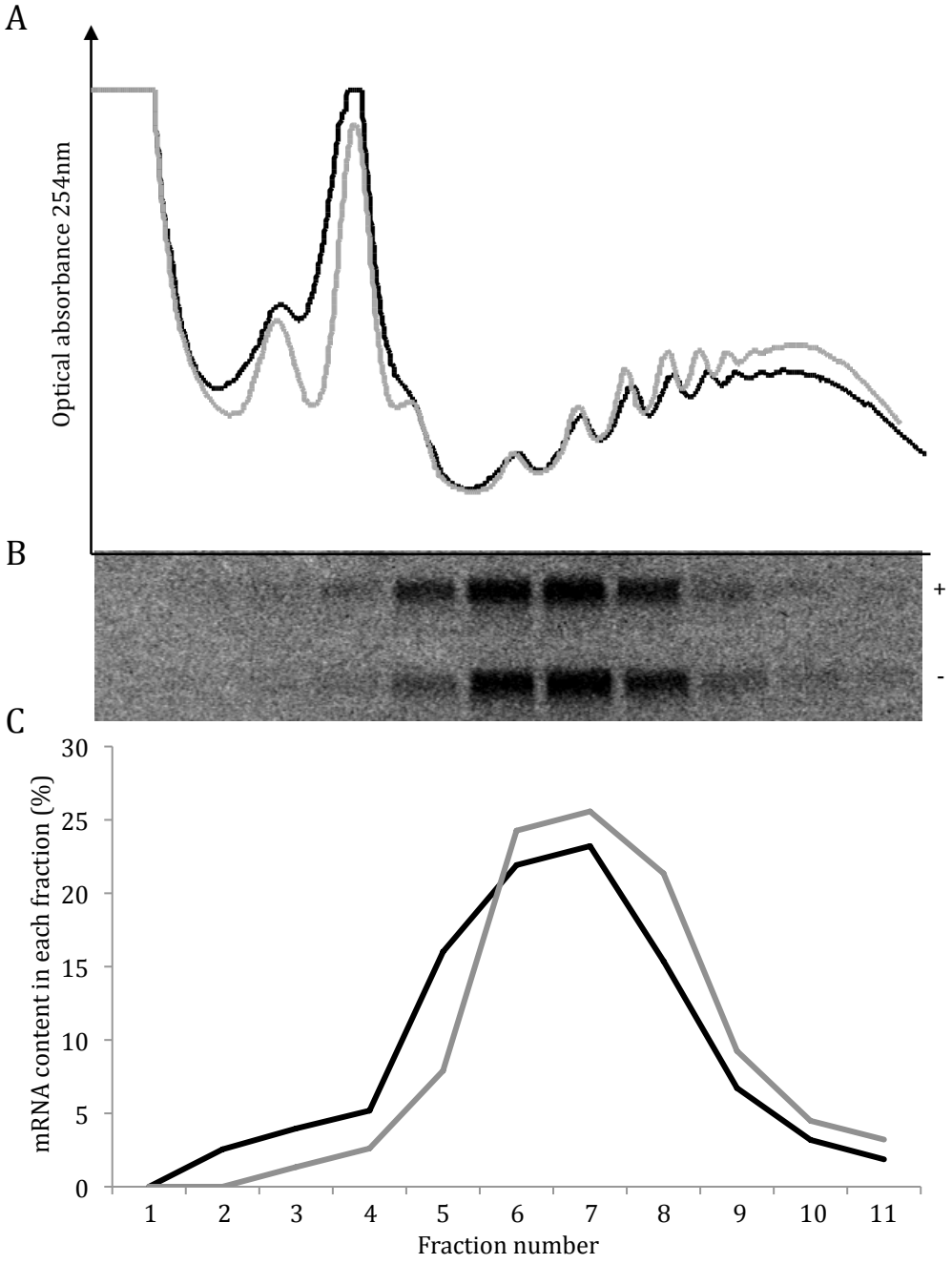

Figure 5.9 Translational repression of DNASE2. A. Polysome profile of 15d-PGJ treated (+, black line) or mock treated (-, grey line) HeLa cells. **B.** The distribution of DNASE2 mRNA throughout polysome fractions as detected by northern blotting. **C.** Image quantification of northern blot performed using ImageJ and normalised to total quantity of mRNA calculated (colours as for polysome profile).

5.8 Ontological clustering

Due to the large amount of data obtained from high-throughput screening techniques such as microarray analysis, a number of data mining software have been developed that are able to cluster genes according to a wide range of criteria. These tools allow the researcher to quickly identify expression patterns within gene lists that are unbiased by preconceptions. DAVID (Database for Annotation, Visualisation and Integrated Discovery) is a web-available program that clusters genes into a number of categories such as function, tissue expression according to the Gene-Ontology (GO) annotations ascribed to them (Dennis *et al.*, 2003). DAVID determines the statistical relevance of clustered gene associations by applying a modified version of the Fischer Exact test to calculate the enrichment of grouped genes compared to the number of genes assigned to that particular group in the human genome. Of the 210 genes entered into the database, DAVID recognised and assigned gene annotations to 202. These genes were assigned to a number of categories according to their associated GO-terms identified in the default annotation database options offered by DAVID. Though additional functions are available, initial data mining of the list generated from 15d-PGJ_2 treated HeLa cells catagorised genes according to tissue distribution and function.

5.9 Tissue distribution

Using the 'UP_TISSUE' annotation source, DAVID grouped 181 genes according to the tissue distribution of their expression. 14 tissues showed an enrichment in genes identified as being differentially expressed that was statistically significant (p. value < 0.01) (figure 5.10). Interestingly a large proportion of the genes identified through microarray analysis are expressed in brain (44.5 %, 90/202). As PGD_2, which is readily converted to the J_2 prostaglandins in the presence of plasma, is one of the most abundantly expressed prostaglandins in the brain this may signify a brain specific function of eIF4AI inhibition (Abdel-Halim *et al.*, 1977; Ogorochi *et al.*, 1984). Also of note is the calculated enrichment of genes in placental (20.3 %, 41/202) and epithelium (19.3 %,

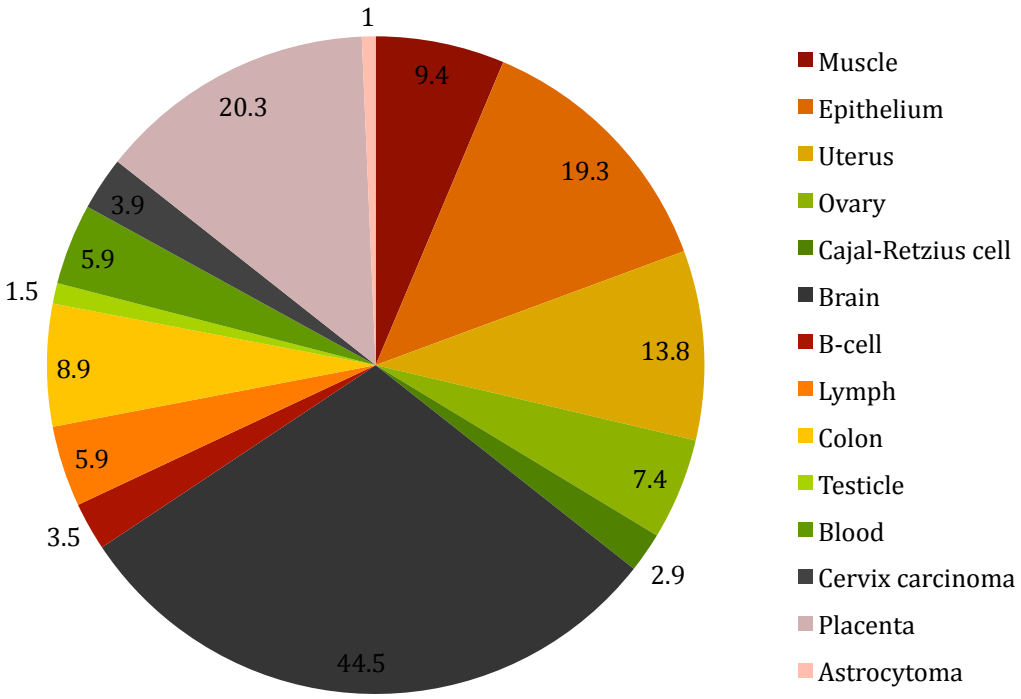

Figure 5.10 Tissue enrichment of differentially expressed genes. Ontological clustering performed using DAVID web-tool calculating tissue expression enrichment of array data. Numbers associated with each wedge represent the percentage of genes expressed in the tissue in comparison to the total number of genes in the list. All enrichment values were statistically significant (p-value < 0.01)

39/202) tissues. The innate immune response plays a major role in pregnancy and placental inflammation is associated with adverse pregnancy outcomes such as miscarriage, preeclampsia and pre-term delivery (Orsi and Tribe, 2008; Challis *et al.*, 2009). The role that prostaglandins play in this response is not well understood, however this data may indicate a specific role of 15d-PGJ_2 in the regulation of placental inflammation.

5.10 Functional group ontology

The enrichment of genes within particular functional annotation groups was also investigated with DAVID. A significant enrichment in the genes involved in ribosome biogenesis and transcription factor activity is seen (figures 5.11 and 5.12). All the ribosomal proteins identified as being differentially expressed were located in the positive list, signifying that the translation of these mRNAs is being maintained when general translation is inhibited. Many ribosomal proteins and proteins involved in translation contain 5' terminal oligopyrimidine tracts (5' TOPs) at the 5' termini which often is capped with a cytosine residue (Hamilton *et al.*, 2006). It is uncertain whether TOP containing mRNAs utilise eIF4F to initiate translation, however this data may indicate that inhibition of eIF4A by 15d-PGJ_2 does not affect the translation of some TOP containing mRNAs.

Of the 17 genes identified as being enriched in transcription five are inhibited by 15d-PGJ_2 as determined by the statistical analysis of microarray data. Of note is BarHL1, a homeodomain transcription factor that is highly conserved amongst species. BarHL1 has been identified as playing a role in neurogenesis in mice and observed mRNA expression is seen to be both tissue specific and tightly regulated (Bulfone *et al.*, 2000; Chellappa *et al.*, 2008). Transcription of BarHL1 is largely influenced by 5' and 3' promoter and enhancer sequences, however translational regulation on gene expression is unresearched. Interestingly, FoxB1 was also identified in translational profiling data obtained after the inhibition of HeLa cells with hippuristanol (A. Bottley, personal communication, 11 March 2008) . These data suggest that 15d-PGJ_2 may alter

Name	logFC	p-value	pfp	15d-PGJ2 (Av)	DMSO (Av)
prolyl-tRNA syntetase 2, mitochondrial	-0.5358	0.0568	14.161	0.0642	0.6616
RpL17	-1.0673	0.0014	0.000	-1.1060	-0.0387
prL31	-0.9104	0.0065	14.161	-0.7044	-0.1904
Rpl35a	-0.6403	0.0266	8.150	-0.4981	0.1422
Rpl36	-0.5522	0.0206	0.000	-0.7142	-0.1620
Rpl37	-0.9445	0.0053	0.000	-0.5977	0.3468
Rpl38	-0.5214	0.0529	14.161	-0.6777	-0.1563
Rps13	-0.7005	0.0238	8.150	-0.7444	-0.0439
Rps21	-0.5503	0.0281	8.150	0.1550	0.7053
Rps24	-0.7690	0.0114	0.000	-0.7566	0.0124
Rps29	-1.4635	0.0919	14.161	0.0038	1.4673
Rps3a	-0.7028	0.0121	0.000	-0.6166	0.3119
Rps6	-0.8961	0.0015	0.000	-0.4259	0.4702

Figure 5.11 Enriched genes involved in ribosome biogenesis. Ontological clustering performed using DAVID web-tool calculating enrichment of array data. FC – log fold change in expression between treated and untreated samples; p-value – calculated for the statistical significance of FC (both using *limma*); pfp – percentage of false positive predictions that a change in rank is observed between the two datasets (calculated with SAM), 15d-PGJ2 (Av) and DMSO (Av) – average FC in each dataset. Enrichment values were statistically significant (p-value < 0.0001)

	Name	logFC	p-value	pfp	15d-PGJ2 (Av)	DMSO (Av)
BARHL1	BarH-like 1 homeobox protein	1.7910	0.0028	0.000	0.0975	-1.6935
CEBPE	CCAAT/enhancer-binding protein epsilon	-0.9022	0.0014	8.150	1.1261	2.0283
FOSL1	Fos-related antigen 1	0.5194	0.0059	15.277	-0.5438	-1.0632
MGA	MAX gene-associated protein	-0.7080	0.0169	14.161	-0.1210	0.3673
NKX2-8	Homeobox protein Nkx-2.8	0.8597	0.0046	0.000	0.4854	-0.3743
NKX2-3	Homeobox protein Nkx-2.3	0.6325	0.0153	13.717	-0.5945	-1.2270
SIX2	Homeobox protein SIX2	-0.8896	0.0032	14.161	0.6135	1.5031
TBX1	T-box transcription factor TBX1	-0.5688	0.0133	8.150	-0.3056	0.2632
CREB3L1	Cyclic AMP-responsive element-binding protein 3-like protein 1	-0.6486	0.0140	14.161	0.9354	1.5839
ETV6	Transcription factor ETV6	-0.8682	0.0013	8.150	0.0209	0.8892
FOXB1	Forkhead box protein B1	1.3955	0.0134	0.000	-0.0494	-1.4449
HNF4A	Hepatocyte nuclear factor 4-alpha	-0.6446	0.0257	8.150	0.4717	1.1163
HOXA9	Homeobox protein Hox-A9	-0.7187	0.0047	0.000	-0.7000	0.0187
HOXB4	Homeobox protein Hox-B4	-0.7370	0.0481	8.150	0.0792	0.8162
NFE2L1	Nuclear factor erythroid 2-related factor 1	0.8651	0.0009	0.000	0.8202	-0.0449
RFX1	MHC class II regulatory factor RFX1	-0.8001	0.0437	8.150	-0.2437	0.5563
ZNF823	Zinc finger protein 823	-0.6122	0.0108	0.000	0.3242	0.9364

Figure 5.12 Enriched genes involved in transcription. Ontological clustering performed using DAVID web-tool calculating enrichment of array data. Data as described in figure 5.11. Enrichment values were statistically significant (p-value = 0.0074)

the transcriptional profile of the cell by mechanisms independent of PPAR-γ and NF-κB signalling.

Of the other functional categories shown to be significantly enriched in the array data, chemical homeostasis, response to wounding and apoptosis are notable due to the role 15d-PGJ_2 plays in the immune response (figures 5.13 - 5.15). Both potassium and calcium homeostasis are key features in the process of apoptosis. A number of events triggering the onset of apoptosis cause potassium efflux, resulting in cell shrinkage caused by osmotic pressure, which is thought to lead to a cascade of events that result in the activation of the caspase signaling cascade (Yu, 2003). Conversely calcium influx is thought to occur at a late stage of apoptosis to cause mitochondrial damage that also leads to the activation of caspases (Rizzuto *et al.*, 2003). Calcium sensing receptor (CaSR) is observed to be translationally repressed in HeLa cells after 15d-PGJ_2 treatment, whereas translation of potassium voltage gated channel member E1 (KCNE1) is upregulated or maintained. Both are important proteins involved in maintaining ion homeostasis in the cell and therefore 15d-PGJ_2-mediated translational regulation of expression may contribute to its influence in apoptosis (Sanguinetti *et al.*, 1996; Saidak *et al.*, 2009).

As the list is yet to be validated, ontological clustering data must be treated with caution, however, should further experimental evidence support this data then this will be a valuable addition to the understanding of gene expression modulation by 15d-PGJ_2.

5.11 Sequence analysis of differentially expressed mRNAs

Inhibition of eIF4AI activity by 15d-PGJ_2 may adversely affect translation initiation by reducing the amount of cap-binding by eIF4F, due to the inhibition of the eIF4GI and eIF4AI interaction, and by reducing the ability of the 48S pre-initiation complex (PIC) to scan the 5' UTR of the mRNA (Morino *et al.*, 2000; Pestova and Kolupaeva, 2002; Kim *et al.*, 2007). The observation that the requirement of eIF4AI in translation initiation is proportional to the amount of

	Name	logFC	p-value	pfp	15d-PGJ2 (Av)	DMSO (Av)
CD52	CAMPATH-1 antigen Precursor	-1.0094	0.0046	0.000	1.1789	2.1883
FKBP1C	Novel protein similar to FK506 binding protein 1A	1.0705	0.0189	15.277	0.2551	-0.8154
AKR1C2	Aldo-keto reductase family 1 member C2	-0.5044	0.1020	14.161	-1.0438	-0.6178
CASR	Extracellular calcium-sensing receptor Precursor	1.4564	0.0088	0.000	0.5479	-0.9085
HNF4A	Hepatocyte nuclear factor 4-alpha	-0.6446	0.0257	8.150	0.4717	1.1163
HAMP	Hepcidin Precursor	-1.6193	0.0407	14.161	1.2743	2.8936
KCNE1	Potassium voltage-gated channel subfamily E member 1	-0.5866	0.0179	14.161	1.3663	1.9529
PTGER3	Prostaglandin E2 receptor EP3 subtype	-0.6765	0.0617	14.161	-0.2669	0.4331
RPS6	40S ribosomal protein S6	-0.8961	0.0015	0.000	-0.4259	0.4702
SLC12A4	Solute carrier family 12 member 4	0.8791	0.0074	0.000	-0.1105	-0.9897
KCNJ3	G protein-activated inward rectifier potassium channel 1	1.6504	0.0522	15.277	-0.5080	-2.1584

Figure 5.13 Enriched genes involved in chemical homeostasis. Ontological clustering performed using DAVID web-tool calculating enrichment of array data. Data as described in figure 5.11. Enrichment values were statistically significant (p-value = 0.0076)

	Name	logFC	p-value	pfp	15d-PGJ2 (Av)	DMSO (Av)
GP1BB	Platelet glycoprotein Ib beta chain Precursor	1.7266	0.0066	13.717	0.0053	-1.7213
HNF4A	Hepatocyte nuclear factor 4-alpha	-0.6446	0.0257	8.150	0.4717	1.1163
HDAC5	Histone deacetylase 5	-0.5550	0.0266	8.150	-0.0539	0.5012
ITGB3	Integrin beta-3 Precursor	0.5295	0.0727	15.277	-0.1092	-0.6387
ITIH4	Inter-alpha-trypsin inhibitor heavy chain H4 Precursor	0.5427	0.0178	13.717	0.2745	-0.2682
NFE2L1	Nuclear factor erythroid 2-related factor 1	0.8651	0.0009	0.000	0.8202	-0.0449
PRDX5	Peroxiredoxin-5, mitochondrial Precursor	-0.5633	0.0219	14.161	-0.7639	-0.1973
PTGER3	Prostaglandin E2 receptor EP3 subtype	-0.6765	0.0617	14.161	-0.2669	0.4331
ERBB3	Receptor tyrosine-protein kinase erbB-3 Precursor	1.2354	0.0993	15.277	0.5030	-0.5962

Figure 5.14 Enriched genes involved in response to wounding. Ontological clustering performed using DAVID web-tool calculating enrichment of array data. Data as described in figure 5.11. Enrichment values were statistically significant (p-value = 0.17)

	Name	logFC	p-value	pfp	15d-PGJ2 (Av)	DMSO (Av)
BARHL1	BarH-like 1 homeobox protein	1.7910	0.0028	0.000	0.0975	-1.6935
FOSL1	Fos-related antigen 1	0.5194	0.0059	15.277	-0.5438	-1.0632
IHH	Indian hedgehog protein Precursor	0.9815	0.0034	0.000	0.0183	-0.9632
SIVA1	Apoptosis regulatory protein Siva	0.6584	0.0158	0.000	0.3818	-0.2766
INPP5D	Phosphatidylinositol-3,4,5-trisphosphate 5-phosphatase 1	1.9813	0.0052	15.277	-0.1295	-2.1108
NUP62	Nuclear pore glycoprotein p62	-0.6565	0.0378	14.161	0.0658	0.7222
PRDX5	Peroxiredoxin-5, mitochondrial Precursor	-0.5633	0.0219	14.161	-0.7639	-0.1973
PTGER3	Prostaglandin E2 receptor EP3 subtype	-0.6765	0.0617	14.161	-0.2669	0.4331
RPS3A	40S ribosomal protein S3a	-0.7028	0.0121	0.000	-0.6166	0.3119
RPS6	40S ribosomal protein S6	-0.8961	0.0015	0.000	-0.4259	0.4702
ERBB3	Receptor tyrosine-protein kinase erbB-3 Precursor	1.2354	0.0993	15.277	0.5030	-0.5962

Figure 5.15 Enriched genes involved in apoptosis. Ontological clustering performed using DAVID web-tool calculating enrichment of array data. Data as described in figure 5.11. Enrichment values were statistically significant (p-value = 0.3)

secondary structure contained in a messages 5' UTR may indicate that eIF4AI inhibition will affect particular subsets of mRNAs above the background level of translational inhibition. The translational microarray profiling described above provides a list of genes that are differentially regulated during a time of translational inhibition. To evaluate whether there is any trend in mRNA sequence length and nucleotide content the genes identified as being upregulated or maintained were compared with the genes identified as being downregulated. The 5' UTR, 3' UTR and coding (CD) and full length sequence data of each gene was accessed through Biomart (Durinck *et al.*, 2005) and then analysed using a linux based program that quantified the length, nucleotide and dinucleotide content of each transcript (figures 5.16 - 5.18). Figure 5.16 displays the mean sequence length of the 5' UTRs (A), the 3' UTRs (B), the CDs (C) and the full length transcripts (based on cDNA data) (D) for the genes that are upregulated/maintained, unaffected or negatively regulated respectively. Data shows that there is no difference in 5' UTR length between the differentially translated transcripts, but a decrease in 3' UTR length, coding sequence and overall transcript length in the upregulated/maintained group. This may indicate that inhibition of eIF4AI activity by 15d-PGJ_2 does not selectively inhibit transcripts with longer 5' UTRs, however, UTR length may not necessarily be an indication of secondary structure. The nucleotide and dinucleotide content, used as a rough estimate of secondary structure of the 5' UTRs, also demonstrated no difference in G:C content between the three groups (5.17 and 5. 18 A). These results imply that translation is being generally inhibited, but mRNAs with shorter coding sequences are preferentially translated. Although a short treatment time of 10 minutes was used to avoid transcriptional influences on the outcome of the experiment, it is possible that 15d-PGJ_2 is influencing other activities within the cell, which are confounding these results. It is also possible that inhibition of eIF4A with 15d-PGJ_2 influences translation in a way that has not been foreseen. Considering the many proteins and molecules that influence eIF4A activity this may represent an interesting possibility.

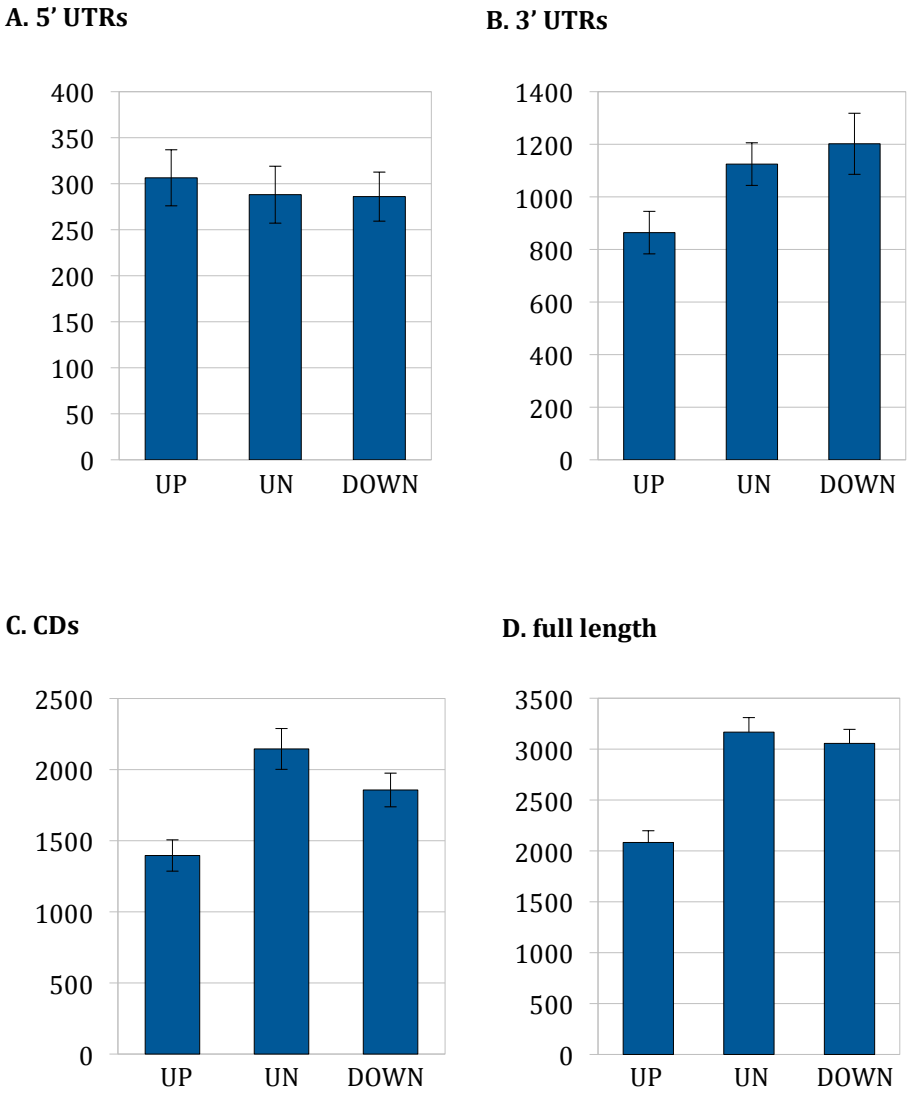

Figure 5.16 Sequence length of differentially translated transcripts. Mean sequence length of 5' UTRs (A), 3' UTRs (B), coding regions (CDs) (C) and full length transcripts (D) of upregulated or maintained genes (UP), unchanged genes (UN) or downregulated genes (DOWN).

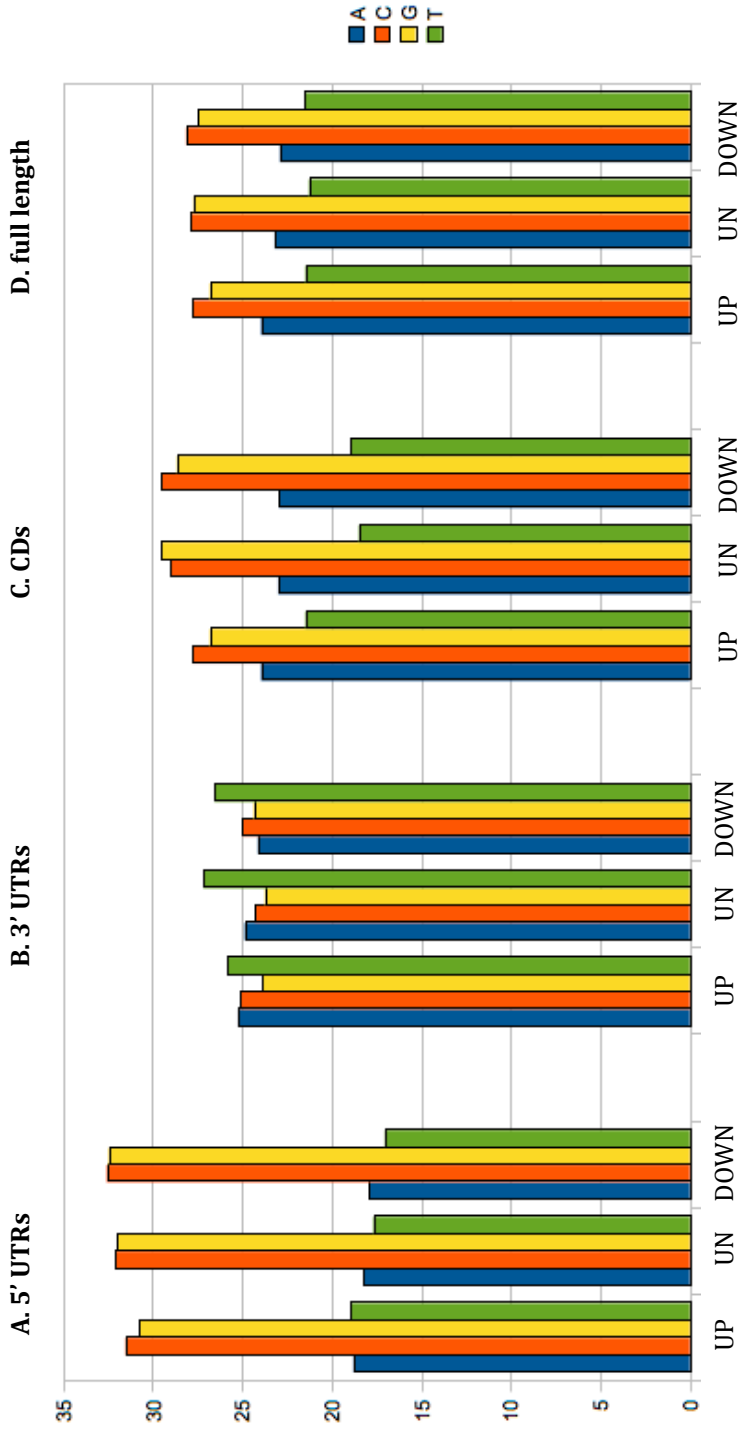

Figure 5.17 Sequence contents of differentially translated transcripts. Mean nucleotide content of 5' UTRs (A), 3' UTRs (B), coding regions (CDs) (C) and full length transcripts (D) of upregulated or maintained genes (UP), unchanged genes (UN) or downregulated genes (DOWN).

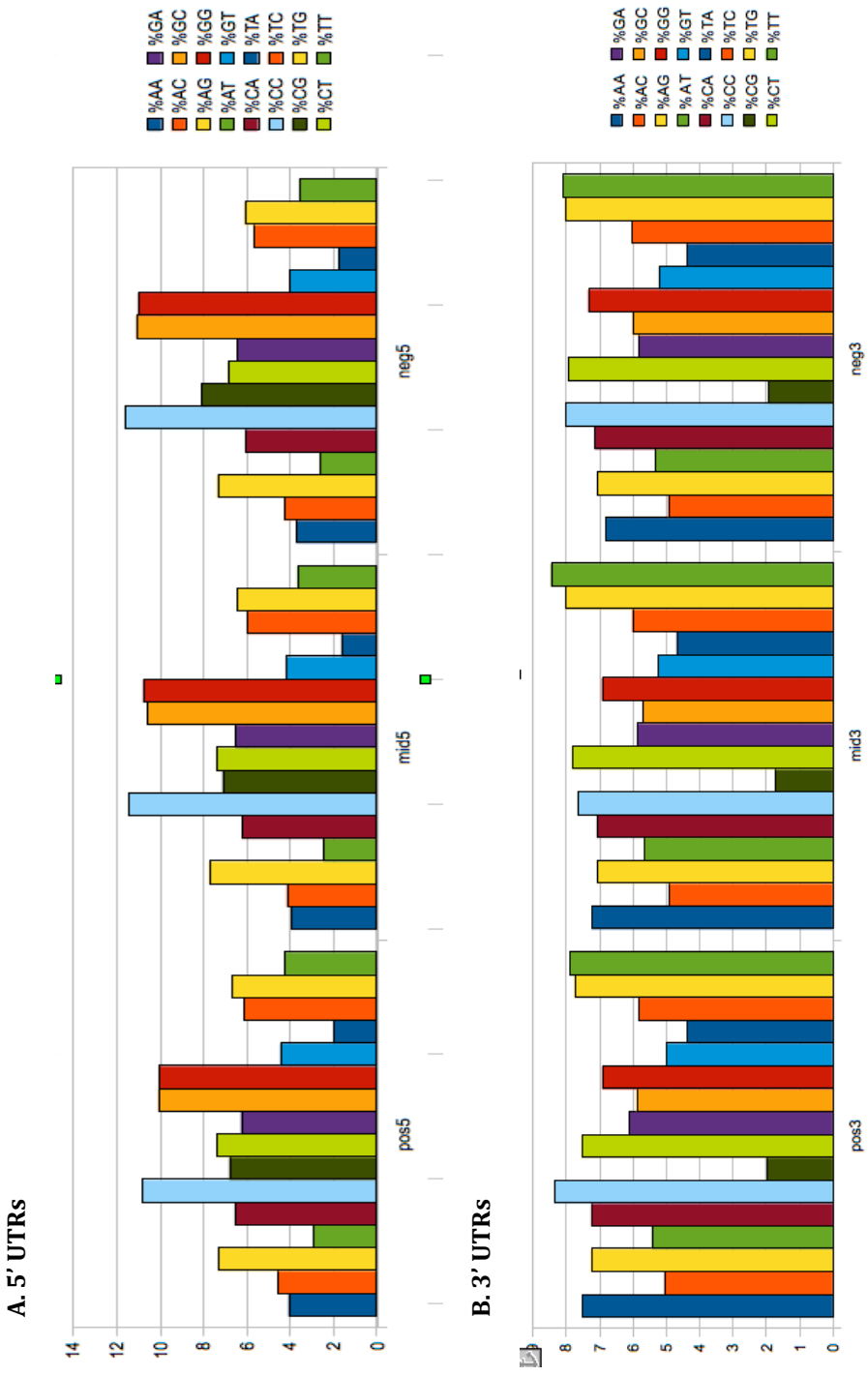

Figure 5.11 Dinucleotide contents of differentially translated transcripts. Mean dinucleotide content of 5' UTRs (A) and 3' UTRs (B) of upregulated or maintained genes (UP), unchanged genes (UN) or downregulated genes (DOWN).

5.12 Discussion

Data presented in this chapter demonstrate the translational profiling of HeLa cells treated with 15d-PGJ_2, a cyclopentenone prostaglandin that has been implicated in many cellular pathways in the control of inflammation resolution and apoptosis. One of the cellular targets of 15d-PGJ_2 is eIF4AI, which it inhibits by preventing the association between eIF4AI and eIF4GI and, as demonstrated in chapter 3 with an *in vitro* helicase assay, by inhibiting helicase activity directly. Differential translation of mRNAs was detected using cDNA microarray profiling to compare subpolysomally and polysomally associated mRNAs. Statistical analysis calculating both the change in rank and the fold change in expression was performed using two separate methods which generated very similar datasets. Initial validation of the lists of positively and negatively regulated genes was performed using northern blot analysis and indicates that the statistical analysis is correct, however more confidence will be associated with the generated data once more mRNAs have been verified. The data mining tool, DAVID, was used to cluster identified transcripts according to tissue expression and functional annotation. This revealed an interesting enrichment of transcripts expressed in the brain, the implications of which will be discussed in more detail below. Functional clustering identified that transcripts were enriched the following groups: ribosome biogenesis, transcription, chemical homeostasis, wound healing and apoptosis. When the array list is validated fully these data may help to understand the role that eIF4A inhibition plays in the cellular modifications caused by 15d-PGJ_2. A comparison of the mean sequence length and nucleotide content of the 5' UTRs, 3' UTRs and coding regions of the mRNAs indicated that the original hypothesis that inhibition of eIF4AI activity would adversely affect the translation of mRNAs with more structured 5' UTRs was not correct for inhibition with 15d-PGJ_2. These results may indicate an alternative mechanism by which eIF4AI inhibition affects protein synthesis; that the involvement of 15d-PGJ_2 in other cellular pathways is influencing our data; or that the results demonstrate a general inhibition of protein synthesis where translation of shorter transcripts is stimulated.

6 Discussion

The aims of this thesis were to investigate eIF4AI helicase activity using a cross-discipline approach to obtain information regarding both the mechanics of helicase activity and the biological impacts of its inhibition. 15d-PGJ_2, a recently identified inhibitor of eIF4A activity, was used in these investigations in order to further clarify its cellular role, mediated through eIF4A inhibition, in inflammation and apoptosis (Kim *et al.*, 2007). Three different types of experiments were performed; the characterisation of recombinant eIF4AI protein and 15d-PGJ_2 using well published ensemble methods; the development of single molecule experiments to investigate helicase activity at a higher resolution and translational microarray profiling to analyse the mRNAs affected by 15d-PGJ_2 inhibition of eIF4AI.

6.1 Recombinant eIF4AI demonstrates helicase activity i*n vitro*

In order to investigate eIF4AI activity, and the stimulatory and inhibitory effects of eIF4B and 15d-PGJ_2 *in vitro*, human recombinant proteins were cloned and expressed in bacterial overexpression systems and investigated in bulk helicase assays as described in (Rogers *et al.*, 1999). Recombinant eIF4AI was able to successfully displace the strands of a radiolabeled duplex RNA molecule with a predicted Gibbs free energy of -17.9 ΔG, however at a rate lower than that previously reported (Rogers *et al.*, 1999). This activity was stimulated 2-fold by the addition of 0.5 molar concentration of recombinant eIF4B, which agreed well with the stimulation recorded in the literature, however an increase in eIF4B to equimolar ratios with eIF4AI did not increase the efficiency of helicase activity further (Rogers *et al.*, 2001b). The difference between these results to the published literature may be due to a number of factors: Rogers and coworkers used eIF4A and eIF4B purified from rabbit reticulocyte lysate (RRL) that may differ in post-translational modification to bacterially expressed recombinant eIF4AI. Indeed post-translational modification of eIF4B is known to alter its binding activity with eIF3 (Raught *et al.*, 2004; Holz *et al.*, 2005; Shahbazian *et al.*, 2006; Kroczynska *et al.*, 2009). Attempts were made to express and purify recombinant eIF4B using a *Drosophila* expression system,

however, although the successful expression of phospho (Ser422) eIF4B was observed by western blotting, purification using nickel affinity chromatography followed by heparin affinity chromatography was unsuccessful. An additional purification step using ion-exchange chromatography to concentrate the protein sample before nickel-affinity chromatography may be beneficial for future purification procedures or the further optimisation of the initial transfection protocol to increase the expression of recombinant protein.

15d-PGJ_2 was identified as an inhibitor of translation initiation through the specific targeting of eIF4AI, preventing its association with eIF4GI and the formation of the cap-binding complex, eIF4F (Kim *et al.*, 2007). In addition to this data, experiments reported in chapter 3 indicate that 15d-PGJ_2 is additionally able to inhibit recombinant eIF4AI helicase activity *in vitro*. Unfortunately comparisons with the inhibition caused by hippuristanol, a well-characterised specific inhibitor of eIF4A activity not possible due to this inhibitor displaying no inhibitory effect in these assays. This is most probably due to a reduced activity of hippuristanol caused by prolonged storage. In addition to these experiments it would be interesting to assess whether 15d-PGJ_2 affected the RNA binding activity of eIF4AI, as other described inhibitors of eIF4A have shown differential modulation of this activity. This may help to gain a better understanding of the mechanism by which 15d-PGJ_2 is able to influence translation initiation.

6.2 Single molecule investigations of eIF4AI

Investigating helicases using ensemble methods can allow a researcher to investigate the basic factors contributing to activity such as substrate specificity, nucleotide specificity and directionality however the heterogeneity of the protein population is lost with these techniques. Single molecule experiments, however, can afford a detailed insight into the dynamic behaviour of a protein, therefore a single molecule technique, based on a protocol developed by the Bustamante group to investigate the hepatitis C viral (HCV) helicase NS3 (Dumont *et al.*, 2006). The manufacture of a dual labeled DNA:RNA hybrid

construct that contained a 60 bp stem-loop hairpin encoded in the 5' UTR of ornithine decarboxylase (ODC) was optimised and then investigated with a series of single molecule techniques. AFM imaging was used to observe the homogeneity and contour length of hybridised molecules. AFM was also used as a tool to measure the force-extension relationship of molecules. Initial experiments were performed with dsDNA to optimise the technique and these experiments were used to explore the structural integrity of dsDNA as it is overstretched using single stranded binding (SSB) protein. These data were used to confirm the experiments performed by W. Zhang and A. Orta which investigated the activity of *Bacillus subtilis* primosome protein DnaD (Zhang *et al.*, 2008). Attempts to adapt this method to investigate the ODC hp construct were unsuccessful and this was thought to be due to a low yield of functionalised product.

A second method using laser optical tweezers to investigate the force extension behaviour of the ODC hp construct was employed. Unfortunately the instrumentation developed at The University of Nottingham by A. Orta failed before the ODC hp construct could be investigated, however a commercial system developed at JPK (Berlin, Germany) became available towards the end of this project. Though time was limited, initial experiments performed with JPK's *Nanotracker* enabled the initial optimisation of force experiments with the ODC hp construct. A number of reproducible force curves that displayed unwinding and refolding events were obtained with this instrumentation, though subsequent analysis identified that the change in distance that occurred at each unwinding/refolding event was too large to be attributed to hairpin unzipping. Future experiments should use a control construct that omits the ODC hp so that the force extension behaviour of the DNA:RNA hybrid arms is calculated. Time limitations caused by initial instrument failures prevented these experiments from being optimised fully, however the data suggest that specific binding of the construct is being observed and therefore further optimisation of the bead:construct ratio should eventually allow the successful investigation of eIF4AI helicase activity.

6.3 Translational profiling of HeLa cells after treatment with 15d-PGJ_2

Translational profiling using cDNA microarrays can be used to compare the translational efficiency of mRNAs between different samples. Dividing mRNAs according to their sub-polysomal or polysomal location, assigned by the examination of the polysome profile of mRNAs fractionated through a sucrose density gradient, can be used as a measure of translational activity. Purified mRNAs from these 'pools' are used as templates to create differentially fluorescently labeled cDNA that are hybridised to cDNA microarrays. These experiments were performed after 15d-PGJ_2 treatment of HeLa cells for 10 minutes. Differentially expressed genes were identified using statistical software to assign a confidence value for each gene change detected. Initial validation analysis of transcript distribution across polysome gradient profiles by northern blotting has corroborated the list, however a larger number of genes must be validated before confident inferences can be drawn from the data.

Associations have been drawn between the amount of secondary structure contained in the 5' UTR of an mRNA and the requirement of eIF4AI helicase activity for its successful translation (Svitkin *et al.*, 2001). It has therefore been suggested that the regulation of translation through the inhibition of eIF4AI may result in a subset of mRNAs with long and highly structured 5' UTRs being preferentially inhibited. As highly regulated genes, such as oncogenes and transcription factors, as a rule contain longer and more structured 5' UTRs it is thought that eIF4AI inhibition may provide a potential opportunity for the development of therapeutics (Kozak, 1987; Davuluri *et al.*, 2000). Sequence data of each transcript identified as being upregulated, downregulated or as uninfluenced by 15d-PGJ_2 treatment of HeLa cells were compared to identify any differences that existed between the length and nucleotide contents of sequences. These data indicated that there was no relationship between 5' UTR length and the mRNAs that were adversely affected by 15d-PGJ_2 treatment. This may therefore indicate that either global translation is being inhibited and there is no defining features in the 5' UTRs that cause an mRNA to be particularly susceptible to translational inhibition caused by 15d-PGJ_2. Alternatively it could

mean that 15d-PGJ_2 inhibition of translation mediated through the inhibition of eIF4AI proceeds via an as yet undefined mechanism.

Ontological clustering of data revealed some interesting enrichment in the various functional groups, some of which are known to be regulated by 15d-PGJ_2 expression during inflammation. Perhaps most interestingly was the observation that a high proportion of transcripts were identified as being expressed in the brain. Both eIF4AI and 15d-PGJ_2 have been shown to be differentially regulated in the brain. eIF4AI is the target of specific inhibition by the non-coding RNA BC1 (Lin *et al.*, 2008), and recent data produced in this laboratory has identified that inhibition of eIF4A activity can downregulate the translation of the Alzheimer's related genes amyloid precursor protein (APP) and microtubule associated protein (MAP) tau (Bottley *et al.* in press). As mentioned previously the expression of PGD_2, which is readily converted to 15d-PGJ_2 in the presence of serum, is highly expressed in brain tissue and activated glial cells (Abdel-Halim *et al.*, 1977; Ogorochi *et al.*, 1984; Minghetti and Levi, 1995). Due to three avenues of eIF4AI inhibition all being linked to processes in the brain, it may be that eIF4AI regulated activity may be important in this tissue. An interesting addition to the microarray data described here, would be to perform these experiments in activated macrophage or glial cells to identify whether 15d-PGJ_2 regulation of eIF4AI activity produces a different set of mRNAs under these conditions.

7 References

Abdel-Halim, M., Hamberg, M., Sjöquist, B., and Anggård, E. (1977). Identification of prostaglandin D2 as a major prostaglandin in homogenates of rat brain. Prostaglandins *14*, 633-643.

Abdelhaleem, M. (2005). RNA helicases: regulators of differentiation. Clin Biochem *38*, 499-503.

Abdelhaleem, M., Maltais, L., and Wain, H. (2003). The human DDX and DHX gene families of putative RNA helicases. Genomics *81*, 618-622.

Abramson, R., Dever, T., and Merrick, W. (1988). Biochemical evidence supporting a mechanism for cap-independent and internal initiation of eukaryotic mRNA. J Biol Chem *263*, 6016-6019.

Acker, M.G., Shin, B.S., Dever, T.E., and Lorsch, J.R. (2006). Interaction between eukaryotic initiation factors 1A and 5B is required for efficient ribosomal subunit joining. Journal of Biological Chemistry *281*, 8469-8475.

Acker, M.G., Shin, B.S., Nanda, J.S., Saini, A.K., Dever, T.E., and Lorsch, J.R. (2009). Kinetic Analysis of Late Steps of Eukaryotic Translation Initiation. Journal of Molecular Biology *385*, 491-506.

Agrawal, R.K., Sharma, M.R., Kiel, M.C., Hirokawa, G., Booth, T.M., Spahn, C.M.T., Grassucci, R.A., Kaji, A., and Frank, J. (2004). Visualization of ribosome-recycling factor on the Escherichia coli 70S ribosome: Functional implications. Proceedings of the National Academy of Sciences of the United States of America *101*, 8900-8905.

Algire, M.A., Maag, D., and Lorsch, J.R. (2005). P-i release from eIF2, not GTP hydrolysis, is the step controlled by start-site selection during eukaryotic translation initiation. Molecular Cell *20*, 251-262.

Ali, I.K., McKendrick, L., Morley, S.J., and Jackson, R.J. (2001). Truncated initiation factor eIF4G lacking an eIF4E binding site can support capped mRNA translation. Embo Journal *20*, 4233-4242.

Altmann, M., Blum, S., Pelletier, J., Sonenberg, N., Wilson, T.M.A., and Trachsel, H. (1990a). Translation initiation factor-dependent extracts from saccharomyces cerevisiae. Biochimica Et Biophysica Acta *1050*, 155-159.

Altmann, M., Blum, S., Wilson, T.M.A., and Trachsel, H. (1990b). The 5' leader sequence of tobacco mosaic virus RNA mediates eIF4E independent, but still eIF4A dependent translation in yeast extracts. Gene *91*, 127-129.

Altmann, M., Müller, P., Wittmer, B., Ruchti, F., Lanker, S., and Trachsel, H. (1993). A Saccharomyces cerevisiae homologue of mammalian translation initiation factor 4B contributes to RNA helicase activity. EMBO J *12*, 3997-4003.

Altmann, M., Wittmer, B., Méthot, N., Sonenberg, N., and Trachsel, H. (1995). The Saccharomyces cerevisiae translation initiation factor Tif3 and its mammalian homologue, eIF-4B, have RNA annealing activity. EMBO J *14*, 3820-3827.

Andersen, C.B., Ballut, L., Johansen, J.S., Chamieh, H., Nielsen, K.H., Oliveira, C.L., Pedersen, J.S., Seraphin, B., Le Hir, H., and Andersen, G.R. (2006). Structure of the exon junction core complex with a trapped DEAD-box ATPase bound to RNA. Science *313*, 1968-1972.

Anderson, P. (2010). Post-transcriptional regulons coordinate the initiation and resolution of inflammation. Nat Rev Immunol *10*, 24-35.

Anderson, P., and Kedersha, N. (2006). RNA granules. J Cell Biol *172*, 803-808.

Anderson, P., and Kedersha, N. (2008). Stress granules: the Tao of RNA triage. Trends Biochem Sci *33*, 141-150.

Arif, A., Jia, J., Mukhopadhyay, R., Willard, B., Kinter, M., and Fox, P. (2009). Two-site phosphorylation of EPRS coordinates multimodal regulation of noncanonical translational control activity. Mol Cell *35*, 164-180.

Asano, K., Clayton, J., Shalev, A., and Hinnebusch, A.G. (2000). A multifactor complex of eukaryotic initiation factors, eIF1, eIF2, eIF3, eIF5, and initiator tRNA(Met) is an important translation initiation intermediate in vivo. Genes & Development *14*, 2534-2546.

Ashkin, A. (1970). Acceleration and trapping of particles by radiation pressure. Physical Review Letters *24*, 156-&.

Ashkin, A., Dziedzic, J.M., Bjorkholm, J.E., and Chu, S. (1986). Observation of a single-beam gradient force optical trap for dielectric particles. Optics Letters *11*, 288-290.

Bakheet, T., Williams, B., and Khabar, K. (2006). ARED 3.0: the large and diverse AU-rich transcriptome. Nucleic Acids Res *34*, D111-114.

Baltimore, D., Boldin, M., O'Connell, R., Rao, D., and Taganov, K. (2008). MicroRNAs: new regulators of immune cell development and function. Nat Immunol *9*, 839-845.

Banroques, J., Cordin, O., Doere, M., Linder, P., and Tanner, N.K. (2008). A conserved phenylalanine of motif IV in superfamily 2 helicases is required for cooperative, ATP-dependent binding of RNA substrates in DEAD-box proteins. Mol Cell Biol *28*, 3359-3371.

Battiste, J.L., Pestova, T.V., Hellen, C.U., and Wagner, G. (2000). The eIF1A solution structure reveals a large RNA-binding surface important for scanning function. Mol Cell *5*, 109-119.

Bauer, C., Brass, N., Diesinger, I., Kayser, K., Grässer, F., and Meese, E. (2002). Overexpression of the eukaryotic translation initiation factor 4G (eIF4G-1) in squamous cell lung carcinoma. Int J Cancer *98*, 181-185.

Bellsolell, L., Cho-Park, P.F., Poulin, F., Sonenberg, N., and Burley, S.K. (2006). Two structurally atypical HEAT domains in the C-terminal portion of human eIF4G support binding to eIF4A and Mnk1. Structure *14*, 913-923.

Benne, R., and Hershey, J. (1978). The mechanism of action of protein synthesis initiation factors from rabbit reticulocytes. J Biol Chem *253*, 3078-3087.

Benne, R., Luedi, M., and Hershey, J.W. (1977). Purification and characterization of initiation factors IF-E4 and IF-E6 from rabbit reticulocytes. J Biol Chem *252*, 5798-5803.

Benne, R., Wong, C., Luedi, M., and Hershey, J.W.B. (1976). Purification and characterisation of initiation factor IF-2 from rabbit reticulocytes. Journal of Biological Chemistry *251*, 7675-7681.

Bentley, D.L. (2005). Rules of engagement: co-transcriptional recruitment of pre-mRNA processing factors. Current Opinion in Cell Biology *17*, 251-256.

Beretta, L., Gingras, A.C., Svitkin, Y.V., Hall, M.N., and Sonenberg, N. (1996). Rapamycin blocks the phosphorylation of 4E-BP1 and inhibits cap-dependent initiation of translation. Embo Journal *15*, 658-664.

Berg-Sorensen, K., and Flyvbjerg, H. (2004). Power spectrum analysis for optical tweezers. Review of Scientific Instruments *75*, 594-612.

Berthelot, K., Muldoon, M., Rajkowitsch, L., Hughes, J., and McCarthy, J.E.G. (2004). Dynamics and processivity of 40S ribosome scanning on mRNA in yeast. Molecular Microbiology *51*, 987-1001.

Bianchini, A., Loiarro, M., Bielli, P., Busa, R., Paronetto, M.P., Loreni, F., Geremia, R., and Sette, C. (2008). Phosphorylation of eIF4E by MNKs supports protein synthesis, cell cycle progression and proliferation in prostate cancer cells. Carcinogenesis *29*, 2279-2288.

Bianco, P., Brewer, L., Corzett, M., Balhorn, R., Yeh, Y., Kowalczykowski, S., and Baskin, R. (2001). Processive translocation and DNA unwinding by individual RecBCD enzyme molecules. Nature *409*, 374-378.

Binnig, G., Quate, C., and Gerber, C. (1986). Atomic force microscope. Phys Rev Lett *56*, 930-933.

Bjornson, K.P., Moore, K.J., and Lohman, T.M. (1996). Kinetic mechanism of DNA binding and DNA-induced dimerization of the Escherichia coli Rep helicase. Biochemistry *35*, 2268-2282.

Blum, S., Mueller, M., Schmid, S.R., Linder, P., and Trachsel, H. (1989). Translation in Saccharomyces cerevisiae: initiation factor 4A-dependent cell-free system. Proc Natl Acad Sci U S A *86*, 6043-6046.

Blum, S., Schmid, S.R., Pause, A., Buser, P., Linder, P., Sonenberg, N., and Trachsel, H. (1992). ATP hydrolysis by initiation factor 4A is required for translation initiation in Saccharomyces cerevisiae. Proc Natl Acad Sci U S A *89*, 7664-7668.

Bono, F., Ebert, J., Lorentzen, E., and Conti, E. (2006). The crystal structure of the exon junction complex reveals how it maintains a stable grip on mRNA. Cell *126*, 713-725.

Bordeleau, M., Robert, F., Gerard, B., Lindqvist, L., Chen, S., Wendel, H., Brem, B., Greger, H., Lowe, S., Porco, J.J., and Pelletier, J. (2008). Therapeutic suppression of translation initiation modulates chemosensitivity in a mouse lymphoma model. J Clin Invest *118*, 2651-2660.

Bordeleau, M.E., Cencic, R., Lindqvist, L., Oberer, M., Northcote, P., Wagner, G., and Pelletier, J. (2006a). RNA-mediated sequestration of the RNA helicase eIF4A by Pateamine A inhibits translation initiation. Chem Biol *13*, 1287-1295.

Bordeleau, M.E., Matthews, J., Wojnar, J.M., Lindqvist, L., Novac, O., Jankowsky, E., Sonenberg, N., Northcote, P., Teesdale-Spittle, P., and Pelletier, J. (2005). Stimulation of mammalian translation initiation factor eIF4A activity by a small molecule inhibitor of eukaryotic translation. Proc Natl Acad Sci U S A *102*, 10460-10465.

Bordeleau, M.E., Mori, A., Oberer, M., Lindqvist, L., Chard, L.S., Higa, T., Belsham, G.J., Wagner, G., Tanaka, J., and Pelletier, J. (2006b). Functional characterization of IRESes by an inhibitor of the RNA helicase eIF4A. Nat Chem Biol *2*, 213-220.

Breitling, R., Armengaud, P., Amtmann, A., and Herzyk, P. (2004). Rank products: a simple, yet powerful, new method to detect differentially regulated genes in replicated microarray experiments. FEBS Lett *573*, 83-92.

Bruand, C., Ehrlich, S., and Jannière, L. (1995). Primosome assembly site in Bacillus subtilis. EMBO J *14*, 2642-2650.

Bruand, C., Farache, M., McGovern, S., Ehrlich, S., and Polard, P. (2001). DnaB, DnaD and DnaI proteins are components of the Bacillus subtilis replication restart primosome. Mol Microbiol *42*, 245-255.

Bulfone, A., Menguzzato, E., Broccoli, V., Marchitiello, A., Gattuso, C., Mariani, M., Consalez, G., Martinez, S., Ballabio, A., and Banfi, S. (2000). Barhl1, a gene belonging to a new subfamily of mammalian homeobox genes, is expressed in migrating neurons of the CNS. Hum Mol Genet *9*, 1443-1452.

Bushell, M., Poncet, D., Marissen, W., Flotow, H., Lloyd, R., Clemens, M., and Morley, S. (2000). Cleavage of polypeptide chain initiation factor eIF4GI during apoptosis in lymphoma cells: characterisation of an internal fragment generated by caspase-3-mediated cleavage. Cell Death Differ *7*, 628-636.

Bushell, M., Stoneley, M., Kong, Y., Hamilton, T., Spriggs, K., Dobbyn, H., Qin, X., Sarnow, P., and Willis, A. (2006). Polypyrimidine tract binding protein regulates IRES-mediated gene expression during apoptosis. Mol Cell *23*, 401-412.

Bushell, M., Wood, W., Carpenter, G., Pain, V., Morley, S., and Clemens, M. (2001). Disruption of the interaction of mammalian protein synthesis eukaryotic initiation factor 4B with the poly(A)-binding protein by caspase- and viral protease-mediated cleavages. J Biol Chem *276*, 23922-23928.

Butt, H.J., and Jaschke, M. (1995). Calculation of thermal noise in atomic force microscopy. Nanotechnology *6*, 1-7.

Böhm, M., Sawicka, K., Siebrasse, J., Brehmer-Fastnacht, A., Peters, R., and Klempnauer, K. (2003). The transformation suppressor protein Pdcd4 shuttles between nucleus and cytoplasm and binds RNA. Oncogene *22*, 4905-4910.

Capecchi, M.R., and Klein, H.A. (1970). Characterisation of three proteins involved in poly peptide chain termination.

Carballo, E., Lai, W., and Blackshear, P. (1998). Feedback inhibition of macrophage tumor necrosis factor-alpha production by tristetraprolin. Science *281*, 1001-1005.

Caron, S., Charon, M., Cramer, E., Sonenberg, N., and Dusanter-Fourt, I. (2004). Selective modification of eukaryotic initiation factor 4F (eIF4F) at the onset of cell differentiation: Recruitment of eIF4GII and long-lasting phosphorylation of eIF4E. Molecular and Cellular Biology *24*, 4920-4928.

Carter, A.P., Clemons, W.M., Brodersen, D.E., Morgan-Warren, R.J., Hartsch, T., Wimberly, B.T., and Ramakrishnan, V. (2001). Crystal structure of an initiation factor bound to the 30S ribosomal subunit. Science *291*, 498-501.

Carter, M.S., Kuhn, K.M., and Sarnow, P. (2000). Cellular internal ribosome entry site elements and the use of cDNA microarrays in their investigation. In: Translational control of gene expression, vol. 2nd edition, eds. N. Sonenberg, J.W.B. Hershey, and M.B. Mathews, Cold Spring Harbor, NY.: Cold Spring Harbor Press, 615 - 635.

Caruthers, J.M., Johnson, E.R., and McKay, D.B. (2000). Crystal structure of yeast initiation factor 4A, a DEAD-box RNA helicase. Proc Natl Acad Sci U S A *97*, 13080-13085.

Caruthers, J.M., and McKay, D.B. (2002). Helicase structure and mechanism. Curr Opin Struct Biol *12*, 123-133.

Casey, J., and Davidson, N. (1977). Rates of formation and thermal stabilities of RNA:DNA and DNA:DNA duplexes at high concentrations of formamide. Nucleic Acids Res *4*, 1539-1552.

Caskey, T., Scolnick, E., Tompkins, R., Goldstein, J., and Milman, G. (1970). Peptide chain termination, codon, protein factor and ribosomal requirements.

Cencic, R., Carrier, M., Galicia-Vázquez, G., Bordeleau, M., Sukarieh, R., Bourdeau, A., Brem, B., Teodoro, J., Greger, H., Tremblay, M., Porco, J.J., and Pelletier, J. (2009). Antitumor activity and mechanism of action of the cyclopenta[b]benzofuran, silvestrol. PLoS One *4*, e5223.

Cencic, R., Carrier, M., Trnkus, A., Porco, J.J., Minden, M., and Pelletier, J. (2010). Synergistic effect of inhibiting translation initiation in combination with cytotoxic agents in acute myelogenous leukemia cells. Leuk Res *34*, 535-541.

Ceulemans, H., and Bollen, M. (2004). Functional diversity of protein phosphatase-1, a cellular economizer and reset button. Physiol Rev *84*, 1-39.

Chakrabarti, A., and Maitra, U. (1991). Function of eukaryotic initiation factor 5 in the formation of an 80S ribosomal polypeptide-chain initiation complex. Journal of Biological Chemistry *266*, 14039-14045.

Challis, J., Lockwood, C., Myatt, L., Norman, J., Strauss, J.r., and Petraglia, F. (2009). Inflammation and pregnancy. Reprod Sci *16*, 206-215.

Chang, J.H., Cho, Y.H., Sohn, S.Y., Choi, J.M., Kim, A., Kim, Y.C., Jang, S.K., and Cho, Y. (2009). Crystal structure of the eIF4A-PDCD4 complex. Proc Natl Acad Sci U S A *106*, 3148-3153.

Chappell, S.A., Dresios, J., Edelman, G.M., and Mauro, V.P. (2006). Ribosomal shunting mediated by a translational enhancer element that base pairs to 18S rRNA. Proceedings of the National Academy of Sciences of the United States of America *103*, 9488-9493.

Chaudhuri, J., Chowdhury, D., and Maitra, U. (1999). Distinct functions of eukaryotic translation initiation factors eIF1A and eIF3 in the formation of the 40 S ribosomal preinitiation complex. Journal of Biological Chemistry *274*, 17975-17980.

Chaudhuri, J., Das, K., and Maitra, U. (1994). Purification and characterisation of bacterially expressed mammalian translation initiation factor 5 (eIF5) - demonstration that eIF5 forms a specific complex with IF2. Biochemistry *33*, 4794-4799.

Chaurasiya, K., Paramanathan, T., McCauley, M., and Williams, M. (2010). Biophysical characterization of DNA binding from single molecule force measurements. Phys Life Rev *7*, 299-341.

Chellappa, R., Li, S., Pauley, S., Jahan, I., Jin, K., and Xiang, M. (2008). Barhl1 regulatory sequences required for cell-specific gene expression and autoregulation in the inner ear and central nervous system. Mol Cell Biol *28*, 1905-1914.

Chen, Y., Potratz, J.P., Tijerina, P., Del Campo, M., Lambowitz, A.M., and Russell, R. (2008). DEAD-box proteins can completely separate an RNA duplex using a single ATP. Proc Natl Acad Sci U S A *105*, 20203-20208.

Cheng, W., Dumont, S., Tinoco, I.J., and Bustamante, C. (2007). NS3 helicase actively separates RNA strands and senses sequence barriers ahead of the opening fork. Proc Natl Acad Sci U S A *104*, 13954-13959.

Cheng, Z., Coller, J., Parker, R., and Song, H. (2005). Crystal structure and functional analysis of DEAD-box protein Dhh1p. RNA *11*, 1258-1270.

Cheung, I., Feng, Y., Danis, K., Shukla, N., Meyers, P., Ladanyi, M., and Cheung, N. (2007a). Novel markers of subclinical disease for Ewing family tumors from gene expression profiling. Clin Cancer Res *13*, 6978-6983.

Cheung, Y.N., Maag, D., Mitchell, S.F., Fekete, C.A., Algire, M.A., Takacs, J.E., Shirokikh, N., Pestova, T., Lorsch, J.R., and Hinnebusch, A.G. (2007b). Dissociation of eIF1 from the 40S ribosomal subunit is a key step in start codon selection in vivo. Genes & Development *21*, 1217-1230.

Chicurel, M., Terrian, D., and Potter, H. (1993). mRNA at the synapse: analysis of a synaptosomal preparation enriched in hippocampal dendritic spines. J Neurosci *13*, 4054-4063.

Chilkoti, A., Boland, T., Ratner, B., and Stayton, P. (1995). The relationship between ligand-binding thermodynamics and protein-ligand interaction forces measured by atomic force microscopy. Biophys J *69*, 2125-2130.

Chuang, R.Y., Weaver, P.L., Liu, Z., and Chang, T.H. (1997). Requirement of the DEAD-box protein Ded1p for messenger RNA translation. Science *275*, 1468-1471.

Cigan, A.M., Feng, L., and Donahue, T.F. (1988). Transfer RNA iMet functions in directing the scanning ribosome to the start site of translation. Science *242*, 93-97.

Clark, B.F.C., and Marcker, K.A. (1966). Role of N-formyl-methionyl-SRNA in protein biosynthesis. Journal of Molecular Biology *17*, 394-&.

Clemens, M., Bushell, M., and Morley, S. (1998). Degradation of eukaryotic polypeptide chain initiation factor (eIF) 4G in response to induction of apoptosis in human lymphoma cell lines. Oncogene *17*, 2921-2931.

Clemens, M.J., Bushell, M., Jeffrey, I.W., Pain, V.M., and Morley, S.J. (2000). Translation initiation factor modifications and the regulation of protein synthesis in apoptotic cells. Cell Death and Differentiation *7*, 603-615.

Clemens, M.J., Pain, V.M., Wong, S.T., and Henshaw, E.C. (1982). Phosphorylation inhibits guanine-nucleotide exchange on eukaryotic initiation factor 2. Nature *296*, 93-95.

Cluzel, P., Lebrun, A., Heller, C., Lavery, R., Viovy, J., Chatenay, D., and Caron, F. (1996). DNA: an extensible molecule. Science *271*, 792-794.

Collins, R., Karlberg, T., Lehtio, L., Schutz, P., van den Berg, S., Dahlgren, L.G., Hammarstrom, M., Weigelt, J., and Schuler, H. (2009). The DEXD/H-box RNA helicase DDX19 is regulated by an alpha-helical switch. J Biol Chem *284*, 10296-10300.

Comtesse, N., Keller, A., Diesinger, I., Bauer, C., Kayser, K., Huwer, H., Lenhof, H., and Meese, E. (2007). Frequent overexpression of the genes FXR1, CLAPM1 and EIF4G located on amplicon 3q26-27 in squamous cell carcinoma of the lung. Int J Cancer *120*, 2538-2544.

Conn, G., Brown, T., and Leonard, G. (1999). The crystal structure of the RNA/DNA hybrid r(GAAGAGAAGC). d(GCTTCTCTTC) shows significant differences to that found in solution. Nucleic Acids Res *27*, 555-561.

Conroy, S.C., Dever, T.E., Owens, C.L., and Merrick, W.C. (1990). Characterisation of the 46,000 dalton subunit of eIF4F. Archives of Biochemistry and Biophysics *282*, 363-371.

Conte, M.R., Kelly, G., Babon, J., Sanfelice, D., Youell, J., Smerdon, S.J., and Proud, C.G. (2006). Structure of the eukaryotic initiation factor (eIF) 5 reveals a fold common to several translation factors. Biochemistry *45*, 4550-4558.

Cooper, H.L., Berger, S.L., and Braverman, R. (1976). Free ribosomes in physiologically nondividing cells - human peripheral lymphocytes. Journal of Biological Chemistry *251*, 4891-4900.

Cordin, O., Banroques, J., Tanner, N.K., and Linder, P. (2006). The DEAD-box protein family of RNA helicases. Gene *367*, 17-37.

Cordin, O., Tanner, N.K., Doere, M., Linder, P., and Banroques, J. (2004). The newly discovered Q motif of DEAD-box RNA helicases regulates RNA-binding and helicase activity. EMBO J *23*, 2478-2487.

Craig, A., Haghighat, A., Yu, A., and Sonenberg, N. (1998). Interaction of polyadenylate-binding protein with the eIF4G homologue PAIP enhances translation. Nature *392*, 520-523.

Crick, F.H., Brenner, S., Watstobi.Rj, and Barnett, L. (1961). General nature of the genetic code for proteins. Nature *192*, 1227-&.

Cuzzocrea, S., Wayman, N., Mazzon, E., Dugo, L., Di Paola, R., Serraino, I., Britti, D., Chatterjee, P., Caputi, A., and Thiemermann, C. (2002). The cyclopentenone prostaglandin 15-deoxy-Delta(12,14)-prostaglandin J(2) attenuates the development of acute and chronic inflammation. Mol Pharmacol *61*, 997-1007.

Damoc, E., Fraser, C.S., Zhou, M., Videler, H., Mayeur, G.L., Hershey, J.W.B., Doudna, J.A., Robinson, C.V., and Leary, J.A. (2007). Structural characterization of the human eukaryotic initiation factor 3 protein complex by mass spectrometry. Molecular & Cellular Proteomics *6*, 1135-1146.

Dang, Y.J., Low, W.K., Xu, J., Gehring, N.H., Dietz, H.C., Romo, D., and Liu, J.O. (2009). Inhibition of Nonsense-mediated mRNA Decay by the Natural Product Pateamine A through Eukaryotic Initiation Factor 4AIII. Journal of Biological Chemistry *284*, 23613-23621.

Davuluri, R.V., Suzuki, Y., Sugano, S., and Zhang, M.Q. (2000). CART classification of human 5 ' UTR sequences. Genome Research *10*, 1807-1816.

De Benedetti, A., and Graff, J. (2004). eIF-4E expression and its role in malignancies and metastases. Oncogene *23*, 3189-3199.

De Gregorio, E., Preiss, T., and Hentze, M.W. (1998). Translational activation of uncapped mRNAs by the central part of human eIF4G is 5 ' end-dependent. Rna-a Publication of the Rna Society *4*, 828-836.

de la Cruz, J., Kressler, D., and Linder, P. (1999). Unwinding RNA in Saccharomyces cerevisiae: DEAD-box proteins and related families. Trends Biochem Sci *24*, 192-198.

de Moor, C.H., Meijer, H., and Lissenden, S. (2005). Mechanisms of translational control by the 3 ' UTR in development and differentiation. Seminars in Cell & Developmental Biology *16*, 49-58.

Deckwerth, T.L., and Johnson, E.M. (1993). Temporal analysis of events associated with programmed cell death (apoptosis) of sympathetic neurons deprived of nerve growth factor. Journal of Cell Biology *123*, 1207-1222.

Dennis, G.J., Sherman, B., Hosack, D., Yang, J., Gao, W., Lane, H., and Lempicki, R. (2003). DAVID: Database for Annotation, Visualization, and Integrated Discovery. Genome Biol *4*, P3.

Deribe, Y.L., Pawson, T., and Dikic, I. (2010). Post-translational modifications in signal integration. Nature Structural & Molecular Biology *17*, 666-672.

Dever, T.E., Feng, L., Wek, R.C., Cigan, A.M., Donahue, T.F., and Hinnebusch, A.G. (1992). Phosphorylation of initiation factor 2 alpha by protein kinase GCN2 mediates gene specific translational control of GCN4 in yeast. Cell *68*, 585-596.

Dimitrova, M., Imbert, I., Kieny, M., and Schuster, C. (2003). Protein-protein interactions between hepatitis C virus nonstructural proteins. J Virol *77*, 5401-5414.

Doepker, R.C., Hsu, W.L., Saffran, H.A., and Smiley, J.R. (2004). Herpes simplex virus virion host shutoff protein is stimulated by translation initiation factors eIF4B and eIF4H. J Virol *78*, 4684-4699.

Dorrello, N.V., Peschiaroli, A., Guardavaccaro, D., Colburn, N.H., Sherman, N.E., and Pagano, M. (2006). S6K1- and beta TRCP-mediated degradation of PDCD4 promotes protein translation and cell growth. Science *314*, 467-471.

Dumont, S., Cheng, W., Serebrov, V., Beran, R., Tinoco, I.J., Pyle, A., and Bustamante, C. (2006). RNA translocation and unwinding mechanism of HCV NS3 helicase and its coordination by ATP. Nature *439*, 105-108.

Duncan, R., and Hershey, J.W.B. (1983). Identification and quantitation of levels of protein-synthesis initiation factors in crude hela cell lysates by two-dimensional polyacrylamide-gel electrophoresis. Journal of Biological Chemistry *258*, 7228-7235.

Durinck, S., Moreau, Y., Kasprzyk, A., Davis, S., De Moor, B., Brazma, A., and Huber, W. (2005). BioMart and Bioconductor: a powerful link between biological databases and microarray data analysis. Bioinformatics *21*, 3439-3440.

Eberle, J., Fecker, L., Bittner, J., Orfanos, C., and Geilen, C. (2002). Decreased proliferation of human melanoma cell lines caused by antisense RNA against translation factor eIF-4A1. Br J Cancer *86*, 1957-1962.

Eberle, J., Krasagakis, K., and Orfanos, C. (1997). Translation initiation factor eIF-4A1 mRNA is consistently overexpressed in human melanoma cells in vitro. Int J Cancer *71*, 396-401.

Edery, I., Humbelin, M., Darveau, A., Lee, K.A.W., Milburn, S., Hershey, J.W.B., Trachsel, H., and Sonenberg, N. (1983). Involvement of eukaryotic initiation factor 4A in the cap recognition process. Journal of Biological Chemistry *258*, 1398-1403.

Ellington, A., and Szostak, J. (1990). In vitro selection of RNA molecules that bind specific ligands. Nature *346*, 818-822.

Ellis, N. (1997). DNA helicases in inherited human disorders. Curr Opin Genet Dev *7*, 354-363.

Ernst, V., Baum, E.Z., and Reddy, P. (1982). Heat shock protein phosphorylation and the control of translation in rabbit reticulocyte lysates and hela cells. Schlesinger, M. J., M. Ashburner and a. Tissieres. Heat Shock: from Bacteria to Man; Meeting, Cold Spring Harbor, N.Y., USA, May 5-9, 1982. Xix+440p. Cold Spring Harbor Laboratory: Cold Spring Harbor, N.Y., USA. Illus, P215-226.

Etchison, D., Milburn, S., Edery, I., Sonenberg, N., and Hershey, J. (1982). Inhibition of HeLa cell protein synthesis following poliovirus infection correlates with the proteolysis of a 220,000-dalton polypeptide associated with eucaryotic initiation factor 3 and a cap binding protein complex. J Biol Chem *257*, 14806-14810.

Fairman-Williams, M.E., Guenther, U.P., and Jankowsky, E. (2010). SF1 and SF2 helicases: family matters. Curr Opin Struct Biol.

Farrell, P.J., Balkow, K., Hunt, T., Jackson, R.J., and Trachsel, H. (1977). Phosphorylation of initiation factor eIF2 and control of reticulocyte protein synthesis. Cell *11*, 187-200.

Feng, P., Everly, D.J., and Read, G. (2001). mRNA decay during herpesvirus infections: interaction between a putative viral nuclease and a cellular translation factor. J Virol *75*, 10272-10280.

Feng, P., Everly, D.J., and Read, G. (2005). mRNA decay during herpes simplex virus (HSV) infections: protein-protein interactions involving the HSV virion host shutoff protein and translation factors eIF4H and eIF4A. J Virol *79*, 9651-9664.

Fenwick, M., and McMenamin, M. (1984). Early virion-associated suppression of cellular protein synthesis by herpes simplex virus is accompanied by inactivation of mRNA. J Gen Virol *65 (Pt 7)*, 1225-1228.

Fischer, U., Janicke, R.U., and Schulze-Osthoff, K. (2003). Many cuts to ruin: a comprehensive update of caspase substrates. Cell Death and Differentiation *10*, 76-100.

Forman, B., Tontonoz, P., Chen, J., Brun, R., Spiegelman, B., and Evans, R. (1995). 15-Deoxy-delta 12, 14-prostaglandin J2 is a ligand for the adipocyte determination factor PPAR gamma. Cell *83*, 803-812.

Freistroffer, D.V., Pavlov, M.Y., MacDougall, J., Buckingham, R.H., and Ehrenberg, M. (1997). Release factor RF3 in E-coli accelerates the dissociation of release factors RF1 and RF2 from the ribosome in a GTP-dependent manner. Embo Journal *16*, 4126-4133.

Fukao, A., Sasano, Y., Imataka, H., Inoue, K., Sakamoto, H., Sonenberg, N., Thoma, C., and Fujiwara, T. (2009). The ELAV protein HuD stimulates cap-dependent translation in a Poly(A)- and eIF4A-dependent manner. Mol Cell *36*, 1007-1017.

Fukushima, M. (1990). Prostaglandin J2--anti-tumour and anti-viral activities and the mechanisms involved. Eicosanoids *3*, 189-199.

Futterer, J., Kiss-Laszlo, Z., and Hohn, T. (1993). Nonlinear ribosome migration on cauliflower mosaic virus 35S RNA. Cell *73*, 788-802.

Galabru, J., and Hovanessian, A. (1987). Autophosphorylation of the protein kinase dependent on double stranded RNA. Journal of Biological Chemistry *262*, 15538-15544.

Gallie, D.R. (1991). The cap and polyA tail function synergistically to regulate messenger RNA translational efficiency. Genes & Development *5*, 2108-2116.

Gallie, D.R. (2004). The role of the initiation surveillance complex in promoting efficient protein synthesis. Biochemical Society Transactions *32*, 585-588.

Gilroy, D., Colville-Nash, P., Willis, D., Chivers, J., Paul-Clark, M., and Willoughby, D. (1999). Inducible cyclooxygenase may have anti-inflammatory properties. Nat Med *5*, 698-701.

Gingras, A.C., Raught, B., and Sonenberg, N. (2001). Regulation of translation initiation by FRAP/mTOR. Genes & Development *15*, 807-826.

Gorbalenya, A.E., and Koonin, E.V. (1993). Helicases: amino acid sequence comparisons and structure-function relationships. Current Opinion in Structural Biology *3*, 419-429.

Gorbalenya, A.E., Koonin, E.V., Donchenko, A.P., and Blinov, V.M. (1988a). A conserved NTP-motif in putative helicases. Nature *333*, 22.

Gorbalenya, A.E., Koonin, E.V., Donchenko, A.P., and Blinov, V.M. (1988b). A novel superfamily of nucleoside triphosphate-binding motif containing proteins which are probably involved in duplex unwinding in DNA and RNA replication and recombination. FEBS Lett *235*, 16-24.

Gorbalenya, A.E., Koonin, E.V., Donchenko, A.P., and Blinov, V.M. (1989). Two related superfamilies of putative helicases involved in replication, recombination, repair and expression of DNA and RNA genomes. Nucleic Acids Res *17*, 4713-4730.

Gorbalenya, A.E., Koonin, E.V., and Wolf, Y.I. (1990). A new superfamily of putative NTP-binding domains encoded by genomes of small DNA and RNA viruses. FEBS Lett *262*, 145-148.

Gradi, A., Imataka, H., Svitkin, Y.V., Rom, E., Raught, B., Morino, S., and Sonenberg, N. (1998). A novel functional human eukaryotic translation initiation factor 4G. Molecular and Cellular Biology *18*, 334-342.

Grens, A., and Scheffler, I. (1990). The 5'- and 3'-untranslated regions of ornithine decarboxylase mRNA affect the translational efficiency. J Biol Chem *265*, 11810-11816.

Grifo, J.A., Tahara, S.M., Morgan, M.A., Shatkin, A.J., and Merrick, W.C. (1983). New initiation factor activity required for globin messenger RNA translation. Journal of Biological Chemistry *258*, 5804-5810.

Grohman, J.K., Del Campo, M., Bhaskaran, H., Tijerina, P., Lambowitz, A.M., and Russell, R. (2007). Probing the mechanisms of DEAD-box proteins as general RNA chaperones: the C-terminal domain of CYT-19 mediates general recognition of RNA. Biochemistry *46*, 3013-3022.

Gross, M., and Mendelewski, J. (1977). Additional evidence that hemin-controlled transaltional repressor from rabbit reticulocytes is a protein kinase. Biochemical and Biophysical Research Communications *74*, 559-569.

Gunawardena, S., Ruis, B., Meyer, J., Kapoor, M., and Conklin, K. (2008). NOM1 targets protein phosphatase I to the nucleolus. J Biol Chem *283*, 398-404.

Guo, H.L., Ingolia, N.T., Weissman, J.S., and Bartel, D.P. (2010). Mammalian microRNAs predominantly act to decrease target mRNA levels. Nature *466*, 835-U866.

Guo, L., Lobenhofer, E., Wang, C., Shippy, R., Harris, S., Zhang, L., Mei, N., Chen, T., Herman, D., Goodsaid, F., Hurban, P., Phillips, K., Xu, J., Deng, X., Sun, Y., Tong, W., Dragan, Y., and Shi, L. (2006). Rat toxicogenomic study reveals analytical consistency across microarray platforms. Nat Biotechnol *24*, 1162-1169.

Göke, A., Göke, R., Knolle, A., Trusheim, H., Schmidt, H., Wilmen, A., Carmody, R., Göke, B., and Chen, Y. (2002). DUG is a novel homologue of translation initiation factor 4G that binds eIF4A. Biochem Biophys Res Commun *297*, 78-82.

Haberl, C., Hültner, L., Flügel, A., Falk, M., Geuenich, S., Wilmanns, W., and Denzlinger, C. (1998). Release of prostaglandin D2 by murine mast cells: importance of metabolite formation for antiproliferative activity. Mediators Inflamm *7*, 79-84.

Haghighat, A., and Sonenberg, N. (1997). eIF4G dramatically enhances the binding of eIF4E to the mRNA 5'-cap structure. Journal of Biological Chemistry *272*, 21677-21680.

Hagner, P., Schneider, A., and Gartenhaus, R. (2010). Targeting the translational machinery as a novel treatment strategy for hematologic malignancies. Blood *115*, 2127-2135.

Hall, M.C., and Matson, S.W. (1999). Helicase motifs: the engine that powers DNA unwinding. Mol Microbiol *34*, 867-877.

Halls, C., Mohr, S., Del Campo, M., Yang, Q., Jankowsky, E., and Lambowitz, A.M. (2007). Involvement of DEAD-box proteins in group I and group II intron splicing. Biochemical characterization of Mss116p, ATP hydrolysis-dependent and -independent mechanisms, and general RNA chaperone activity. J Mol Biol *365*, 835-855.

Hamilton, T., Stoneley, M., Spriggs, K., and Bushell, M. (2006). TOPs and their regulation. Biochem Soc Trans *34*, 12-16.

Harding, H.P., Zhang, Y.H., and Ron, D. (1999). Protein translation and folding are coupled by an endoplasmic-reticulum-resident kinase. Nature *397*, 271-274.

Henis-Korenblit, S., Strumpf, N., Goldstaub, D., and Kimchi, A. (2000). A novel form of DAP5 protein accumulates in apoptotic cells as a result of caspase cleavage and internal ribosome entry site-mediated translation. Mol Cell Biol *20*, 496-506.

Henn, A., Cao, W., Hackney, D.D., and De La Cruz, E.M. (2008). The ATPase cycle mechanism of the DEAD-box rRNA helicase, DbpA. J Mol Biol *377*, 193-205.

Henn, A., Medalia, O., Shi, S., Steinberg, M., Franceschi, F., and Sagi, I. (2001). Visualization of unwinding activity of duplex RNA by DbpA, a DEAD box helicase, at single-molecule resolution by atomic force microscopy. Proc Natl Acad Sci U S A *98*, 5007-5012.

Henn, A., Shi, S.P., Zarivach, R., Ben-Zeev, E., and Sagi, I. (2002). The RNA helicase DbpA exhibits a markedly different conformation in the ADP-bound state when compared with the ATP- or RNA-bound states. J Biol Chem *277*, 46559-46565.

Hilbert, M., Karow, A.R., and Klostermeier, D. (2009). The mechanism of ATP-dependent RNA unwinding by DEAD box proteins. Biol Chem *390*, 1237-1250.

Hilliard, A., Hilliard, B., Zheng, S., Sun, H., Miwa, T., Song, W., Göke, R., and Chen, Y. (2006). Translational regulation of autoimmune inflammation and lymphoma genesis by programmed cell death 4. J Immunol *177*, 8095-8102.

Hinman, M., and Lou, H. (2008). Diverse molecular functions of Hu proteins. Cell Mol Life Sci *65*, 3168-3181.

Hitti, E., Iakovleva, T., Brook, M., Deppenmeier, S., Gruber, A., Radzioch, D., Clark, A., Blackshear, P., Kotlyarov, A., and Gaestel, M. (2006). Mitogen-activated protein kinase-activated protein kinase 2 regulates tumor necrosis factor mRNA stability and translation mainly by altering tristetraprolin expression, stability, and binding to adenine/uridine-rich element. Mol Cell Biol *26*, 2399-2407.

Hodgman, T.C. (1988). A new superfamily of replicative proteins. Nature *333*, 22-23.

Hofmann, I., Casella, M., Schnölzer, M., Schlechter, T., Spring, H., and Franke, W. (2006). Identification of the junctional plaque protein plakophilin 3 in cytoplasmic particles containing RNA-binding proteins and the recruitment of plakophilins 1 and 3 to stress granules. Mol Biol Cell *17*, 1388-1398.

Holz, M.K., Ballif, B.A., Gygi, S.P., and Blenis, J. (2005). mTOR and S6K1 mediate assembly of the translation preinitiation complex through dynamic protein interchange and ordered phosphorylation events. Cell *123*, 569-580.

Hood, K.A., West, L.M., Northcote, P.T., Berridge, M.V., and Miller, J.H. (2001). Induction of apoptosis by the marine sponge (Mycale) metabolites, mycalamide A and pateamine. Apoptosis *6*, 207-219.

Hutchins, A.P., Roberts, G.R., Lloyd, C.W., and Doonan, J.H. (2004). In vivo interaction between CDKA and eIF4A: a possible mechanism linking translation and cell proliferation. FEBS Lett *556*, 91-94.

Hutter, J.L., and Bechhoefer, J. (1993). Calibration of atomic force microscope tips. Review of Scientific Instruments *64*, 1868-1873.

Hwang, B., Su, B., Chai, H., Mi, Q., Kardono, L., Afriastini, J., Riswan, S., Santarsiero, B., Mesecar, A., Wild, R., Fairchild, C., Vite, G., Rose, W., Farnsworth, N., Cordell, G., Pezzuto, J., Swanson, S., and Kinghorn, A. (2004). Silvestrol and episilvestrol, potential anticancer rocaglate derivatives from Aglaia silvestris. J Org Chem *69*, 3350-3358.

Hwang, S., Jin, H., Kwon, J., Chang, S., Kim, T., Cho, C., Lee, K., Young, M., Colburn, N., Beck, G.J., Yang, H., and Cho, M. (2007). Aerosol-delivered programmed cell death 4 enhanced apoptosis, controlled cell cycle and suppressed AP-1 activity in the lungs of AP-1 luciferase reporter mice. Gene Ther *14*, 1353-1361.

Höck, J., Weinmann, L., Ender, C., Rüdel, S., Kremmer, E., Raabe, M., Urlaub, H., and Meister, G. (2007). Proteomic and functional analysis of Argonaute-containing mRNA-protein complexes in human cells. EMBO Rep *8*, 1052-1060.

Iacono, M., Mignone, F., and Pesole, G. (2005). uAUG and uORFs in human and rodent 5 ' untranslated mRNAs. Gene *349*, 97-105.

Imataka, H., Olsen, H., and Sonenberg, N. (1997). A new translational regulator with homology to eukaryotic translation initiation factor 4G. EMBO J *16*, 817-825.

Imataka, H., and Sonenberg, N. (1997). Human eukaryotic translation initiation factor 4G (eIF4G) possesses two separate and independent binding sites for eIF4A. Mol Cell Biol *17*, 6940-6947.

Inokuchi, Y., Hirashima, A., Sekine, Y., Janosi, L., and Kaji, A. (2000). Role of ribosome recycling factor (RRF) in translational coupling. Embo Journal *19*, 3788-3798.

Iost, I., Dreyfus, M., and Linder, P. (1999). Ded1p, a DEAD-box protein required for translation initiation in Saccharomyces cerevisiae, is an RNA helicase. J Biol Chem *274*, 17677-17683.

Ito, T., Marintchev, A., and Wagner, G. (2004). Solution structure of human initiation factor eIF2 alpha reveals homology to the elongation factor eEF1B. Structure *12*, 1693-1704.

Janosi, L., Hara, H., Zhang, S.J., and Kaji, A. (1996). Ribosome recycling by ribosome recycling factor (RRF) - An important but overlooked step of protein biosynthesis. Advances in Biophysics, Vol 32, 1996 *32*, 121-201.

Jansen, A., Camalier, C., and Colburn, N. (2005). Epidermal expression of the translation inhibitor programmed cell death 4 suppresses tumorigenesis. Cancer Res *65*, 6034-6041.

Jaramillo, M., Dever, T.E., Merrick, W.C., and Sonenberg, N. (1991). RNA unwinding in translation - assembly of helicase complex intermediates comprising eukaryotic initiation factors eIF4F and eIF4B. Molecular and Cellular Biology *11*, 5992-5997.

Jefferies, H.B.J., Fumagalli, S., Dennis, P.B., Reinhard, C., Pearson, R.B., and Thomas, G. (1997). Rapamycin suppresses 5'TOP mRNA translation through inhibition of p70(S6k). Embo Journal *16*, 3693-3704.

Jeffery, I., Higgins, D., and Culhane, A. (2006). Comparison and evaluation of methods for generating differentially expressed gene lists from microarray data. BMC Bioinformatics *7*, 359.

Jeffrey, I., Bushell, M., Tilleray, V., Morley, S., and Clemens, M. (2002). Inhibition of protein synthesis in apoptosis: differential requirements by the tumor necrosis factor alpha family and a DNA-damaging agent for caspases and the double-stranded RNA-dependent protein kinase. Cancer Res *62*, 2272-2280.

Jennings, M.D., and Pavitt, G.D. (2010). eIF5 has GDI activity necessary for translational control by eIF2 phosphorylation. Nature *465*, 378-U142.

Jiang, C., Ting, A., and Seed, B. (1998). PPAR-gamma agonists inhibit production of monocyte inflammatory cytokines. Nature *391*, 82-86.

Jin, H., Kim, T., Hwang, S., Chang, S., Kim, H., Anderson, H., Lee, H., Lee, K., Colburn, N., Yang, H., Cho, M., and Cho, C. (2006). Aerosol delivery of urocanic acid-modified chitosan/programmed cell death 4 complex regulated apoptosis, cell cycle, and angiogenesis in lungs of K-ras null mice. Mol Cancer Ther *5*, 1041-1049.

Johannes, G., Carter, M., Eisen, M., Brown, P., and Sarnow, P. (1999). Identification of eukaryotic mRNAs that are translated at reduced cap binding complex eIF4F concentrations using a cDNA microarray. Proc Natl Acad Sci U S A *96*, 13118-13123.

Johnstone, O., and Lasko, P. (2004). Interaction with eIF5B is essential for Vasa function during development. Development *131*, 4167-4178.

Kaempfer, R. (1969). Ribosomal subunit exchange in cytoplasm of a eukaryote. Nature *222*, 950-&.

Kaempfer, R. (1970). Dissociation of ribosomes on polypeptide chain termination and origin of single ribosomes. Nature *228*, 534-&.

Kang, M., Ahn, H., Lee, J., Matsuhashi, S., and Park, W. (2002). Up-regulation of PDCD4 in senescent human diploid fibroblasts. Biochem Biophys Res Commun *293*, 617-621.

Kapasi, P., Chaudhuri, S., Vyas, K., Baus, D., Komar, A., Fox, P., Merrick, W., and Mazumder, B. (2007). L13a blocks 48S assembly: role of a general initiation factor in mRNA-specific translational control. Mol Cell *25*, 113-126.

Kapp, L.D., and Lorsch, J.R. (2004). GTP-dependent recognition of the methionine moiety on initiator tRNA by translation factor eIF2. Journal of Molecular Biology *335*, 923-936.

Karginov, F.V., Caruthers, J.M., Hu, Y., McKay, D.B., and Uhlenbeck, O.C. (2005). YxiN is a modular protein combining a DEx(D/H) core and a specific RNA-binding domain. J Biol Chem *280*, 35499-35505.

Karimi, R., Pavlov, M.Y., Buckingham, R.H., and Ehrenberg, M. (1999). Novel roles for classical factors at the interface between translation termination and initiation. Molecular Cell *3*, 601-609.

Karow, A., and Klostermeier, D. (2010). A Structural Model for the DEAD Box Helicase YxiN in Solution: Localization of the RNA Binding Domain. J Mol Biol.

Karow, A.R., Theissen, B., and Klostermeier, D. (2007). Authentic interdomain communication in an RNA helicase reconstituted by expressed protein ligation of two helicase domains. FEBS J *274*, 463-473.

Kay, J.E., Ahern, T., and Atkins, M. (1971). Control of protein synthesis during activation of lymphocytes by phytomaglutinin. Biochimica Et Biophysica Acta *247*, 322-&.

Kedersha, N., Stoecklin, G., Ayodele, M., Yacono, P., Lykke-Andersen, J., Fritzler, M., Scheuner, D., Kaufman, R., Golan, D., and Anderson, P. (2005). Stress granules and processing bodies are dynamically linked sites of mRNP remodeling. J Cell Biol *169*, 871-884.

Keiper, B.D., Gan, W.N., and Rhoads, R.E. (1999). Protein synthesis initiation factor 4G. International Journal of Biochemistry & Cell Biology *31*, 37-41.

Kim, S.H., Quigley, G.J., Suddath, F.L., McPherso.A, Sneden, D., Kim, J.J., Weinzier.J, and Rich, A. (1973). 3-dimensional structure of yeast phenylalanine transfer-RNA - folding of polynucleotide chain. Science *179*, 285-288.

Kim, W.J., Kim, J.H., and Jang, S.K. (2007). Anti-inflammatory lipid mediator 15d-PGJ2 inhibits translation through inactivation of eIF4A. EMBO J *26*, 5020-5032.

Kliewer, S., Lenhard, J., Willson, T., Patel, I., Morris, D., and Lehmann, J. (1995). A prostaglandin J2 metabolite binds peroxisome proliferator-activated receptor gamma and promotes adipocyte differentiation. Cell *83*, 813-819.

Kolupaeva, V.G., Unbehaun, A., Lomakin, I.B., Hellen, C.U.T., and Pestova, T.V. (2005). Binding of eukaryotic initiation factor 3 to ribosomal 40S subunits and its role in ribosomal dissociation and anti-association. Rna-a Publication of the Rna Society *11*, 470-486.

Kondrashov, A., Kiefmann, M., Ebnet, K., Khanam, T., Muddashetty, R., and Brosius, J. (2005). Inhibitory effect of naked neural BC1 RNA or BC200 RNA on eukaryotic in vitro translation systems is reversed by poly(A)-binding protein (PABP). J Mol Biol *353*, 88-103.

Korneeva, N.L., Lamphear, B.J., Hennigan, F.L., Merrick, W.C., and Rhoads, R.E. (2001). Characterization of the two eIF4A-binding sites on human eIF4G-1. J Biol Chem *276*, 2872-2879.

Korneeva, N.L., Lamphear, B.J., Hennigan, F.L., and Rhoads, R.E. (2000). Mutually cooperative binding of eukaryotic translation initiation factor (eIF) 3 and eIF4A to human eIF4G-1. J Biol Chem *275*, 41369-41376.

Koromilas, A.E., Lazariskaratzas, A., and Sonenberg, N. (1992). Messenger RNAs containing extensive secondary structure in their 5' noncoding region translate efficiently in cells overexpressing initiation factor eIF4E. Embo Journal *11*, 4153-4158.

Kozak, M. (1978). How do eukaryotic ribosomes select initiation regions in messenger-RNA. Cell *15*, 1109-1123.

Kozak, M. (1980a). Evaluation of the scanning model for initiation of protein-synthesis in eukaryotes. Cell *22*, 7-8.

Kozak, M. (1980b). Role of ATP in binding and migration of 40S ribosomal subunits. Cell *22*, 459-467.

Kozak, M. (1981). Possible role of flanking nucleotides in recognition of the AUG initiator codon by eukaryotic ribosomes. Nucleic Acids Research *9*, 5233-5252.

Kozak, M. (1983). Translation of insulin-related polypeptides from messenger RNAs with tandemly reiterated copies of the ribosome binding site. Cell *34*, 971-978.

Kozak, M. (1986a). Influences of messenger RNA secondary structure on initiation by eukaryotic ribosomes. Proceedings of the National Academy of Sciences of the United States of America *83*, 2850-2854.

Kozak, M. (1986b). Point mutations define a sequence flanking the AUG initiator codon that modulates translation by eukaryotic ribosomes. Cell *44*, 283-292.

Kozak, M. (1987). An analysis of 5' non-coding sequences from 699 vertebrate messenger RNAs. Nucleic Acids Research *15*, 8125-8148.

Kozak, M. (1991). An analysis of vertebrate messenger RNA sequences - intimations of translational control. Journal of Cell Biology *115*, 887-903.

Kroczynska, B., Kaur, S., Katsoulidis, E., Majchrzak-Kita, B., Sassano, A., Kozma, S.C., Fish, E.N., and Platanias, L.C. (2009). Interferon-Dependent Engagement of Eukaryotic Initiation Factor 4B via S6 Kinase (S6K)-and Ribosomal Protein S6K-Mediated Signals. Molecular and Cellular Biology *29*, 2865-2875.

La Teana, A., Gualerzi, C.O., and Brimacombe, R. (1995). From standby to decoding site - adjustment of the messenger RNA on the 30S ribosomal subunit under the influence of the initiation factors. Rna-a Publication of the Rna Society *1*, 772-782.

Lai, M., Kuo, H., Chang, W., and Tarn, W. (2003). A novel splicing regulator shares a nuclear import pathway with SR proteins. EMBO J *22*, 1359-1369.

Lal, A., Navarro, F., Maher, C., Maliszewski, L., Yan, N., O'Day, E., Chowdhury, D., Dykxhoorn, D., Tsai, P., Hofmann, O., Becker, K., Gorospe, M., Hide, W., and Lieberman, J. (2009). miR-24 Inhibits cell proliferation by targeting E2F2, MYC,

and other cell-cycle genes via binding to "seedless" 3'UTR microRNA recognition elements. Mol Cell *35*, 610-625.

Lamphear, B.J., Kirchweger, R., Skern, T., and Rhoads, R.E. (1995). Mapping of functional domains in eukaryotic protein synthesis initiation factor 4G (eIF4G) with picornaviral proteases - implications for cap-dependent and cap independent translational initiation. Journal of Biological Chemistry *270*, 21975-21983.

Lang, C., Frost, R., and Vary, T. (2007). Regulation of muscle protein synthesis during sepsis and inflammation. Am J Physiol Endocrinol Metab *293*, E453-459.

Lankat-Buttgereit, B., and Göke, R. (2009). The tumour suppressor Pdcd4: recent advances in the elucidation of function and regulation. Biol Cell *101*, 309-317.

Lankat-Buttgereit, B., Lenschen, B., Schmidt, H., and Göke, R. (2008). The action of Pdcd4 may be cell type specific: evidence that reduction of dUTPase levels might contribute to its tumor suppressor activity in Bon-1 cells. Apoptosis *13*, 157-164.

LaRonde-LeBlanc, N., Santhanam, A., Baker, A., Wlodawer, A., and Colburn, N. (2007). Structural basis for inhibition of translation by the tumor suppressor Pdcd4. Mol Cell Biol *27*, 147-156.

Laursen, B.S., Sorensen, H.P., Mortensen, K.K., and Sperling-Petersen, H.U. (2005). Initiation of protein synthesis in bacteria. Microbiology and Molecular Biology Reviews *69*, 101-+.

Lawson, T.G., Lee, K.A., Maimone, M.M., Abramson, R.D., Dever, T.E., Merrick, W.C., and Thach, R.E. (1989). Dissociation of double stranded polynucleotide helical structures by eukaryotic initiation factors, as revealed by a novel assay. Biochemistry *28*, 4729-4734.

Lee, C.P., Dyson, M.R., Mandal, N., Varshney, U., Bahramian, B., and Rajbhandary, U.L. (1992). Striking effects of coupling mutations in the acceptor stem on recognition of tRNAs by Escherichia coli Met-tRNA synthetase and met-tRNA transformylase. Proceedings of the National Academy of Sciences of the United States of America *89*, 9262-9266.

Lee, C.P., Seong, B.L., and Rajbhandary, U.L. (1991). Structural and sequence elements important for recognition of Escherichia coli formylmethionine tRNA by methionyl-tRNA transformylase are clustered in the acceptor stem. Journal of Biological Chemistry *266*, 18012-18017.

Lee, C.S., Dias, A.P., Jedrychowski, M., Patel, A.H., Hsu, J.L., and Reed, R. (2008). Human DDX3 functions in translation and interacts with the translation initiation factor eIF3. Nucleic Acids Research *36*, 4708-4718.

Lee, S., Cui, B., Mehta, R., Kinghorn, A., and Pezzuto, J. (1998). Cytostatic mechanism and antitumor potential of novel 1H-cyclopenta[b]benzofuran lignans isolated from Aglaia elliptica. Chem Biol Interact *115*, 215-228.

Lee, S., and McCormick, F. (2006). p97/DAP5 is a ribosome-associated factor that facilitates protein synthesis and cell proliferation by modulating the synthesis of cell cycle proteins. EMBO J *25*, 4008-4019.

LeFebvre, A.K., Korneeva, N.L., Trutschl, M., Cvek, U., Duzan, R.D., Bradley, C.A., Hershey, J.W.B., and Rhoads, R.E. (2006). Translation initiation factor eIF4G-1 binds to eIF3 through the eIF3e subunit. Journal of Biological Chemistry *281*, 22917-22932.

Leger, J.F., Romano, G., Sarkar, A., Robert, J., Bourdieu, L., Chatenay, D., and Marko, J.F. (1999). Structural transitions of a twisted and stretched DNA molecule. Physical Review Letters *83*, 1066-1069.

Leung, Y., and Cavalieri, D. (2003). Fundamentals of cDNA microarray data analysis. Trends Genet *19*, 649-659.

Levy-Strumpf, N., Deiss, L., Berissi, H., and Kimchi, A. (1997). DAP-5, a novel homolog of eukaryotic translation initiation factor 4G isolated as a putative modulator of gamma interferon-induced programmed cell death. Mol Cell Biol *17*, 1615-1625.

Lewis, S., Cerquozzi, S., Graber, T., Ungureanu, N., Andrews, M., and Holcik, M. (2008). The eIF4G homolog DAP5/p97 supports the translation of select mRNAs during endoplasmic reticulum stress. Nucleic Acids Res *36*, 168-178.

Li, J., Li, W., and Gelbart, W. (2005). A genetic screen for maternal-effect suppressors of decapentaplegic identifies the eukaryotic translation initiation factor 4A in Drosophila. Genetics *171*, 1629-1641.

Li, J., and Li, W.X. (2006). A novel function of Drosophila eIF4A as a negative regulator of Dpp/BMP signalling that mediates SMAD degradation. Nat Cell Biol *8*, 1407-1414.

Li, Q.Y., Imataka, H., Morino, S., Rogers, G.W., Richter-Cook, N.J., Merrick, W.C., and Sonenberg, N. (1999). Eukaryotic translation initiation factor 4AIII (eTF4AIII) is functionally distinct from eIF4AI and eIF4AII. Molecular and Cellular Biology *19*, 7336-7346.

Li, W., Dang, Y., Liu, J.O., and Yu, B. (2009). Expeditious synthesis of hippuristanol and congeners with potent antiproliferative activities. Chemistry *15*, 10356-10359.

Li, W., Dang, Y., Liu, J.O., and Yu, B. (2010). Structural and stereochemical requirements of the spiroketal group of hippuristanol for antiproliferative activity. Bioorg Med Chem Lett *20*, 3112-3115.

Liberman, N., Marash, L., and Kimchi, A. (2009). The translation initiation factor DAP5 is a regulator of cell survival during mitosis. Cell Cycle *8*, 204-209.

Lin, D., Pestova, T., Hellen, C., and Tiedge, H. (2008). Translational control by a small RNA: dendritic BC1 RNA targets the eukaryotic initiation factor 4A helicase mechanism. Mol Cell Biol *28*, 3008-3019.

Lin, J., Hsu, M., and Tarn, W. (2007). Cell stress modulates the function of splicing regulatory protein RBM4 in translation control. Proc Natl Acad Sci U S A *104*, 2235-2240.

Linder, P. (2006). Dead-box proteins: a family affair--active and passive players in RNP-remodeling. Nucleic Acids Res *34*, 4168-4180.

Linder, P., Lasko, P.F., Ashburner, M., Leroy, P., Nielsen, P.J., Nishi, K., Schnier, J., and Slonimski, P.P. (1989). Birth of the D-E-A-D box. Nature *337*, 121-122.

Linder, P., and Slonimski, P.P. (1989). An essential yeast protein, encoded by duplicated genes TIF1 and TIF2 and homologous to the mammalian translation initiation factor eIF-4A, can suppress a mitochondrial missense mutation. Proc Natl Acad Sci U S A *86*, 2286-2290.

Lindqvist, L., Oberer, M., Reibarkh, M., Cencic, R., Bordeleau, M., Vogt, E., Marintchev, A., Tanaka, J., Fagotto, F., Altmann, M., Wagner, G., and Pelletier, J. (2008). Selective pharmacological targeting of a DEAD box RNA helicase. PLoS One *3*, e1583.

Ling, J., Morley, S.J., and Traugh, J.A. (2005). Inhibition of cap-dependent translation via phosphorylation of eIF4G by protein kinase Pak2. Embo Journal *24*, 4094-4105.

Liphardt, J., Onoa, B., Smith, S., Tinoco, I.J., and Bustamante, C. (2001). Reversible unfolding of single RNA molecules by mechanical force. Science *292*, 733-737.

Liu, F., Putnam, A., and Jankowsky, E. (2008). ATP hydrolysis is required for DEAD-box protein recycling but not for duplex unwinding. Proc Natl Acad Sci U S A *105*, 20209-20214.

Loh, P., Yang, H., Walsh, M., Wang, Q., Wang, X., Cheng, Z., Liu, D., and Song, H. (2009). Structural basis for translational inhibition by the tumour suppressor Pdcd4. EMBO J *28*, 274-285.

Lomakin, I.B., Hellen, C.U., and Pestova, T.V. (2000). Physical association of eukaryotic initiation factor 4G (eIF4G) with eIF4A strongly enhances binding of eIF4G to the internal ribosomal entry site of encephalomyocarditis virus and is required for internal initiation of translation. Mol Cell Biol *20*, 6019-6029.

Lomakin, I.B., Kolupaeva, V.G., Marintchev, A., Wagner, G., and Pestova, T.V. (2003). Position of eukaryotic initiation factor eIF1 on the 40S ribosomal subunit determined by directed hydroxyl radical probing. Genes & Development *17*, 2786-2797.

Lomakin, I.B., Shirokikh, N.E., Yusupov, M.M., Hellen, C.U.T., and Pestova, T.V. (2006). The fidelity of translation initiation: reciprocal activities of eIF1, IF3 and YciH. Embo Journal *25*, 196-210.

Lorsch, J.R., and Herschlag, D. (1998a). The DEAD box protein eIF4A. 1. A minimal kinetic and thermodynamic framework reveals coupled binding of RNA and nucleotide. Biochemistry *37*, 2180-2193.

Lorsch, J.R., and Herschlag, D. (1998b). The DEAD box protein eIF4A. 2. A cycle of nucleotide and RNA-dependent conformational changes. Biochemistry *37*, 2194-2206.

Low, W.K., Dang, Y., Bhat, S., Romo, D., and Liu, J.O. (2007). Substrate-dependent targeting of eukaryotic translation initiation factor 4A by pateamine A: negation of domain-linker regulation of activity. Chem Biol *14*, 715-727.

Low, W.K., Dang, Y., Schneider-Poetsch, T., Shi, Z., Choi, N.S., Merrick, W.C., Romo, D., and Liu, J.O. (2005). Inhibition of eukaryotic translation initiation by the marine natural product pateamine A. Mol Cell *20*, 709-722.

Maag, D., Algire, M.A., and Lorsch, J.R. (2006). Communication between eukaryotic translation initiation factors 5 and 1A within the ribosomal pre-initiation complex plays a role in start site selection. Journal of Molecular Biology *356*, 724-737.

Maag, D., Fekete, C.A., Gryczynski, Z., and Lorsch, J.R. (2005). A conformational change in the eukaryotic translation preinitiation complex and release of eIF1 signal recognition of the start codon. Molecular Cell *17*, 265-275.

Marash, L., and Kimchi, A. (2005). DAP5 and IRES-mediated translation during programmed cell death. Cell Death Differ *12*, 554-562.

Marash, L., Liberman, N., Henis-Korenblit, S., Sivan, G., Reem, E., Elroy-Stein, O., and Kimchi, A. (2008). DAP5 promotes cap-independent translation of Bcl-2 and CDK1 to facilitate cell survival during mitosis. Mol Cell *30*, 447-459.

Marcker, K. (1965). Formation of N-formylmethionyl sRNA. Journal of Molecular Biology *14*, 63-&.

Marcker, K., and Sanger, F. (1964). N-formyl methionyl sRNA. Journal of Molecular Biology *8*, 835-&.

Marcotrigiano, J., Lomakin, I.B., Sonenberg, N., Pestova, T.V., Hellen, C.U.T., and Burley, S.K. (2001). A conserved HEAT domain within eIF4G directs assembly of the translation initiation machinery. Molecular Cell *7*, 193-203.

Marintchev, A., Edmonds, K.A., Marintcheva, B., Hendrickson, E., Oberer, M., Suzuki, C., Herdy, B., Sonenberg, N., and Wagner, G. (2009). Topology and regulation of the human eIF4A/4G/4H helicase complex in translation initiation. Cell *136*, 447-460.

Marintchev, A., and Wagner, G. (2005). EIF4G and CBP80 share a common origin and similar domain organization: Implications for the structure and function of eIF4W. Biochemistry *44*, 12265-12272.

Marissen, W., Gradi, A., Sonenberg, N., and Lloyd, R. (2000). Cleavage of eukaryotic translation initiation factor 4GII correlates with translation inhibition during apoptosis. Cell Death Differ *7*, 1234-1243.

Marsden, S., Nardelli, M., Linder, P., and McCarthy, J. (2006). Unwinding single RNA molecules using helicases involved in eukaryotic translation initiation. J Mol Biol *361*, 327-335.

Martineau, Y., Derry, M., Wang, X., Yanagiya, A., Berlanga, J., Shyu, A., Imataka, H., Gehring, K., and Sonenberg, N. (2008). Poly(A)-binding protein-interacting protein 1 binds to eukaryotic translation initiation factor 3 to stimulate translation. Mol Cell Biol *28*, 6658-6667.

Matson, S., Tabor, S., and Richardson, C. (1983). The gene 4 protein of bacteriophage T7. Characterization of helicase activity. J Biol Chem *258*, 14017-14024.

Mazroui, R., Sukarieh, R., Bordeleau, M., Kaufman, R., Northcote, P., Tanaka, J., Gallouzi, I., and Pelletier, J. (2006). Inhibition of ribosome recruitment induces stress granule formation independently of eukaryotic initiation factor 2alpha phosphorylation. Mol Biol Cell *17*, 4212-4219.

Mazumder, B., Sampath, P., Seshadri, V., Maitra, R., DiCorleto, P., and Fox, P. (2003). Regulated release of L13a from the 60S ribosomal subunit as a mechanism of transcript-specific translational control. Cell *115*, 187-198.

Mazumder, B., Seshadri, V., Imataka, H., Sonenberg, N., and Fox, P. (2001). Translational silencing of ceruloplasmin requires the essential elements of mRNA circularization: poly(A) tail, poly(A)-binding protein, and eukaryotic translation initiation factor 4G. Mol Cell Biol *21*, 6440-6449.

McGrath, J., McMillan, J., Shemanko, C., Runswick, S., Leigh, I., Lane, E., Garrod, D., and Eady, R. (1997). Mutations in the plakophilin 1 gene result in ectodermal dysplasia/skin fragility syndrome. Nat Genet *17*, 240-244.

Methot, N., Pickett, G., Keene, J., and Sonenberg, N. (1996a). In vitro RNA selection identifies RNA ligands that specifically bind to eukaryotic translation initiation factor 4B: the role of the RNA remotif. RNA *2*, 38-50.

Methot, N., Song, M.S., and Sonenberg, N. (1996b). A region rich in aspartic acid, arginine, tyrosine, and glycine (DRYG) mediates eukaryotic initiation factor 4B (eIF4B) self-association and interaction with eIF3. Mol Cell Biol *16*, 5328-5334.

Meurs, E., Chong, K., Galabru, J., Thomas, N.S.B., Kerr, I.M., Williams, B.R.G., and Hovanessian, A.G. (1990). Molecular cloning and characterisation of the human double stranded RNA activated protein kinase induced by interferon. Cell *62*, 379-390.

Milburn, S., Hershey, J., Davies, M., Kelleher, K., and Kaufman, R. (1990). Cloning and expression of eukaryotic initiation factor 4B cDNA: sequence determination identifies a common RNA recognition motif. EMBO J *9*, 2783-2790.

Minghetti, L., and Levi, G. (1995). Induction of prostanoid biosynthesis by bacterial lipopolysaccharide and isoproterenol in rat microglial cultures. J Neurochem *65*, 2690-2698.

Mitchell, S.F., and Lorsch, J.R. (2008). Should I stay or should I go? Eukaryotic translation initiation factors 1 and 1A control start codon recognition. Journal of Biological Chemistry *283*, 27345-27349.

Mitkevich, V.A., Kononenko, A.V., Petrushanko, I.Y., Yanvarev, D.V., Makarov, A.A., and Kisselev, L.L. (2006). Termination of translation in eukaryotes is mediated by the quaternary eRF1 center dot eRF3 center dot GTP center dot Mg2+ complex. The biological roles of eRF3 and prokaryotic RF3 are profoundly distinct. Nucleic Acids Research *34*, 3947-3954.

Miyakawa, S., Oguro, A., Ohtsu, T., Imataka, H., Sonenberg, N., and Nakamura, Y. (2006). RNA aptamers to mammalian initiation factor 4G inhibit cap-dependent translation by blocking the formation of initiation factor complexes. RNA *12*, 1825-1834.

Mochizuki, K., Oguro, A., Ohtsu, T., Sonenberg, N., and Nakamura, Y. (2005). High affinity RNA for mammalian initiation factor 4E interferes with mRNA-cap binding and inhibits translation. RNA *11*, 77-89.

Moerschell, R.P., Hosokawa, Y., Tsunasawa, S., and Sherman, F. (1990). The specificities of yeast methionine aminopeptidase and acetylation of amino-terminal methionine in vivo - processing of altered iso-1-cytochromes-cis created by oligonucleotide transformation. Journal of Biological Chemistry *265*, 19638-19643.

Mohr, G., Del Campo, M., Mohr, S., Yang, Q., Jia, H., Jankowsky, E., and Lambowitz, A.M. (2008). Function of the C-terminal domain of the DEAD-box protein Mss116p analyzed in vivo and in vitro. J Mol Biol *375*, 1344-1364.

Mokas, S., Mills, J., Garreau, C., Fournier, M., Robert, F., Arya, P., Kaufman, R., Pelletier, J., and Mazroui, R. (2009). Uncoupling stress granule assembly and translation initiation inhibition. Mol Biol Cell *20*, 2673-2683.

Molloy, J.E., and Padgett, M.J. (2002). Lights, action: optical tweezers. Contemporary Physics *43*, 241-258.

Morino, S., Imataka, H., Svitkin, Y.V., Pestova, T.V., and Sonenberg, N. (2000). Eukaryotic translation initiation factor 4E (eIF4E) binding site and the middle one-third of eIF4GI constitute the core domain for cap-dependent translation, and the C-terminal one-third functions as a modulatory region. Molecular and Cellular Biology *20*, 468-477.

Morley, S.J., McKendrick, L., and Bushell, M. (1998). Cleavage of translation initiation factor 4G (eIF4G) during anti-Fas IgM-induced apoptosis does not require signalling through the p38 mitogen-activated protein (MAP) kinase. Febs Letters *438*, 41-48.

Mukhopadhyay, R., Jia, J., Arif, A., Ray, P., and Fox, P. (2009). The GAIT system: a gatekeeper of inflammatory gene expression. Trends Biochem Sci *34*, 324-331.

Mukhopadhyay, R., Ray, P., Arif, A., Brady, A., Kinter, M., and Fox, P. (2008). DAPK-ZIPK-L13a axis constitutes a negative-feedback module regulating inflammatory gene expression. Mol Cell *32*, 371-382.

Murakami, A., Nishizawa, T., Egawa, K., Kawada, T., Nishikawa, Y., Uenakai, K., and Ohigashi, H. (2005). New class of linoleic acid metabolites biosynthesized by corn and rice lipoxygenases: suppression of proinflammatory mediator expression via attenuation of MAPK- and Akt-, but not PPARgamma-, dependent pathways in stimulated macrophages. Biochem Pharmacol *70*, 1330-1342.

Muslimov, I., Iacoangeli, A., Brosius, J., and Tiedge, H. (2006). Spatial codes in dendritic BC1 RNA. J Cell Biol *175*, 427-439.

Muslimov, I., Santi, E., Homel, P., Perini, S., Higgins, D., and Tiedge, H. (1997). RNA transport in dendrites: a cis-acting targeting element is contained within neuronal BC1 RNA. J Neurosci *17*, 4722-4733.

Muthukrishnan, S., Both, G.W., Furuichi, Y., and Shatkin, A.J. (1975). 5'-terminal 7-methylguanosine in eukaryotic messenger RNA is required for translation. Nature *255*, 33-37.

Myong, S., Bruno, M., Pyle, A., and Ha, T. (2007). Spring-loaded mechanism of DNA unwinding by hepatitis C virus NS3 helicase. Science *317*, 513-516.

Méthot, N., Pause, A., Hershey, J., and Sonenberg, N. (1994). The translation initiation factor eIF-4B contains an RNA-binding region that is distinct and independent from its ribonucleoprotein consensus sequence. Mol Cell Biol *14*, 2307-2316.

Mühl, H., and Pfeilschifter, J. (2003). Anti-inflammatory properties of pro-inflammatory interferon-gamma. Int Immunopharmacol *3*, 1247-1255.

Nadanaciva, S., Weber, J., Wilke-Mounts, S., and Senior, A.E. (1999). Importance of F1-ATPase residue alpha-Arg-376 for catalytic transition state stabilization. Biochemistry *38*, 15493-15499.

Nanda, J.S., Cheung, Y.N., Takacs, J.E., Martin-Marcos, P., Saini, A.K., Hinnebusch, A.G., and Lorsch, J.R. (2009). eIF1 Controls Multiple Steps in Start Codon Recognition during Eukaryotic Translation Initiation. Journal of Molecular Biology *394*, 268-285.

Naranda, T., Strong, W., Menaya, J., Fabbri, B., and Hershey, J. (1994). Two structural domains of initiation factor eIF-4B are involved in binding to RNA. J Biol Chem *269*, 14465-14472.

Neuman, K., and Block, S. (2004). Optical trapping. Rev Sci Instrum *75*, 2787-2809.

Nielsen, K.H., Chamieh, H., Andersen, C.B., Fredslund, F., Hamborg, K., Le Hir, H., and Andersen, G.R. (2009). Mechanism of ATP turnover inhibition in the EJC. RNA *15*, 67-75.

Nielsen, P.J., McMaster, G.K., and Trachsel, H. (1985). Cloning of eukaryotic protein synthesis initiation factor genes - isolation and characterisation of cDNA clones encoding eIF4A. Nucleic Acids Research *13*, 6867-6880.

Nielsen, P.J., and Trachsel, H. (1988). The mouse protein-synthesis initiation factor 4A gene family includes two related functional genes which are differentially expressed. Embo Journal *7*, 2097-2105.

Nika, J., Yang, W.M., Pavitt, G.D., Hinnebusch, A.G., and Hannig, E.M. (2000). Purification and kinetic analysis of eIF2B from Saccharomyces cerevisiae. Journal of Biological Chemistry *275*, 26011-26017.

Nirenberg, M., Leder, P., Bernfiel, M., Brimacom, R., Trupin, J., Rottman, F., and Oneal, C. (1965). RNA codewords and protein synthesis. VII. On general nature of RNA code. Proceedings of the National Academy of Sciences of the United States of America *53*, 1161-&.

Nirenberg, M.W., and Leder, P. (1964). RNA codewords and protein synthesis - effect of trinucleotides upon binding of SRNA to ribosomes. Science *145*, 1399-&.

Northcote, P.T., Blunt, J.W., and Munro, M.H.G. (1991). Pateamine: a potent cytotoxin from the New Zealand marine sponge, Mycale sp. Tetrahedron Letters *32*, 6259, 6411-6414.

Nousch, M., Reed, V., Bryson-Richardson, R., Currie, P., and Preiss, T. (2007). The eIF4G-homolog p97 can activate translation independent of caspase cleavage. RNA *13*, 374-384.

Oberer, M., Marintchev, A., and Wagner, G. (2005). Structural basis for the enhancement of eIF4A helicase activity by eIF4G. Genes Dev *19*, 2212-2223.

Ogorochi, T., Narumiya, S., Mizuno, N., Yamashita, K., Miyazaki, H., and Hayaishi, O. (1984). Regional distribution of prostaglandins D2, E2, and F2 alpha and related enzymes in postmortem human brain. J Neurochem *43*, 71-82.

Oguro, A., Ohtsu, T., Svitkin, Y., Sonenberg, N., and Nakamura, Y. (2003). RNA aptamers to initiation factor 4A helicase hinder cap-dependent translation by blocking ATP hydrolysis. RNA *9*, 394-407.

Ohse, T., Ohba, S., Yamamoto, T., Koyano, T., and Umezawa, K. (1996). Cyclopentabenzofuran lignan protein synthesis inhibitors from Aglaia odorata. J Nat Prod *59*, 650-652.

Okano, H., and Darnell, R. (1997). A hierarchy of Hu RNA binding proteins in developing and adult neurons. J Neurosci *17*, 3024-3037.

Oliva, J., Pérez-Sala, D., Castrillo, A., Martínez, N., Cañada, F., Boscá, L., and Rojas, J. (2003). The cyclopentenone 15-deoxy-delta 12,14-prostaglandin J2 binds to and activates H-Ras. Proc Natl Acad Sci U S A *100*, 4772-4777.

Orsi, N., and Tribe, R. (2008). Cytokine networks and the regulation of uterine function in pregnancy and parturition. J Neuroendocrinol *20*, 462-469.

Orta, A. (2008). Development and automation of optical tweezers for single molecule bioforce measurements, Nottingham, Nottingham.

Orton, K.C., Ling, J., Waskiewicz, A.J., Cooper, J.A., Merrick, W.C., Korneeva, N.L., Rhoads, R.E., Sonenberg, N., and Traugh, J.A. (2004). Phosphorylation of Mnk1 by caspase-activated pak2/gamma-PAK inhibits phosphorylation and interaction of eIF4G with Mnk. Journal of Biological Chemistry *279*, 38649-38657.

Pang, P., Jankowsky, E., Planet, P., and Pyle, A. (2002). The hepatitis C viral NS3 protein is a processive DNA helicase with cofactor enhanced RNA unwinding. EMBO J *21*, 1168-1176.

Passmore, L.A., Schmeing, T.M., Maag, D., Applefield, D.J., Acker, M.G., Algire, M.A., Lorsch, J.R., and Ramakrishnan, V. (2007). The eukaryotic translation initiation factors eIF1 and eIF1A induce an open conformation of the 40S ribosome. Molecular Cell *26*, 41-50.

Patel, S.S., and Picha, K.M. (2000). Structure and function of hexameric helicases. Annu Rev Biochem *69*, 651-697.

Paulin, F.E.M., Campbell, L.E., O'Brien, K., Loughlin, J., and Proud, C.G. (2001). Eukaryotic translation initiation factor 5 (elF5) acts as a classical GTPase-activator protein. Current Biology *11*, 55-59.

Pause, A., Methot, N., and Sonenberg, N. (1993). The HRIGRXXR region of the DEAD box RNA helicase eukaryotic translation initiation factor 4A is required for RNA binding and ATP hydrolysis. Mol Cell Biol *13*, 6789-6798.

Pause, A., Methot, N., Svitkin, Y., Merrick, W.C., and Sonenberg, N. (1994). Dominant negative mutants of mammalian translation initiation factors eIF4A define a critical role for eIF4F in cap dependent initiation of translation. Embo Journal *13*, 1205-1215.

Pause, A., and Sonenberg, N. (1992). Mutational analysis of a DEAD box RNA helicase: the mammalian translation initiation factor eIF-4A. EMBO J *11*, 2643-2654.

Peck, M.L., and Herschlag, D. (1999). Effects of oligonucleotide length and atomic composition on stimulation of the ATPase activity of translation initiation factor elF4A. RNA *5*, 1210-1221.

Pegg, A. (1988). Polyamine metabolism and its importance in neoplastic growth and a target for chemotherapy. Cancer Res *48*, 759-774.

Pelletier, J., and Sonenberg, N. (1985). Insertion mutagenesis to increase secondary structure within the 5' noncoding region of a eukaryotic messenger RNA reduces translational efficiency. Cell *40*, 515-526.

Pende, M., Um, S.H., Mieulet, V., Sticker, M., Goss, V.L., Mestan, J., Mueller, M., Fumagalli, S., Kozma, S.C., and Thomas, G. (2004). S6K1(-/-)/S6K2(-/-) mice exhibit perinatal lethality and rapamycin-sensitive 5 '-terminal oligopyrimidine mRNA translation and reveal a mitogen-activated protein kinase-dependent S6 kinase pathway. Molecular and Cellular Biology *24*, 3112-3124.

Person, E., Waite, L., Taylor, R., and Scanlan, T. (2001). Albumin regulates induction of peroxisome proliferator-activated receptor-gamma (PPARgamma) by 15-deoxy-delta(12-14)-prostaglandin J(2) in vitro and may be an important regulator of PPARgamma function in vivo. Endocrinology *142*, 551-556.

Pesole, G., Gissi, C., Grillo, G., Licciulli, F., Liuni, S., and Saccone, C. (2000). Analysis of oligonucleotide AUG start codon context in eukariotic mRNAs. Gene *261*, 85-91.

Pestova, T., Hellen, C., and Shatsky, I. (1996a). Canonical eukaryotic initiation factors determine initiation of translation by internal ribosomal entry. Mol Cell Biol *16*, 6859-6869.

Pestova, T., Shatsky, I., Fletcher, S., Jackson, R., and Hellen, C. (1998a). A prokaryotic-like mode of cytoplasmic eukaryotic ribosome binding to the initiation codon during internal translation initiation of hepatitis C and classical swine fever virus RNAs. Genes Dev *12*, 67-83.

Pestova, T.V., Borukhov, S.I., and Hellen, C.U.T. (1998b). Eukaryotic ribosomes require initiation factors 1 and 1A to locate initiation codons. Nature *394*, 854-859.

Pestova, T.V., and Kolupaeva, V.G. (2002). The roles of individual eukaryotic translation initiation factors in ribosomal scanning and initiation codon selection. Genes & Development *16*, 2906-2922.

Pestova, T.V., Shatsky, I.N., and Hellen, C.U.T. (1996b). Functional dissection of eukaryotic initiation factor 4F: The 4A subunit and the central domain of the 4G subunit are sufficient to mediate internal entry of 43S preinitiation complexes. Molecular and Cellular Biology *16*, 6870-6878.

Petersen, H.U., Danchin, A., and Grunbergmanago, M. (1976). Toward an understanding of initiator tRNA methionine in prokaryotic protein synthesis. II. A two-state model for 70S ribosome. Biochemistry *15*, 1362-1369.

Pisarev, A.V., Kolupaeva, V.G., Pisareva, V.P., Merrick, W.C., Hellen, C.U.T., and Pestova, T.V. (2006). Specific functional interactions of nucleotides at key (-)3 and (+)4 positions flanking the initiation codon with components of the mammalian 48S translation initiation complex. Genes & Development *20*, 624-636.

Pisareva, V.P., Pisarev, A.V., Komar, A.A., Hellen, C.U.T., and Pestova, T.V. (2008). Translation Initiation on Mammalian mRNAs with Structured 5 ' UTRs Requires DExH-Box Protein DHX29. Cell *135*, 1237-1250.

Powers, T., and Walter, P. (1999). Regulation of ribosome biogenesis by the rapamycin-sensitive TOR-signaling pathway in Saccharomyces cerevisiae. Molecular Biology of the Cell *10*, 987-1000.

Pyronnet, S., Pradayrol, L., and Sonenberg, N. (2000). A cell cycle-dependent internal ribosome entry site. Mol Cell *5*, 607-616.

Pérez-Sala, D., Cernuda-Morollón, E., and Cañada, F. (2003). Molecular basis for the direct inhibition of AP-1 DNA binding by 15-deoxy-Delta 12,14-prostaglandin J2. J Biol Chem *278*, 51251-51260.

Qin, H., Raught, B., Sonenberg, N., Goldstein, E.G., and Edelman, A.M. (2003). Phosphorylation screening identifies translational initiation factor 4GII as an intracellular target of Ca2+/Calmodulin-dependent protein kinase I. Journal of Biological Chemistry *278*, 48570-48579.

Ramírez-Valle, F., Braunstein, S., Zavadil, J., Formenti, S., and Schneider, R. (2008). eIF4GI links nutrient sensing by mTOR to cell proliferation and inhibition of autophagy. J Cell Biol *181*, 293-307.

Raught, B., Gingras, A.C., Gygi, S.P., Imataka, H., Morino, S., Gradi, A., Aebersold, R., and Sonenberg, N. (2000). Serum-stimulated, rapamycin-sensitive phosphorylation sites in the eukaryotic translation initiation factor 4GI. Embo Journal *19*, 434-444.

Raught, B., Peiretti, F., Gingras, A.C., Livingstone, M., Shahbazian, D., Mayeur, G.L., Polakiewicz, R.D., Sonenberg, N., and Hershey, J.W.B. (2004). Phosphorylation of eucaryotic translation initiation factor 4B Ser422 is modulated by S6 kinases. Embo Journal *23*, 1761-1769.

Ray, B.K., Lawson, T.G., Kramer, J.C., Cladaras, M.H., Grifo, J.A., Abramson, R.D., Merrick, W.C., and Thach, R.E. (1985). ATP-dependent unwinding of messenger RNA structure by eukaryotic initiation factors. Journal of Biological Chemistry *260*, 7651-7658.

Reiter, A.K., Bolster, D.R., Crozier, S.J., Kimball, S.R., and Jefferson, L.S. (2008). AMPK represses TOP mRNA translation but not global protein synthesis in liver. Biochemical and Biophysical Research Communications *374*, 345-350.

Richter-Cook, N., Dever, T., Hensold, J., and Merrick, W. (1998). Purification and characterization of a new eukaryotic protein translation factor. Eukaryotic initiation factor 4H. J Biol Chem *273*, 7579-7587.

Ricote, M., Li, A., Willson, T., Kelly, C., and Glass, C. (1998). The peroxisome proliferator-activated receptor-gamma is a negative regulator of macrophage activation. Nature *391*, 79-82.

Ritchie, M., Silver, J., Oshlack, A., Holmes, M., Diyagama, D., Holloway, A., and Smyth, G. (2007). A comparison of background correction methods for two-colour microarrays. Bioinformatics *23*, 2700-2707.

Rittinger, K., Walker, P.A., Eccleston, J.F., Nurmahomed, K., Owen, D., Laue, E., Gamblin, S.J., and Smerdon, S.J. (1997). Crystal structure of a small G protein in complex with the GTPase-activating protein rhoGAP. Nature *388*, 693-697.

Rizzuto, R., Pinton, P., Ferrari, D., Chami, M., Szabadkai, G., Magalhães, P., Di Virgilio, F., and Pozzan, T. (2003). Calcium and apoptosis: facts and hypotheses. Oncogene *22*, 8619-8627.

Robertus, J.D., Ladner, J.E., Finch, J.T., Rhodes, D., Brown, R.S., Clark, B.F.C., and Klug, A. (1974a). Correlation between 3-dimensional structure and chemical reactivity of transfer-RNA. Nucleic Acids Research *1*, 927-932.

Robertus, J.D., Ladner, J.E., Finch, J.T., Rhodes, D., Brown, R.S., Clark, B.F.C., and Klug, A. (1974b). Structure of yeast phenylalanine transfer-RNA at 3 A resolution. Nature *250*, 546-551.

Rogers, G.W., Jr., Lima, W.F., and Merrick, W.C. (2001a). Further characterization of the helicase activity of eIF4A. Substrate specificity. J Biol Chem *276*, 12598-12608.

Rogers, G.W., Jr., Richter, N.J., Lima, W.F., and Merrick, W.C. (2001b). Modulation of the helicase activity of eIF4A by eIF4B, eIF4H, and eIF4F. J Biol Chem *276*, 30914-30922.

Rogers, G.W., Jr., Richter, N.J., and Merrick, W.C. (1999). Biochemical and kinetic characterization of the RNA helicase activity of eukaryotic initiation factor 4A. J Biol Chem *274*, 12236-12244.

Roig, J., Huang, Z.D., Lytle, C., and Traugh, J.A. (2000). p21-activated protein kinase gamma-PAK is translocated and activated in response to hyperosmolarity - Implication of Cdc42 and phosphoinositide 3-kinase in a two-step mechanism for gamma-PAK activation. Journal of Biological Chemistry *275*, 16933-16940.

Roy, G., De Crescenzo, G., Khaleghpour, K., Kahvejian, A., O'Connor-McCourt, M., and Sonenberg, N. (2002). Paip1 interacts with poly(A) binding protein through two independent binding motifs. Mol Cell Biol *22*, 3769-3782.

Rozen, F., Edery, I., Meerovitch, K., Dever, T.E., Merrick, W.C., and Sonenberg, N. (1990). Bidirectional RNA helicase activity of eukaryotic translation initiation factor 4A and factor 4F. Molecular and Cellular Biology *10*, 1134-1144.

Rozovsky, N., Butterworth, A.C., and Moore, M.J. (2008). Interactions between eIF4AI and its accessory factors eIF4B and eIF4H. RNA *14*, 2136-2148.

Safer, B., Adams, S.L., Kemper, W.M., Berry, K.W., Lloyd, M., and Merrick, W.C. (1976). Purification and characterization of two initiation factors required for maximal activity of a highly fractionated globin mRNA translation system. Proc Natl Acad Sci U S A *73*, 2584-2588.

Saidak, Z., Mentaverri, R., and Brown, E. (2009). The role of the calcium-sensing receptor in the development and progression of cancer. Endocr Rev *30*, 178-195.

Sanchez, J. (2008). Alanine is the main second amino acid in vertebrate proteins and its coding entails increased use of the rare codon GCG. Biochemical and Biophysical Research Communications *373*, 589-592.

Sandler, H., and Stoecklin, G. (2008). Control of mRNA decay by phosphorylation of tristetraprolin. Biochem Soc Trans *36*, 491-496.

Sanguinetti, M., Curran, M., Zou, A., Shen, J., Spector, P., Atkinson, D., and Keating, M. (1996). Coassembly of K(V)LQT1 and minK (IsK) proteins to form cardiac I(Ks) potassium channel. Nature *384*, 80-83.

Saraste, M., Sibbald, P.R., and Wittinghofer, A. (1990). The P-loop--a common motif in ATP- and GTP-binding proteins. Trends Biochem Sci *15*, 430-434.

Sauer, I., Schaljo, B., Vogl, C., Gattermeier, I., Kolbe, T., Müller, M., Blackshear, P., and Kovarik, P. (2006). Interferons limit inflammatory responses by induction of tristetraprolin. Blood *107*, 4790-4797.

Scheffzek, K., Ahmadian, M.R., Kabsch, W., Wiesmuller, L., Lautwein, A., Schmitz, F., and Wittinghofer, A. (1997). The Ras-RasGAP complex: structural basis for GTPase activation and its loss in oncogenic Ras mutants. Science *277*, 333-338.

Schek, N., and Bachenheimer, S. (1985). Degradation of cellular mRNAs induced by a virion-associated factor during herpes simplex virus infection of Vero cells. J Virol *55*, 601-610.

Scheper, G.C., and Proud, C.G. (2002). Does phosphorylation of the cap-binding protein eIF4E play a role in translation initiation? European Journal of Biochemistry *269*, 5350-5359.

Schmitt, E., Blanquet, S., and Mechulam, Y. (2002). The large subunit of initiation factor alF2 is a close structural homologue of elongation factors. Embo Journal *21*, 1821-1832.

Schreier, M.H., Erni, B., and Staehelin, T. (1977). Initiation of mammalian protein synthesis. 1. purification and characterisation of seven initiation factors. Journal of Molecular Biology *116*, 727-753.

Schutz, P., Bumann, M., Oberholzer, A.E., Bieniossek, C., Trachsel, H., Altmann, M., and Baumann, U. (2008). Crystal structure of the yeast eIF4A-eIF4G complex: an RNA-helicase controlled by protein-protein interactions. Proc Natl Acad Sci U S A *105*, 9564-9569.

Scolnick, E., Tompkins, R., Caskey, T., and Nirenber.M. (1968). Release factors differing in specificity for terminator codons. Proceedings of the National Academy of Sciences of the United States of America *61*, 768-&.

Scott, C.E., and Adebodun, F. (1999). C-13-NMR investigation of protein synthesis during apoptosis in human leukemic cell lines. Journal of Cellular Physiology *181*, 147-152.

Seal, S.N., Schmidt, A., and Marcus, A. (1983). Eukaryotic initiation factor 4A is the component that interacts with ATP in protein chain initiation. Proceedings of the National Academy of Sciences of the United States of America-Biological Sciences *80*, 6562-6565.

Sengoku, T., Nureki, O., Nakamura, A., Kobayashi, S., and Yokoyama, S. (2006). Structural basis for RNA unwinding by the DEAD-box protein Drosophila Vasa. Cell *125*, 287-300.

Serhan, C., Chiang, N., and Van Dyke, T. (2008). Resolving inflammation: dual anti-inflammatory and pro-resolution lipid mediators. Nat Rev Immunol *8*, 349-361.

Shahbazian, D., Parsyan, A., Petroulakis, E., Topisirovic, I., Martineau, Y., Gibbs, B., Svitkin, Y., and Sonenberg, N. (2010). Control of cell survival and proliferation by mammalian eukaryotic initiation factor 4B. Mol Cell Biol *30*, 1478-1485.

Shahbazian, D., Roux, P.P., Mieulet, V., Cohen, M.S., Raught, B., Taunton, J., Hershey, J.W., Blenis, J., Pende, M., and Sonenberg, N. (2006). The mTOR/PI3K and MAPK pathways converge on eIF4B to control its phosphorylation and activity. EMBO J *25*, 2781-2791.

Shatkin, A.J. (1976). Capping of eukaryotic mRNAs. Cell *9*, 645-653.

Sheedy, F., Palsson-McDermott, E., Hennessy, E., Martin, C., O'Leary, J., Ruan, Q., Johnson, D., Chen, Y., and O'Neill, L. (2010). Negative regulation of TLR4 via targeting of the proinflammatory tumor suppressor PDCD4 by the microRNA miR-21. Nat Immunol *11*, 141-147.

Shen, Y., Prakash, C., and Chang, Y. (2001). Two new polyhydroxysteroids from the gorgonian Isis hippuris. Steroids *66*, 721-725.

Sherrill, K.W., and Lloyd, R.E. (2008). Translation of cIAP2 mRNA is mediated exclusively by a stress-modulated ribosome shunt. Molecular and Cellular Biology *28*, 2011-2022.

Shi, H., Cordin, O., Minder, C.M., Linder, P., and Xu, R.M. (2004). Crystal structure of the human ATP-dependent splicing and export factor UAP56. Proc Natl Acad Sci U S A *101*, 17628-17633.

Shi, L., Reid, L., Jones, W., Shippy, R., Warrington, J., Baker, S., Collins, P., de Longueville, F., Kawasaki, E., Lee, K., Luo, Y., Sun, Y., Willey, J., Setterquist, R., Fischer, G., Tong, W., Dragan, Y., Dix, D., Frueh, F., Goodsaid, F., Herman, D., Jensen, R., Johnson, C., Lobenhofer, E., Puri, R., Schrf, U., Thierry-Mieg, J., Wang, C., Wilson, M., Wolber, P., Zhang, L., Amur, S., Bao, W., Barbacioru, C., Lucas, A., Bertholet, V., Boysen, C., Bromley, B., Brown, D., Brunner, A., Canales, R., Cao, X., Cebula, T., Chen, J., Cheng, J., Chu, T., Chudin, E., Corson, J., Corton, J., Croner, L., Davies, C., Davison, T., Delenstarr, G., Deng, X., Dorris, D., Eklund, A., Fan, X., Fang, H., Fulmer-Smentek, S., Fuscoe, J., Gallagher, K., Ge, W., Guo, L., Guo, X., Hager, J., Haje, P., Han, J., Han, T., Harbottle, H., Harris, S., Hatchwell, E., Hauser, C., Hester, S., Hong, H., Hurban, P., Jackson, S., Ji, H., Knight, C., Kuo, W., LeClerc, J., Levy, S., Li, Q., Liu, C., Liu, Y., Lombardi, M., Ma, Y., Magnuson, S., Maqsodi, B., McDaniel, T., Mei, N., Myklebost, O., Ning, B., Novoradovskaya, N., Orr, M., Osborn, T., Papallo, A., Patterson, T., Perkins, R., Peters, E., Peterson, R., Philips, K., Pine, P., Pusztai, L., Qian, F., Ren, H., Rosen, M., Rosenzweig, B., Samaha, R., Schena, M., Schroth, G., Shchegrova, S., Smith, D., Staedtler, F., Su, Z., Sun, H., Szallasi, Z., Tezak, Z., Thierry-Mieg, D., Thompson, K., Tikhonova, I., Turpaz, Y., Vallanat, B., Van, C., Walker, S., Wang, S., Wang, Y., Wolfinger, R., Wong, A., Wu, J., Xiao, C., Xie, Q., Xu, J., Yang, W., Zhong, S., Zong, Y., Slikker, W.J., and Consortium, M. (2006). The MicroArray Quality Control (MAQC) project shows inter- and intraplatform reproducibility of gene expression measurements. Nat Biotechnol *24*, 1151-1161.

Shi, L., Tong, W., Fang, H., Scherf, U., Han, J., Puri, R., Frueh, F., Goodsaid, F., Guo, L., Su, Z., Han, T., Fuscoe, J., Xu, Z., Patterson, T., Hong, H., Xie, Q., Perkins, R., Chen, J., and Casciano, D. (2005). Cross-platform comparability of microarray technology: intra-platform consistency and appropriate data analysis procedures are essential. BMC Bioinformatics *6 Suppl 2*, S12.

Shibahara, K., Asano, M., Ishida, Y., Aoki, T., Koike, T., and Honjo, T. (1995). Isolation of a novel mouse gene MA-3 that is induced upon programmed cell death. Gene *166*, 297-301.

Shine, J., and Dalgarno, L. (1974). The 3' terminal sequence of Escherichia coli 16S ribosomal RNA complementarity to nonsense triplets and ribosome binding sites. Proceedings of the National Academy of Sciences of the United States of America *71*, 1342-1346.

Shine, J., and Dalgarno, L. (1975). Determinant of cistron specificity in bacterial ribosomes. Nature *254*, 34-38.

Silvera, D., Arju, R., Darvishian, F., Levine, P., Zolfaghari, L., Goldberg, J., Hochman, T., Formenti, S., and Schneider, R. (2009). Essential role for eIF4GI overexpression in the pathogenesis of inflammatory breast cancer. Nat Cell Biol *11*, 903-908.

Simmons, H., Oseth, L., Nguyen, P., O'Leary, M., Conklin, K., and Hirsch, B. (2002). Cytogenetic and molecular heterogeneity of 7q36/12p13 rearrangements in childhood AML. Leukemia *16*, 2408-2416.

Simmons, H.M., Ruis, B.L., Kapoor, M., Hudacek, A.W., and Conklin, K.F. (2005). Identification of NOM1, a nucleolar, eIF4A binding protein encoded within the chromosome 7q36 breakpoint region targeted in cases of pediatric acute myeloid leukemia. Gene *347*, 137-145.

Singleton, M.R., Dillingham, M.S., and Wigley, D.B. (2007). Structure and mechanism of helicases and nucleic acid translocases. Annu Rev Biochem *76*, 23-50.

Siridechadilok, B., Fraser, C.S., Hall, R.J., Doudna, J.A., and Nogales, E. (2005). Structural roles for human translation factor eIF3 in initiation of protein synthesis. Science *310*, 1513-1515.

Smibert, C., Johnson, D., and Smiley, J. (1992). Identification and characterization of the virion-induced host shutoff product of herpes simplex virus gene UL41. J Gen Virol *73 (Pt 2)*, 467-470.

Smith, C.A., and Rayment, I. (1996). Active site comparisons highlight structural similarities between myosin and other P-loop proteins. Biophys J *70*, 1590-1602.

Smith, S., Cui, Y., and Bustamante, C. (1996). Overstretching B-DNA: the elastic response of individual double-stranded and single-stranded DNA molecules. Science *271*, 795-799.

Smyth, G. (2004). Linear models and empirical bayes methods for assessing differential expression in microarray experiments. Stat Appl Genet Mol Biol *3*, Article3.

Smyth, G., and Speed, T. (2003). Normalization of cDNA microarray data. Methods *31*, 265-273.

Smyth, G.K. (2005). Limma: linear models for microarray data. In: Bioinformatics and Computational Biology Solutions using R and Bioconductor eds. R. Gentlman, V. Carey, S. Dudoit, R. Irizarry, and W. Huber, New York: Springer, 397 - 420.

Sonenberg, N., Morgan, M.A., Merrick, W.C., and Shatkin, A.J. (1978). Polypeptide in eukaryotic initiation factors that crosslinks specifically to 5' terminal cap in messenger RNAs. Proceedings of the National Academy of Sciences of the United States of America *75*, 4843-4847.

Spies, M., Amitani, I., Baskin, R., and Kowalczykowski, S. (2007). RecBCD enzyme switches lead motor subunits in response to chi recognition. Cell *131*, 694-705.

Spies, M., Bianco, P., Dillingham, M., Handa, N., Baskin, R., and Kowalczykowski, S. (2003). A molecular throttle: the recombination hotspot chi controls DNA translocation by the RecBCD helicase. Cell *114*, 647-654.

Steitz, J.A., and Jakes, K. (1975). How ribosomes select initiator regions in mRNA - base pair formation between 3' terminus of 16S ribosomal RNA and messenger RNA during initiation of protein synthesis in Escherichia coli. Proceedings of the National Academy of Sciences of the United States of America *72*, 4734-4738.

Stoecklin, G., Stubbs, T., Kedersha, N., Wax, S., Rigby, W., Blackwell, T., and Anderson, P. (2004). MK2-induced tristetraprolin:14-3-3 complexes prevent stress granule association and ARE-mRNA decay. EMBO J *23*, 1313-1324.

Stoneley, M., Chappell, S., Jopling, C., Dickens, M., MacFarlane, M., and Willis, A. (2000). c-Myc protein synthesis is initiated from the internal ribosome entry segment during apoptosis. Mol Cell Biol *20*, 1162-1169.

Stoneley, M., and Willis, A. (2004). Cellular internal ribosome entry segments: structures, trans-acting factors and regulation of gene expression. Oncogene *23*, 3200-3207.

Story, R.M., Li, H., and Abelson, J.N. (2001). Crystal structure of a DEAD box protein from the hyperthermophile Methanococcus jannaschii. Proc Natl Acad Sci U S A *98*, 1465-1470.

Straus, D., and Glass, C. (2001). Cyclopentenone prostaglandins: new insights on biological activities and cellular targets. Med Res Rev *21*, 185-210.

Straus, D., and Glass, C. (2007). Anti-inflammatory actions of PPAR ligands: new insights on cellular and molecular mechanisms. Trends Immunol *28*, 551-558.

Straus, D., Pascual, G., Li, M., Welch, J., Ricote, M., Hsiang, C., Sengchanthalangsy, L., Ghosh, G., and Glass, C. (2000). 15-deoxy-delta 12,14-prostaglandin J2 inhibits multiple steps in the NF-kappa B signaling pathway. Proc Natl Acad Sci U S A *97*, 4844-4849.

Strom, T., and Frenkel, N. (1987). Effects of herpes simplex virus on mRNA stability. J Virol *61*, 2198-2207.

Subkhankulova, T., Mitchell, S., and Willis, A. (2001). Internal ribosome entry segment-mediated initiation of c-Myc protein synthesis following genotoxic stress. Biochem J *359*, 183-192.

Sugimoto, N., Nakano, S., Katoh, M., Matsumura, A., Nakamuta, H., Ohmichi, T., Yoneyama, M., and Sasaki, M. (1995). Thermodynamic parameters to predict stability of RNA/DNA hybrid duplexes. Biochemistry *34*, 11211-11216.

Sundararajan, T.A., and Thach, R.E. (1966). Role of formylmethionine codon AUG in phasing translation of synthetic messenger RNA. Journal of Molecular Biology *19*, 74-&.

Sundkvist, I.C., and Staehelin, T. (1975). Structure and function of free 40 S ribosome subunits: Characterization of initiation factors. J Mol Biol *99*, 401-418.

Suzuki, C., Garces, R.G., Edmonds, K.A., Hiller, S., Hyberts, S.G., Marintchev, A., and Wagner, G. (2008). PDCD4 inhibits translation initiation by binding to eIF4A using both its MA3 domains. Proc Natl Acad Sci U S A *105*, 3274-3279.

Svitkin, Y.V., Pause, A., Haghighat, A., Pyronnet, S., Witherell, G., Belsham, G.J., and Sonenberg, N. (2001). The requirement for eukaryotic initiation factor 4A (elF4A) in translation is in direct proportion to the degree of mRNA 5' secondary structure. RNA *7*, 382-394.

Talavera, M.A., and De La Cruz, E.M. (2005). Equilibrium and kinetic analysis of nucleotide binding to the DEAD-box RNA helicase DbpA. Biochemistry *44*, 959-970.

Tang, H., Hornstein, E., Stolovich, M., Levy, G., Livingstone, M., Templeton, D., Avruch, J., and Meyuhas, O. (2001). Amino acid-induced translation of TOP mRNAs is fully dependent on phosphatidylinositol 3-kinase-mediated signaling, is partially inhibited by rapamycin and is independent of S6K1 and rpS6 phosphorylation. Molecular and Cellular Biology *21*, 8671-8683.

Tanner, N.K., Cordin, O., Banroques, J., Doere, M., and Linder, P. (2003). The Q motif: a newly identified motif in DEAD box helicases may regulate ATP binding and hydrolysis. Mol Cell *11*, 127-138.

Theissen, B., Karow, A.R., Kohler, J., Gubaev, A., and Klostermeier, D. (2008). Cooperative binding of ATP and RNA induces a closed conformation in a DEAD box RNA helicase. Proc Natl Acad Sci U S A *105*, 548-553.

Tiedge, H., Chen, W., and Brosius, J. (1993). Primary structure, neural-specific expression, and dendritic location of human BC200 RNA. J Neurosci *13*, 2382-2390.

Tiedge, H., Fremeau, R.J., Weinstock, P., Arancio, O., and Brosius, J. (1991). Dendritic location of neural BC1 RNA. Proc Natl Acad Sci U S A *88*, 2093-2097.

Tomoo, K., Shen, X., Okabe, K., Nozoe, Y., Fukuhara, S., Morino, S., Ishida, T., Taniguchi, T., Hasegawa, H., Terashima, A., Sasaki, M., Katsuya, Y., Kitamura, K., Miyoshi, H., Ishikawa, M., and Miura, K.I. (2002). Crystal structures of 7-methylguanosine 5 '-triphosphate (m(7)GTP)- and P-1-7-methylguanosine-P-3-adenosine-5 ',5 '-triphosphate (m7GpppA)-bound human full-length eukaryotic initiation factor 4E: biological importance of the C-terminal flexible region. Biochemical Journal *362*, 539-544.

Topisirovic, I., Ruiz-Gutierrez, M., and Borden, K.L.B. (2004). Phosphorylation of the eukaryotic translation initiation factor eIF4E contributes to its transformation and mRNA transport activities. Cancer Research *64*, 8639-8642.

Trachsel, H., Erni, B., Schreier, M., and Staehelin, T. (1977). Initiation of mammalian protein synthesis. II. The assembly of the initiation complex with purified initiation factors. J Mol Biol *116*, 755-767.

Tu, L., Liu, Z., He, X., He, Y., Yang, H., Jiang, Q., Xie, S., Xiao, G., Li, X., Yao, K., and Fang, W. (2010). Over-expression of eukaryotic translation initiation factor 4 gamma 1 correlates with tumor progression and poor prognosis in nasopharyngeal carcinoma. Mol Cancer *9*, 78.

Tudor, C., Marchese, F., Hitti, E., Aubareda, A., Rawlinson, L., Gaestel, M., Blackshear, P., Clark, A., Saklatvala, J., and Dean, J. (2009). The p38 MAPK pathway inhibits tristetraprolin-directed decay of interleukin-10 and pro-inflammatory mediator mRNAs in murine macrophages. FEBS Lett *583*, 1933-1938.

Tuerk, C., and Gold, L. (1990). Systematic evolution of ligands by exponential enrichment: RNA ligands to bacteriophage T4 DNA polymerase. Science *249*, 505-510.

Turner, I., Scott, D., Allen, S., Roberts, C., and Soultanas, P. (2004). The Bacillus subtilis DnaD protein: a putative link between DNA remodeling and initiation of DNA replication. FEBS Lett *577*, 460-464.

Tusher, V., Tibshirani, R., and Chu, G. (2001). Significance analysis of microarrays applied to the ionizing radiation response. Proc Natl Acad Sci U S A *98*, 5116-5121.

Tuteja, N., and Tuteja, R. (2004). Prokaryotic and eukaryotic DNA helicases. Essential molecular motor proteins for cellular machinery. Eur J Biochem *271*, 1835-1848.

Ueda, T., Watanabe-Fukunaga, R., Fukuyama, H., Nagata, S., and Fukunaga, R. (2004). Mnk2 and Mnk1 are essential for constitutive and inducible phosphorylation of eukaryotic initiation factor 4E but not for cell growth or development. Molecular and Cellular Biology *24*, 6539-6549.

Uma, S., Yun, B.G., and Matts, R.L. (2001). The heme-regulated eukaryotic initiation factor 2 alpha kinase - A potential regulatory target for control of protein synthesis by diffusible cases. Journal of Biological Chemistry *276*, 14875-14883.

Vale, R.D. (1996). Switches, latches, and amplifiers: common themes of G proteins and molecular motors. J Cell Biol *135*, 291-302.

Vary, T.C., Deiter, G., and Lynch, C.J. (2007). Rapamycin limits formation of active eukaryotic initiation factor 4F complex following meal feeding in rat hearts. Journal of Nutrition *137*, 1857-1862.

Vary, T.C., and Lynch, C.J. (2006). Meal feeding enhances formation of eIF4F in skeletal muscle: role of increased eIF4E availability and eIF4G phosphorylation. American Journal of Physiology-Endocrinology and Metabolism *290*, E631-E642.

Vasudevan, S., Tong, Y., and Steitz, J. (2007). Switching from repression to activation: microRNAs can up-regulate translation. Science *318*, 1931-1934.

Veigel, C., Bartoo, M., White, D., Sparrow, J., and Molloy, J. (1998). The stiffness of rabbit skeletal actomyosin cross-bridges determined with an optical tweezers transducer. Biophys J *75*, 1424-1438.

Venkatesan, M., Silver, L., and Nossal, N. (1982). Bacteriophage T4 gene 41 protein, required for the synthesis of RNA primers, is also a DNA helicase. J Biol Chem *257*, 12426-12434.

Villaret, D., Wang, T., Dillon, D., Xu, J., Sivam, D., Cheever, M., and Reed, S. (2000). Identification of genes overexpressed in head and neck squamous cell carcinoma using a combination of complementary DNA subtraction and microarray analysis. Laryngoscope *110*, 374-381.

von der Haar, T., and McCarthy, J.E.G. (2002). Intracellular translation initiation factor levels in Saccharomyces cerevisiae and their role in cap-complex function. Molecular Microbiology *46*, 531-544.

von Moeller, H., Basquin, C., and Conti, E. (2009). The mRNA export protein DBP5 binds RNA and the cytoplasmic nucleoporin NUP214 in a mutually exclusive manner. Nat Struct Mol Biol *16*, 247-254.

Von Pawel-Rammingen, U., Astrom, S., and Bystrom, A.S. (1992). Mutational analysis of conserved positions potentially important for initiator tRNA function in Saccharomyces cerevisiae. Molecular and Cellular Biology *12*, 1432-1442.

Walker, J.E., Saraste, M., Runswick, M.J., and Gay, N.J. (1982). Distantly related sequences in the alpha- and beta-subunits of ATP synthase, myosin, kinases and other ATP-requiring enzymes and a common nucleotide binding fold. EMBO J *1*, 945-951.

Wang, H., Iacoangeli, A., Lin, D., Williams, K., Denman, R., Hellen, C., and Tiedge, H. (2005). Dendritic BC1 RNA in translational control mechanisms. J Cell Biol *171*, 811-821.

Wang, H., Iacoangeli, A., Popp, S., Muslimov, I., Imataka, H., Sonenberg, N., Lomakin, I., and Tiedge, H. (2002). Dendritic BC1 RNA: functional role in regulation of translation initiation. J Neurosci *22*, 10232-10241.

Wang, X.M., Paulin, F.E.M., Campbell, L.E., Gomez, E., O'Brien, K., Morrice, N., and Proud, C.G. (2001). Eukaryotic initiation factor 2B: identification of multiple phosphorylation sites in the epsilon-subunit and their functions in vivo. Embo Journal *20*, 4349-4359.

Warner, J.R. (1999). The economics of ribosome biosynthesis in yeast. Trends in Biochemical Sciences *24*, 437-440.

Waskiewicz, A.J., Flynn, A., Proud, C.G., and Cooper, J.A. (1997). Mitogen-activated protein kinases activate the serine/threonine kinases Mnk1 and Mnk2. Embo Journal *16*, 1909-1920.

Wells, S.E., Hillner, P.E., Vale, R.D., and Sachs, A.B. (1998). Circularization of mRNA by eukaryotic translation initiation factors. Molecular Cell *2*, 135-140.

Wen, J.D., Lancaster, L., Hodges, C., Zeri, A.C., Yoshimura, S.H., Noller, H.F., Bustamante, C., and Tinoco, I. (2008). Following translation by single ribosomes one codon at a time. Nature *452*, 598-U592.

Wen, L., Huang, J., and Blackshear, P. (1989). Rat ornithine decarboxylase gene. Nucleotide sequence, potential regulatory elements, and comparison to the mouse gene. J Biol Chem *264*, 9016-9021.

Wendel, H.G., Silva, R.L.A., Malina, A., Mills, J.R., Zhu, H., Ueda, T., Watanabe-Fukunaga, R., Fukunaga, R., Teruya-Feldstein, J., Pelletier, J., and Lowe, S.W. (2007). Dissecting eIF4E action in tumorigenesis. Genes & Development *21*, 3232-3237.

White, R., and Sharrocks, A. (2010). Coordinated control of the gene expression machinery. Trends Genet *26*, 214-220.

Williams, D.D., Price, N.T., Loughlin, A.J., and Proud, C.G. (2001). Characterization of the mammalian initiation factor eIF2B complex as a GDP dissociation stimulator protein. Journal of Biological Chemistry *276*, 24697-24703.

Williams-Hill, D.M., Duncan, R.F., Nielsen, P.J., and Tahara, S.M. (1997). Differential expression of the murine eukaryotic translation initiation factor isogenes eIF4A(I) and eIF4A(II) is dependent upon cellular growth status. Arch Biochem Biophys *338*, 111-120.

Witten, D.M., and Tibshirani, R. (2007). A comparison of fold-change and the t-statistic for microarray data analysis. Stanford University, Stanford, CA, CA.

Wolf, A., Krause-Gruszczynska, M., Birkenmeier, O., Ostareck-Lederer, A., Hüttelmaier, S., and Hatzfeld, M. (2010). Plakophilin 1 stimulates translation by promoting eIF4A1 activity. J Cell Biol *188*, 463-471.

Woods, Y.L., Cohen, P., Becker, W., Jakes, R., Goedert, M., Wang, X.M., and Proud, C.G. (2001). The kinase DYRK phosphorylates protein-synthesis initiation factor eIF2B epsilon at Ser(539) and the microtubule-associated protein tau at Thr(212): potential role for DYRK as a glycogen synthase kinase 3-priming kinase. Biochemical Journal *355*, 609-615.

Xia, X.H. (2007). The +4G site in Kozak consensus is not related to the efficiency of translation initiation. Plos One *2*.

Yang, H., Matthews, C., Clair, T., Wang, Q., Baker, A., Li, C., Tan, T., and Colburn, N. (2006). Tumorigenesis suppressor Pdcd4 down-regulates mitogen-activated protein kinase kinase kinase kinase 1 expression to suppress colon carcinoma cell invasion. Mol Cell Biol *26*, 1297-1306.

Yang, H.S., Cho, M.H., Zakowicz, H., Hegamyer, G., Sonenberg, N., and Colburn, N.H. (2004). A novel function of the MA-3 domains in transformation and translation suppressor Pdcd4 is essential for its binding to eukaryotic translation initiation factor 4A. Molecular and Cellular Biology *24*, 3894-3906.

Yang, Q., and Jankowsky, E. (2005). ATP- and ADP-dependent modulation of RNA unwinding and strand annealing activities by the DEAD-box protein DED1. Biochemistry *44*, 13591-13601.

Yang, Y., Dudoit, S., Luu, P., Lin, D., Peng, V., Ngai, J., and Speed, T. (2002). Normalization for cDNA microarray data: a robust composite method addressing single and multiple slide systematic variation. Nucleic Acids Res *30*, e15.

Yasuda, M., Nishizawa, T., Ohigashi, H., Tanaka, T., Hou, D., Colburn, N., and Murakami, A. (2009). Linoleic acid metabolite suppresses skin inflammation and tumor promotion in mice: possible roles of programmed cell death 4 induction. Carcinogenesis *30*, 1209-1216.

Yatime, L., Mechulam, Y., Blanquet, S., and Schmitt, E. (2006). Structural switch of the gamma subunit in an archaeal alF2 alpha y heterodimer. Structure *14*, 119-128.

Yu, S. (2003). Regulation and critical role of potassium homeostasis in apoptosis. Prog Neurobiol *70*, 363-386.

Yueh, A., and Schneider, R.J. (2000). Translation by ribosome shunting on adenovirus and hsp70 mRNAs facilitated by complementarity to 18S rRNA. Genes & Development *14*, 414-421.

Zavialov, A.V., Buckingham, R.H., and Ehrenberg, M. (2001). A posttermination ribosomal complex is the guanine nucleotide exchange factor for peptide release factor RF3. Cell *107*, 115-124.

Zavialov, A.V., Mora, L., Buckingham, R.H., and Ehrenberg, M. (2002). Release of peptide promoted by the GGQ motif of class 1 release factors regulates the GTPase activity of RF3. Molecular Cell *10*, 789-798.

Zhang, W., Allen, S., Roberts, C., and Soultanas, P. (2006). The Bacillus subtilis primosomal protein DnaD untwists supercoiled DNA. J Bacteriol *188*, 5487-5493.

Zhang, W., Barbagallo, R., Madden, C., Roberts, C., Woolford, A., and Allen, S. (2005). Progressing single biomolecule force spectroscopy measurements for the screening of DNA binding agents. Nanotechnology *16*, 2325-2333.

Zhang, W., Dillingham, M., Thomas, C., Allen, S., Roberts, C., and Soultanas, P. (2007). Directional loading and stimulation of PcrA helicase by the replication initiator protein RepD. J Mol Biol *371*, 336-348.

Zhang, W., Machón, C., Orta, A., Phillips, N., Roberts, C., Allen, S., and Soultanas, P. (2008). Single-molecule atomic force spectroscopy reveals that DnaD forms scaffolds and enhances duplex melting. J Mol Biol *377*, 706-714.

Zhang, X., Wang, J., Gong, W., Mukaida, N., and Young, H. (2001). Differential regulation of chemokine gene expression by 15-deoxy-delta 12,14 prostaglandin J2. J Immunol *166*, 7104-7111.

Zhou, B.B., Li, H.L., Yuan, J.Y., and Kirschner, M.W. (1998). Caspase-dependent activation of cyclin-dependent kinases during fas-induced apoptosis in Jurkat cells. Proceedings of the National Academy of Sciences of the United States of America *95*, 6785-6790.

Zhouravleva, G., Frolova, L., Legoff, X., Leguellec, R., Ingevechtomov, S., Kisselev, L., and Philippe, M. (1995). Termination of translation in eukaryotes is governed by two interacting polypeptide-chain release factors, eRF1 and eRF3. Embo Journal *14*, 4065-4072.